Towards deeper molecular insight into familial exudative vitreoretinopathy

Zinc-ing deep into the vessels

Dyah Winiarty Karjosukarso

DONDERS
SERIES

Towards deeper molecular insight into familial exudative vitreoretinopathy

Zinc-ing deep into the vessels

Dyah Winiarty Karjosukarso

Colophon:
The work presented in this thesis was carried out within the Department of Human Genetics, the Donders Institute for Brain, Cognition, and Behaviour, Radboud university medical center, Nijmegen, the Netherlands

The printing of this thesis was financially supported by the Radboud University Nijmegen and the Donders Institute for Brain, Cognition, and Behaviour.

Printed by:	Proefschriftmaken.nl
Cover design by:	Bella Monica
Lay-out by:	Ferdinand van Nispen, *my*-thesis.nl
ISBN:	978-94-6380-381-6

Towards deeper molecular insight into familial exudative vitreoretinopathy

Zinc-ing deep into the vessels

Proefschrift

ter verkrijging van de graad van doctor
aan de Radboud Universiteit Nijmegen
op gezag van de rector magnificus prof. dr. J.H.J.M. van Krieken,
volgens besluit van het college van decanen
in het openbaar te verdedigen op donderdag 4 juli 2019
om 10.30 uur precies

door

Dyah Winiarty Karjosukarso
geboren op 1 maart 1992
te Ujung Pandang, Indonesië

Promotoren:
Dr. R.W.J. Collin
Prof. dr. F.P.M. Cremers

Copromotor:
Dr. H. Zhou

Manuscriptcommissie:
Prof. dr. M. Vermeulen
Dr. C. Toomes (St James's University Hospital, Leeds VK)
Prof. dr. J.H. Jansen

Paranimfen:
Lonneke Duijkers
Bella Monica

Towards deeper molecular insight into familial exudative vitreoretinopathy

Zinc-ing deep into the vessels

Doctoral Thesis

to obtain the degree of doctor
from Radboud University Nijmegen
on the authority of the Rector Magnificus prof. dr. J.H.J.M. van Krieken,
according to the decision of the Council of Deans
to be defended in public on Thursday, July 4, 2019
at 10.30 hours

by

Dyah Winiarty Karjosukarso
born on March 1, 1992
in Ujung Pandang, Indonesia

Supervisors:
Dr. R.W.J. Collin
Prof. dr. F.P.M. Cremers

Co-supervisor:
Dr. H. Zhou

Doctoral Thesis Committee:
Prof. dr. M. Vermeulen
Dr. C. Toomes (St James's University Hospital, Leeds, UK)
Prof. dr. J.H. Jansen

Paranymphs:
Lonneke Duijkers
Bella Monica

Table of contents

List of abbreviations

*	stop codon
2D	two-dimensional
3D	three-dimensional
ANOVA	analysis of variance
ATOH7	atonal bHLH transcription factor 7
BCVA	best corrected visual acuity
BRB	blood-retinal barrier
Cas9	CRISPR-associated protein 9
cDNA	complementary DNA
ChIP	chromatin immunoprecipitation
CRISPR	clustered regulatory interspaced short palindromic repeat
CT	computer tomography
CTNNB1	catenin beta 1
DNA	deoxyribonucleic acid
dpf	day(s) post fertilization
DRV	dorsal radial vessel
EC	endothelial cell
EGM2	endothelial growth medium 2
ENU	N-ethyl-N-nitrosurea
FACS	fluorescent activated cell sorting
FEVR	familial exudative vitreoretinopathy
FPKM	fragments per kilobase of exon model per million reads mapped
FZD4	frizzled class receptor 4
GCL	ganglion cell layer
GFP	green fluorescent protein
GO	gene ontology
HA	hemagglutinin
HDR	homology-directed repair
HEK293T	human embryonic kidney 293 T
hESC	human embryonic stem cell
hpf	hour(s) post fertilization
HUVEC	human umbilical vein endothelial cell
iBRB	inner blood-retinal barrier
INL	inner nuclear layer

IPL	inner plexiform layer
iPSC	induced pluripotent stem cell
KIF11	kinesin family member 11
LOVD	Leiden Open (source) Variation Database
LRP5	low density lipoprotein receptor-related protein 5
NDP	Norrie disease protein
NGS	next-generation sequencing
NHEJ	non-homologous end-joining
NRV	nasal radial vessel
oBRB	outer blood-retinal barrier
OIR	oxygen-induced retinopathy
ONL	outer nuclear layer
OPL	outer plexiform layer
PCA	principal component analysis
PCR	polymerase chain reaction
PRDM	positive regulatory domain I-binding factor 1/PRDI-BF1 and retinoblastoma-interacting zinc finger protein/RIZ1 homology domain containing
qPCR	quantitative polymerase chain reaction
RCBTB1	regulator of chromosome condensation (RCC1) and BTB (POZ) domain containing protein 1
RNA	ribonucleic acid
ROP	retinopathy of prematurity
RP	retinitis pigmentosa
RPE	retinal pigment epithelium
SET	Su3-9, Enhancer-of-zeste and Trithorax
TALEN	transcription activator-like effector nucleases
TLF	Tupfel long fin
TNFα	tumor necrosis factor alpha
TSPAN12	tetraspanin 12
TSS	transcription start site
UMC	unaffected mutant carrier
VEGF	vascular endothelial growth factor
VHL	von Hippel-Lindau syndrome
VMR	visuomotor response
VRV	ventral radial vessel

WES	whole exome sequencing
WG	week(s) of gestation
WGS	whole genome sequencing
ZFN	zinc finger nuclease
ZNF408	zinc finger protein 408

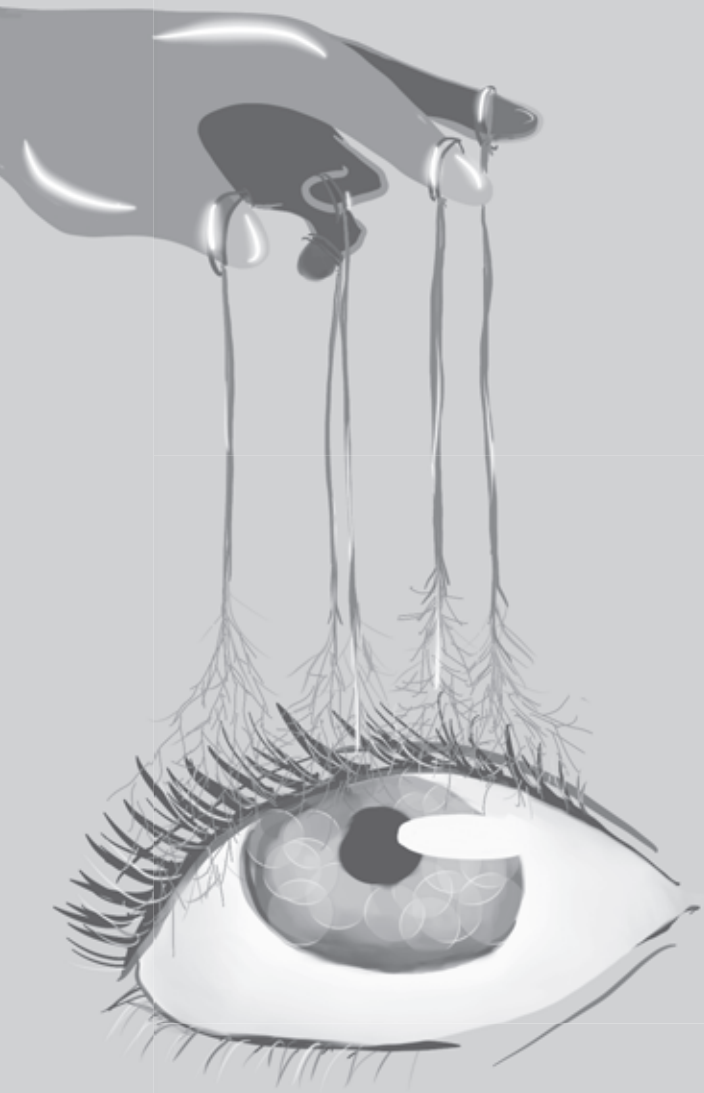

Chapter 1

General introduction

1.1 The eye

1.1.1 Anatomy of human eye

The human eye is composed of three layers (Figure 1) [1]. The outer layer consists of the cornea and the sclera. The cornea is the most anterior part of the eye and it transmits light through the lens to the retina. It also acts as a shield against infection and damage of the inner part of the eye [1, 2]. The sclera is built of connective tissue and maintains the spherical shape of the eye, protecting it from internal and external pressure [1]. The middle layer of the eye consists of the iris, the ciliary body, and the choroid. The iris is a thin circular structure within the eye which is responsible for controlling the size of the pupil and thereby, controls the amount of light transmitted to the retina. The iris is heavily pigmented which determines the eye color of an individual [1, 2]. The ciliary body is composed of the ciliary muscle and the ciliary epithelium. The ciliary muscle controls the shape of the lens, enabling one to focus on close or far objects. The ciliary epithelium is responsible for producing the aqueous humor [1, 2]. The last part of the middle layer, the choroid, contains the vascular beds which supports the outer retina [1, 2]. The innermost layer of the eye is called the retina. It is a complex layered structure of different types of cells that converts the light signal from the environment into a neural impulse which is subsequently transmitted to the brain creating visual perception [1, 2].

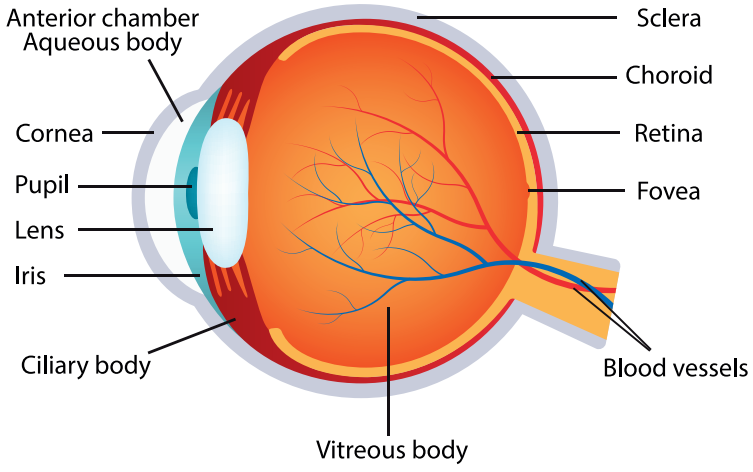

Figure 1. Anatomy of the human eye. The different parts of the human eye are indicated.©Adobe Stock.

The three layers of the eye surround three transparent structures, namely the aqueous humor, the vitreous, and the lens. The aqueous humor is secreted by the aforementioned ciliary epithelium. It is a transparent liquid which fills both the anterior and posterior chamber of the eye and is responsible for maintaining the intraocular pressure to keep the eye globe inflated as well as transporting nutrients to avascular eye parts [1]. The vitreous is a gelatinous transparent substance that fills the cavity between the lens and the retina. It consists of mainly water and obtains its gel-like consistency from collagen fibers and hyaluronic acid [1]. The lens, together with the cornea, refracts light onto the retina. Its ability to change shape under the control of the ciliary muscle allows one to focus on objects at various distances [1].

1.1.2 Retina structure

The retina is the photosensitive layer of the eye which is a part of the central nervous system [2]. It is a ~0.2 mm thick tissue which is composed of several layers of different cell types, among which are five types of neuronal cells, namely photoreceptor cells, horizontal cells, bipolar cells, amacrine cells, and ganglion cells [3]. These cells are organized into three nuclear layers that are separated by two synaptic layers (Figure 2). The outer nuclear layer (ONL), which is the first nuclear layer, consists of photoreceptor cells. The second layer is termed the inner nuclear layer (INL) and includes horizontal cells, bipolar cells and amacrine cells. The innermost layer is the ganglion cell layer (GCL), which as indicated by the name is composed of ganglion cells [2, 3]. The first synaptic layer is called the outer plexiform layer (OPL) which separates the ONL from the INL. It is the site where photoreceptor cells are in contact with horizontal cells and bipolar cells. The INL and the GCL are separated by the inner plexiform layer (IPL) where the bipolar and amacrine cells make synaptic contacts with ganglion cells [2, 3]. Besides the five types of neuronal cells, the retina also consists of Müller glial cells and retinal pigment epithelium cells (RPE). The Müller glial cells span across the retina and support the neuronal cells. The RPE is a layer of epithelial cells adjacent to the photoreceptor cell layer, which is essential for photoreceptor cells maintenance [2, 3].

Photoreceptor cells are specialized neurons which are responsible for the conversion of light into an electrical signal [2, 3]. Most vertebrates have two types of photoreceptor cells, the rods and the cones. The rods mediate vision in dim

light and are not involved in color vision, whereas the cones mediate vision in bright light and are involved in color vision [2]. The rods contain pigment with an absorption peak in the blue-green spectrum, while the cones contain pigments with absorption peaks in the blue, green or yellow parts of the color spectra. In human retina, the rods are approximately 20 times more abundant than cones [2]. However, the density of rods and cones differs between different regions of the retina. The peripheral retina is dominated by rods, whereas the very central region of the human retina, also known as the fovea, is dominated by cones. The center of the fovea, the foveola, is exclusively populated by cones [2, 4].

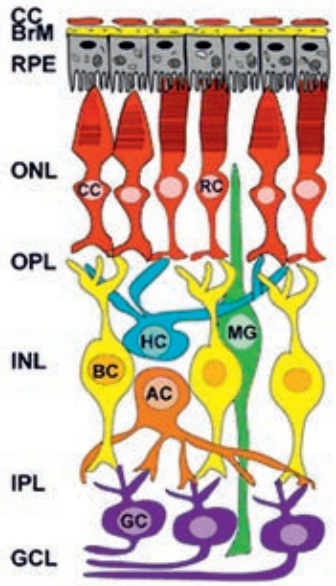

Figure 2. Schematic diagram of healthy retinal circuits. The mammalian retina consists of five major types of neuronal cells –photoreceptor cells (i.e. rod cells (RC) and cone cells (CC)), horizontal cells (HC), bipolar cells (BC), amacrine cells (AC), and retinal ganglion cells (RGC). The Müller cells (MC) are glial cells that span the retina and their somata. The RPE provides metabolic and transport functions essential for homeostasis of the neural retina. Bruch's membrane (BrM) is a highly specialized and multi-laminar structure separating the RPE from the choroid and mediates exchange of oxygen and nutrients between vasculature of choroid and neural retina. The RPE and BrM form the outer blood-retinal barrier. Choroidal capillaries (CC) are the blood capillaries present in the choroid that supply oxygen and nourishment to the outer layer of the retina. Reprinted with permission from Singh *et al.* (2018) [3].

The RPE is a monolayer of cuboidal pigmented epithelial cells that makes up the outermost part of the retina [2, 5, 6]. The apical side of the RPE faces the photoreceptor cells, whereas its basolateral side faces Bruch's membrane which separates the RPE from the choriocapillaris [5]. The RPE is involved in multiple

mechanisms which are fundamental to the maintenance of structural integrity and function of the retina. The functions of the RPE include the maintenance of photoreceptor function by phagocytosis of outer segments shed by photoreceptors as well as synthesis and regeneration of visual pigments [5, 6]. The pigmented cells allow the RPE to absorb scattered light which protects the retina from phototoxicity. The RPE's role as blood-retinal barrier (BRB) involves the transport of nutrients, growth factors, and waste from blood to the subretinal space and *vice versa* [5, 6]. Furthermore, the RPE is involved in the transport and metabolism of vitamin A as well as secreting growth factors and immunosuppressive factors required by neighbouring cells [5]. Additionally, the RPE is also involved in retinal adhesion [6].

1.1.3 Vasculature of the eye

The metabolic needs of the different ocular structures are supplied by separate circulation systems [7]. The avascular structures, such as the cornea, the lens, and the vitreous humor are served by an internal circulation of the aqueous humor [7]. The fovea, the central region of the retina which provides sharp vision, also lacks blood vessels and gets its nutrients by diffusion from the choroid. The retina is known to be the most metabolically active tissue in the body [7, 8]. Its high metabolic activity is served by two vasculature beds, the choroidal vasculature and the retinal vasculature. The choroidal vasculature is responsible for the RPE and the outer layer of the retina (mainly photoreceptors), whereas the retinal vasculature serves the inner layer of the retina (Figure 3) [7, 9]. Circulation in the choroidal vasculature is characterized by a high blood flow and a low oxygen extraction, while the retinal circulation typically has a low blood flow with a high oxygen extraction. The choroidal capillaries are much wider compared to the retinal capillaries, resulting in low resistance in the choroidal capillaries and thereby facilitate the high blood flow. Furthermore, unlike the retinal capillaries, the choroidal capillaries are fenestrated and tend to leak plasma protein [7]. Both vasculature beds are also regulated by different mechanisms. The choroidal circulation is mainly controlled by autonomic innervations, whereas the retinal circulation is mostly controlled by autoregulatory mechanisms and local factors, such as variations in perfusion pressure, variations in oxygen and carbon dioxide level, pH, etc [7].

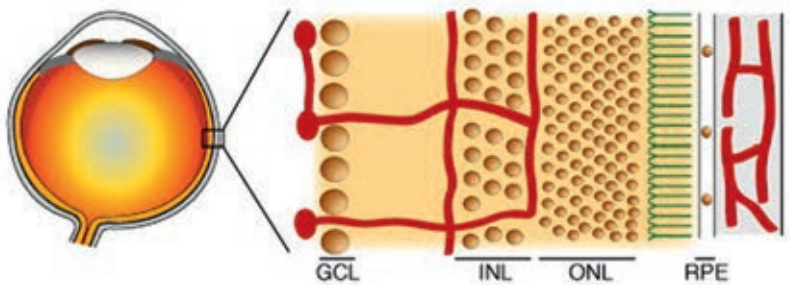

Figure 3. Anatomy of eye vasculature. Left, the human eye in cross-section; right, the anatomy of the retinal and choroidal vasculatures (red). The retinal vasculature spans the GCL and INL; the choroidal vasculature is immediately beyond (to the right of) the RPE. Abbreviations: GCL, ganglion cell layer; INL, inner nuclear layer; ONL, outer nuclear layer; RPE, retinal pigment epithelium. Reprinted with permission from Ye *et al.* (2010) [8].

Blood vessels can be formed by two different mechanisms, namely vasculogenesis and angiogenesis. Vasculogenesis is defined as *de novo* formation of vessels from endothelial precursor cells, whereas angiogenesis is a term describing the development of new vessels from pre-existing vascular network [10]. In humans, the development of retinal vasculature occurs *in utero* by both vasculogenesis and angiogenesis [8, 10, 11]. Initially, the retina develops avascularly and is supplied by the choroidal vasculature as well as the hyaloid vasculature [12]. The hyaloid vasculature is an arterial network in the vitreous which develops from the central hyaloid artery at around 6 weeks of gestation (WG). It runs through the vitreous to the posterior lens and exits through choroidal veins at the front of the eye (Figure 4a) [12, 13]. The hyaloid vasculature starts to regress around 13 WG and simultaneously, a vascular plexus emerges from the optic nerve head by vasculogenesis [10]. This gives rise to the retinal vasculature, which contains both arteries and veins that both enter and exit through the optic nerve (Figure 4b) [12, 13]. Subsequently, the primary plexus undergoes remodeling into three parallel but inter-connected networks, located in the nerve fiber layer and the plexiform layers (Figure 4c) [12]. The development of the retinal vasculature is complete by 38-40 WG, by which time the hyaloid vasculature has fully regressed [13].

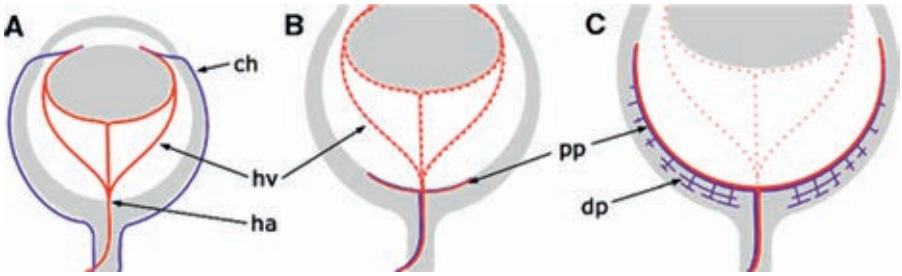

Figure 4. The vascular network inside the eye is remodeled during development. (A) The hyaloid vasculature (hv) is supplied by the hyaloid artery (ha) and drained into the venous, choroidal net (ch) on the outside of the eye (the choroidal net is not shown in B and C). (B) The hyaloid vasculature regresses as the primary plexus (pp) of the retinal vasculature grows into the retina. The primary plexus consists of arteries and veins. (C) The deeper plexus (dp) of the retinal vasculature develops from veins in the primary plexus. Reprinted with permission from Fruttiger (2007) [12].

The angiogenic sprouting of the primary plexus requires differential behavior of endothelial cells, based on their location [13]. Endothelial cells at the leading edge of the vascular network, usually termed "tip cells", are more motile and less proliferative compared to those in the stalk (also called "stalk cells") [14]. Tip cells sense the vascular endothelial growth factor (VEGF) gradient as well as other angiogenic factors and thereby guide the direction of growth. Conversely, the stalk cells proliferate and form the vessel lumen, sustaining sprout extension and perfusion [15, 16]. The two types of endothelial cells also have different transcriptional profiles [17, 18]. The tip-stalk state of endothelial cells are dynamically regulated by Delta like 4 (DLL4)-NOTCH signaling. Tip cells express DLL4, which activates NOTCH1 in adjacent cells where DLL4 transcription is suppressed, thereby inhibiting the tip cell state [19]. A VEGF gradient influences this switch mechanism, by inducing the transcription of DLL4 upon VEGFR2 activation by VEGF, thereby promoting the tip state. Furthermore, Notch1 activation de-sensitizes the stalk cells to VEGF by downregulation of VEGFR2/3 while activating the VEGF antagonist, VEGFR1 [20-22]. Since the VEGF concentration is highest at the leading edge of the growing plexus, the tip-stalk phenotype of endothelial cells is dependent on their location [13]. Such a VEGF gradient is likely to be also present in the retina. Higher VEGF mRNA expression has been observed in the peripheral retina which is not yet vascularized and hypoxic, compared to the central retina where oxygen is supplied by the developing vessels and represses VEGF expression [23]. Additionally, multiple other molecules have been demonstrated to modulate the endothelial tip-stalk state (reviewed in [13]), which creates a balance in the expansion of the primitive plexus.

The primitive plexus is subsequently remodeled into structured, hierarchical vascular trees. This remodeling takes place by vessel regression as well as vessel stabilization. De-stabilizing factors such as lack of perfusion, endothelial cell migration, and apoptosis may eventually lead to vessel regression. Conversely, perfusion, endothelial-mural cell interactions, as well as vessel maturity positively contribute to vessel stabilization [24]. Vessels are highly proliferative at the growing edge of the developing primary plexus, while towards the centre of the retina less proliferation and more remodeling of the generated primitive plexus was observed. Despite the quiescent state of vessels at the remodeling region, they are unstable and either differentiate into more mature vessels or are pruned [13]. Vessel maturation includes differentiation of newly formed vessels into mature types, such as capillaries, arteries, and veins [13]. This process involves the interaction of endothelial cells with mural cells (pericytes and smooth muscle cells) [25].

The deeper plexus of the retinal vasculature sprouts from the primary plexus veins, starting from the center of the retina and expanding towards the periphery (Figure 4c) [26]. It grows along the Müller cells into the retina. Once reaching the INL, it forms two networks in parallel to the primary plexus. Unlike the primary plexus, retinal astrocytes are not involved in the development of the deeper plexus [12]. Furthermore, the cellular and molecular mechanisms of deeper plexus development are also less well studied. Nonetheless, some signaling pathways that are involved in the primary plexus development, also seem to be relevant in the development of the deeper plexus. For example, deletion of genes in the transforming growth factor beta (TGFB) and Norrin signaling pathways, not only hindered the primary plexus development, but also that of the deeper plexus. Additionally, VEGF has been speculated as the molecule guiding angiogenic sprouting towards the outer retina (reviewed in [13]).

The development of retinal vasculature requires cell-cell interactions between the endothelial cells in the developing vessels, retinal astrocytes, as well as retinal ganglion cells [13]. Retinal astrocytes emerge from the optic nerve head towards the retina, where they serve as a template for retinal angiogenesis [27, 28]. Retinal astrocytes are only found in species which have retinal vasculature and are the only astrocyte type in the central nervous system that express platelet derived growth factor receptor alpha (PDGFRA) [29, 30]. RGCs secrete platelet derived

growth factor alpha (PDGFA), which is a ligand of PDGFRA and a mitogen for retinal astrocytes [27]. Retinal astrocytes proliferate and migrate across the retina, establishing a mesh-like network. Since this occurs prior to the development of retinal vasculature, they experience hypoxia and express VEGF, a key inducer of angiogenesis [12]. As the retinal vasculature develops, the astrocytes stop proliferating and differentiate into a more mature phenotype. Molecularly, this is marked by the upregulation of glial fibrillary protein (GFAP) and downregulation of VEGF [23]. Furthermore, retinal astrocytes secrete apelin (APLN) which stimulates leukemia inhibitory factor (LIF) production in endothelial cells, which is an inducer of astrocytes maturation as well as inhibitor of retinal astrocytes proliferation [31, 32]. The close proximity to astrocytes that is required by endothelial cells also suggest that they might have a role in providing physical growth substrate for the vessels [13]. RGCs constitute another cell type that is involved in the retinal angiogenesis, which are crucial in detecting hypoxia in the developing retina. Moreover, they produce semaphorin 3E (SEMA3E) which is anti-angiogenic and thereby prevents misdirection of developing vessels as well as limits the growth of the primary plexus to the nerve fiber layer [33, 34].

1.1.4 Blood-retinal barrier

The blood-ocular barriers are crucial in the maintenance of a suitable environment of optimal visual function by regulating the contents of the inner fluids in the eye, as well as protecting the internal ocular tissues from variations that occur in the circulation [35, 36]. The barriers keep the eye as a privileged site in the human body. There are two main barrier systems, namely the blood-aqueous barrier and the blood-retinal barrier [35, 36]. The blood-aqueous barrier is located in the anterior segment of the eye and is formed by tight junctions in the non-pigmented epithelial cells of the ciliary epithelium, the endothelial cells in the iris vasculature, and the inner wall endothelium of Schlemm's canal [35]. The blood-retinal barrier is located in the posterior segment of the eye and acts similar to the blood-brain barrier. It is a physiological barrier that regulates movement of molecules into and out of the retina, maintaining its appropriate microenvironment. The blood-retinal barrier (BRB) consists of the inner BRB (iBRB) and the outer BRB (oBRB) [36]. The iBRB is composed of tight junctions between adjacent endothelial cells, which are resting on a basal lamina covered by astrocytes and Müller cells. Although pericytes are also present in the basal lamina, they do not form a continuous layer and thereby, are not involved in the diffusional barrier. On the other hand, the

oBRB is formed by tight junctions of the neighboring RPE cells. It is important in gate-keeping exchange of nutrients and waste products between blood and the photoreceptors [36].

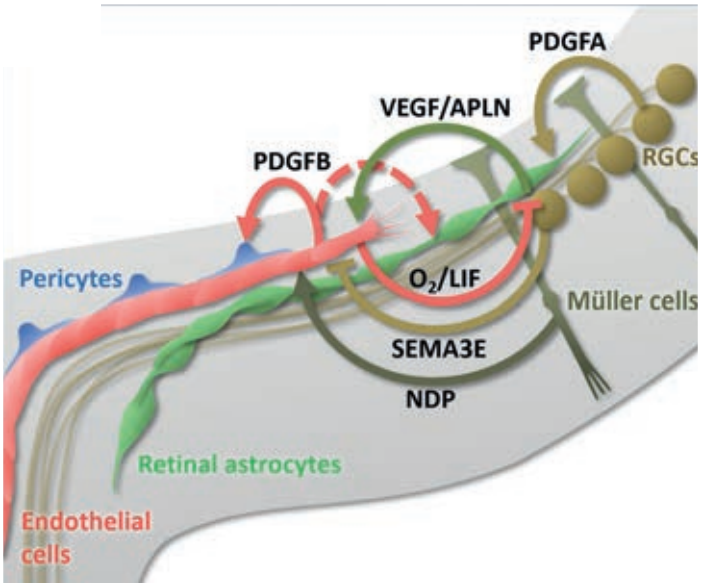

Figure 5. Cell-cell signaling between RGCs, retinal astrocytes and developing vessels controls the development of retinal vasculature. PDGFA released by RGCs acts on astrocytes to promote proliferation and migration. VEGF and APLN produced by retinal astrocytes and VEGF produced by RGCs and other neural cells act on endothelial cells. In reverse, endothelial cells stabilize retinal astrocytes via LIF. Similarly, oxygen provided by the growing vasculature feeds back on VEGF expression from retinal astrocytes and other neural cells. SEMA3E restricts growth of the developing plexus to the nerve fiber layer. Endothelial derived PDGFB has chemo-attractant and mitotic effects on pericytes, but might also influence retinal astrocytes (stippled arrow). Reprinted with permission from Selvam *et al.* (2018) [13].

1.2 Familial exudative vitreoretinopathy

Familial exudative vitreoretinopathy (FEVR) was first described by Criswick and Schepens in 1969 [37]. It is an inherited retinal disorder, which is characterized by an abnormal vascularization in the peripheral retina. An avascular peripheral retina is observed in most FEVR patients. However, the clinical features and visual function of FEVR patients may be asymmetric and highly variable. In mild cases, the aberrant vasculature in the peripheral retina does not cause any symptoms. Neovascularization and fibrosis at the junction between the vascular and avascular retina may occur in the moderate to severe cases, which causes traction of the

macula and retinal vessels, thereby leading to varying degrees of macular ectopia and visual dysfunction. This traction, however, may also lead to retinal folds and detachment in severe cases that result in very poor vision in the most severe cases. FEVR can be diagnosed in an individual at any age, if there is evidence of avascularity in the peripheral retina in one or both eyes. These ocular features are overlapping with those observed in retinopathy of prematurity (ROP) cases, in which the clinical signs are due to incomplete retinal vascularization after premature birth and hyperoxia (in comparison to in *utero*) experienced during neonatal care. Therefore, it is important that a person diagnosed with FEVR is born at full term [38].

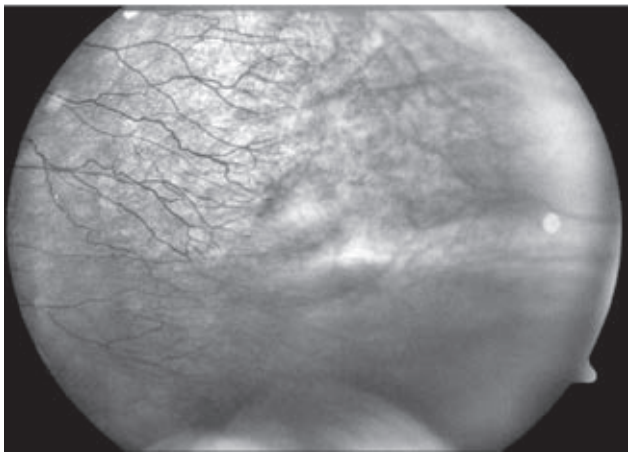

Figure 6. Fundus photograph showing part of the avascular periphery of an FEVR patient. This picture shows temporal periphery of the left fundus of the patient. The retinal vasculature (at the left side) ends in small aberrant ramifications in the equatorial area of the fundus. The peripheral retina (at the right side) is avascular, only choroidal vessels are present in this area. Reprinted with permission from Nikopoulos *et al.* (2010) [39].

Next to its heterogeneous clinical manifestations, FEVR is also genetically heterogeneous. It can be inherited in an autosomal dominant, autosomal recessive or X-linked manner. Mutations in several genes have been associated with FEVR, such as *NDP* [40], *FZD4* [41, 42], *LRP5* [42, 43], *TSPAN12* [39, 44], *ZNF408* [45], *CTNNB1* [46, 47], *RCBTB1* [48], and *ATOH7*. Four of these genes (*NDP*, *FZD4*, *LRP5*, and *TSPAN12*) are most commonly mutated in FEVR patients and are also the most well-studied FEVR-associated genes. The proteins encoded by these genes are involved in the Norrin signaling pathway. In this pathway, FZD4 and LRP5 act as receptor and co-receptor for Norrin, the protein encoded by *NDP*. TSPAN12

is required for the multimerization of FZD4-LRP5 complex and is exclusively involved in Norrin signaling. Binding of Norrin to its receptor complex, activates this signaling pathway. This leads to the translocation of β-catenin, the protein encoded by *CTNNB1*, to the nucleus where it subsequently activates the expression of its downstream genes [49]. Knock-out of *Ndp*, *Fzd4*, *Lrp5*, and *Tspan12* in mice resulted in retinal vasculature defects, including the absence of two intraretinal capillaries that flank the INL, abnormal primary arteries and veins, as well as a delayed regression of hyaloid vessels (reviewed in [8]). Moreover, conditional knockout mice showed that the depletion of β-catenin in endothelial cells resulted in defective angiogenesis in the complete central nervous system including the retina [50, 51].

Defects in the aforementioned genes may also results in other clinical features, which may or may not overlap with the features of FEVR. Mutations in *LRP5* can result in FEVR-like features accompanied by bone abnormalities, a syndrome termed osteoporosis pseudoglioma [52]. Norrie disease, which is due to mutations in *NDP*, is a severe X-linked syndrome with ocular features overlapping with those of FEVR as well as developmental delay and hearing impairment [40, 53]. Besides FEVR, *RCBTB1* mutations have been associated with Coats disease, a sporadic, unilateral retinal vasculopathy, and retinitis pigmentosa, an inherited retinal disease hallmarked by photoreceptor degeneration [48, 54]. Biallelic mutations in *ZNF408* have also been implicated in autosomal recessive retinitis pigmentosa [55]. Finally, FEVR features have been described to be accompanied by microcephaly, a condition associated with mutations in *KIF11* [56].

FEVR belongs to a spectrum of disease with overlapping clinical features. These diseases, termed vitreoretinopathies, are mainly characterized by defects of the vitreous and the retina accompanied by typical features that specify the different diseases. Other clinical features may also be observed next to the ocular features in the syndromic form of these diseases, some of which have been discussed earlier in this section. The diseases that belong to the vitreoretinopathy spectrum are listed in Table 1.

Table 1 Clinical characteristics and known causative genes for vitreoretinopathies. Summarized from [57, 58]

Disease name	Main clinical characteristics	Genes
FEVR	Avascular peripheral retina, retinal neovascularization, fibrosis, retinal traction and detachment	*NDP, FZD4, LRP5, TSPAN12, ZNF408, RCBTB1, CTNNB1, ATOH7*
Snowflake vitreoretinal degeneration	Early onset cataract, vitreoretinal dystrophy, fibrillal degeneration of the vitreous, shiny crystalline-like deposits resembling snowflakes, retinal detachment	*KCNJ13*
Enhanced S cone syndrome, Goldmann-Favre syndrome (severe form)	Retinal degeneration, enhanced response of S cones. Severe manifestations constitute vitreoretinal degeneration and cataract	*NR2E3*
Autosomal dominant vitreoretinochoroidopathy	Hyperpigmented cells at the peripheral retina with white opacities, breakdown of blood-retinal barrier with retinal neovascularization, presenile cataract, and choroidal atrophy	*VMD2*
Wagner syndrome/ Erosive vitreoretinopathy	Syneresis of the vitreous, cataract, high myopia, night blindness, and retinal detachment	*VCAN*
Osteoporosis pseudoglioma	Osteoporosis, FEVR-like ocular features	*LRP5*
Norrie disease	Mental retardation, hearing impairment, intraocular mass in the retina, FEVR-like ocular features	*NDP*
Stickler syndrome	Mid-face hypoplasia, small chin, cleft palate, hearing impairment, vitreous abnormalities, cataract, retinal detachment	*COL2A1, COL11A1, COL11A2, COL9A1*

A range of disease severity within an individual or within families has been observed in FEVR. Relatives of patients presenting severe FEVR may have mild to asymptomatic symptoms, although they have the same mutation. This suggests incomplete penetrance of the associated mutation [38, 49, 59]. Such a reduced penetrance is observed in ~25% of mutation carriers in FEVR [45, 59]. Non-penetrance itself is defined as a state in which a particular genetic trait fails to manifest itself in the phenotype. The penetrance of a mutation can be influenced by many factors, among others epigenetic modification, allele dosage, modifier genes, copy number variants, gene expression level, and environmental factors [60].

1.3 Animal models for retinal vasculature diseases

As described above, abnormal ocular vasculature development can underlie a broad spectrum of eye disorders. Over the last decades, numerous animal models have been generated to mimic these diseases with defective retinal, choroidal, or corneal angiogenesis. Studies employing these animal models not only broaden

our insight on the basic mechanisms of angiogenesis, but also shed light in the understanding of disease pathology. Various methods have been employed to generate these models, such as oxygen level manipulation, laser treatment, surgical treatment, as well as genetic modification. Besides, multiple species have been used to model ocular angiogenesis, such as feline, canine, rat, mouse, and zebrafish (reviewed in [61]). In this chapter, mouse and zebrafish models of retinal angiogenesis will be discussed in more detail.

1.3.1 Mouse models

Mice are the most commonly used animals to model both development and disease. The procedures of creating transgenic strains as well as the characterization of the generated animals are well established, thanks to the extensive availability of recombinant proteins and antibodies that are compatible with mice [62]. Although mice as well as other rodents are nocturnal and therefore their eye and retinal architecture differs from that of human [63], the postnatal development of retinal vasculature in mice facilitated the investigation of retinal angiogenesis in development and disease. For instance, the pruning of hyaloid vessels as well as the parallel development of the intraretinal vasculature that occurs postnatally in mice has allowed the study of mechanisms underlying these processes [61, 62].

The time course of normal retinal vasculature development in wild-type mice varies between different strains, usually with a few days difference. As an approximation, in C57BL/6 mice, the superficial vascular plexus grows from the optic nerve into the periphery during the first week after birth. It starts sprouting to form the deep and intermediate vascular plexus from postnatal day 7 (P7) onwards. The deep plexus in the OPL reaches the retinal periphery at approximately P12, while the intermediate plexus in the IPL does so between P12 and P15. All three vascular layers are fully mature by the end of the third postnatal week (Figure 7) [62].

One of the most popular mouse models to study retinal angiogenesis is the oxygen-induced retinopathy (OIR) model. This model is mainly used to mimic the pathological mechanisms present in patients with ROP or diabetic retinopathy. Abnormal retinal angiogenesis is the hallmark of both diseases, in which abnormal retinal avascularity is followed by aberrant neovascularization. Diabetes is associated with these clinical features in DR, whereas in ROP cases, these are associated with incomplete retinal vascularization after premature birth

followed by hyperoxia during neonatal care (compared to *in utero* condition). To generate OIR models, neonatal mice are exposed to 75% oxygen from P7 to P12, which leads to vaso-obliteration that mimics the initial phase of ROP. Normoxic conditions are applied from P12 onwards for 5 days, leading to uncontrolled compensatory pathologic neovascularization resembling human proliferative retinopathies. It reaches its maximum at P17, which is a usual end point of this mouse model. Afterwards, the abnormal vascularization gradually regresses and disappears by P25 [64].

Mouse models mimicking pathologic neovascularization have also been generated by genetic modification. For example, *vldlr*$^{-/-}$ mice, which were generated by targeted disruption, showed subretinal neovascularization as well as choroidal anastomosis [65, 66]. Another example is the *rho/VEGF* mice, in which full-length cDNA of human VEGF is put under a bovine *rho* promoter to overexpress VEGF in the photoreceptor cells. This model showed intraretinal and subretinal neovascularization with vascular leakage as well as substantial photoreceptor degeneration [67, 68]. Both models are mainly used to investigate retinal angiomatous proliferation, a variant of neovascular age-related macular degeneration [61].

Mice with deficient retinal angiogenesis such as that observed in FEVR and Norrie disease have also been generated, such as the knock-out mice models of the four genes that are most frequently mutated in FEVR, namely *Fzd4*$^{-/-}$, *Lrp5*$^{-/-}$, *Tspan12*$^{-/-}$, and *Ndp*$^{-/-}$. Loss of function of each of these genes showed comparable phenotypes [69-73]. These mice usually lack two intraretinal capillary beds flanking the INL and the sprouting that gives rise to these vessels are also stunted. Persistent hyaloid vasculature was also observed in these mice [69-73]. Moreover, the defective inner retina vascularization leads to hypoxia, which in turn upregulates VEGF and subsequently, compensatory vascularization [74].

1.3.2 Zebrafish models

In recent years, zebrafish have become more and more popular as a model organism to study vertebrate development as well as disease modeling. Zebrafish are easy to maintain and also breed in large quantities in a short time with relatively low costs. The transparent embryo facilitates visualization during development. Furthermore, 70% of human genes as well as 84% of known human disease-associated genes have a zebrafish orthologue. These, together with the possibilities

for genetic manipulation, render zebrafish a suitable model organism for human inherited diseases [75].

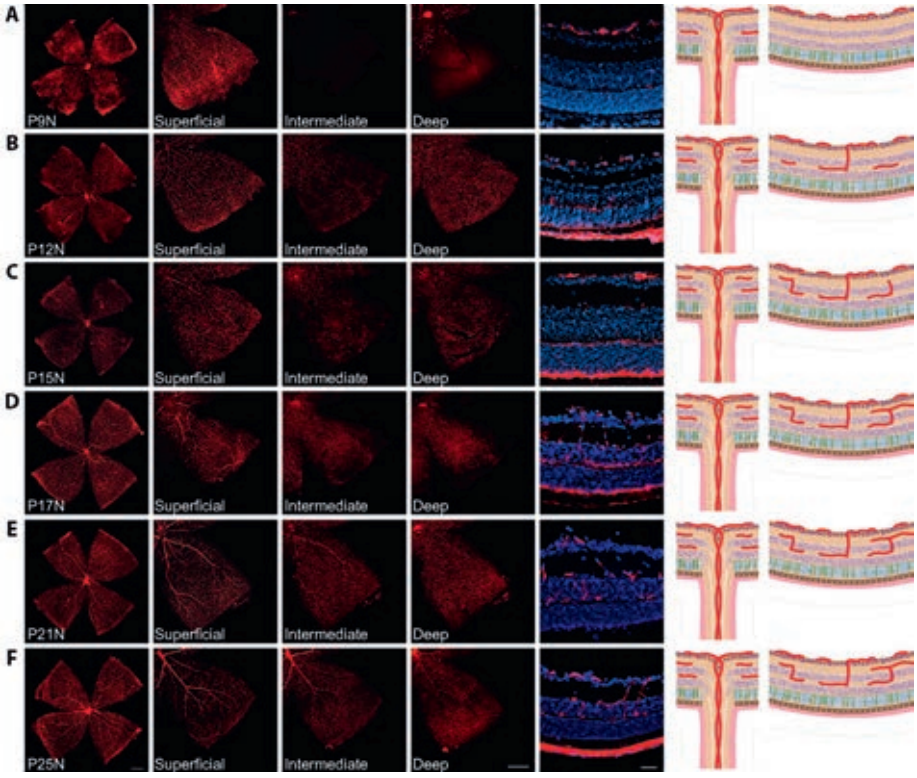

Figure 7. Development of the deep and intermediate vascular plexus in C57BL/6 mouse retinas. Retinal whole mounts and cross sections from postnatal day (P)9 to P25 were stained for endothelial cells with isolectin B4-Alexa 594 (red) and for cell nuclei with DAPI (blue). N (normoxia) signifies normal development. (A) At P9N, the superficial plexus has fully extended to the peripheral retina. The deep vascular plexus begins forming centrally from vertical vessels diving down from the superficial plexus. The intermediate vascular plexus has not begun to form yet. On cross section, the three neuronal layers of the retina and the superficial vascular plexus can be identified. Representative drawings on the right illustrate both superficial and deep vascular plexus in the immediate vicinity of the optic nerve, whereas in the periphery the superficial plexus remains the only vascular network. (B) At P12N, the intermediate vascular plexus becomes visible on retinal whole mounts. The deep vascular plexus is nearly fully developed. On cross section, vertical sprouting of vessels toward the intermediate plexus can be observed. Representative drawings illustrate the beginning of a three-layered vascular plexus around the optic nerve and superficial and deep vascular plexus with interconnecting vessels in the periphery. (C) At P15N, the intermediate vascular plexus continues to develop throughout the retina as illustrated both on retinal whole mounts and cross sections. Representative drawings illustrate complete formation of superficial and deep plexus with continued development of the intermediate vascular plexus in the periphery. (D) At P17N, the superficial, intermediate, and deep plexus can be seen both centrally and in the peripheral retina. Cross sections and representative drawings illustrate the three-layered vascular system in all parts of the retina along with multiple interconnecting vessels. (E, F) Between P21N and P25N, further maturation of especially the intermediate plexus can be observed. Cross sections and representative drawings illustrate the mature retinal vasculature. Note that isolectin B4 binds to choroidal vessels as well as nonspecifically to RPE and the scleral wall in some of the cross sections (A-F). Reprinted with permission from Stahl *et al.* (2010) [62].

Vision disorders are among the wide variety of human diseases that have been modeled in zebrafish [75]. One might wonder how similar a human eye is to the zebrafish eye. The visual system of zebrafish is principally comparable to that of humans. Structurally, zebrafish and human eyes differ in the shape of the lens as well as the space between the lens and the retina [76]. The retina of zebrafish also contains five layers (ONL, OPL, INL, IPL, and GCL), similar to the human retina (Figure 8). Since zebrafish are diurnal species, they possess cone-rich retinas with a cone density close to humans. However, a macula is absent in the zebrafish retina [75, 76].

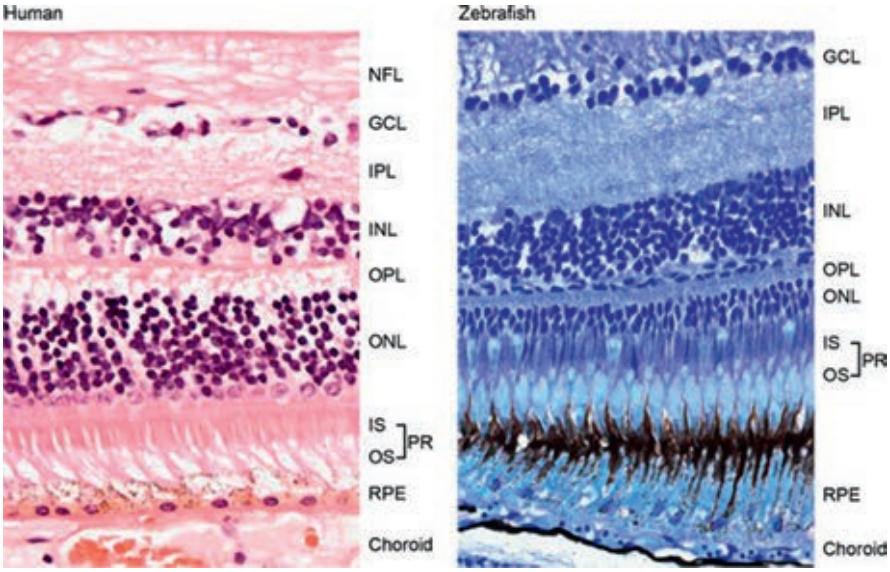

Figure 8. Cross-sectional histology of the human and zebrafish retina demonstrating similarities in the arrangement of cells and structural features that define the distinct retinal layers. RPE, pigmented epithelium; IS, inner segment; OS, outer segment; PR, photoreceptor; ONL, outer nuclear layer; OPL, outer plexiform layer; INL, inner nuclear layer; GCL, ganglion cell layer; and NFL, nerve fibre layer. Reprinted with permission from Richardson *et al.* (2016) [75].

Similar to humans, hyaloid vasculature is also present in zebrafish. The hyaloid artery originates from the optic fissure at 18-20 hours post fertilization (hpf), after which it grows and branches to surround the medial part of the lens at around 48 hpf. In parallel, another vasculature system develops at the surface of the eye, which is termed the superficial system. It is connected to the hyaloid vein and leads the formation of choroidal vessels [77]. The superficial system consists of three major

vessels which are interconnected by a ring-shaped vessel. The three major vessels are the nasal radial vessel (NRV), the dorsal radial vessel (DRV), and the ventral radial vessel (VRV) (Figure 9). Blood enters through the NRV and exits through the DRV and VRV [78]. At 5 days post fertilization (dpf), the hyaloid vasculature completely embraces the lens and continues branching forming a complex network. Unlike hyaloid vasculature regression that is observed in humans, the hyaloid vasculature starts loosening its contact with the lens and simultaneously, becomes more attached to the retina from approximately 15 dpf onwards. The zebrafish retina shows an elaborate vasculature network similar to adults at 60 dpf and maintains the morphology to 18 months. Around 18-20 months, the retinal vessels progressively degenerate, consistent with an age-related loss of retinal vasculature function (Figure 10). Of note, zebrafish lack intraretinal plexus which is present in human and other mammals, possibly because the surface retinal and choroidal vasculature are sufficient to supply the thinner zebrafish retina [79].

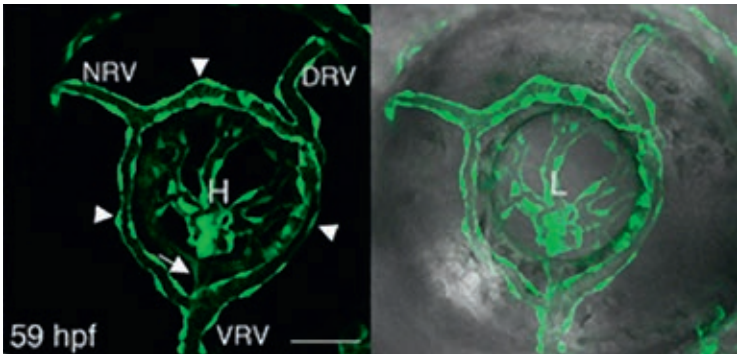

Figure 9. The hyaloid and superficial system vasculature of zebrafish. On the left side, a projection of confocal z-stacks showing ocular vessels in *Tg(kdrl:EGFP)* live embryos at 59 hpf are shown and on the right side, the same confocal image is combined with a bright field image showing the position of vessel relative to the eye. Arrows point at the hyaloid vein and arrowheads at the ring-shaped vessel where the three major superficial system vessels are interconnected. H: hyaloid, NRV: nasal radial vessel, DRV: dorsal radial vessel, and VRV: ventral radial vessel, L: lens. Both images are lateral views, anterior to the left, dorsal up. Scale bar is 50 µm. Adapted with permission from Kaufman *et al.* (2015) [77].

Zebrafish have been used extensively to model multiple ocular disorders, including ocular coloboma, microphthalmia/anophthalmia, cyclopia, corneal dystrophies, cataract, retinal and RPE abnormalities, as well as vasculature defects (reviewed in [75]). The availability of transgenic zebrafish with fluorescent reporters on the blood vessels, such as *Tg(fli1:EGFP)* line [80] and *Tg(flk1:GFP)* line [81], facilitates *in vivo* investigation of vasculature-related ocular disease. For instance,

vhl$^{-/-}$ zebrafish showed an aberrant vasculature development in the brain, eye, and trunk, as observed in von Hippel-Lindau (VHL) syndrome. Moreover, hyaloid and choroid neovascularization together with the vascular leakage and retinal detachment that is also observed in *vhl*$^{-/-}$ zebrafish, is similar to those observed in proliferative diabetic retinopathy and age-related macular degeneration [82]. Gene expression alteration by antisense oligonucleotides such as morpholinos has also been used to study vasculature-related ocular disease. For example, morpholino-induced knockdown of *znf408*, a gene mutated in FEVR, resulted in aberrant development eye and trunk vasculature [45]. In addition, hypoxia treatment on adult zebrafish has been used to mimic adult retinopathy. After 3-10 days of hypoxia treatment, retinal neovascularization was observed in the adult zebrafish [83]. Lastly, zebrafish have also been used in small molecule screening for compounds that affect vascular development in the zebrafish retina [78].

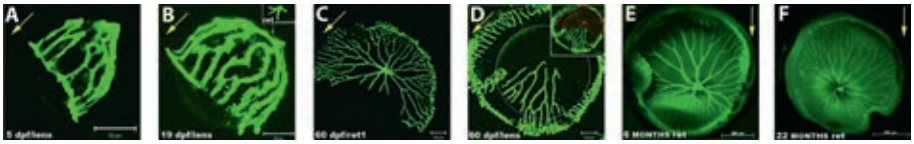

Figure 10. Dynamic development of the hyaloid and retinal vasculature in zebrafish. Shown are fluorescent images of blood vessels on lenses and wholemount retinas dissected from *Tg(fli1:EGFP)* zebrafish. A) At 5 dpf the vasculature covers the lens from the optic disk to the inner optic circle. B) At 19 dpf an intricate network of hyaloid vessels branches around the lens. Some vessels at the posterior lens have lost contact and are attached to the retina (inset). C) Retina and D) lens from a 60 dpf zebrafish. In this specimen some vessels are attached to the lens although most of them are found on the retina. Inset in D: Overlay of the retina from pseudo-colored in red, and the lens from D depicts the complementing network of vessels. E) Typical vascular pattern of intraocular vasculature in a 6 month old fish. F) Inner retina of a 22 month old senescent zebrafish showing slightly thinner and more fragile vessels. White circumferences demarcate the lens in A-D. Yellow arrows point from the posterior to the anterior lens in A, B, and D and from the dorsal to the ventral retina in C, E, and F. Scale bars: 50 μm in A and B; 100 μm in C and D; and 500 μm in E and F. Adapted with permission from Alvarez *et al.* (2007) [79].

1.4 Cellular models for vasculature-related diseases

Besides animal models, endothelial cells are mainly used as an *in vitro* model in vasculature-related research. These cells form a monolayer that line the vascular lumen and are involved in various physiological processes of the vasculature, such as control of permeability, angiogenesis, coagulation, and inflammation [84]. Primary endothelial cells have been isolated from various species, including bovine, canine, porcine, murine, and human. Endothelial cells have also been

isolated from various locations, such as the dermis for microvessels as well as the umbilical vein, jugular vein, and aorta for large vessels [85]. Endothelial cells are a heterogeneous population, that has differences in expression patterns across developmental stage, vascular classes (i.e. capillary, artery, venous), and tissue types [86].

Human umbilical vein endothelial cells (HUVEC) are the most commonly used primary endothelial cells in vascular biology research. The second most popular are human dermal microvascular endothelial cells (HDMEC). Both cell types are widely used, since they are relatively easy to isolate and culture [85]. Although the use of primary cells gives the advantage of having the most similar characteristics as compared to an *in vivo* situation, the primary cells have a limited life-span which may complicate their application in long-term experiments. Many studies have attempted to generate endothelial cells with prolonged life-span or even immortalized endothelial cell lines (reviewed in [84]). However, these cells are often developed using malignant factors, for instance SV40 large antigen or telomerase. Such procedures may alter the genetic and epigenetic properties of the cells and thereby, the immortalized cell lines may be less representative of the *in vivo* situation. The results obtained with such cell lines should thus be confirmed using primary cells [84].

In recent years, multiple methods have been employed to generate endothelial cells from pluripotent stem cells [87, 88]. The term 'pluripotent stem cells' describes any undifferentiated cells that have the ability to differentiate to any cell type of the body, excluding extra embryonic tissue. Pluripotent stem cells can be of embryonic origin, such as human embryonic stem cells (hESCs), or reprogrammed from somatic cells, which are termed induced pluripotent stem cells (iPSCs). Somatic cells are reprogrammed into iPSCs using a cocktail of reprograming factors (Oct3/4, Klf4, Sox2, c-Myc), originally described by Yamanaka *et al.* [89]. Various compositions of this cocktail as well as the delivery methods have been developed since the original finding. Many cell types have been successfully reprogrammed into iPSCs, but dermal fibroblasts remain the most commonly used cell type [90]. The possibility to obtain iPSCs from patients and differentiate them into relevant cell type has benefited many disease investigations. It is applicable to studies in which it is challenging to obtain the disease-relevant cell type. Patient-derived iPSCs also present the advantage that they represent the genetic background of

the patient without the need of any manipulation. It is especially advantageous in research requiring cell types for which genetic modification is challenging, for instance, endothelial cells.

iPSC cultures on OP9 feeder cell layer as well as embryoid body formation have been employed in the initial attempts to differentiate iPSCs into endothelial cells. Nowadays, monolayer differentiation employing defined factors directing iPSCs differentiation to mesoderm and subsequently endothelial lineage is the most popular technique. The differentiation efficiency is improved using this method, compared to previous attempts. BMP4, Activin A/Nodal, FGF2, and GSK3β inhibitors or WNT ligands are usually used to induce differentiation towards mesoderm layer, while VEGF and endothelial promoting culture conditions are employed to further direct the differentiation into endothelial cells. The generated cells can be further selected for those expressing endothelial cell surface marker(s) by flow cytometry or immunomagnetic separation, to increase the purity of the generated endothelial cell population. As mentioned previously, endothelial cells represent a heterogeneous population and therefore, methods to further specify iPSC-derived endothelial cells are currently being investigated. Nonetheless, the existence of robust protocols to differentiate human iPSCs into endothelial cells not only provides tools to study disease mechanisms, but also pave the way for cell-therapy of vascular-related diseases [88].

Next to its typical cobble-stone morphology (Figure 11), endothelial cells possess other distinctive *in vitro* characteristics. Endothelial cells isolated from donor (primary endothelial cells) as well as stem cell-derived endothelial cells need to be tested for these characteristics. Immunostaining is often used to check for the expression of endothelial cell surface markers, such as CD31 (Figure 11), CD144 (VE-cadherin), VEGFR2 (KDR) and von Willebrand factor (vWF). Furthermore, endothelial cells are also often tested for their *in vitro* behaviors, which include tube formation on a 3D matrix (Figure 10), uptake of acetylated-LDL (Figure 11), migration in response to VEGF, as well as secretion of certain pro-angiogenic growth factors and cytokines [88].

Lastly, the increasing availability of *in vitro* models of endothelial cells as well as other cells supporting the vasculature, such as pericytes and vascular smooth muscle cells, allowed the development of an *in vitro* physiological model of

vasculature using organ-on-a-chip technology. It allows the investigation of vessel development in the presence of fluid flow as well as supporting cells (e.g. pericytes) in co-culture. Such a system mimics the *in vivo* situation more closely than the 2D culture system and has been applied in multiple vascular investigations. For instance, it has been used in research on endothelial cell barrier functions; regulation of blood flow, hemostasis and thrombosis, as well as vasculogenesis and angiogenesis [87].

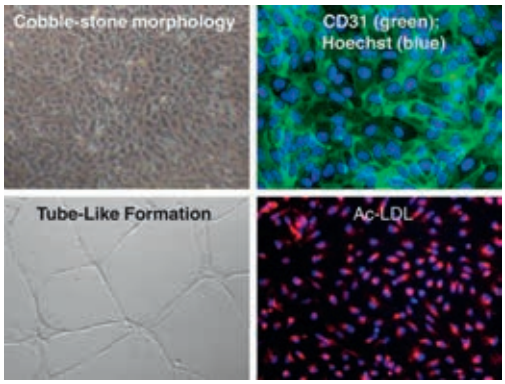

Figure 11. Endothelial cell characteristics. Endothelial cells have a characteristic endothelial cell cobblestone morphology, express the endothelial marker CD31, form tube-like structures in Matrigel and incorporate acetylated low-density lipoprotein (ac-LDL). Reprinted with permission from Wong *et al.* (2012) [91].

1.5 Technologies to unravel molecular mechanisms of disease

1.5.1 Genetic defect identification

The first step in studying the mechanisms underlying an inherited disease is to determine the genetic defect causing this disease. Linkage analysis is a popular way to map Mendelian traits with familial segregation. This approach employs genetic markers to identify regions in the genome that are associated with a disease. Even now, in the advanced sequencing era, linkage analysis is still utilized to narrow down the disease locus, thereby reducing the number of variants to follow-up [92].

Sanger sequencing was the gold-standard in finding the genetic defect underlying Mendelian disorders. It allows very low rates of false-positive results and is also

very specific. However, it only allows sequencing of a (fraction of) gene in each reaction, rendering the process extremely expensive and time consuming. Recent advances in sequencing technologies, particularly massive parallel sequencing, often termed next-generation sequencing (NGS), provide possibilities to screen a handful of genes in a single reaction or even to examine the whole genome of an individual.

A targeted approach can be used to investigate the genetic cause of diseases for which there is a strong causative association with a gene or multiple genes. The use of NGS technology provides information of how many molecules have been sequenced (also termed number of reads), which allows one to determine the precise percentage of the detected variant. It provides high sensitivity, especially in a single gene approach, allowing the detection of low-grade mosaicisms (i.e. a genetic defect that is only present in some cells of an individual) which often is not detected by Sanger sequencing. The possibility to sequence a panel of genes in a single step provides efficient and rapid identification of genetic defects in a genetically heterogenous disorder [93].

Hypothesis-free approaches, such as whole exome sequencing (WES) and whole genome sequencing (WGS), are applied in investigating the genetic cause of diseases for which there is no clear causative gene(s) as well as in finding novel causative genes. In WES, all protein coding regions (~1% of human genome) are analysed, whereas WGS targets the whole human genome. WES has been successfully applied to identify genetic cause in multiple diseases. It is particularly useful in highly heterogeneous diseases for which there are a large number of candidate genes. The technological development and a continuous decrease in sequencing costs have allowed more and more application of WGS, especially in finding genetic variant(s) that are not located in the coding regions. Nonetheless, both WES and WGS generate vast amounts of data which are often challenging in terms of storage as well as analysis and interpretation. Furthermore, one should note that these techniques may generate incidental findings, such as pathogenic or possibly pathogenic variant(s), that are not relevant to the clinical features for which the analysis was initially performed [93, 94].

1.5.2 Characterization of gene expression regulation

the advances in sequencing technologies not only revolutionized the identification of genetic variants, but also enabled the study of different aspects of gene regulation at a genome-wide level. Various high-throughput techniques have been applied on different cell types and tissues to gain insight in the gene regulation networks. Two techniques that are relevant for the scope of this thesis will be discussed here.

Chromatin immunoprecipitation followed by high-throughput sequencing (ChIP-Seq) is a technique utilized to identify DNA binding sequences of transcription factors as well as histone modifications. In a ChIP experiment, proteins are crosslinked to DNA by formaldehyde treatment, followed by chromatin shearing by means of sonication. Subsequently, an antibody specific to the protein of interest is used to precipitate the DNA-protein complex after which the crosslinks are reversed to allow analysis of the DNA sequences bound to the protein of interest by high-throughput sequencing. Subsequent analysis of the obtained sequence then allows one to determine the genome-wide distribution of histone modifications or transcription factors investigated in the study [95, 96].

The identification of DNA binding sequences of a transcription factor or histone modification does not provide information of its impact to gene expression. Therefore, such experiments should be complemented with gene expression measurements at the RNA level to gain further knowledge in gene expression regulation, especially in determining the function of a transcription factor or histone modification [97]. High-throughput RNA sequencing (RNA-Seq) enables the identification and quantification of genome-wide gene expression in a given cell type/tissue under certain conditions. RNA isolated from the sample of interest is fragmented and reverse-transcribed into complementary DNA (cDNA). Subsequently, cDNA is amplified and subjected to high-throughput sequencing. The obtained sequences can be mapped to reference transcriptome or used in *de novo* transcript assembly prior to subsequent analysis such as differential expression analysis, splicing analysis, etc [94].

1.5.3 Generation of animal models by genetic modification

The animal models used to study genetic diseases, such as inherited retinal diseases, may develop their phenotype as the result of a naturally occurring mutation or due to genetic modification. Both forward and reverse genetic screens have been

used to generate animal models. In forward genetic screens, lots of different loci are mutated simultaneously, allowing the generation of many different mutant animals. The mutation can be introduced by using mutagenic chemicals (e.g. N-Ethyl-N-nitrosourea (ENU)) or by viral-mediated DNA insertion. However, due to the high number of animals to be screened, this method may be costly and labor intensive. Conversely, in reverse genetic screens, specific modifications can be introduced to a region of interest. Homologous recombination is one of the methods used to introduce specific modification. DNA double-strand breaks have been induced using nucleases, such as zinc finger nuclease (ZFN) or transcription activator-like effector nucleases (TALENs). Following cleavage, cellular non-homologous end-joining (NHEJ) repair mechanisms will join the DNA ends, a process in which insertion and/or deletions may be introduced. If a donor template DNA is provided, the repair mechanisms can also be directed towards homologous recombination (reviewed in [98]).

In the last few years, a new tool that uses similar principles as ZFN and TALENs, but with higher efficiency, has become available. Clustered regulatory interspaced short palindromic repeat (CRISPR)-associated protein 9 (Cas9) originates from bacteria, specifically *Streptococcus pyogenes*. A short RNA sequence (guide RNA/gRNA) guides Cas9 to the target sequence, where it induces DNA double-strand breaks. Similar to ZFN and TALENs systems, both NHEJ and homology-directed repair (HDR) can be used to repair the cleavage [99]. Following its original application to cut DNA at various sites *in vitro* in 2012 [100], this system has been applied in genetic modification of a variety of cell types and organisms [99].

1.6 ZNF408 - What do we know about it?

In the following chapters in this thesis, the topic will mainly be around a single gene, *ZNF408*. Initially, a mutation (p.His455Tyr) in *ZNF408* was reported in an autosomal dominant FEVR family by Collin *et al.* (2013) [45]. *ZNF408* is ubiquitously expressed with highest expression in the retina. Subcellular localization showed that wild-type ZNF408 resides in the nucleus, whereas the p.His455Tyr mutant ZNF408 is mislocalized in the cytoplasm. Co-transfection of wild-type and mutant ZNF408 resulted in mislocalization to the cytoplasm, suggesting a dominant negative mode of action. Morpholino-induced knockdown of *znf408*

in zebrafish led to abnormal development of eye and trunk vasculature [45]. Following these findings, several other groups also reported *ZNF408* mutations in FEVR [101-104]. Intriguingly, mutations in *ZNF408* have also been identified in patients with retinitis pigmentosa, an inherited retinal disorder which is caused by photoreceptor degeneration [55, 105, 106]. Immunostaining showed that ZNF408 is expressed in the retinal vasculature as well as the photoreceptor layer of human retina [55]. *ZNF408* mutations reported in both FEVR and retinitis pigmentosa are spread throughout the gene without a clear correlation between the positions of the mutation with the resulting phenotype. How different mutations in *ZNF408* result in different clinical features is currently unclear.

ZNF408 has five exons and the encoded protein belongs to the PRDM (positive regulatory domain I-binding factor 1/PRDI-BF1 and retinoblastoma-interacting zinc finger protein 1/RIZ1 homology domain containing) family. Members of this family have been described to be highly cell-type and tissue-specific transcriptional regulators using either enzymatic activity towards histones or by recruitment of interaction partners to modify the expression of target genes. This protein family is characterized by an N-terminal PR domain and multiple zinc finger domains. The PR domain is a subfamily of SET methyltransferase, although enzymatic activity was only found in a few PRDM proteins [107, 108]. Zinc finger domains refer to a small peptide domain whose secondary structure is stabilized by a zinc ion bound to the cysteine and histidine residues of the finger. Such a domain is generally known to be involved in DNA binding, although RNA and protein binding have also been described [109, 110]. ZNF408 is predicted to have 10 zinc finger domains, each of which consists of two histidine and two cysteine residues [45].

Although the findings so far suggest an involvement of ZNF408 in the development of retinal vasculature as well as in photoreceptor degeneration, its molecular role is currently unknown. As a member of the PRDM family, it potentially acts as a transcriptional regulator in those processes. Investigation of the molecular role of ZNF408, particularly in the development of retinal vasculature as well as the pathogenesis of FEVR, will be described in the following chapters of this thesis.

1.7 Aim of the thesis

The main aim of this thesis is to elucidate the role of *ZNF408* in the regulation of (retinal) vasculature development. Both *in vitro* and *in vivo* models were used to study the function of ZNF408 and how its defect leads to FEVR.

Chapter 1 provides the background information on the retina structure, development of retinal vasculature, the clinical and genetic features of FEVR as well as relevant models and technologies.

Chapter 2 presents an *in vitro* study on the role of ZNF408 in regulating gene expression and how the p.His455Tyr mutation affects its function. Transcriptome profiling showed that ZNF408 regulates the expression of genes relevant to the development of vasculature, which are altered by the mutation.

Chapter 3 describes the generation of zebrafish models of *ZNF408*. A knock-in model mimicking the mutation in FEVR patients as well as knock-out models were generated using CRISPR-Cas9 technology. The zebrafish models showed abnormal development of retinal vasculature, mimicking the clinical features of FEVR.

Chapter 4 presents a preliminary study of the reduced penetrance of *ZNF408*--associated FEVR. Fibroblasts, derived from an FEVR patient and an unaffected mutation carrier, were reprogrammed into iPSCs and subsequently differentiated into endothelial cells. The pilot study showed the possibility to generate patient-specific endothelial cells to study reduced penetrance in FEVR.

Chapter 5 reports the finding of a novel *KIF11* mutation in a patient presenting FEVR and microcephaly. Deep sequencing revealed that the mutation is inherited from the mother who is mosaic for the mutation.

Chapter 6 and 7 provide the general discussion and summary.

References

1. Forrester, J.V., et al., *Chapter 1 - Anatomy of the eye and orbit*, in *The Eye (Fourth Edition)*. 2016, W.B. Saunders. p. 1-102.e2.
2. E, W.C., et al., *Anatomy and physiology of the human eye: effects of mucopolysaccharidoses disease on structure and function – a review.* Clinical & Experimental Ophthalmology, 2010. **38**(s1): p. 2-11.
3. Singh, R., et al., *Pluripotent Stem Cells for Retinal Tissue Engineering: Current Status and Future Prospects.* Stem Cell Rev, 2018. **14**(4): p. 463-483.
4. Purves D, A.G., Fitzpatrick D, et al., editors, *Anatomical Distribution of Rods and Cones*, in *Neuroscience 2nd edition*. 2001, Sinauer Associates: Sunderland (MA).
5. Strauss, O., *The retinal pigment epithelium in visual function.* Physiol Rev, 2005. **85**(3): p. 845-81.
6. Marmorstein, A.D., et al., *Morphogenesis of the retinal pigment epithelium: toward understanding retinal degenerative diseases.* Ann N Y Acad Sci, 1998. **857**: p. 1-12.
7. Delaey, C. and J. Van De Voorde, *Regulatory mechanisms in the retinal and choroidal circulation.* Ophthalmic Res, 2000. **32**(6): p. 249-56.
8. Ye, X., Y. Wang, and J. Nathans, *The Norrin/Frizzled4 signaling pathway in retinal vascular development and disease.* Trends Mol Med, 2010. **16**(9): p. 417-25.
9. *Front Matter A2 - Forrester, John V*, in *The Eye (Fourth Edition)*, A.D. Dick, et al., Editors. 2016, W.B. Saunders. p. i-iii.
10. Chan-Ling, T., *Development of the Retinal Vasculature*. Encyclopedia of the Eye. Vol. 2. 2010: Academic Press.
11. Hughes, S., H. Yang, and T. Chan-Ling, *Vascularization of the human fetal retina: roles of vasculogenesis and angiogenesis.* Invest Ophthalmol Vis Sci, 2000. **41**(5): p. 1217-28.
12. Fruttiger, M., *Development of the retinal vasculature.* Angiogenesis, 2007. **10**(2): p. 77-88.
13. Selvam, S., T. Kumar, and M. Fruttiger, *Retinal vasculature development in health and disease.* Prog Retin Eye Res, 2018. **63**: p. 1-19.
14. Gerhardt, H., et al., *VEGF guides angiogenic sprouting utilizing endothelial tip cell filopodia.* J Cell Biol, 2003. **161**(6): p. 1163-77.
15. Adams, R.H. and A. Eichmann, *Axon guidance molecules in vascular patterning.* Cold Spring Harb Perspect Biol, 2010. **2**(5): p. a001875.
16. Carmeliet, P. and M. Tessier-Lavigne, *Common mechanisms of nerve and blood vessel wiring.* Nature, 2005. **436**(7048): p. 193-200.
17. del Toro, R., et al., *Identification and functional analysis of endothelial tip cell-enriched genes.* Blood, 2010. **116**(19): p. 4025-33.
18. Strasser, G.A., J.S. Kaminker, and M. Tessier-Lavigne, *Microarray analysis of retinal endothelial tip cells identifies CXCR4 as a mediator of tip cell morphology and branching.* Blood, 2010. **115**(24): p. 5102-10.
19. Benedito, R., et al., *The notch ligands Dll4 and Jagged1 have opposing effects on angiogenesis.* Cell, 2009. **137**(6): p. 1124-35.
20. Benedito, R., et al., *Notch-dependent VEGFR3 upregulation allows angiogenesis without VEGF-VEGFR2 signalling.* Nature, 2012. **484**(7392): p. 110-4.
21. Siekmann, A.F., L. Covassin, and N.D. Lawson, *Modulation of VEGF signalling output by the Notch pathway.* Bioessays, 2008. **30**(4): p. 303-13.
22. Zarkada, G., et al., *VEGFR3 does not sustain retinal angiogenesis without VEGFR2.* Proc Natl Acad Sci U S A, 2015. **112**(3): p. 761-6.
23. West, H., W.D. Richardson, and M. Fruttiger, *Stabilization of the retinal vascular network by reciprocal feedback between blood vessels and astrocytes.* Development, 2005. **132**(8): p. 1855-62.
24. Korn, C. and H.G. Augustin, *Mechanisms of Vessel Pruning and Regression.* Dev Cell, 2015. **34**(1): p. 5-17.
25. Winkler, E.A., R.D. Bell, and B.V. Zlokovic, *Central nervous system pericytes in health and disease.* Nat Neurosci, 2011. **14**(11): p. 1398-1405.

26. Gariano, R.F., M.L. Iruela-Arispe, and A.E. Hendrickson, *Vascular development in primate retina: comparison of laminar plexus formation in monkey and human.* Invest Ophthalmol Vis Sci, 1994. **35**(9): p. 3442-55.
27. Fruttiger, M., et al., *PDGF mediates a neuron-astrocyte interaction in the developing retina.* Neuron, 1996. **17**(6): p. 1117-31.
28. Ling, T.L. and J. Stone, *The development of astrocytes in the cat retina: evidence of migration from the optic nerve.* Brain Res Dev Brain Res, 1988. **44**(1): p. 73-85.
29. Mudhar, H.S., et al., *PDGF and its receptors in the developing rodent retina and optic nerve.* Development, 1993. **118**(2): p. 539-52.
30. Tao, C. and X. Zhang, *Development of astrocytes in the vertebrate eye.* Dev Dyn, 2014. **243**(12): p. 1501-10.
31. Sakimoto, S., et al., *A role for endothelial cells in promoting the maturation of astrocytes through the apelin/APJ system in mice.* Development, 2012. **139**(7): p. 1327-35.
32. Kubota, Y., et al., *Leukemia inhibitory factor regulates microvessel density by modulating oxygen-dependent VEGF expression in mice.* J Clin Invest, 2008. **118**(7): p. 2393-403.
33. Fukushima, Y., et al., *Sema3E-PlexinD1 signaling selectively suppresses disoriented angiogenesis in ischemic retinopathy in mice.* J Clin Invest, 2011. **121**(5): p. 1974-85.
34. Kim, J., et al., *Semaphorin 3E-Plexin-D1 signaling regulates VEGF function in developmental angiogenesis via a feedback mechanism.* Genes Dev, 2011. **25**(13): p. 1399-411.
35. Coca-Prados, M., *The blood-aqueous barrier in health and disease.* J Glaucoma, 2014. **23**(8 Suppl 1): p. S36-8.
36. Cunha-Vaz, J., R. Bernardes, and C. Lobo, *Blood-retinal barrier.* Eur J Ophthalmol, 2011. **21 Suppl 6**: p. S3-9.
37. Criswick, V.G. and C.L. Schepens, *Familial exudative vitreoretinopathy.* Am J Ophthalmol, 1969. **68**(4): p. 578-94.
38. Gilmour, D.F., *Familial exudative vitreoretinopathy and related retinopathies.* Eye (Lond), 2015. **29**(1): p. 1-14.
39. Nikopoulos, K., et al., *Next-generation sequencing of a 40 Mb linkage interval reveals TSPAN12 mutations in patients with familial exudative vitreoretinopathy.* Am J Hum Genet, 2010. **86**(2): p. 240-7.
40. Chen, Z.Y., et al., *A mutation in the Norrie disease gene (NDP) associated with X-linked familial exudative vitreoretinopathy.* Nat Genet, 1993. **5**(2): p. 180-3.
41. Toomes, C., et al., *Mutations in LRP5 or FZD4 underlie the common familial exudative vitreoretinopathy locus on chromosome 11q.* Am J Hum Genet, 2004. **74**(4): p. 721-30.
42. Robitaille, J., et al., *Mutant frizzled-4 disrupts retinal angiogenesis in familial exudative vitreoretinopathy.* Nat Genet, 2002. **32**(2): p. 326-30.
43. Jiao, X., et al., *Autosomal recessive familial exudative vitreoretinopathy is associated with mutations in LRP5.* Am J Hum Genet, 2004. **75**(5): p. 878-84.
44. Poulter, J.A., et al., *Mutations in TSPAN12 cause autosomal-dominant familial exudative vitreoretinopathy.* Am J Hum Genet, 2010. **86**(2): p. 248-53.
45. Collin, R.W., et al., *ZNF408 is mutated in familial exudative vitreoretinopathy and is crucial for the development of zebrafish retinal vasculature.* Proc Natl Acad Sci U S A, 2013. **110**(24): p. 9856-61.
46. Dixon, M.W., et al., *CTNNB1 mutation associated with familial exudative vitreoretinopathy (FEVR) phenotype.* Ophthalmic Genet, 2016. **37**(4): p. 468-470.
47. Panagiotou, E.S., et al., *Defects in the Cell Signaling Mediator beta-Catenin Cause the Retinal Vascular Condition FEVR.* Am J Hum Genet, 2017. **100**(6): p. 960-968.
48. Wu, J.H., et al., *Haploinsufficiency of RCBTB1 is associated with Coats disease and familial exudative vitreoretinopathy.* Hum Mol Genet, 2016. **25**(8): p. 1637-47.
49. Nikopoulos, K., et al., *Overview of the mutation spectrum in familial exudative vitreoretinopathy and Norrie disease with identification of 21 novel variants in FZD4, LRP5, and NDP.* Hum Mutat, 2010. **31**(6): p. 656-66.
50. Daneman, R., et al., *Wnt/beta-catenin signaling is required for CNS, but not non-CNS, angiogenesis.* Proc Natl Acad Sci U S A, 2009. **106**(2): p. 641-6.

51. Zhou, Y., et al., *Canonical WNT signaling components in vascular development and barrier formation.* J Clin Invest, 2014. **124**(9): p. 3825-46.
52. Gong, Y., et al., *LDL receptor-related protein 5 (LRP5) affects bone accrual and eye development.* Cell, 2001. **107**(4): p. 513-23.
53. Meindl, A., et al., *Norrie disease is caused by mutations in an extracellular protein resembling C-terminal globular domain of mucins.* Nat Genet, 1992. **2**(2): p. 139-43.
54. Coppieters, F., et al., *Isolated and Syndromic Retinal Dystrophy Caused by Biallelic Mutations in RCBTB1, a Gene Implicated in Ubiquitination.* Am J Hum Genet, 2016. **99**(2): p. 470-80.
55. Avila-Fernandez, A., et al., *Whole-exome sequencing reveals ZNF408 as a new gene associated with autosomal recessive retinitis pigmentosa with vitreal alterations.* Hum Mol Genet, 2015. **24**(14): p. 4037-48.
56. Robitaille, J.M., et al., *Phenotypic overlap between familial exudative vitreoretinopathy and microcephaly, lymphedema, and chorioretinal dysplasia caused by KIF11 mutations.* JAMA Ophthalmol, 2014. **132**(12): p. 1393-9.
57. Berger, W., B. Kloeckener-Gruissem, and J. Neidhardt, *The molecular basis of human retinal and vitreoretinal diseases.* Prog Retin Eye Res, 2010. **29**(5): p. 335-75.
58. Edwards, A.O., *Clinical features of the congenital vitreoretinopathies.* Eye (Lond), 2008. **22**(10): p. 1233-42.
59. Tauqeer, Z. and Y. Yonekawa, *Familial Exudative Vitreoretinopathy: Pathophysiology, Diagnosis, and Management.* Asia Pac J Ophthalmol (Phila), 2018. **7**(3): p. 176-182.
60. Cooper, D.N., et al., *Where genotype is not predictive of phenotype: towards an understanding of the molecular basis of reduced penetrance in human inherited disease.* Hum Genet, 2013. **132**(10): p. 1077-130.
61. Liu, C.H., et al., *Animal models of ocular angiogenesis: from development to pathologies.* FASEB J, 2017. **31**(11): p. 4665-4681.
62. Stahl, A., et al., *The mouse retina as an angiogenesis model.* Invest Ophthalmol Vis Sci, 2010. **51**(6): p. 2813-26.
63. Veleri, S., et al., *Biology and therapy of inherited retinal degenerative disease: insights from mouse models.* Dis Model Mech, 2015. **8**(2): p. 109-29.
64. Smith, L.E., et al., *Oxygen-induced retinopathy in the mouse.* Invest Ophthalmol Vis Sci, 1994. **35**(1): p. 101-11.
65. Frykman, P.K., et al., *Normal plasma lipoproteins and fertility in gene-targeted mice homozygous for a disruption in the gene encoding very low density lipoprotein receptor.* Proc Natl Acad Sci U S A, 1995. **92**(18): p. 8453-7.
66. Heckenlively, J.R., et al., *Mouse model of subretinal neovascularization with choroidal anastomosis.* Retina, 2003. **23**(4): p. 518-22.
67. Okamoto, N., et al., *Transgenic mice with increased expression of vascular endothelial growth factor in the retina: a new model of intraretinal and subretinal neovascularization.* Am J Pathol, 1997. **151**(1): p. 281-91.
68. Tobe, T., et al., *Evolution of neovascularization in mice with overexpression of vascular endothelial growth factor in photoreceptors.* Invest Ophthalmol Vis Sci, 1998. **39**(1): p. 180-8.
69. Xu, Q., et al., *Vascular development in the retina and inner ear: control by Norrin and Frizzled-4, a high-affinity ligand-receptor pair.* Cell, 2004. **116**(6): p. 883-95.
70. Kato, M., et al., *Cbfa1-independent decrease in osteoblast proliferation, osteopenia, and persistent embryonic eye vascularization in mice deficient in Lrp5, a Wnt coreceptor.* J Cell Biol, 2002. **157**(2): p. 303-14.
71. Junge, H.J., et al., *TSPAN12 regulates retinal vascular development by promoting Norrin- but not Wnt-induced FZD4/beta-catenin signaling.* Cell, 2009. **139**(2): p. 299-311.
72. Luhmann, U.F., et al., *Role of the Norrie disease pseudoglioma gene in sprouting angiogenesis during development of the retinal vasculature.* Invest Ophthalmol Vis Sci, 2005. **46**(9): p. 3372-82.
73. Richter, M., et al., *Retinal vasculature changes in Norrie disease mice.* Invest Ophthalmol Vis Sci, 1998. **39**(12): p. 2450-7.

74. Rattner, A., et al., *The role of the hypoxia response in shaping retinal vascular development in the absence of Norrin/Frizzled4 signaling.* Invest Ophthalmol Vis Sci, 2014. **55**(12): p. 8614-25.
75. Richardson, R., et al., *The zebrafish eye-a paradigm for investigating human ocular genetics.* Eye (Lond), 2017. **31**(1): p. 68-86.
76. Chhetri, J., G. Jacobson, and N. Gueven, *Zebrafish--on the move towards ophthalmological research.* Eye (Lond), 2014. **28**(4): p. 367-80.
77. Kaufman, R., et al., *Development and origins of zebrafish ocular vasculature.* BMC Dev Biol, 2015. **15**: p. 18.
78. Kitambi, S.S., et al., *Small molecule screen for compounds that affect vascular development in the zebrafish retina.* Mech Dev, 2009. **126**(5-6): p. 464-77.
79. Alvarez, Y., et al., *Genetic determinants of hyaloid and retinal vasculature in zebrafish.* BMC Dev Biol, 2007. **7**: p. 114.
80. Lawson, N.D. and B.M. Weinstein, *In vivo imaging of embryonic vascular development using transgenic zebrafish.* Dev Biol, 2002. **248**(2): p. 307-18.
81. Choi, J., et al., *FoxH1 negatively modulates flk1 gene expression and vascular formation in zebrafish.* Dev Biol, 2007. **304**(2): p. 735-44.
82. van Rooijen, E., et al., *von Hippel-Lindau tumor suppressor mutants faithfully model pathological hypoxia-driven angiogenesis and vascular retinopathies in zebrafish.* Dis Model Mech, 2010. **3**(5-6): p. 343-53.
83. Cao, Z., et al., *Hypoxia-induced retinopathy model in adult zebrafish.* Nat Protoc, 2010. **5**(12): p. 1903-10.
84. Bouis, D., et al., *Endothelium in vitro: a review of human vascular endothelial cell lines for blood vessel-related research.* Angiogenesis, 2001. **4**(2): p. 91-102.
85. Morin, K.T. and R.T. Tranquillo, *In vitro models of angiogenesis and vasculogenesis in fibrin gel.* Exp Cell Res, 2013. **319**(16): p. 2409-17.
86. Wilson, H.K., et al., *Concise review: tissue-specific microvascular endothelial cells derived from human pluripotent stem cells.* Stem Cells, 2014. **32**(12): p. 3037-45.
87. Cochrane, A., et al., *Advanced in vitro models of vascular biology: Human induced pluripotent stem cells and organ-on-chip technology.* Adv Drug Deliv Rev, 2018.
88. Klein, D., *iPSCs-based generation of vascular cells: reprogramming approaches and applications.* Cell Mol Life Sci, 2018. **75**(8): p. 1411-1433.
89. Takahashi, K. and S. Yamanaka, *Induction of pluripotent stem cells from mouse embryonic and adult fibroblast cultures by defined factors.* Cell, 2006. **126**(4): p. 663-76.
90. Clayton, Z.E., S. Sadeghipour, and S. Patel, *Generating induced pluripotent stem cell derived endothelial cells and induced endothelial cells for cardiovascular disease modelling and therapeutic angiogenesis.* Int J Cardiol, 2015. **197**: p. 116-22.
91. Wong, W.T., et al., *Endothelial cells derived from nuclear reprogramming.* Circ Res, 2012. **111**(10): p. 1363-75.
92. Bailey-Wilson, J.E. and A.F. Wilson, *Linkage analysis in the next-generation sequencing era.* Hum Hered, 2011. **72**(4): p. 228-36.
93. Pinto, A.M., et al., *Exploiting the potential of next-generation sequencing in genomic medicine.* Expert Rev Mol Diagn, 2016. **16**(9): p. 1037-47.
94. Chaitankar, V., et al., *Next generation sequencing technology and genomewide data analysis: Perspectives for retinal research.* Prog Retin Eye Res, 2016. **55**: p. 1-31.
95. Park, P.J., *ChIP-seq: advantages and challenges of a maturing technology.* Nat Rev Genet, 2009. **10**(10): p. 669-80.
96. Yan, H., et al., *ChIP-seq in studying epigenetic mechanisms of disease and promoting precision medicine: progresses and future directions.* Epigenomics, 2016. **8**(9): p. 1239-58.
97. Wade, J.T., *Mapping Transcription Regulatory Networks with ChIP-seq and RNA-seq.* Adv Exp Med Biol, 2015. **883**: p. 119-34.
98. Slijkerman, R.W., et al., *The pros and cons of vertebrate animal models for functional and therapeutic research on inherited retinal dystrophies.* Prog Retin Eye Res, 2015. **48**: p. 137-59.

99. Sander, J.D. and J.K. Joung, *CRISPR-Cas systems for editing, regulating and targeting genomes.* Nat Biotechnol, 2014. **32**(4): p. 347-55.
100. Jinek, M., et al., *A programmable dual-RNA-guided DNA endonuclease in adaptive bacterial immunity.* Science, 2012. **337**(6096): p. 816-21.
101. Musada, G.R., et al., *Mutation spectrum of the FZD-4, TSPAN12 AND ZNF408 genes in Indian FEVR patients.* BMC Ophthalmol, 2016. **16**: p. 90.
102. Salvo, J., et al., *Next-generation sequencing and novel variant determination in a cohort of 92 familial exudative vitreoretinopathy patients.* Invest Ophthalmol Vis Sci, 2015. **56**(3): p. 1937-46.
103. Li, Y., et al., *The characteristics of digenic familial exudative vitreoretinopathy.* Graefes Arch Clin Exp Ophthalmol, 2018. **256**(11): p. 2149-2156.
104. Su, N., et al., *[Analysis of pathological mutation in a Chinese pedigree affected with familial exudative vitreoretinopathy].* Zhonghua Yi Xue Yi Chuan Xue Za Zhi, 2018. **35**(2): p. 193-196.
105. Habibi, I., et al., *Exome sequencing confirms ZNF408 mutations as a cause of familial retinitis pigmentosa.* Ophthalmic Genet, 2017. **38**(5): p. 494-497.
106. Biswas, P., et al., *Whole-Exome Sequencing Identifies Novel Variants that Co-segregates with Autosomal Recessive Retinal Degeneration in a Pakistani Pedigree.* Adv Exp Med Biol, 2018. **1074**: p. 219-228.
107. Fog, C.K., G.G. Galli, and A.H. Lund, *PRDM proteins: important players in differentiation and disease.* Bioessays, 2012. **34**(1): p. 50-60.
108. Hohenauer, T. and A.W. Moore, *The Prdm family: expanding roles in stem cells and development.* Development, 2012. **139**(13): p. 2267-82.
109. Iuchi, S., *Three classes of C2H2 zinc finger proteins.* Cell Mol Life Sci, 2001. **58**(4): p. 625-35.
110. Brayer, K.J. and D.J. Segal, *Keep your fingers off my DNA: protein-protein interactions mediated by C2H2 zinc finger domains.* Cell Biochem Biophys, 2008. **50**(3): p. 111-31.

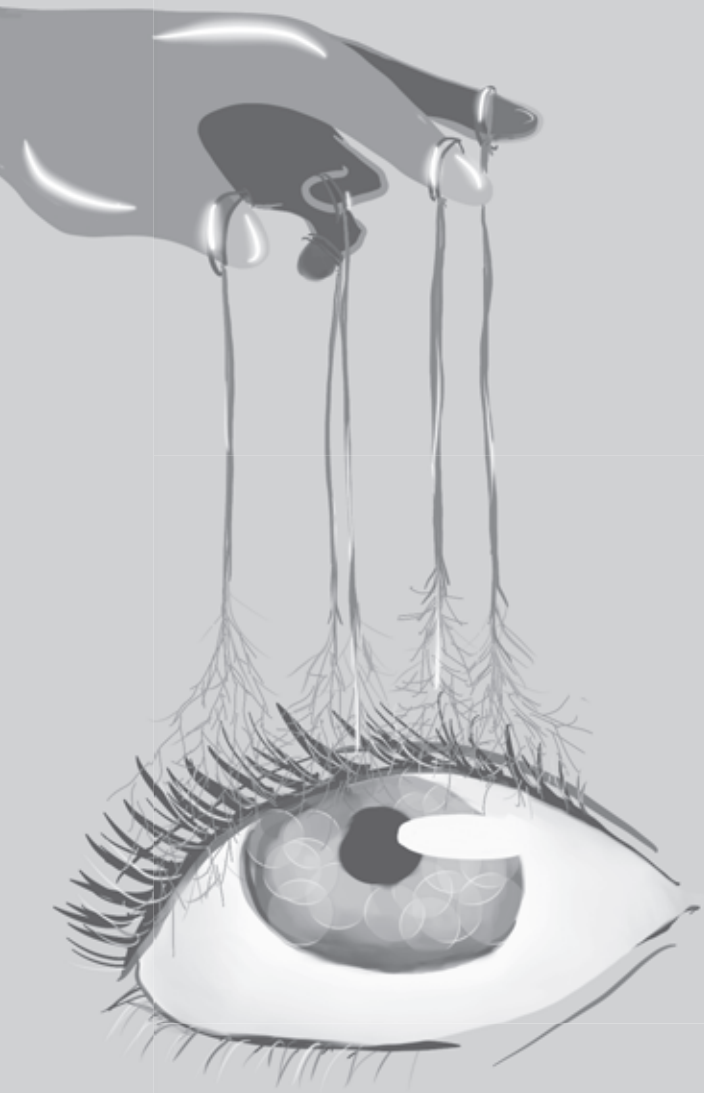

Chapter 2

An FEVR-associated mutation in *ZNF408* alters the expression of genes involved in the development of vasculature

Dyah W Karjosukarso[1], Sebastianus HC van Gestel[1,2], Jieqiong Qu[2], Evelyn N Kouwenhoven[2,3], Lonneke Duijkers[4], Alejandro Garanto[1], Huiqing Zhou[2,3,¶], Rob WJ Collin[1,¶]

[1]Department of Human Genetics, Donders Institute for Brain, Cognition and Behaviour, Radboud University Medical Center, Nijmegen, the Netherlands; [2]Department of Molecular Developmental Biology, Faculty of Science, Radboud Institute for Molecular Life Sciences, Radboud University, Nijmegen, the Netherlands; [3]Department of Human Genetics, Radboud Institute for Molecular Life Sciences, Radboud University Medical Center, Nijmegen, the Netherlands; [4]Department of Human Genetics, Radboud University Medical Center, Nijmegen, the Netherlands

[¶] These authors contributed equally to this work

Human Molecular Genetics (2018) **27:** 3519-3527

Abstract

Familial exudative vitreoretinopathy (FEVR) is an inherited retinal disorder hallmarked by an abnormal development of retinal vasculature. A missense mutation in *ZNF408* (p.His455Tyr) was reported to underlie autosomal dominant FEVR in a large Dutch family, and *ZNF408* was shown to play a role in the development of vasculature. Nonetheless, little is known about the molecular mechanism of *ZNF408*-associated FEVR. To investigate this, an *in vitro* model of *ZNF408*-associated FEVR was generated by overexpressing wild-type and p.His455Tyr ZNF408 in Human Umbilical Vein Endothelial Cells (HUVEC). Cells overexpressing mutant ZNF408 were unable to form a capillary-like network in *in vitro* tube formation assay, thereby mimicking the clinical feature observed in FEVR patients. Intriguingly, transcriptome analysis revealed that genes involved in the development of vasculature were deregulated by the p.His455Tyr mutation. Chromatin immunoprecipitation (ChIP) showed that p.His455Tyr ZNF408 has reduced DNA-binding ability, as compared to the wild-type protein. The fact that the p.His455Tyr mutation disrupts the expression of genes important for the development of vasculature, sheds further light on the molecular mechanisms underlying *ZNF408*-associated FEVR.

2.1 Introduction

Familial exudative vitreoretinopathy (FEVR, MIM 133780) is an inherited retinal disorder that was first described by Criswick and Schepens [1]. It is primarily characterized by abnormal and incomplete vascularisation of the peripheral retina [2-4]. Thus far, mutations in *NDP* [5], *FZD4* [6, 7], *TSPAN12* [8], *LRP5* [6, 9], *ZNF408* [10], *ATOH7* [11], *RCBTB1* [12], and *CTNNB1* [13, 14] have been reported in FEVR cases. Besides those of *ZNF408*, *ATOH7*, and *RCBTB1*, the proteins encoded by FEVR genes are involved in the Norrin/β-catenin signaling pathway [15]. Next to the genetic heterogeneity, various clinical manifestations can be observed in FEVR, ranging from asymptomatic to complete blindness [16].

We previously discovered a mutation in *ZNF408* (c.1363C>T, p.His455Tyr, NM_024741.2) that segregates in a large autosomal dominant FEVR family [10]. The protein encoded by *ZNF408* belongs to the PRDM (positive regulatory domain I-binding factor 1/PRD1-BF1 and retinoblastoma-interacting zinc finger protein 1/RIZ1 homology domain containing) family [17]. Members of this family typically have an N-terminal PR domain and multiple zinc finger domains. The PR domain belongs to a subfamily of SET methyltransferase domains, whereas zinc finger domains are generally involved in DNA binding and protein-protein interactions [17, 18]. ZNF408 is predicted to harbor ten zinc finger domains, each of which consists of two histidine and two cysteine residues. The p.His455Tyr mutation changes a histidine in the fourth zinc finger domain into a tyrosine [10]. We demonstrated that the mutant protein is mislocalised in the cell and knockdown of *znf408* in zebrafish resulted in abnormal development of eye and trunk vasculature [10]. These data support the causality of the mutation and implicate an important role of ZNF408 in the development of vasculature. Nonetheless, very little is known about the exact molecular function of ZNF408.

To unravel the role of ZNF408 in the development of vasculature and to assess their angiogenic ability, *in vitro* tube formation assays were performed on endothelial cells overexpressing wild-type or mutant p.His455Tyr ZNF408. These cells were also subjected to transcriptome analysis to identify genes regulated by ZNF408, as well as the effect of the mutation on gene expression. Furthermore, chromatin immunoprecipitation followed by high-throughput sequencing (ChIP-Seq was employed to reveal the binding sites of ZNF408 in the human genome. Our

data suggest that ZNF408 indirectly regulates the expression of genes important for the development of vasculature, and that this regulation is disrupted by the p.His455Tyr mutation.

2.2 Materials and Methods

2.2.1 Cell culture

Human umbilical vein endothelial cells (HUVEC, a kind gift from Dr. William Leenders) were cultured in Endothelial Growth Medium 2 (EGM2, Promocell) supplemented with 1% penicillin/streptomycin or other required antibiotics. Culture dishes were coated with 0.01 mg/ml bovine fibronectin (Promocell) for at least 1 h at 37°C before use for HUVEC culture. HEK293T cells (ATCC) were cultured in DMEM (Sigma) supplemented with 10% FCS, 1% sodium pyruvate and 1% penicillin/streptomycin. HUVEC and HEK293T cells were maintained at 37°C and 5% CO_2.

2.2.2 Lentivirus production

To generate lentiviral constructs that enable inducible expression of N-terminally HA-tagged ZNF408, the $2K7_{bsd}$ lentivirus vector [19] was used. A tetracycline inducible promoter was cloned into the pDONR-P4P1R entry clone, whereas full-length human ZNF408 cDNA (wild-type and p.His455Tyr mutant) fused with sequence encoding HA-tag were cloned into the pDONR201 entry clone. LR Clonase II Plus enzyme mix (Thermo Fisher Scientific) was used to insert the promoter and fusion gene into the $2K7_{bsd}$ lentiviral vector. To produce lentivirus particles, 5 µg of $2K7_{bsd}$_Tet_HA-ZNF408 construct was co-transfected with 3.2 µg psPAX2 and 1.8 µg pMD2.G into HEK293T cells using $CaPO_4$ (final concentration of 250 mM $CaCl_2$, 0.5 mM Tris pH 7.5, EDTA, 25 mM HEPES-NaOH pH 7.3, 280 mM NaCl, 1.5 mM $NaPO_4$) transfection method. Medium was refreshed 8 hours post-transfection and the supernatant containing lentivirus particles were collected 48 hours post-transfection. Lentiviral particles of tetracycline-controlled transcriptional activator (rtTA, pLVX-EtO) were produced following similar procedures.

2.2.3 Stable cells generation

HUVEC were seeded on 12-well plate with 2.5 x 10^5 cells/well density. After 6-8 hours, they were transduced with supernatant containing lentiviral particles of

$2K7_{bsd}$_Tet_HA-ZNF408 and rtTA with 1:1 ratio overnight. The following day, the medium was changed to EGM2 without selection antibiotics. Ninety-six hours post-transduction, 4 μg/ml blasticidin (Sigma) and 1000 μg/ml G418 (Sigma) were added to EGM2 to select for positively transduced cells. The selection medium was applied every 48 hours for 6 days. The obtained stable cells were further cultured in medium containing 25% of the antibiotics dose used for selection.

2.2.4 Stable cells validation

The stable cells were validated for the integration of $2K7_{bsd}$_Tet_HA-ZNF408 (wild-type and p.His455Tyr mutant) and rtTA constructs at the genomic DNA level. DNA was isolated from cell pellet using DNeasy Blood and Tissue kit (Qiagen) following manufacturer's instructions. Twenty nanograms DNA was used as template for amplification. The expression of HA-ZNF408 was examined at RNA and protein level. Total RNA was isolated using Macherey-Nagel RNA isolation kit according to the kit manual. iScript kit (Bio-Rad) was used to synthesise cDNA from 250 ng RNA. Subsequently, GoTaq Green Master Mix (Promega) was used in the quantitative (qPCR) PCR reaction. Primers used in the genomic DNA amplification and qPCR are listed in Table S1. Western blot analysis was performed to check the expression at protein level. Mouse anti-HA (Sigma, 1:1,000) and rabbit anti-ZNF408 (Biorbyt, 1:500) was used to detect the expression of HA-ZNF408 at the protein level. Tubulin was stained as loading control using mouse anti-tubulin (Abcam, 1:2,000). Donkey anti-mouse IRDye 680 RD and donkey anti-rabbit 800 CW (LI-COR, 1:20,000) were used as secondary antibodies. The blot was scanned on LI-COR Odyssey CLx system.

2.2.5 *In vitro* tube formation assay

Non-transduced HUVEC as well as stable HUVEC were seeded at the density of 1.5 x 10^5 cells in 12-well plate format. Forty-eight hours post-seeding, the overexpression of wild-type and p.His455Tyr ZNF408 was induced by doxycycline treatment (100 ng/ml and 500 ng/ml, respectively) for 48 hours. The cells were then trypsinised and seeded on 96-well plate coated with Matrigel (BD Biosciences) at the density of 1.5 x 10^4 cell per well. After 20 hours, the cells were stained with Calcein Red (Thermo Scientific) at a 6 μM final concentration, followed by imaging on EVOS cell imaging station.

2.2.6 RNA-Seq

Non-transduced HUVEC as well as the stable HUVECs were seeded in duplicate at a density of 2.5 x 10^5 cells in 6-well plate format. Overexpression of wild-type and p.His455Tyr ZNF408 was induced in similar manner as mentioned previously. The cells were harvested for total RNA isolation using Macherey-Nagel RNA isolation kit, following manufacturer's instructions. Ribo-Zero rRNA removal kit (Illumina) was used to eliminate rRNA from the sample. RNA fragmentation was performed as well as first and second strand cDNA synthesis as described in [20], with the deviation that RNA fragmentation was performed for 3 minutes at 95°C instead of 1.5 minutes. The obtained cDNA was used for next generation sequencing on Illumina NextSeq 500 platform.

2.2.7 RNA-Seq data analysis

Sequence reads were mapped to the human genome (build hg19) using the STAR algorithm [21]. Number of reads per gene were counted using HTseq [22] followed by differential gene expression analysis using DESeq2 package [23]. The cutoff used to determine a significant difference in gene expression was set at a Benjamini-Hochberg adjusted p-value of <0.05 and a fold-change of ≥ 1.5. The FPKM of differentially expressed genes was calculated using Cuffdiff [24]. GO-terms enrichment analysis was performed on the lists of differentially expressed genes by DAVID with default settings [25, 26]. The list of enriched GO-terms was summarized using REVIGO, with the settings: small list (allowed similarity = 0.5), *Homo sapiens* database, and SimRel for semantic similarity measure [27].

2.2.8 Real-time quantitative PCR

Some of the differentially regulated genes detected in the RNA-Seq data were validated by means of real-time quantitative PCR (qPCR) using GoTaq Green Master Mix (Promega). qPCR was performed on three biological replicates and Student's t-test was used to determine significance difference. The primers used for this are listed in Table S1.

2.2.9 ChIP-Seq

Full-length human wild-type and p.His455Tyr mutant ZNF408 cDNA were cloned into pcDNA3-HA vector, to generate a construct encoding ZNF408 with the HA-tag at the N-terminus. These constructs were transiently transfected into HEK293T cells cultured in 15-cm dishes using Fugene HD reagent (Promega). Forty-eight

hours post-transfection, the cells were crosslinked using 1% formaldehyde at room temperature for 10 minutes. The crosslinking was stopped with 0.125 M glycine and the nuclear fraction was harvested as described in Denissov, *et al.*, 2007 [28]. DNA was fragmented by sonication using Bioruptor (Diagenode). The settings of the sonication were high power, 16 cycles of 30 seconds ON and 30 seconds OFF. In each immunoprecipitation reaction, 100 µl sonicated nuclear lysate, 30 µl ProtA/G beads (Santa Cruz), and 1-2 µg antibody was used. The antibodies used for chromatin immunoprecipitation were mouse monoclonal anti-HA (1 µg per reaction, Sigma) and rabbit polyclonal anti-ZNF408 (2 µg per reaction, Biorbyt). Immunoprecipitation reactions were incubated at 4°C overnight. Immunoprecipitated DNA was purified by phenol/chloroform extraction. Next generation sequencing was performed on Illumina HiSeq 2000 using 5 ng of the immunoprecipitated DNA.

2.2.10 ChIP-Seq Data Analysis

The sequence reads were uniquely mapped to the human genome build hg19 using bwa algorithm [29]. Peak calling was performed using MACS2 [30] with default settings and a p-value threshold of 1E-05. Data from non-transfected HEK293T cells were used as control file. The functional significance of the detected peaks were assessed using GREAT with basal plus extension settings [31]. The list of enriched GO-terms was summarized using REVIGO, with the settings: small list (allowed similarity = 0.5), *Homo sapiens* database, and SimRel for semantic similarity measure [27].

2.2.11 Transactivation assay

Putative ZNF408 binding sites on the human genome were amplified and subsequently cloned into Gateway adapted pGL3-Enhancer vector. The constructs were co-transfected with pcDNA3-HA, pcDNA3-HA-ZNF408 wild-type, or pcDNA3-HA-ZNF408 p.His455Tyr vector into HEK293T cells using Fugene HD transfection reagent (Promega). The transfection was performed in triplicates on 24-well format. Forty-eight hours after transfection, the cells were lysed and luciferase expression was measured using Dual Luciferase Assay kit (Promega) following the manufacturer's instructions. Luciferase measurement was performed in duplicate using 5 µl of cell lysate. Student's t-test was performed to test for significant differences between wild-type and mutant.

2.2.12 Statistical analysis

Statistical tests used in the data analysis of the different experiments are described in detail in the sections that belongs to the corresponding experiments.

2.3 Results

2.3.1 Overexpression of ZNF408 p.His455Tyr prevents HUVEC from forming capillary-like structures

To study the role of ZNF408, particularly in the development of vasculature, a cellular model for *ZNF408*-associated FEVR was established. A widely used endothelial cell system, Human Umbilical Vein Endothelial Cells (HUVEC), was transduced with lentiviral particles that contain constructs encoding HA-tagged wild-type or p.His455Tyr ZNF408. These transgenes were stably integrated into the HUVEC genome, and allowed inducible overexpression of wild-type and p.His455Tyr ZNF408 (Figure 1a and b). The integration of *ZNF408* wild-type and p.His455Tyr was confirmed at the genomic DNA level (Figure S1a), and their overexpression was validated both at the transcript and protein levels (Figure S1b and S1c). The phenotype of these cellular models was assessed by *in vitro* tube formation assay, which is commonly used to examine the angiogenic ability of endothelial cells [32]. Unlike overexpression of wild-type ZNF408, which did not interfere with the formation of capillary-like structures in this assay, overexpression of ZNF408 p.His455Tyr clearly inhibited the formation of these structures (Figure 1c). This result showed that the *in vitro* models mimic the abnormal vasculature development observed in FEVR patients, demonstrating their suitability to study the role of ZNF408 in this process.

2.3.2 Overexpression of ZNF408 p.His455Tyr alters the expression of genes involved in development of vasculature

Next, we performed transcriptome analysis of the generated cells to study the underlying molecular mechanisms of the observed phenotype. Two biological replicates of each experimental condition, non-transduced HUVEC (NT), HUVEC overexpressing wild-type ZNF408 (WT), and HUVEC overexpressing p.His455Tyr ZNF408 (MUT), were included. The biological replicates clustered together in the principal component analysis (PCA), demonstrating their similarities. Notably, the three different conditions were separated from each other in PCA (Figure

1d), indicating their distinct gene expression profiles. Furthermore, NT and MUT were located on the same end of PC2 axis, in contrast to WT that was located on the other end of PC2. The distinct gene expression profiles observed are consistent with the heatmap of gene expression in the three experimental conditions (Figure S1d). Subsequently, differential expressed genes between the conditions were determined. In this analysis, three pairwise comparisons were made, namely a comparison of WT *vs* MUT (Dataset S1, Figure 1e), NT *vs* WT (Dataset S2, Figure 1f), as well as NT *vs* MUT (Dataset S3, Figure S1e). Gene ontology (GO) analysis was performed to investigate the biological processes associated with the differentially regulated genes. The terms nucleosome assembly and protein heterotetramerization were enriched for genes upregulated by WT (Figure 1f), as compared to NT. The genes associated with these two terms mainly encode for histone H1 and H2. For the genes downregulated by WT, the terms cell adhesion and response to hypoxia were enriched (Figure 1f), and included *ITGA4*, *CTGF*, *COL8A1*, and *VCAM1*, or *MMP2*, *ANGPT2*, *TGFB2*, and *VCAM1*, respectively. Interestingly, the GO terms enriched for the genes differentially upregulated by WT as compared to NT, were rather similar to those downregulated by MUT as compared to WT, and vice versa (Figure 1e and 1f). These findings indicate that many genes that were up-/downregulated by wildtype ZNF408 can be de-regulated due to the p.His455Tyr mutation, suggesting that MUT can disrupt the regulation of gene expression which is controlled by WT.

To further focus on the mechanisms that are disrupted by MUT, we focused on genes whose expression is deregulated by MUT. In total, there were 122 genes that were exclusively upregulated by WT as compared to NT, but downregulated by MUT as compared to WT (WT > MUT, Table S2, Figure 2a and 2c), while there were 102 genes that were uniquely downregulated by WT as compared to NT, but upregulated by MUT as compared to WT (WT < MUT, Table S3, Figure 2b and 2d). Some of these genes were regulated in opposite direction by WT and MUT. For instance, *HIST1H1D* and *HIST1H3C* were upregulated by WT as compared to NT, but downregulated by MUT as compared to NT. Another example is *VCAM1*, which is downregulated by WT as compared to NT, but upregulated by MUT as compared to NT. Consistently, these deregulated genes were similar to the genes that mark the difference on the PC2 axis in the PCA analysis (Table S4), further highlighting the fact that MUT can disrupt the regulation of these genes. The GO terms enriched for these genes were similar to those enriched

in the pairwise comparisons. For instance, nucleosome assembly and protein heterotetramerisation, which are relevant to chromatin organization and remodeling, were enriched for genes upregulated by WT (Figure 2e). Likewise, terms relevant to the development of vasculature were again enriched for genes downregulated by WT. Besides response to hypoxia and cell adhesion, the term angiogenesis was also enriched in this set of genes (Figure 2f), and included *CTGF*, *COL8A1*, *ANGPT2*, *MMP2*, *FN1* and *TGFB2*. These data provide novel insights into the function of ZNF408, probably in chromatin organization and remodeling, and also confirm our previous findings of its role in vasculature development.

Given the fact that *ZNF408* is mutated in FEVR, we further focused on genes that are relevant to vasculature development. Quantitative PCR (qPCR) was performed to confirm the expression pattern of 15 genes known to be associated with vasculature development including *HMOX1*, *CTGF*, *ITGA4*, *ANGPT2*, and *MMP2* (Figure S2). The difference in expression level between WT and MUT was validated for all of them, demonstrating the reliability of the RNA-Seq data.

2.3.3 ZNF408 p.His455Tyr has reduced DNA-binding ability

The data obtained from the transcriptome analysis indicate a regulatory role for ZNF408 in the development of vasculature. Due to the presence of ten zinc finger domains in ZNF408, we hypothesized that this protein regulates gene expression by binding to regulatory genomic regions. Therefore, a chromatin immunoprecipitation followed by high-throughput sequencing (ChIP-Seq experiment was performed. HEK293T cells were transfected with HA-tagged wild-type and p.His455Tyr mutant ZNF408 and the immunoprecipitation was performed using antibodies targeting either the HA-tag or the ZNF408 protein (Figure 3a). There were 1,548 and 3,074 binding sites detected for wild-type ZNF408, while there were only 56 and 58 binding sites detected for p.His455Tyr ZNF408 in the HA-ChIP and ZNF408-ChIP, respectively. The overlapping binding sites between HA-ChIP and ZNF408-ChIP were considered the most reliable, which were 730 for wild-type ZNF408 and 10 for p.His455Tyr ZNF408. Interestingly, these results showed that p.His455Tyr ZNF408 has remarkably less binding sites compared to wild-type ZNF408 (Figure 3b), examples of which are shown for *ANXA5*, *GPR180*, and *LZTS2* (Figure S3a). To validate the ChIP-Seq results, the identified regulatory regions were cloned upstream of the luciferase sequence in the pGL3-Enhancer vector. The overexpression of these constructs, together with constructs encoding wild-type or p.His455Tyr ZNF408, showed

activation of luciferase gene transcription by wild-type ZNF408, but not by p.His455Tyr ZNF408 (Figure S3b), thereby confirming the reduced DNA-binding ability of p.His455Tyr that was observed in the ChIP-Seq experiment.

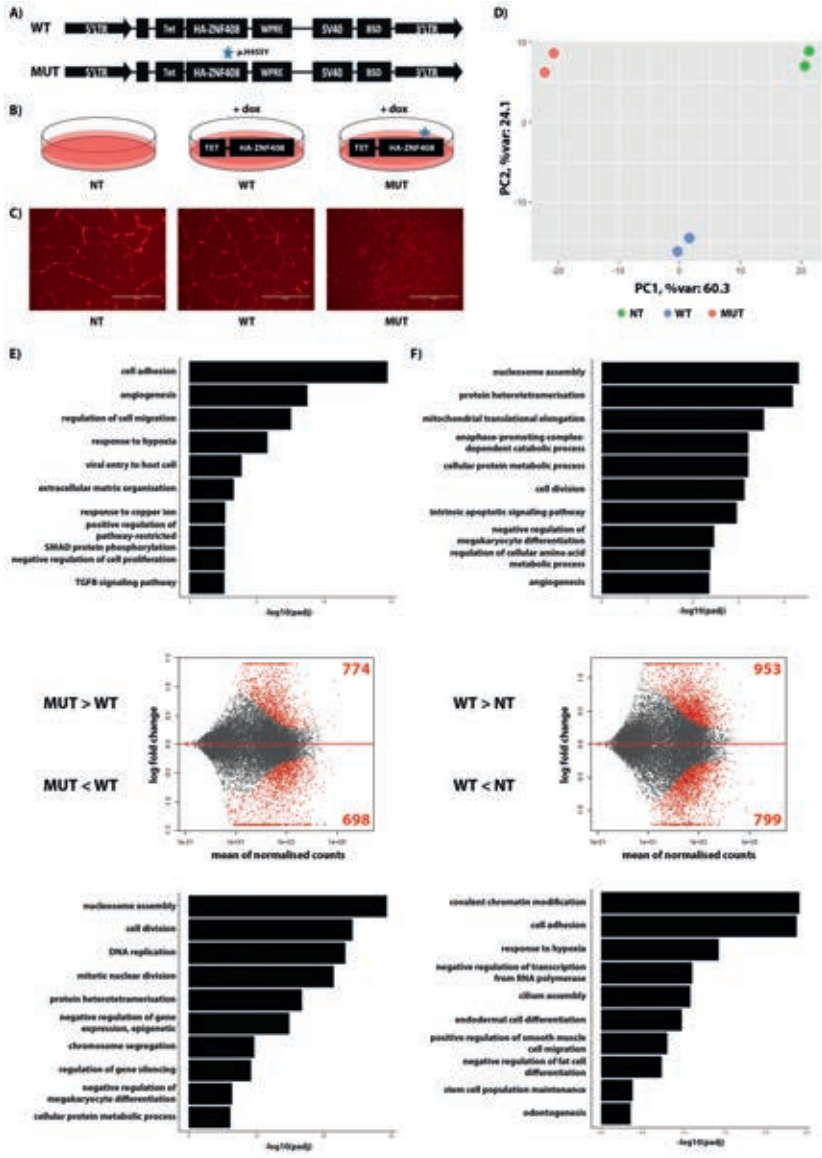

Figure 1. Overexpression of ZNF408 p.His455Tyr (p.H455Y) resulted in absence of capillary-like structures in tube-formation assay and disrupts the normal gene expression regulated by wild-type ZNF408. A) Lentiviral constructs for wild-type and p.His455Tyr mutant ZNF408 overexpression. LTR: long terminal repeats, Tet: tetracycline-inducible promoter, WPRE: woodchuck hepatitis virus post-transcriptional regulatory element, SV40: Simian virus 40, BSD: blasticidin resistance gene. B) Schematic illustration of the experimental setup. NT: non-transduced HUVEC, WT: HUVEC transduced with wild-

type ZNF408, and MUT: HUVEC transduced with mutant ZNF408. ZNF408 overexpression was induced by doxycycline. C) Fluorescent images of the capillary-like structures formed by NT and WT cells, but not MUT cells in an *in vitro* tube formation assay. Scale bars = 1000 µm. D) Principal component analysis of the transcriptome data. Two biological replicates were analysed in each condition. E) and F) MA-plot of the differential expression analysis, comparing WT to MUT and WT to NT, respectively. Red dots represent genes differentially expressed between conditions, black dots represent no difference in expression. The number of genes with significant difference in expression is depicted on the corner of the plot. The top 10 biological process GO-terms associated to genes belonging to the upper and lower panel of the MA-plot are depicted above and below the MA-plot, respectively. The p-values were adjusted using the Benjamini-Hochberg method.

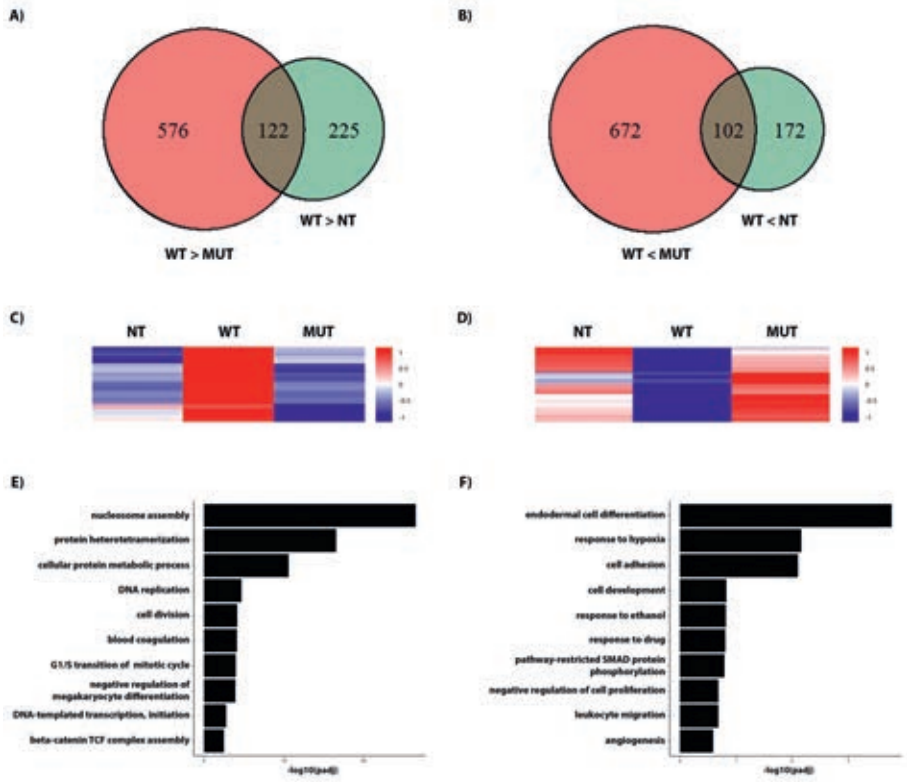

Figure 2. p.His455Tyr ZNF408 deregulates the expression of some genes. A) Venn diagrams showing the overlap of genes that are exclusively upregulated in WT compared to NT (WT > NT) and downregulated in MUT compared to WT (WT > MUT) and B) Venn diagrams showing the overlap of genes that are exclusively downregulated in WT compared to NT (WT < NT) and upregulated in MUT compared to WT (WT < MUT). C) and D) Heatmap of the expression of these genes described in (A) and (B), respectively. The z-score was calculated based on the FPKM values of these genes. E) and F) The enriched biological process GO-terms for the genes described in (A) and (B), respectively. The p-values were adjusted using the Benjamini-Hochberg method.

The binding sites of wild-type ZNF408 were predominantly located around the transcription start site (Figure 3c) and associated with 778 genes (Dataset S4). Gene ontology analysis showed that these genes are involved in diverse

biological processes, such as nucleosome assembly, regulation of gene expression, megakaryocyte differentiation, and protein processing (Figure 3d). Despite the clear loss of binding demonstrated by p.His455Tyr ZNF408, only 15 of these genes are differentially regulated by wild-type and p.His455Tyr ZNF408 in HUVEC (Table S5). Two of these 15 genes, *HMOX1* and *ITGA4,* are involved in biological processes relevant to the development of vasculature. Intriguingly, gene expression analysis showed that wild-type ZNF408 upregulated the expression of *HMOX1* while downregulating that of *ITGA4*, processes that were reversed by the p.His455Tyr mutation (Figure S2). ZNF408 binds to a region around 8 kb upstream the transcription start site (TSS) of *HMOX1*, whereas it binds approximately 350 bp downstream of the TSS in *ITGA4* (Figure S4a and S4b). Cloning of these regions upstream of luciferase sequence followed by transactivation assay in HEK293T cells validated direct binding of wild-type ZNF408 to the *ITGA4* TSS (Figure S4c and S4d).

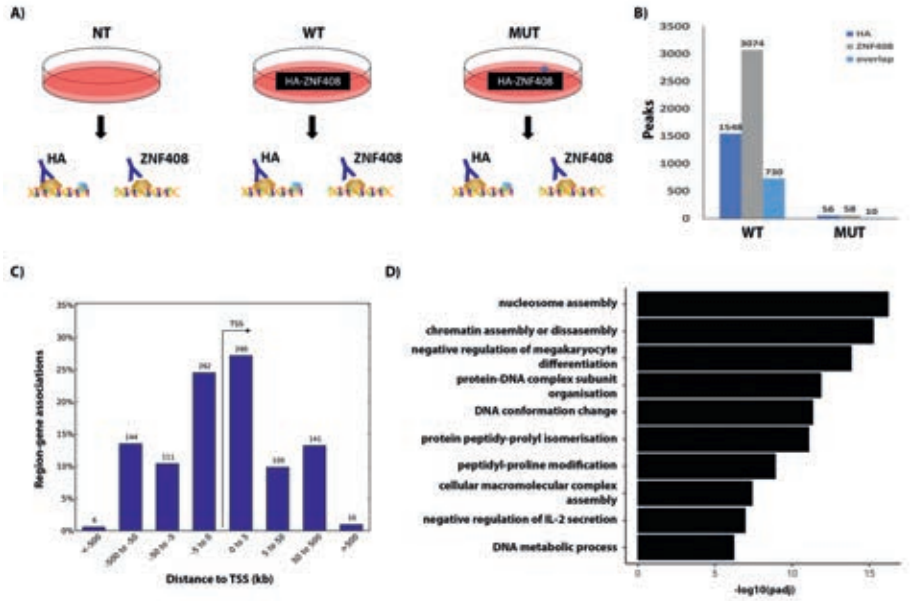

Figure 3. ZNF408 p.His455Tyr has reduced DNA-binding ability. A) Schematic illustration of the experimental setup. NT: non-transduced HEK293T, WT: HEK293T transfected with wild-type ZNF408, and MUT: HEK293T transfected with mutant ZNF408. B) Number of peaks detected in ChIP using HA antibody, ZNF408 antibody and the overlap of both. C) The distance of the overlapping peaks to transcription start site (TSS). D) The top 10 biological process GO-terms of genes associated with ZNF408 binding sites. The p-values are adjusted with false discovery rate (FDR) method.

2.4 Discussion

In this study, the role of ZNF408 in the development of vasculature was investigated. An *in vitro* model of *ZNF408*-associated FEVR was generated by overexpressing wild-type or p.His455Tyr mutant ZNF408 in HUVEC. The overexpression of p.His455Tyr ZNF408 disrupted the ability of HUVEC to form a capillary-like network *in vitro*, which mimics the aberrant retinal vasculature development observed in FEVR patients. Transcriptome analyses of the cellular models showed that the mutation altered the normal gene expression regulated by wild-type ZNF408, which may underlie the observed cellular phenotype. Chromatin immunoprecipitation in HEK293T cells showed that the p.His455Tyr mutation reduced the DNA-binding ability of mutant ZNF408.

The results obtained in this study suggest a role of ZNF408 in various biological processes. Nucleosome assembly and protein heterotetramerization are two terms that were highly enriched for genes upregulated by wild-type ZNF408. The genes associated with these terms are mainly encoding for histones H1 and H2, implying a role for ZNF408 in chromatin remodeling. Interestingly, the term nucleosome assembly was also highly enriched for the genes identified in the ChIP-Seq experiment and is mainly associated with genes encoding histone H1, H2, and H3. Although little overlap was observed between genes identified by ChIP-Seq and the transcriptome analysis, our results suggest the involvement of ZNF408 in chromatin remodeling, which may directly or indirectly contribute to the observed vascular phenotype.

Response to hypoxia, cell adhesion, and most importantly angiogenesis are processes that are directly relevant to the development of vasculature. Genes related to these terms were downregulated by wild-type ZNF408, which was deregulated by p.His455Tyr ZNF408. Given that the overexpression of wild-type ZNF408 did not inhibit *in vitro* tube formation, we hypothesize that wild-type ZNF408 promotes the vasculature development by downregulating genes inhibiting angiogenesis, explaining why reversal of this process by p.His455Tyr ZNF408 led to a disruption of *in vitro* tube formation. Indeed, based on literature, some of the genes associated with these terms (*e.g. CTGF* and *ANGPT2)*, are proposed to act as angiogenesis inhibitors in some circumstances [33, 34].

Hypoxia has been widely described as one of the inducers of angiogenesis, including in the retina [35]. Hypoxic retinal astrocytes in avascular areas express the vascular endothelial growth factor (VEGF) and can direct endothelial cells to a specific site to form a vascular network [36, 37]. The downregulation of genes associated to a response to hypoxia by ZNF408 implies a role for this protein in regulating this response, albeit via an unknown mechanism. The de-regulation of these genes by p.His455Tyr ZNF408 suggests a prevention of compensatory hypoxia-induced angiogenesis in FEVR patients, despite the presence of an avascular peripheral retina that would normally induce hypoxia.

Since ZNF408 is predicted to have ten zinc finger domains, we hypothesized that it regulates gene expression by binding to genomic regulatory regions and therefore, performed ChIP-Seq experiment to determine ZNF408 binding sites. Relatively a small number of peaks were detected in the ChIP-Seq experiment. This, together with the difference in cellular systems used - HEK293T in ChIP-Seq experiment and HUVEC in transcriptome analysis - may contribute to the little overlap with the differentially expressed genes. The small number of peaks also suggests that ZNF408 does not bind directly to DNA to regulate gene expression. Despite DNA binding being the primary role of many zinc finger domains, binding activity to other ligands such as RNA and protein have been described as well [38, 39]. Moreover, ZNF408 belongs to the PRDM family. Although some members of this family have been shown to bind DNA directly, other members of the family are known to regulate gene expression either by acting as direct histone methyltransferase or by recruiting other histone modifying enzymes. PRDM family proteins have also been shown to bind to transcription factors to target gene promoters or to act as non-DNA binding cofactors [17, 18]. These not only further suggest the role of ZNF408 in chromatin remodeling, but also support the hypothesis that ZNF408 acts in concert with other molecules to regulate gene expression instead of directly binding to its target genes. Further investigation on ZNF408 interacting partners will enable a more detailed understanding of the mechanism by which this protein regulates gene expression.

The data obtained in our ChIP-Seq experiment showed ZNF408 binding sites near two differentially regulated genes which are relevant to the development of vasculature, namely *HMOX1* and *ITGA4*. *HMOX1* encodes for heme oxygenase 1 (HO-1), which is an enzyme that catalyzes the conversion of heme into carbon

monoxide, free iron, and biliverdin. HO-1 has a dual role in the development of blood vessels, in which its activation is required in vascular endothelial growth factor (VEGF)-induced angiogenesis, while its inhibition promotes inflammatory angiogenesis (reviewed in [40, 41]). Overexpression of wild-type ZNF408 in HUVEC resulted in an upregulation of *HMOX1*. Interestingly, overexpression of *HMOX1* inhibits the expression of VCAM-1, a cell adhesion molecule that, together with its receptor α4 integrin (the protein encoded by *ITGA4*), mediates TNFα-induced angiogenesis [40, 42]. Induction of VCAM-1 expression by TNFα during inflammation triggers leukocyte migration through the cell junctions, which subsequently may lead to endothelial cell barrier breakdown [43, 44]. Blockade of α4 integrin has been shown to reduce leukocyte adhesion, and thereby prevent vascular leakage in a diabetic retinopathy model [45]. The overexpression of wild-type ZNF408 also resulted in a downregulation of *ITGA4*, *VCAM1*, and of genes associated to leukocyte migration, whilst their expression was de-regulated by the p.His455Tyr mutation. This suggests an involvement of ZNF408 in protecting the endothelial cell barrier, thereby preventing vascular leakage. Additionally, binding of ZNF408 to the proximity of *ITGA4*, but not *HMOX1*, was further validated by a transactivation assay in HEK293T cells. This indicates that ZNF408 represses the expression of *ITGA4* by binding directly to its TSS, whereas *HMOX1* activation is more likely due to an indirect effect of ZNF408 overexpression.

Mutations in *ZNF408* have also been reported in retinitis pigmentosa (RP), another type of inherited visual impairment in which the patients suffer from photoreceptor degeneration [46]. Immunohistochemistry revealed that ZNF408 is expressed in both retinal vasculature as well as the photoreceptor layer of the human retina [46]. The hypothesis that ZNF408 works together with other molecules to regulate gene expression may contribute to distinct phenotypes that can result from different *ZNF408* mutations. However, it remains unclear what determines the exact outcome of the different mutations, as those reported in both FEVR and RP are spread throughout the gene [10, 46-49], implying that there is not yet a clear correlation between the exact position of the mutation and the corresponding phenotype.

In summary, the results obtained in this study indicate that ZNF408 is involved in the regulation of genes involved in the development of vasculature as well as other biological processes. Our data also imply that ZNF408 mainly acts in

concert with other molecules to regulate gene expression. This process is clearly disrupted by the FEVR-associated p.His455Tyr mutation, leading to the observed cellular phenotype, and thereby increases our understanding on the molecular mechanisms underlying *ZNF408*-associated vitreoretinopathy.

Acknowledgements

We would like to thank William Leenders for providing the HUVEC used in this study, Martin Oti for helpful discussions on data analysis, Simon van Heeringen for helpful discussions on motif finding, Bert van den Heuvel for providing endothelial cell RNA, as well as Saskia van der Velde-Visser and Marlie Jacobs-Camps for cell culture assistance.

Funding

This work is funded by a Radboudumc PhD Grant to Dyah W. Karjosukarso.

Conflict of interest

The authors declare no conflict of interest.

References

1. Criswick VG, Schepens CL (1969) Familial exudative vitreoretinopathy. *American journal of ophthalmology* **68:** 578-594
2. Canny CL, Oliver GL (1976) Fluorescein angiographic findings in familial exudative vitreoretinopathy. *Archives of ophthalmology* **94:** 1114-1120
3. Miyakubo H, Hashimoto K, Miyakubo S (1984) Retinal vascular pattern in familial exudative vitreoretinopathy. *Ophthalmology* **91:** 1524-1530
4. Miyakubo H, Inohara N, Hashimoto K (1982) Retinal involvement in familial exudative vitreoretinopathy. *Ophthalmologica. Journal international d'ophtalmologie. International journal of ophthalmology. Zeitschrift fur Augenheilkunde* **185:** 125-135
5. Chen ZY, Battinelli EM, Fielder A, Bundey S, Sims K, Breakefield XO, Craig IW (1993) A mutation in the Norrie disease gene (NDP) associated with X-linked familial exudative vitreoretinopathy. *Nature genetics* **5:** 180-183
6. Toomes C, Bottomley HM, Jackson RM, Towns KV, Scott S, Mackey DA, Craig JE, Jiang L, Yang Z, Trembath R, *et al.* (2004) Mutations in LRP5 or FZD4 underlie the common familial exudative vitreoretinopathy locus on chromosome 11q. *American journal of human genetics* **74:** 721-730
7. Robitaille J, MacDonald ML, Kaykas A, Sheldahl LC, Zeisler J, Dube MP, Zhang LH, Singaraja RR, Guernsey DL, Zheng B, *et al.* (2002) Mutant frizzled-4 disrupts retinal angiogenesis in familial exudative vitreoretinopathy. *Nature genetics* **32:** 326-330
8. Nikopoulos K, Gilissen C, Hoischen A, van Nouhuys CE, Boonstra FN, Blokland EA, Arts P, Wieskamp N, Strom TM, Ayuso C, *et al.* (2010) Next-generation sequencing of a 40 Mb linkage interval reveals TSPAN12 mutations in patients with familial exudative vitreoretinopathy. *American journal of human genetics* **86:** 240-247
9. Jiao X, Ventruto V, Trese MT, Shastry BS, Hejtmancik JF (2004) Autosomal recessive familial exudative vitreoretinopathy is associated with mutations in LRP5. *American journal of human genetics* **75:** 878-884
10. Collin RW, Nikopoulos K, Dona M, Gilissen C, Hoischen A, Boonstra FN, Poulter JA, Kondo H, Berger W, Toomes C, *et al.* (2013) *ZNF408* is mutated in familial exudative vitreoretinopathy and is crucial for the development of zebrafish retinal vasculature. *Proceedings of the National Academy of Sciences of the United States of America* **110:** 9856-9861
11. Kondo H, Matsushita I, Tahira T, Uchio E, Kusaka S (2016) Mutations in ATOH7 gene in patients with nonsyndromic congenital retinal nonattachment and familial exudative vitreoretinopathy. *Ophthalmic genetics* **37:** 462-464
12. Wu JH, Liu JH, Ko YC, Wang CT, Chung YC, Chu KC, Liu TT, Chao HM, Jiang YJ, Chen SJ, *et al.* (2016) Haploinsufficiency of RCBTB1 is associated with Coats disease and familial exudative vitreoretinopathy. *Human molecular genetics* **25:** 1637-1647
13. Dixon MW, Stem MS, Schuette JL, Keegan CE, Besirli CG (2016) CTNNB1 mutation associated with familial exudative vitreoretinopathy (FEVR) phenotype. *Ophthalmic genetics*, 10.3109/13816810.2015.11203181-3
14. Panagiotou ES, Sanjurjo Soriano C, Poulter JA, Lord EC, Dzulova D, Kondo H, Hiyoshi A, Chung BH, Chu YW, Lai CHY, *et al.* (2017) Defects in the Cell Signaling Mediator beta-Catenin Cause the Retinal Vascular Condition FEVR. *American journal of human genetics* **100:** 960-968
15. Nikopoulos K, Venselaar H, Collin RW, Riveiro-Alvarez R, Boonstra FN, Hooymans JM, Mukhopadhyay A, Shears D, van Bers M, de Wijs IJ, *et al.* (2010) Overview of the mutation spectrum in familial exudative vitreoretinopathy and Norrie disease with identification of 21 novel variants in FZD4, LRP5, and NDP. *Human mutation* **31:** 656-666
16. Boonstra FN, van Nouhuys CE, Schuil J, de Wijs IJ, van der Donk KP, Nikopoulos K, Mukhopadhyay A, Scheffer H, Tilanus MA, Cremers FP, *et al.* (2009) Clinical and molecular evaluation of probands and family members with familial exudative vitreoretinopathy. *Investigative ophthalmology & visual science* **50:** 4379-4385
17. Fog CK, Galli GG, Lund AH (2012) PRDM proteins: important players in differentiation and disease. *Bioessays* **34:** 50-60

18. Hohenauer T, Moore AW (2012) The Prdm family: expanding roles in stem cells and development. *Development* **139:** 2267-2282
19. Suter DM, Cartier L, Bettiol E, Tirefort D, Jaconi ME, Dubois-Dauphin M, Krause KH (2006) Rapid generation of stable transgenic embryonic stem cell lines using modular lentivectors. *Stem cells* **24:** 615-623
20. Kouwenhoven EN, Oti M, Niehues H, van Heeringen SJ, Schalkwijk J, Stunnenberg HG, van Bokhoven H, Zhou H (2015) Transcription factor p63 bookmarks and regulates dynamic enhancers during epidermal differentiation. *EMBO reports* **16:** 863-878
21. Dobin A, Davis CA, Schlesinger F, Drenkow J, Zaleski C, Jha S, Batut P, Chaisson M, Gingeras TR (2013) STAR: ultrafast universal RNA-seq aligner. *Bioinformatics* **29:** 15-21
22. Anders S, Pyl PT, Huber W (2015) HTSeq--a Python framework to work with high-throughput sequencing data. *Bioinformatics* **31:** 166-169
23. Love MI, Huber W, Anders S (2014) Moderated estimation of fold change and dispersion for RNA-seq data with DESeq2. *Genome biology* **15:** 550
24. Trapnell C, Roberts A, Goff L, Pertea G, Kim D, Kelley DR, Pimentel H, Salzberg SL, Rinn JL, Pachter L (2012) Differential gene and transcript expression analysis of RNA-seq experiments with TopHat and Cufflinks. *Nat Protoc* **7:** 562-578
25. Huang da W, Sherman BT, Lempicki RA (2009) Systematic and integrative analysis of large gene lists using DAVID bioinformatics resources. *Nature protocols* **4:** 44-57
26. Huang da W, Sherman BT, Zheng X, Yang J, Imamichi T, Stephens R, Lempicki RA (2009) Extracting biological meaning from large gene lists with DAVID. *Current protocols in bioinformatics* **Chapter 13:** Unit 13 11
27. Supek F, Bosnjak M, Skunca N, Smuc T (2011) REVIGO summarizes and visualizes long lists of gene ontology terms. *PLoS One* **6:** e21800
28. Denissov S, van Driel M, Voit R, Hekkelman M, Hulsen T, Hernandez N, Grummt I, Wehrens R, Stunnenberg H (2007) Identification of novel functional TBP-binding sites and general factor repertoires. *The EMBO journal* **26:** 944-954
29. Li H, Durbin R (2009) Fast and accurate short read alignment with Burrows-Wheeler transform. *Bioinformatics* **25:** 1754-1760
30. Zhang Y, Liu T, Meyer CA, Eeckhoute J, Johnson DS, Bernstein BE, Nusbaum C, Myers RM, Brown M, Li W, *et al.* (2008) Model-based analysis of ChIP-Seq (MACS). *Genome biology* **9:** R137
31. McLean CY, Bristor D, Hiller M, Clarke SL, Schaar BT, Lowe CB, Wenger AM, Bejerano G (2010) GREAT improves functional interpretation of cis-regulatory regions. *Nat Biotechnol* **28:** 495-501
32. Arnaoutova I, Kleinman HK (2010) In vitro angiogenesis: endothelial cell tube formation on gelled basement membrane extract. *Nat Protoc* **5:** 628-635
33. Hashimoto G, Inoki I, Fujii Y, Aoki T, Ikeda E, Okada Y (2002) Matrix metalloproteinases cleave connective tissue growth factor and reactivate angiogenic activity of vascular endothelial growth factor 165. *The Journal of biological chemistry* **277:** 36288-36295
34. Augustin HG, Koh GY, Thurston G, Alitalo K (2009) Control of vascular morphogenesis and homeostasis through the angiopoietin-Tie system. *Nat Rev Mol Cell Biol* **10:** 165-177
35. Germain S, Monnot C, Muller L, Eichmann A (2010) Hypoxia-driven angiogenesis: role of tip cells and extracellular matrix scaffolding. *Curr Opin Hematol* **17:** 245-251
36. Gerhardt H, Golding M, Fruttiger M, Ruhrberg C, Lundkvist A, Abramsson A, Jeltsch M, Mitchell C, Alitalo K, Shima D, *et al.* (2003) VEGF guides angiogenic sprouting utilizing endothelial tip cell filopodia. *The Journal of cell biology* **161:** 1163-1177
37. Tammela T, Zarkada G, Wallgard E, Murtomaki A, Suchting S, Wirzenius M, Waltari M, Hellstrom M, Schomber T, Peltonen R, *et al.* (2008) Blocking VEGFR-3 suppresses angiogenic sprouting and vascular network formation. *Nature* **454:** 656-660
38. Iuchi S (2001) Three classes of C2H2 zinc finger proteins. *Cell Mol Life Sci* **58:** 625-635
39. Brayer KJ, Segal DJ (2008) Keep your fingers off my DNA: protein-protein interactions mediated by C2H2 zinc finger domains. *Cell Biochem Biophys* **50:** 111-131
40. Kim YM, Pae HO, Park JE, Lee YC, Woo JM, Kim NH, Choi YK, Lee BS, Kim SR, Chung HT (2011) Heme oxygenase in the regulation of vascular biology: from molecular mechanisms to therapeutic opportunities. *Antioxid Redox Signal* **14:** 137-167

41. Bussolati B, Mason JC (2006) Dual role of VEGF-induced heme-oxygenase-1 in angiogenesis. *Antioxid Redox Signal* **8:** 1153-1163

42. Vanderslice P, Munsch CL, Rachal E, Erichsen D, Sughrue KM, Truong AN, Wygant JN, McIntyre BW, Eskin SG, Tilton RG*, et al.* (1998) Angiogenesis induced by tumor necrosis factor-agr; is mediated by alpha4 integrins. *Angiogenesis* **2:** 265-275

43. Marcos-Ramiro B, Garcia-Weber D, Millan J (2014) TNF-induced endothelial barrier disruption: beyond actin and Rho. *Thrombosis and haemostasis* **112:** 1088-1102

44. Mehta D, Ravindran K, Kuebler WM (2014) Novel regulators of endothelial barrier function. *Am J Physiol Lung Cell Mol Physiol* **307:** L924-935

45. Iliaki E, Poulaki V, Mitsiades N, Mitsiades CS, Miller JW, Gragoudas ES (2009) Role of alpha 4 integrin (CD49d) in the pathogenesis of diabetic retinopathy. *Investigative ophthalmology & visual science* **50:** 4898-4904

46. Avila-Fernandez A, Perez-Carro R, Corton M, Lopez-Molina MI, Campello L, Garanto A, Fernandez-Sanchez L, Duijkers L, Lopez-Martinez MA, Riveiro-Alvarez R*, et al.* (2015) Whole-exome sequencing reveals *ZNF408* as a new gene associated with autosomal recessive retinitis pigmentosa with vitreal alterations. *Human molecular genetics* **24:** 4037-4048

47. Habibi I, Chebil A, Kort F, Schorderet DF, El Matri L (2017) Exome sequencing confirms *ZNF408* mutations as a cause of familial retinitis pigmentosa. *Ophthalmic genetics*, 10.1080/13816810.2016.12750201-4

48. Musada GR, Syed H, Jalali S, Chakrabarti S, Kaur I (2016) Mutation spectrum of the FZD-4, TSPAN12 AND *ZNF408* genes in Indian FEVR patients. *BMC Ophthalmol* **16:** 90

49. Salvo J, Lyubasyuk V, Xu M, Wang H, Wang F, Nguyen D, Wang K, Luo H, Wen C, Shi C*, et al.* (2015) Next-generation sequencing and novel variant determination in a cohort of 92 familial exudative vitreoretinopathy patients. *Investigative ophthalmology & visual science* **56:** 1937-1946

Supplementary materials

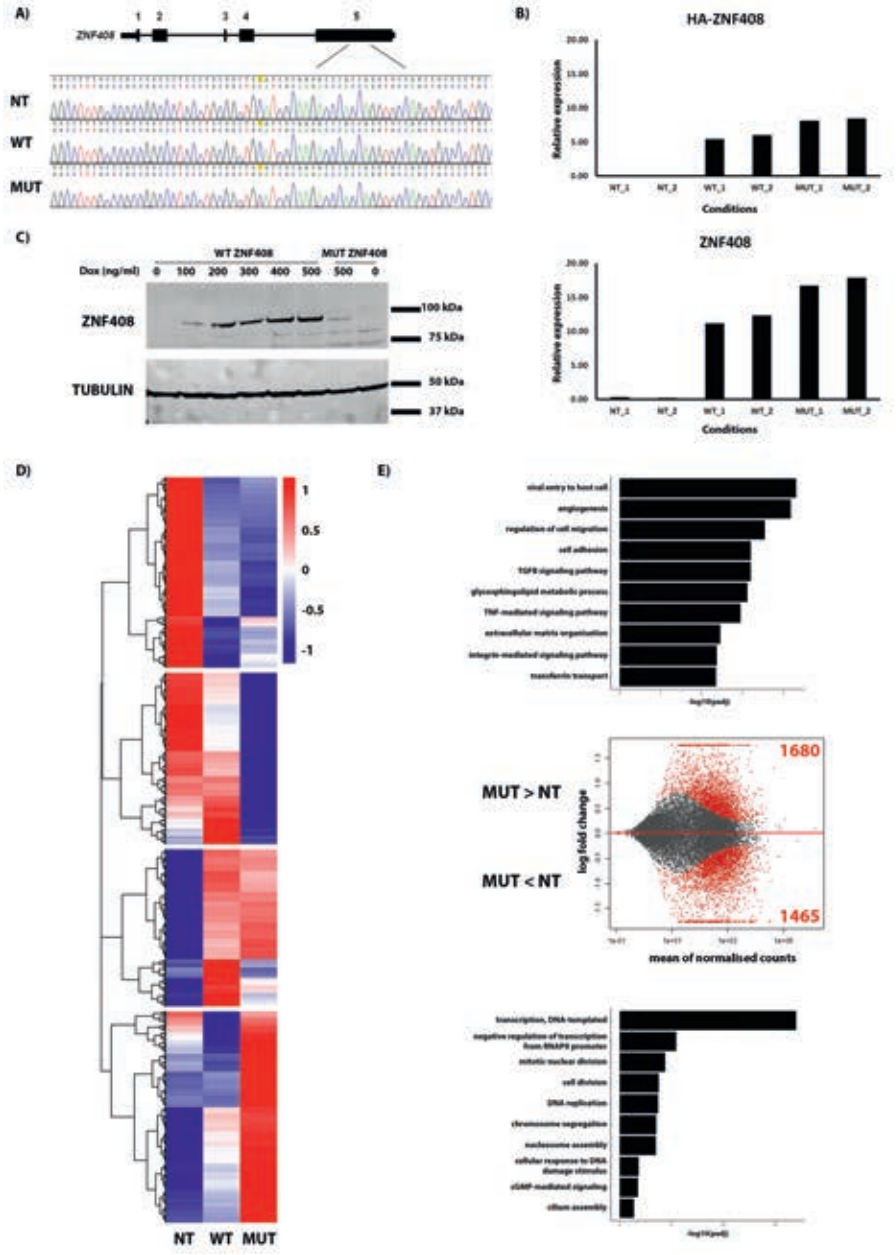

Figure S1. Stable cells validation and the effect of wild-type and p.His455Tyr ZNF408 overexpression to global transcriptome. A) Validation of the generated stable cells at the genomic DNA level. The c.1363C>T (p.His455Tyr) mutation is highlighted in yellow on the chromatogram. The presence of both endogenous and exogenous *ZNF408* results in a heterozygous peak. B) Measurement of *ZNF408* overexpression at RNA level by qPCR. Two biological replicates were tested separately (denoted as 1 and 2) and the depicted expression is relative to the housekeeping gene (*GUSB*). Primers targeting *HA-ZNF408* transgene (upper

panel) and endogenous *ZNF408* (lower panel) were used. C) Western blot analysis of ZNF408 overexpression. WT cells were induced with different doses of doxycycline to determine the dose required to have equal expression level of wild-type and p.His455Tyr ZNF408 protein. D) Heatmap of differentially expressed genes between the three conditions. Two biological replicates of each condition were included in the analysis. The z-score was calculated from the FPKM value of each gene. E) MA-plot of the differential expression analysis, comparing MUT to NT. Red dots represent genes with differential expression between the two conditions compared, black dots represent no difference in expression. The number of genes with significant difference in expression is depicted on the corner of the plot. The top 10 biological process GO-terms of genes belonging to the upper and lower part of the MA-plot are depicted above and below the MA-plot, respectively. The p-values were adjusted using the Benjamini-Hochberg method.

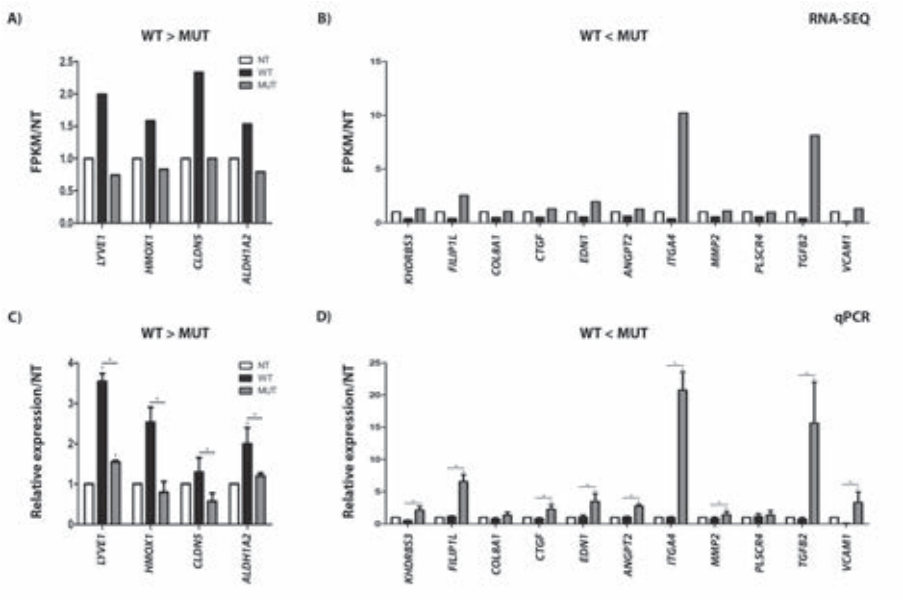

Figure S2. The expression of genes relevant to angiogenesis process detected by RNA-Seq (A and B) and qPCR (C and D). The expression of genes detected by RNA-Seq is depicted in FPKM values relative to NT condition (NT = 1). The gene expression detected by qPCR is also shown relative to NT condition (NT = 1). Error bars in c) and d) represent standard deviation of three biological replicates. Significance is illustrated with *(p-value < 0.05).

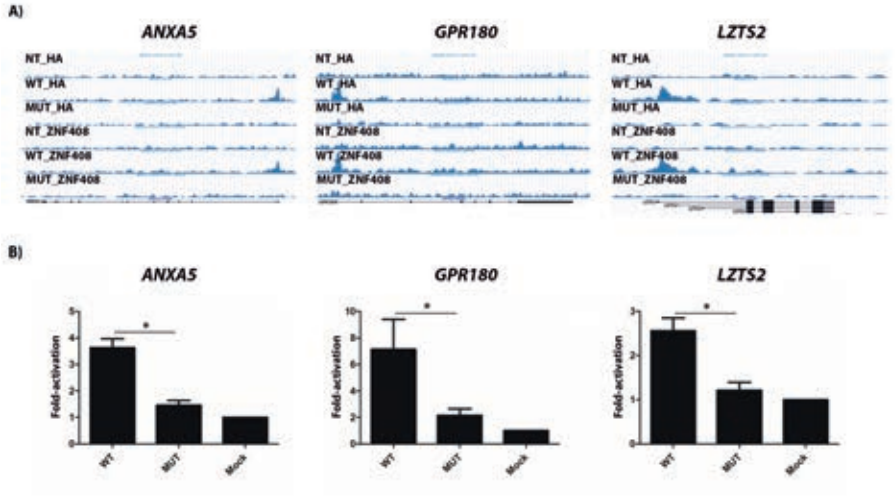

Figure S3. Validation of p.His455Tyr ZNF408 reduced DNA-binding ability by transactivation assay. A) Screenshot of UCSC Genome Browser track of example ChIP peaks. B) Fold-activation of transcription detected in luciferase-based transactivation assay. The fold-activation of WT and MUT is relative to mock. Error bars denote standard deviation of three biological replicates. Significance is illustrated with * (p-value < 0.05).

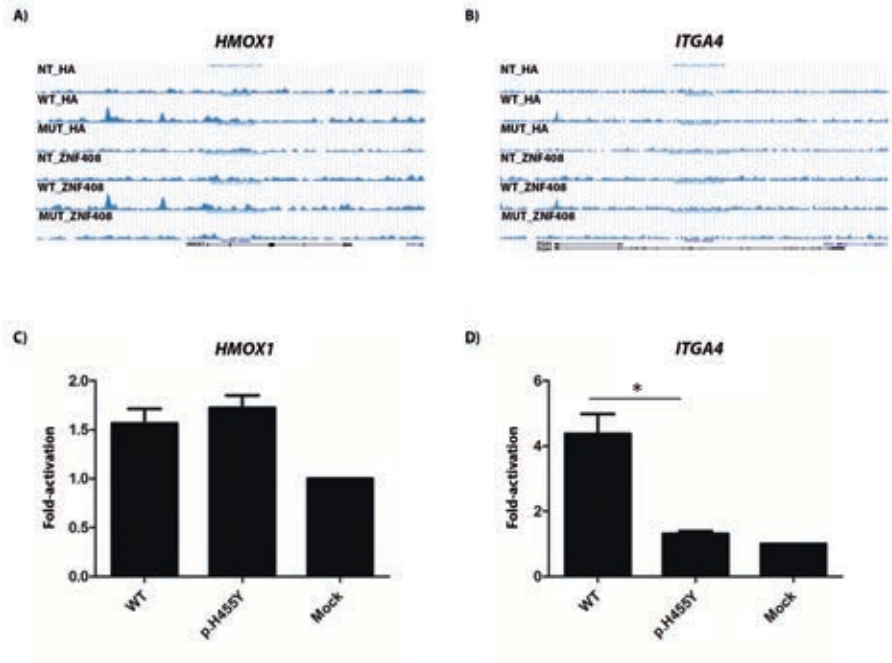

Figure S4. Validation of ZNF408 binding to a locus near *HMOX1* and *ITGA4*. A) and B) Screenshot of UCSC Genome Browser track of wild-type ZNF408 binding in the proximity of *HMOX1* and *ITGA4*, respectively. Antibody targeting ZNF408 was used for immunoprecipitation. Error bars represent standard deviation of two biological replicates. C) and D) Fold-activation of transcription detected in luciferase-based transactivation assay. The fold-activation of WT and MUT is relative to mock. Error bars denote standard deviation of three biological replicates. Significance is illustrated with * (p-value < 0.05).

Table S1 Primer list

Target	Sequence (5'- 3')
qPCR_*LYVE1*_Forward	TTTGGAAGGTTCCAGTGAGC
qPCR_*LYVE1*_Reverse	GAATATGGGATCTTTGGTGGTG
qPCR_*HMOX1*_Forward	CTTTCAGAAGGGCCAGGTG
qPCR_*HMOX1*_Reverse	GTAGACAGGGGCGAAGACTG
qPCR_*CLDN5*_Forward	CCTTCCTGGACCACAACATC
qPCR_*CLDN5*_Reverse	ACCGAGTCGTACACTTTGCAC
qPCR_*ALDH1A2*_Forward	ATGATATGCGGATTGCCAAG
qPCR_*ALDH1A2*_Reverse	CAGCTGCTACGAGTCCAAAG
qPCR_*KHDRBS3*_Forward	TGAAGCTGGGACAGAAAGTG
qPCR_*KHDRBS3*_Reverse	AACCTTTCCCAAGGATGGAC
qPCR_*FILIP1L*_Forward	AACGCTGGTATCATGGCTGAA
qPCR_*FILIP1L*_Reverse	ATCTCTTGCACTGCTCCTCCATT
qPCR_*COL8A1*_Forward	TGGCAAAGAGTATCCACACC
qPCR_*COL8A1*_Reverse	TTGTTCCCCTCGTAAACTGG
qPCR_*CTGF*_Forward	GCAGGCTAGAGAAGCAGAGC
qPCR_*CTGF*_Reverse	TGGAGATTTTGGGAGTACGG
qPCR_*EDN1*_Forward	ACTTCTGCCACCTGGACATC
qPCR_*EDN1*_Reverse	GGCATCTATTTTCACGGTCTG
qPCR_*ANGPT2*_Forward	AGGGACAAACCTGTTGAACC
qPCR_*ANGPT2*_Reverse	TTGTCGAGAGGGAGTGTTCC
qPCR_*ITGA4*_Forward	ACCTCAATGCAGATGGCTTC
qPCR_*ITGA4*_Reverse	ACGAGGTTTGTTTCCATTGC
qPCR_*MMP2*_Forward	GAGAAGGATGGCAAGTACGG
qPCR_*MMP2*_Reverse	CATAGGATGTGCCCTGGAAG
qPCR_*PLSCR4*_Forward	ACAGCCTGCAGGTGAAATG
qPCR_*PLSCR4*_Reverse	TGGGTAGCCAGTAGGTGGAG
qPCR_*TGFB2*_Forward	AGCCAGAGTGCCTGAACAAC
qPCR_*TGFB2*_Reverse	ACATCGAAGGAGAGCCATTC
qPCR_*VCAM1*_Forward	GGCAGGCTGTAAAAGAATTGC
qPCR_*VCAM1*_Reverse	TTCTTGCAGCTTTGTGGATG
qPCR_*GUSB*_Forward	AGAGTGGTGCTGAGGATTGG
qPCR_*GUSB*_Reverse	CCCTCATGCTCTAGCGTGTC
gDNA_*ZNF408*_Forward	CCTGGCCAAGAAGTTACACAG
gDNA_*ZNF408*_Reverse	TTTCTCCTGTATGGAGCCTCA
qPCR_*ZNF408*_Forward	GAGGAGTCTGCCTCCAAGG
qPCR_*ZNF408*_Reverse	CCAGCCAGAACTCTGCTCAC
qPCR_*HA-ZNF408*_Forward	TTACGATGTACCGGATTACGC
qPCR_*HA-ZNF408*_Reverse	CGGAAGGGTTCCATCCTAAG

Table S2 Genes that are upregulated in WT, but not in MUT

Ensembl ID	Symbol	Ensembl ID	Symbol	Ensembl ID	Symbol
ENSG00000135451	*TROAP*	ENSG00000276410	*HIST1H2BB*	ENSG00000185130	*HIST1H2BL*
ENSG00000197182	*MIR4763*	ENSG00000100292	*HMOX1*	ENSG00000274290	*HIST1H2BE*
ENSG00000127528	*KLF2*	ENSG00000184270	*HIST2H2AB*	ENSG00000275713	*HIST1H2BH*
ENSG00000013810	*TACC3*	ENSG00000079616	*KIF22*	ENSG00000278588	*HIST1H2BI*
ENSG00000233922	*LOC105372840*	ENSG00000171345	*KRT19*	ENSG00000111665	*CDCA3*
ENSG00000133800	*LYVE1*	ENSG00000197182	*MIRLET7BHG*	ENSG00000274641	*HIST1H2BO*
ENSG00000122952	*ZWINT*	ENSG00000197182	*MIRLET7A3*	ENSG00000275714	*HIST1H3A*
ENSG00000146670	*CDCA5*	ENSG00000197182	*MIRLET7B*	ENSG00000278272	*HIST1H3C*
ENSG00000104147	*OIP5*	ENSG00000164109	*MAD2L1*	ENSG00000275379	*HIST1H3I*
ENSG00000162639	*HENMT1*	ENSG00000073111	*MCM2*	ENSG00000273983	*HIST1H3G*
ENSG00000163923	*RPL39L*	ENSG00000100297	*MCM5*	ENSG00000197153	*HIST1H3J*
ENSG00000197837	*HIST4H4*	ENSG00000166508	*MCM7*	ENSG00000278828	*HIST1H3H*
ENSG00000181885	*CLDN7*	ENSG00000085840	*ORC1*	ENSG00000274267	*HIST1H3B*
ENSG00000165071	*TMEM71*	ENSG00000131153	*GINS2*	ENSG00000278637	*HIST1H4A*
ENSG00000188643	*S100A16*	ENSG00000197594	*ENPP1*	ENSG00000197061	*HIST1H4C*
ENSG00000101331	*CCM2L*	ENSG00000166851	*PLK1*	ENSG00000158406	*HIST1H4H*
ENSG00000161888	*SPC24*	ENSG00000102575	*ACP5*	ENSG00000167747	*C19orf48*
ENSG00000186281	*GPAT2*	ENSG00000129195	*FAM64A*	ENSG00000274997	*HIST1H2AH*
ENSG00000123977	*DAW1*	ENSG00000134690	*CDCA8*	ENSG00000118640	*VAMP8*
ENSG00000204161	*C10orf128*	ENSG00000105011	*ASF1B*	ENSG00000157873	*TNFRSF14*
ENSG00000130511	*SSBP4*	ENSG00000035499	*DEPDC1B*	ENSG00000128918	*ALDH1A2*
ENSG00000140873	*ADAMTS18*	ENSG00000163638	*ADAMTS9*	ENSG00000134057	*CCNB1*
ENSG00000090776	*EFNB1*	ENSG00000171848	*RRM2*	ENSG00000277775	*HIST1H3F*
ENSG00000175899	*A2M*	ENSG00000127586	*CHTF18*	ENSG00000196787	*HIST1H2AG*
ENSG00000163584	*RPL22L1*	ENSG00000186283	*TOR3A*	ENSG00000124635	*HIST1H2BJ*
ENSG00000144554	*FANCD2*	ENSG00000110080	*ST3GAL4*	ENSG00000119333	*WDR34*
ENSG00000184232	*OAF*	ENSG00000183598	*HIST2H3D*	ENSG00000162063	*CCNF*
ENSG00000161513	*FDXR*	ENSG00000252481	*SCARNA13*	ENSG00000110711	*AIP*
ENSG00000168496	*FEN1*	ENSG00000159167	*STC1*	ENSG00000178999	*AURKB*
ENSG00000001561	*ENPP4*	ENSG00000137310	*TCF19*	ENSG00000071539	*TRIP13*
ENSG00000100304	*TTLL12*	ENSG00000270141	*TERC*	ENSG00000158859	*ADAMTS4*
ENSG00000179604	*CDC42EP4*	ENSG00000167900	*TK1*	ENSG00000100034	*PPM1F*
ENSG00000186994	*KANK3*	ENSG00000184113	*CLDN5*	ENSG00000135476	*ESPL1*
ENSG00000164087	*POC1A*	ENSG00000176890	*TYMS*	ENSG00000007312	*CD79B*
ENSG00000107719	*PALD1*	ENSG00000100162	*CENPM*	ENSG00000166803	*KIAA0101*
ENSG00000161800	*RACGAP1*	ENSG00000131652	*THOC6*	ENSG00000117399	*CDC20*
ENSG00000276043	*UHRF1*	ENSG00000171241	*SHCBP1*	ENSG00000100918	*REC8*
ENSG00000160447	*PKN3*	ENSG00000276180	*HIST1H4I*	ENSG00000198327	NA
ENSG00000124575	*HIST1H1D*	ENSG00000093009	*CDC45*	ENSG00000124529	NA
ENSG00000184357	*HIST1H1B*	ENSG00000196747	*HIST1H2AI*	ENSG00000259001	NA
ENSG00000277075	*HIST1H2AE*	ENSG00000276903	*HIST1H2AL*	ENSG00000267325	NA
ENSG00000164032	*H2AFZ*	ENSG00000278463	*HIST1H2AB*		

Table S3 **Genes that are downregulated in WT, but not in MUT**

Ensembl ID	Symbol	Ensembl ID	Symbol	Ensembl ID	Symbol
ENSG00000227124	*ZNF717*	ENSG00000115457	*IGFBP2*	ENSG00000169439	*SDC2*
ENSG00000139187	*KLRG1*	ENSG00000163453	*IGFBP7*	ENSG00000154864	*PIEZO2*
ENSG00000131773	*KHDRBS3*	ENSG00000122641	*INHBA*	ENSG00000214944	*ARHGEF28*
ENSG00000168386	*FILIP1L*	ENSG00000117595	*IRF6*	ENSG00000143429	*LOC645166*
ENSG00000180787	*ZFP3*	ENSG00000115232	*ITGA4*	ENSG00000206432	*TMEM200C*
ENSG00000144810	*COL8A1*	ENSG00000206538	*VGLL3*	ENSG00000196632	*WNK3*
ENSG00000111799	*COL12A1*	ENSG00000156466	*GDF6*	ENSG00000189223	*PAX8-AS1*
ENSG00000164318	*EGFLAM*	ENSG00000095015	*MAP3K1*	ENSG00000144681	*STAC*
ENSG00000139971	*C14orf37*	ENSG00000170430	*MGMT*	ENSG00000130303	*BST2*
ENSG00000118523	*CTGF*	ENSG00000087245	*MMP2*	ENSG00000092969	*TGFB2*
ENSG00000143869	*GDF7*	ENSG00000198938	*COX3*	ENSG00000162692	*VCAM1*
ENSG00000198947	*DMD*	ENSG00000198727	*CYTB*	ENSG00000147180	*ZNF711*
ENSG00000183044	*ABAT*	ENSG00000198840	*ND3*	ENSG00000075785	*RAB7A*
ENSG00000078401	*EDN1*	ENSG00000086991	*NOX4*	ENSG00000129680	*MAP7D3*
ENSG00000123572	*NRK*	ENSG00000124785	*NRN1*	ENSG00000175471	*MCTP1*
ENSG00000225383	*SFTA1P*	ENSG00000154678	*PDE1C*	ENSG00000122786	*CALD1*
ENSG00000148218	*ALAD*	ENSG00000184588	*PDE4B*	ENSG00000138759	*FRAS1*
ENSG00000165092	*ALDH1A1*	ENSG00000057294	*PKP2*	ENSG00000118473	*SGIP1*
ENSG00000177409	*SAMD9L*	ENSG00000128567	*PODXL*	ENSG00000184384	*MAML2*
ENSG00000083857	*FAT1*	ENSG00000170891	*CYTL1*	ENSG00000154556	*SORBS2*
ENSG00000184254	*ALDH1A3*	ENSG00000196368	*NUDT11*	ENSG00000102802	*MEDAG*
ENSG00000146555	*SDK1*	ENSG00000022556	*NLRP2*	ENSG00000180543	*TSPYL5*
ENSG00000189134	*NKAPL*	ENSG00000198185	*ZNF334*	ENSG00000138735	*PDE5A*
ENSG00000179399	*GPC5*	ENSG00000114698	*PLSCR4*	ENSG00000133101	*CCNA1*
ENSG00000162631	*NTNG1*	ENSG00000134247	*PTGFRN*	ENSG00000003096	*KLHL13*
ENSG00000115414	*FN1*	ENSG00000095303	*PTGS1*	ENSG00000162614	*NEXN*
ENSG00000118407	*FILIP1*	ENSG00000136383	*ALPK3*	ENSG00000128487	*SPECC1*
ENSG00000118946	*PCDH17*	ENSG00000138771	*SHROOM3*	ENSG00000170160	*CCDC144A*
ENSG00000177990	*DPY19L2*	ENSG00000105426	*PTPRS*	ENSG00000184867	*ARMCX2*
ENSG00000091879	*ANGPT2*	ENSG00000148143	*ZNF462*	ENSG00000228495	NA
ENSG00000095951	*HIVEP1*	ENSG00000169213	*RAB3B*	ENSG00000205664	NA
ENSG00000180806	*HOXC9*	ENSG00000114200	*BCHE*	ENSG00000226702	NA
ENSG00000147036	*LANCL3*	ENSG00000074527	*NTN4*	ENSG00000237973	NA
ENSG00000140443	*IGF1R*	ENSG00000126950	*TMEM35A*	ENSG00000254635	NA

Table S4 Top 1000 genes on principal component 1 and 2 axis

Principal Component 1		Principal Component 2	
Ensembl ID	Symbol	Ensembl ID	Symbol
ENSG00000170558	*CDH2*	ENSG00000170558	*CDH2*
ENSG00000234420	*ZNF37BP*	ENSG00000136560	*TANK*
ENSG00000204767	*FAM196B*	ENSG00000198865	*CCDC152*
ENSG00000221676	*RNU6ATAC*	ENSG00000255737	*AGAP2-AS1*
ENSG00000234456	*MAGI2-AS3*	ENSG00000205078	*SYCE1L*
ENSG00000204520	*MICA*	ENSG00000227124	*ZNF717*
ENSG00000113810	*SMC4*	ENSG00000221676	*RNU6ATAC*
ENSG00000025434	*NR1H3*	ENSG00000135451	*TROAP*
ENSG00000254986	*DPP3*	ENSG00000260260	*SNHG19*
ENSG00000113163	*COL4A3BP*	ENSG00000025434	*NR1H3*
ENSG00000140937	*CDH11*	ENSG00000230630	*DNM3OS*
ENSG00000241553	*ARPC4*	ENSG00000184281	*TSSC4*
ENSG00000140391	*TSPAN3*	ENSG00000140937	*CDH11*
ENSG00000188042	*ARL4C*	ENSG00000140945	*CDH13*
ENSG00000122644	*ARL4A*	ENSG00000127914	*AKAP9*
ENSG00000073910	*FRY*	ENSG00000245648	*LOC101928100*
ENSG00000139679	*LPAR6*	ENSG00000235448	*LURAP1L-AS1*
ENSG00000245648	*LOC101928100*	ENSG00000123136	*DDX39A*
ENSG00000227517	*LINC01483*	ENSG00000139187	*KLRG1*
ENSG00000235448	*LURAP1L-AS1*	ENSG00000128606	*LRRC17*
ENSG00000064989	*CALCRL*	ENSG00000070404	*FSTL3*
ENSG00000105810	*CDK6*	ENSG00000123080	*CDKN2C*
ENSG00000105355	*PLIN3*	ENSG00000100526	*CDKN3*
ENSG00000136158	*SPRY2*	ENSG00000264462	*MIR3648-2*
ENSG00000124762	*CDKN1A*	ENSG00000107833	*NPM3*
ENSG00000131477	*RAMP2*	ENSG00000127528	*KLF2*
ENSG00000111276	*CDKN1B*	ENSG00000164442	*CITED2*
ENSG00000070404	*FSTL3*	ENSG00000075213	*SEMA3A*
ENSG00000103266	*STUB1*	ENSG00000188229	*TUBB4B*
ENSG00000147889	*CDKN2A*	ENSG00000101335	*MYL9*
ENSG00000147883	*CDKN2B*	ENSG00000064225	*ST3GAL6*
ENSG00000174130	*TLR6*	ENSG00000080986	*NDC80*
ENSG00000154258	*ABCA9*	ENSG00000104324	*CPQ*
ENSG00000264462	*MIR3648-2*	ENSG00000134215	*VAV3*
ENSG00000141338	*ABCA8*	ENSG00000130204	*TOMM40*
ENSG00000164442	*CITED2*	ENSG00000013810	*TACC3*
ENSG00000124406	*ATP8A1*	ENSG00000250508	*LOC105369364*
ENSG00000101335	*MYL9*	ENSG00000233922	*LOC105372840*
ENSG00000080986	*NDC80*	ENSG00000105404	*RABAC1*
ENSG00000104324	*CPQ*	ENSG00000184990	*SIVA1*
ENSG00000137693	*YAP1*	ENSG00000086504	*MRPL28*
ENSG00000134375	*TIMM17A*	ENSG00000135624	*CCT7*
ENSG00000106400	*ZNHIT1*	ENSG00000115163	*CENPA*

Table S4 continued

Principal Component 1		Principal Component 2	
Ensembl ID	Symbol	Ensembl ID	Symbol
ENSG00000131236	*CAP1*	ENSG00000183751	*TBL3*
ENSG00000107175	*CREB3*	ENSG00000076382	*SPAG5*
ENSG00000108828	*VAT1*	ENSG00000113356	*POLR3G*
ENSG00000257219	*LOC105369848*	ENSG00000133110	*POSTN*
ENSG00000254486	*LOC105376554*	ENSG00000111247	*RAD51AP1*
ENSG00000136938	*ANP32B*	ENSG00000131773	*KHDRBS3*
ENSG00000151640	*DPYSL4*	ENSG00000048740	*CELF2*
ENSG00000184470	*TXNRD2*	ENSG00000051341	*POLQ*
ENSG00000138778	*CENPE*	ENSG00000142731	*PLK4*
ENSG00000113356	*POLR3G*	ENSG00000132970	*WASF3*
ENSG00000265972	*TXNIP*	ENSG00000173083	*HPSE*
ENSG00000117724	*CENPF*	ENSG00000183207	*RUVBL2*
ENSG00000133110	*POSTN*	ENSG00000133800	*LYVE1*
ENSG00000167642	*SPINT2*	ENSG00000148671	*ADIRF*
ENSG00000253522	*MIR3142HG*	ENSG00000143554	*SLC27A3*
ENSG00000077514	*POLD3*	ENSG00000142945	*KIF2C*
ENSG00000185737	*NRG3*	ENSG00000175602	*CCDC85B*
ENSG00000132970	*WASF3*	ENSG00000099203	*TMED1*
ENSG00000170271	*FAXDC2*	ENSG00000123124	*WWP1*
ENSG00000173083	*HPSE*	ENSG00000175063	*UBE2C*
ENSG00000125966	*MMP24*	ENSG00000164283	*ESM1*
ENSG00000104356	*POP1*	ENSG00000070778	*PTPN21*
ENSG00000213190	*MLLT11*	ENSG00000138080	*EMILIN1*
ENSG00000136026	*CKAP4*	ENSG00000053254	*FOXN3*
ENSG00000118508	*RAB32*	ENSG00000122952	*ZWINT*
ENSG00000139278	*GLIPR1*	ENSG00000169306	*IL1RAPL1*
ENSG00000243244	*STON1*	ENSG00000173598	*NUDT4*
ENSG00000080561	*MID2*	ENSG00000168309	*FAM107A*
ENSG00000119397	*CNTRL*	ENSG00000170955	*PRKCDBP*
ENSG00000091428	*RAPGEF4*	ENSG00000168386	*FILIP1L*
ENSG00000276023	*DUSP14*	ENSG00000222041	*CYTOR*
ENSG00000162616	*DNAJB4*	ENSG00000135324	*MRAP2*
ENSG00000164283	*ESM1*	ENSG00000137491	*SLCO2B1*
ENSG00000150687	*PRSS23*	ENSG00000146670	*CDCA5*
ENSG00000138738	*PRDM5*	ENSG00000104147	*OIP5*
ENSG00000138080	*EMILIN1*	ENSG00000138435	*CHRNA1*
ENSG00000026950	*BTN3A1*	ENSG00000247596	*TWF2*
ENSG00000136504	*KAT7*	ENSG00000162639	*HENMT1*
ENSG00000164985	*PSIP1*	ENSG00000207445	*SNORD15B*
ENSG00000160326	*SLC2A6*	ENSG00000164796	*CSMD3*
ENSG00000090376	*IRAK3*	ENSG00000156804	*FBXO32*
ENSG00000139629	*GALNT6*	ENSG00000157657	*ZNF618*
ENSG00000166073	*GPR176*	ENSG00000144741	*SLC25A26*

Table S4 continued

Principal Component 1		Principal Component 2	
Ensembl ID	Symbol	Ensembl ID	Symbol
ENSG00000168386	*FILIP1L*	ENSG00000164932	*CTHRC1*
ENSG00000222041	*CYTOR*	ENSG00000150551	*LYPD1*
ENSG00000135324	*MRAP2*	ENSG00000183617	*MRPL54*
ENSG00000161013	*MGAT4B*	ENSG00000163923	*RPL39L*
ENSG00000011009	*LYPLA2*	ENSG00000132622	*HSPA12B*
ENSG00000105669	*COPE*	ENSG00000156398	*SFXN2*
ENSG00000138435	*CHRNA1*	ENSG00000197837	*HIST4H4*
ENSG00000074416	*MGLL*	ENSG00000151136	*BTBD11*
ENSG00000247596	*TWF2*	ENSG00000151572	*ANO4*
ENSG00000164796	*CSMD3*	ENSG00000180787	*ZFP3*
ENSG00000166897	*ELFN2*	ENSG00000202198	*RN7SK*
ENSG00000164484	*TMEM200A*	ENSG00000161677	*JOSD2*
ENSG00000079156	*OSBPL6*	ENSG00000161618	*ALDH16A1*
ENSG00000156804	*FBXO32*	ENSG00000164692	*COL1A2*
ENSG00000178695	*KCTD12*	ENSG00000168542	*COL3A1*
ENSG00000164849	*GPR146*	ENSG00000187498	*COL4A1*
ENSG00000157107	*FCHO2*	ENSG00000183856	*IQGAP3*
ENSG00000186446	*ZNF501*	ENSG00000134871	*COL4A2*
ENSG00000164932	*CTHRC1*	ENSG00000130635	*COL5A1*
ENSG00000166265	*CYYR1*	ENSG00000163092	*XIRP2*
ENSG00000150551	*LYPD1*	ENSG00000144810	*COL8A1*
ENSG00000135842	*FAM129A*	ENSG00000111799	*COL12A1*
ENSG00000132622	*HSPA12B*	ENSG00000065618	*COL17A1*
ENSG00000131584	*ACAP3*	ENSG00000175182	*FAM131A*
ENSG00000131386	*GALNT15*	ENSG00000164509	*IL31RA*
ENSG00000106367	*AP1S1*	ENSG00000164318	*EGFLAM*
ENSG00000178338	*ZNF354B*	ENSG00000197261	*C6orf141*
ENSG00000163297	*ANTXR2*	ENSG00000163751	*CPA3*
ENSG00000120885	*CLU*	ENSG00000109472	*CPE*
ENSG00000139263	*LRIG3*	ENSG00000181885	*CLDN7*
ENSG00000151136	*BTBD11*	ENSG00000155975	*VPS37A*
ENSG00000151572	*ANO4*	ENSG00000165071	*TMEM71*
ENSG00000172590	*MRPL52*	ENSG00000188643	*S100A16*
ENSG00000139926	*FRMD6*	ENSG00000101331	*CCM2L*
ENSG00000167703	*SLC43A2*	ENSG00000179630	*LACC1*
ENSG00000161091	*MFSD12*	ENSG00000139971	*C14orf37*
ENSG00000169991	*IFFO2*	ENSG00000216588	*IGSF23*
ENSG00000197982	*C1orf122*	ENSG00000161888	*SPC24*
ENSG00000164692	*COL1A2*	ENSG00000118523	*CTGF*
ENSG00000187498	*COL4A1*	ENSG00000116761	*CTH*
ENSG00000134871	*COL4A2*	ENSG00000186281	*GPAT2*
ENSG00000130635	*COL5A1*	ENSG00000143869	*GDF7*
ENSG00000204262	*COL5A2*	ENSG00000091986	*CCDC80*

Table S4 continued

Principal Component 1		Principal Component 2	
Ensembl ID	Symbol	Ensembl ID	Symbol
ENSG00000163092	*XIRP2*	ENSG00000256043	*CTSO*
ENSG00000162944	*RFTN2*	ENSG00000180611	*MB21D2*
ENSG00000197467	*COL13A1*	ENSG00000163131	*CTSS*
ENSG00000057019	*DCBLD2*	ENSG00000137075	*RNF38*
ENSG00000145247	*OCIAD2*	ENSG00000122694	*GLIPR2*
ENSG00000151466	*SCLT1*	ENSG00000174899	*PQLC2L*
ENSG00000254535	*PABPC4L*	ENSG00000154639	*CXADR*
ENSG00000164284	*GRPEL2*	ENSG00000178343	*SHISA3*
ENSG00000163751	*CPA3*	ENSG00000008283	*CYB561*
ENSG00000180938	*ZNF572*	ENSG00000051523	*CYBA*
ENSG00000198832	*SELENOM*	ENSG00000196715	*VKORC1L1*
ENSG00000125995	*ROMO1*	ENSG00000184661	*CDCA2*
ENSG00000152404	*CWF19L2*	ENSG00000183354	*KIAA2026*
ENSG00000178882	*RFLNA*	ENSG00000153071	*DAB2*
ENSG00000167767	*KRT80*	ENSG00000196352	*CD55*
ENSG00000198324	*FAM109A*	ENSG00000166750	*SLFN5*
ENSG00000140511	*HAPLN3*	ENSG00000167554	*ZNF610*
ENSG00000038427	*VCAN*	ENSG00000123977	*DAW1*
ENSG00000159176	*CSRP1*	ENSG00000173200	*PARP15*
ENSG00000101439	*CST3*	ENSG00000178175	*ZNF366*
ENSG00000216588	*IGSF23*	ENSG00000204161	*C10orf128*
ENSG00000196659	*TTC30B*	ENSG00000130511	*SSBP4*
ENSG00000164733	*CTSB*	ENSG00000140873	*ADAMTS18*
ENSG00000213160	*KLHL23*	ENSG00000228716	*DHFR*
ENSG00000143869	*GDF7*	ENSG00000147202	*DIAPH2*
ENSG00000091986	*CCDC80*	ENSG00000211448	*DIO2*
ENSG00000180611	*MB21D2*	ENSG00000075711	*DLG1*
ENSG00000163131	*CTSS*	ENSG00000198947	*DMD*
ENSG00000154639	*CXADR*	ENSG00000124721	*DNAH8*
ENSG00000164463	*CREBRF*	ENSG00000115325	*DOK1*
ENSG00000051523	*CYBA*	ENSG00000183044	*ABAT*
ENSG00000153721	*CNKSR3*	ENSG00000113070	*HBEGF*
ENSG00000171115	*GIMAP8*	ENSG00000107404	*DVL1*
ENSG00000168672	*FAM84B*	ENSG00000213694	*S1PR3*
ENSG00000176853	*FAM91A1*	ENSG00000078401	*EDN1*
ENSG00000153071	*DAB2*	ENSG00000136160	*EDNRB*
ENSG00000176438	*SYNE3*	ENSG00000247077	*PGAM5*
ENSG00000176435	*CLEC14A*	ENSG00000237624	*OXCT2P1*
ENSG00000167657	*DAPK3*	ENSG00000090776	*EFNB1*
ENSG00000159640	*ACE*	ENSG00000125266	*EFNB2*
ENSG00000179144	*GIMAP7*	ENSG00000106780	*MEGF9*
ENSG00000181444	*ZNF467*	ENSG00000165244	*ZNF367*
ENSG00000213203	*GIMAP1*	ENSG00000203805	*PLPP4*

Table S4 continued

Principal Component 1		Principal Component 2	
Ensembl ID	Symbol	Ensembl ID	Symbol
ENSG00000172893	*DHCR7*	ENSG00000161996	*WDR90*
ENSG00000211448	*DIO2*	ENSG00000175899	*A2M*
ENSG00000075711	*DLG1*	ENSG00000163584	*RPL22L1*
ENSG00000124721	*DNAH8*	ENSG00000185909	*KLHDC8B*
ENSG00000013563	*DNASE1L1*	ENSG00000159314	*ARHGAP27*
ENSG00000197102	*DYNC1H1*	ENSG00000169689	*CENPX*
ENSG00000119772	*DNMT3A*	ENSG00000169683	*LRRC45*
ENSG00000197635	*DPP4*	ENSG00000074800	*ENO1*
ENSG00000157514	*TSC22D3*	ENSG00000123572	*NRK*
ENSG00000134769	*DTNA*	ENSG00000145242	*EPHA5*
ENSG00000113070	*HBEGF*	ENSG00000225383	*SFTA1P*
ENSG00000120129	*DUSP1*	ENSG00000157554	*ERG*
ENSG00000133740	*E2F5*	ENSG00000148218	*ALAD*
ENSG00000078401	*EDN1*	ENSG00000173153	*ESRRA*
ENSG00000111752	*PHC1*	ENSG00000182197	*EXT1*
ENSG00000125266	*EFNB2*	ENSG00000165092	*ALDH1A1*
ENSG00000106546	*AHR*	ENSG00000144554	*FANCD2*
ENSG00000111145	*ELK3*	ENSG00000078098	*FAP*
ENSG00000158711	*ELK4*	ENSG00000177409	*SAMD9L*
ENSG00000169621	*APLF*	ENSG00000083857	*FAT1*
ENSG00000154240	*CEP112*	ENSG00000107731	*UNC5B*
ENSG00000134531	*EMP1*	ENSG00000184254	*ALDH1A3*
ENSG00000213853	*EMP2*	ENSG00000184232	*OAF*
ENSG00000142227	*EMP3*	ENSG00000172738	*TMEM217*
ENSG00000170006	*TMEM154*	ENSG00000160813	*PPP1R35*
ENSG00000112297	*AIM1*	ENSG00000106009	*BRAT1*
ENSG00000106991	*ENG*	ENSG00000146555	*SDK1*
ENSG00000183323	*CCDC125*	ENSG00000189134	*NKAPL*
ENSG00000116016	*EPAS1*	ENSG00000166924	*NYAP1*
ENSG00000145242	*EPHA5*	ENSG00000161513	*FDXR*
ENSG00000151491	*EPS8*	ENSG00000168496	*FEN1*
ENSG00000213462	*ERV3-1*	ENSG00000138675	*FGF5*
ENSG00000173153	*ESRRA*	ENSG00000179399	*GPC5*
ENSG00000182197	*EXT1*	ENSG00000087303	*NID2*
ENSG00000164251	*F2RL1*	ENSG00000158186	*MRAS*
ENSG00000068366	*ACSL4*	ENSG00000162631	*NTNG1*
ENSG00000078098	*FAP*	ENSG00000001561	*ENPP4*
ENSG00000169710	*FASN*	ENSG00000135299	*ANKRD6*
ENSG00000083857	*FAT1*	ENSG00000141337	*ARSG*
ENSG00000183621	*ZNF438*	ENSG00000118985	*ELL2*
ENSG00000069122	*ADGRF5*	ENSG00000129116	*PALLD*
ENSG00000172738	*TMEM217*	ENSG00000020577	*SAMD4A*
ENSG00000180537	*RNF182*	ENSG00000187239	*FNBP1*

Table S4 continued

Principal Component 1		Principal Component 2	
Ensembl ID	Symbol	Ensembl ID	Symbol
ENSG00000164651	*SP8*	ENSG00000102935	*ZNF423*
ENSG00000146555	*SDK1*	ENSG00000123200	*ZC3H13*
ENSG00000005108	*THSD7A*	ENSG00000082397	*EPB41L3*
ENSG00000180354	*MTURN*	ENSG00000100304	*TTLL12*
ENSG00000161040	*FBXL13*	ENSG00000107104	*KANK1*
ENSG00000153993	*SEMA3D*	ENSG00000137573	*SULF1*
ENSG00000138685	*FGF2*	ENSG00000160796	*NBEAL2*
ENSG00000138675	*FGF5*	ENSG00000171735	*CAMTA1*
ENSG00000149925	*ALDOA*	ENSG00000049759	*NEDD4L*
ENSG00000105967	*TFEC*	ENSG00000131018	*SYNE1*
ENSG00000135315	*CEP162*	ENSG00000115414	*FN1*
ENSG00000071246	*VASH1*	ENSG00000121152	*NCAPH*
ENSG00000107890	*ANKRD26*	ENSG00000169946	*ZFPM2*
ENSG00000169760	*NLGN1*	ENSG00000127603	*MACF1*
ENSG00000096060	*FKBP5*	ENSG00000179604	*CDC42EP4*
ENSG00000064932	*SBNO2*	ENSG00000011454	*RABGAP1*
ENSG00000138722	*MMRN1*	ENSG00000133265	*HSPBP1*
ENSG00000118985	*ELL2*	ENSG00000130147	*SH3BP4*
ENSG00000107984	*DKK1*	ENSG00000123892	*RAB38*
ENSG00000054598	*FOXC1*	ENSG00000128228	*SDF2L1*
ENSG00000085831	*TTC39A*	ENSG00000125848	*FLRT3*
ENSG00000020577	*SAMD4A*	ENSG00000198691	*ABCA4*
ENSG00000187239	*FNBP1*	ENSG00000102384	*CENPI*
ENSG00000150907	*FOXO1*	ENSG00000180071	*ANKRD18A*
ENSG00000102935	*ZNF423*	ENSG00000126709	*IFI6*
ENSG00000151702	*FLI1*	ENSG00000143469	*SYT14*
ENSG00000109436	*TBC1D9*	ENSG00000186994	*KANK3*
ENSG00000010327	*STAB1*	ENSG00000141424	*SLC39A6*
ENSG00000011523	*CEP68*	ENSG00000130520	*LSM4*
ENSG00000019144	*PHLDB1*	ENSG00000117308	*GALE*
ENSG00000137573	*SULF1*	ENSG00000108479	*GALK1*
ENSG00000054654	*SYNE2*	ENSG00000185432	*METTL7A*
ENSG00000037280	*FLT4*	ENSG00000205356	*TECPR1*
ENSG00000186866	*POFUT2*	ENSG00000164087	*POC1A*
ENSG00000064999	*ANKS1A*	ENSG00000196155	*PLEKHG4*
ENSG00000131018	*SYNE1*	ENSG00000197555	*SIPA1L1*
ENSG00000103187	*COTL1*	ENSG00000152217	*SETBP1*
ENSG00000107130	*NCS1*	ENSG00000198624	*CCDC69*
ENSG00000154262	*ABCA6*	ENSG00000181722	*ZBTB20*
ENSG00000154589	*LY96*	ENSG00000119403	*PHF19*
ENSG00000103066	*PLA2G15*	ENSG00000137507	*LRRC32*
ENSG00000117758	*STX12*	ENSG00000161956	*SENP3*
ENSG00000185022	*MAFF*	ENSG00000154027	*AK5*

Table S4 continued

Principal Component 1		Principal Component 2	
Ensembl ID	Symbol	Ensembl ID	Symbol
ENSG00000125848	*FLRT3*	ENSG00000131979	*GCH1*
ENSG00000099968	*BCL2L13*	ENSG00000135441	*BLOC1S1*
ENSG00000137409	*MTCH1*	ENSG00000100558	*PLEK2*
ENSG00000110218	*PANX1*	ENSG00000099800	*TIMM13*
ENSG00000172031	*EPHX4*	ENSG00000134809	*TIMM10*
ENSG00000126709	*IFI6*	ENSG00000238578	*SNORD4A*
ENSG00000184465	*WDR27*	ENSG00000225091	*SNORA71A*
ENSG00000137700	*SLC37A4*	ENSG00000204136	*GGTA1P*
ENSG00000166046	*TCP11L2*	ENSG00000200959	*SNORA74A*
ENSG00000143469	*SYT14*	ENSG00000200156	*RNU5B-1*
ENSG00000184005	*ST6GALNAC3*	ENSG00000070756	*PABPC1*
ENSG00000165072	*MAMDC2*	ENSG00000143322	*ABL2*
ENSG00000172159	*FRMD3*	ENSG00000265107	*GJA5*
ENSG00000172260	*NEGR1*	ENSG00000148677	*ANKRD1*
ENSG00000151014	*NOCT*	ENSG00000105327	*BBC3*
ENSG00000198792	*TMEM184B*	ENSG00000050165	*DKK3*
ENSG00000185432	*METTL7A*	ENSG00000107719	*PALD1*
ENSG00000196155	*PLEKHG4*	ENSG00000118407	*FILIP1*
ENSG00000143641	*GALNT2*	ENSG00000250510	*GPR162*
ENSG00000170011	*MYRIP*	ENSG00000146072	*TNFRSF21*
ENSG00000198795	*ZNF521*	ENSG00000150593	*PDCD4*
ENSG00000066279	*ASPM*	ENSG00000118946	*PCDH17*
ENSG00000104951	*IL4I1*	ENSG00000102359	*SRPX2*
ENSG00000132424	*PNISR*	ENSG00000154553	*PDLIM3*
ENSG00000020181	*ADGRA2*	ENSG00000078053	*AMPH*
ENSG00000197324	*LRP10*	ENSG00000178445	*GLDC*
ENSG00000138604	*GLCE*	ENSG00000137502	*RAB30*
ENSG00000152217	*SETBP1*	ENSG00000108106	*UBE2S*
ENSG00000109046	*WSB1*	ENSG00000244509	*APOBEC3C*
ENSG00000137507	*LRRC32*	ENSG00000136717	*BIN1*
ENSG00000066735	*KIF26A*	ENSG00000211450	*SELENOH*
ENSG00000157214	*STEAP2*	ENSG00000250303	*LOC283140*
ENSG00000134242	*PTPN22*	ENSG00000149380	*P4HA3*
ENSG00000154217	*PITPNC1*	ENSG00000165434	*PGM2L1*
ENSG00000092621	*PHGDH*	ENSG00000177990	*DPY19L2*
ENSG00000146021	*KLHL3*	ENSG00000255874	*LINC00346*
ENSG00000154027	*AK5*	ENSG00000139508	*SLC46A3*
ENSG00000177628	*GBA*	ENSG00000154188	*ANGPT1*
ENSG00000114480	*GBE1*	ENSG00000154874	*CCDC144B*
ENSG00000152137	*HSPB8*	ENSG00000224877	*NDUFAF8*
ENSG00000106852	*LHX6*	ENSG00000227195	*MIR663AHG*
ENSG00000187210	*GCNT1*	ENSG00000091879	*ANGPT2*
ENSG00000172927	*MYEOV*	ENSG00000144792	*ZNF660*

Table S4 continued

Principal Component 1		Principal Component 2	
Ensembl ID	Symbol	Ensembl ID	Symbol
ENSG00000185352	*HS6ST3*	ENSG00000099875	*MKNK2*
ENSG00000204136	*GGTA1P*	ENSG00000233276	*GPX1*
ENSG00000200959	*SNORA74A*	ENSG00000115290	*GRB14*
ENSG00000099998	*GGT5*	ENSG00000102760	*RGCC*
ENSG00000164647	*STEAP1*	ENSG00000168701	*TMEM208*
ENSG00000196511	*TPK1*	ENSG00000120217	*CD274*
ENSG00000265107	*GJA5*	ENSG00000161800	*RACGAP1*
ENSG00000148677	*ANKRD1*	ENSG00000276043	*UHRF1*
ENSG00000078081	*LAMP3*	ENSG00000163739	*CXCL1*
ENSG00000114861	*FOXP1*	ENSG00000025770	*NCAPH2*
ENSG00000050165	*DKK3*	ENSG00000164116	*GUCY1A3*
ENSG00000102393	*GLA*	ENSG00000061918	*GUCY1B3*
ENSG00000198075	*SULT1C4*	ENSG00000121957	*GPSM2*
ENSG00000102359	*SRPX2*	ENSG00000160447	*PKN3*
ENSG00000130768	*SMPDL3B*	ENSG00000136732	*GYPC*
ENSG00000108106	*UBE2S*	ENSG00000197019	*SERTAD1*
ENSG00000250303	*LOC283140*	ENSG00000089486	*CDIP1*
ENSG00000171435	*KSR2*	ENSG00000123636	*BAZ2B*
ENSG00000139508	*SLC46A3*	ENSG00000147010	*SH3KBP1*
ENSG00000099814	*CEP170B*	ENSG00000187837	*HIST1H1C*
ENSG00000166450	*PRTG*	ENSG00000124575	*HIST1H1D*
ENSG00000180229	*HERC2P3*	ENSG00000184357	*HIST1H1B*
ENSG00000154188	*ANGPT1*	ENSG00000277075	*HIST1H2AE*
ENSG00000186665	*C17orf58*	ENSG00000188486	*H2AFX*
ENSG00000154874	*CCDC144B*	ENSG00000164032	*H2AFZ*
ENSG00000196268	*ZNF493*	ENSG00000158373	*HIST1H2BD*
ENSG00000267519	*LOC284454*	ENSG00000276410	*HIST1H2BB*
ENSG00000227195	*MIR663AHG*	ENSG00000124610	*HIST1H1A*
ENSG00000198719	*DLL1*	ENSG00000099937	*SERPIND1*
ENSG00000180376	*CCDC66*	ENSG00000000971	*CFH*
ENSG00000249464	*LINC01091*	ENSG00000013016	*EHD3*
ENSG00000126882	*FAM78A*	ENSG00000177374	*HIC1*
ENSG00000233276	*GPX1*	ENSG00000095951	*HIVEP1*
ENSG00000081087	*OSTM1*	ENSG00000231389	*HLA-DPA1*
ENSG00000087884	*AAMDC*	ENSG00000223865	*HLA-DPB1*
ENSG00000102760	*RGCC*	ENSG00000138356	*AOX1*
ENSG00000163884	*KLF15*	ENSG00000072571	*HMMR*
ENSG00000166825	*ANPEP*	ENSG00000100292	*HMOX1*
ENSG00000120217	*CD274*	ENSG00000129514	*FOXA1*
ENSG00000163739	*CXCL1*	ENSG00000184270	*HIST2H2AB*
ENSG00000213366	*GSTM2*	ENSG00000107282	*APBA1*
ENSG00000100027	*YPEL1*	ENSG00000180806	*HOXC9*
ENSG00000164116	*GUCY1A3*	ENSG00000126457	*PRMT1*

Table S4 continued

Principal Component 1		Principal Component 2	
Ensembl ID	Symbol	Ensembl ID	Symbol
ENSG00000061918	*GUCY1B3*	ENSG00000086696	*HSD17B2*
ENSG00000106266	*SNX8*	ENSG00000089685	*BIRC5*
ENSG00000197019	*SERTAD1*	ENSG00000135914	*HTR2B*
ENSG00000124593	*PRICKLE4*	ENSG00000090339	*ICAM1*
ENSG00000089486	*CDIP1*	ENSG00000108622	*ICAM2*
ENSG00000147650	*LRP12*	ENSG00000254004	*ZNF260*
ENSG00000151967	*SCHIP1*	ENSG00000100036	*SLC35E4*
ENSG00000189060	*H1F0*	ENSG00000125968	*ID1*
ENSG00000187837	*HIST1H1C*	ENSG00000010404	*IDS*
ENSG00000168298	*HIST1H1E*	ENSG00000205403	*CFI*
ENSG00000182718	*ANXA2*	ENSG00000147036	*LANCL3*
ENSG00000063854	*HAGH*	ENSG00000130203	*APOE*
ENSG00000099937	*SERPIND1*	ENSG00000140443	*IGF1R*
ENSG00000138772	*ANXA3*	ENSG00000115457	*IGFBP2*
ENSG00000000971	*CFH*	ENSG00000167779	*IGFBP6*
ENSG00000213977	*TAX1BP3*	ENSG00000163453	*IGFBP7*
ENSG00000127946	*HIP1*	ENSG00000198931	*APRT*
ENSG00000164104	*HMGB2*	ENSG00000115008	*IL1A*
ENSG00000138356	*AOX1*	ENSG00000115594	*IL1R1*
ENSG00000103415	*HMOX2*	ENSG00000131724	*IL13RA1*
ENSG00000163412	*EIF4E3*	ENSG00000122641	*INHBA*
ENSG00000180806	*HOXC9*	ENSG00000163083	*INHBB*
ENSG00000115756	*HPCAL1*	ENSG00000117595	*IRF6*
ENSG00000086696	*HSD17B2*	ENSG00000115232	*ITGA4*
ENSG00000090339	*ICAM1*	ENSG00000138448	*ITGAV*
ENSG00000148488	*ST8SIA6*	ENSG00000259207	*ITGB3*
ENSG00000197841	*ZNF181*	ENSG00000132470	*ITGB4*
ENSG00000185860	*CCDC190*	ENSG00000105855	*ITGB8*
ENSG00000165949	*IFI27*	ENSG00000182118	*FAM89A*
ENSG00000122483	*CCDC18*	ENSG00000135976	*ANKRD36*
ENSG00000162687	*KCNT2*	ENSG00000069020	*MAST4*
ENSG00000176771	*NCKAP5*	ENSG00000157404	*KIT*
ENSG00000234284	*ZNF879*	ENSG00000237649	*KIFC1*
ENSG00000188107	*EYS*	ENSG00000079616	*KIF22*
ENSG00000157593	*SLC35B2*	ENSG00000186081	*KRT5*
ENSG00000168528	*SERINC2*	ENSG00000205420	*KRT6A*
ENSG00000130203	*APOE*	ENSG00000171401	*KRT13*
ENSG00000242498	*ARPIN*	ENSG00000203760	*CENPW*
ENSG00000115457	*IGFBP2*	ENSG00000171345	*KRT19*
ENSG00000167779	*IGFBP6*	ENSG00000175155	*YPEL2*
ENSG00000163453	*IGFBP7*	ENSG00000264343	*NOTCH2NL*
ENSG00000142871	*CYR61*	ENSG00000168887	*C2orf68*
ENSG00000198931	*APRT*	ENSG00000206538	*VGLL3*

Table S4 continued

Principal Component 1		Principal Component 2	
Ensembl ID	Symbol	Ensembl ID	Symbol
ENSG00000115008	*IL1A*	ENSG00000115963	*RND3*
ENSG00000115594	*IL1R1*	ENSG00000130702	*LAMA5*
ENSG00000185291	*IL3RA*	ENSG00000091136	*LAMB1*
ENSG00000136244	*IL6*	ENSG00000058085	*LAMC2*
ENSG00000168685	*IL7R*	ENSG00000156466	*GDF6*
ENSG00000169429	*CXCL8*	ENSG00000182541	*LIMK2*
ENSG00000240583	*AQP1*	ENSG00000169756	*LIMS1*
ENSG00000163083	*INHBB*	ENSG00000079435	*LIPE*
ENSG00000171105	*INSR*	ENSG00000160789	*LMNA*
ENSG00000169083	*AR*	ENSG00000113368	*LMNB1*
ENSG00000005884	*ITGA3*	ENSG00000197182	*MIRLET7BHG*
ENSG00000115232	*ITGA4*	ENSG00000186479	*RGS7BP*
ENSG00000161638	*ITGA5*	ENSG00000177570	*SAMD12*
ENSG00000138448	*ITGAV*	ENSG00000188921	*HACD4*
ENSG00000259207	*ITGB3*	ENSG00000182489	*XKRX*
ENSG00000132470	*ITGB4*	ENSG00000119681	*LTBP2*
ENSG00000242372	*EIF6*	ENSG00000164109	*MAD2L1*
ENSG00000082781	*ITGB5*	ENSG00000101846	*STS*
ENSG00000105855	*ITGB8*	ENSG00000111885	*MAN1A1*
ENSG00000184916	*JAG2*	ENSG00000132561	*MATN2*
ENSG00000162434	*JAK1*	ENSG00000103495	*MAZ*
ENSG00000177606	*JUN*	ENSG00000073111	*MCM2*
ENSG00000182118	*FAM89A*	ENSG00000104738	*MCM4*
ENSG00000135976	*ANKRD36*	ENSG00000100297	*MCM5*
ENSG00000188157	*AGRN*	ENSG00000076003	*MCM6*
ENSG00000143603	*KCNN3*	ENSG00000166508	*MCM7*
ENSG00000140859	*KIFC3*	ENSG00000111339	*ART4*
ENSG00000186081	*KRT5*	ENSG00000095015	*MAP3K1*
ENSG00000135480	*KRT7*	ENSG00000049130	*KITLG*
ENSG00000171401	*KRT13*	ENSG00000170430	*MGMT*
ENSG00000171346	*KRT15*	ENSG00000002586	*CD99*
ENSG00000181350	*LRRC75A*	ENSG00000187098	*MITF*
ENSG00000253368	*TRNP1*	ENSG00000087245	*MMP2*
ENSG00000155366	*RHOC*	ENSG00000166670	*MMP10*
ENSG00000206538	*VGLL3*	ENSG00000204899	*MZT1*
ENSG00000115963	*RND3*	ENSG00000206149	*HERC2P9*
ENSG00000185896	*LAMP1*	ENSG00000203995	*ZYG11A*
ENSG00000058085	*LAMC2*	ENSG00000215146	*LOC441666*
ENSG00000156466	*GDF6*	ENSG00000198899	*ATP6*
ENSG00000130164	*LDLR*	ENSG00000228253	*ATP8*
ENSG00000116678	*LEPR*	ENSG00000198804	*COX1*
ENSG00000100097	*LGALS1*	ENSG00000198712	*COX2*
ENSG00000113594	*LIFR*	ENSG00000198938	*COX3*

Table S4 continued

Principal Component 1		Principal Component 2	
Ensembl ID	Symbol	Ensembl ID	Symbol
ENSG00000099204	*ABLIM1*	ENSG00000198727	*CYTB*
ENSG00000221968	*FADS3*	ENSG00000100714	*MTHFD1*
ENSG00000135363	*LMO2*	ENSG00000198888	*ND1*
ENSG00000136153	*LMO7*	ENSG00000198763	*ND2*
ENSG00000124374	*PAIP2B*	ENSG00000198840	*ND3*
ENSG00000184305	*CCSER1*	ENSG00000198886	*ND4*
ENSG00000186479	*RGS7BP*	ENSG00000212907	*ND4L*
ENSG00000134013	*LOXL2*	ENSG00000198786	*ND5*
ENSG00000163956	*LRPAP1*	ENSG00000157601	*MX1*
ENSG00000154102	*C16orf74*	ENSG00000099860	*GADD45B*
ENSG00000160285	*LSS*	ENSG00000133026	*MYH10*
ENSG00000111144	*LTA4H*	ENSG00000176658	*MYO1D*
ENSG00000119681	*LTBP2*	ENSG00000157483	*MYO1E*
ENSG00000226380	*MIR29A*	ENSG00000196586	*MYO6*
ENSG00000120693	*SMAD9*	ENSG00000137474	*MYO7A*
ENSG00000100299	*ARSA*	ENSG00000145555	*MYO10*
ENSG00000166963	*MAP1A*	ENSG00000117650	*NEK2*
ENSG00000132561	*MATN2*	ENSG00000103024	*NME3*
ENSG00000076706	*MCAM*	ENSG00000164867	*NOS3*
ENSG00000106511	*MEOX2*	ENSG00000169418	*NPR1*
ENSG00000049130	*KITLG*	ENSG00000065057	*NTHL1*
ENSG00000111341	*MGP*	ENSG00000185483	*ROR1*
ENSG00000143198	*MGST3*	ENSG00000115758	*ODC1*
ENSG00000104763	*ASAH1*	ENSG00000116213	*WRAP73*
ENSG00000204516	*MICB*	ENSG00000085840	*ORC1*
ENSG00000171843	*MLLT3*	ENSG00000086991	*NOX4*
ENSG00000196611	*MMP1*	ENSG00000106366	*SERPINE1*
ENSG00000166670	*MMP10*	ENSG00000197632	*SERPINB2*
ENSG00000157227	*MMP14*	ENSG00000149269	*PAK1*
ENSG00000119711	*ALDH6A1*	ENSG00000204387	*C6orf48*
ENSG00000182534	*MXRA7*	ENSG00000173599	*PC*
ENSG00000015133	*CCDC88C*	ENSG00000169851	*PCDH7*
ENSG00000206149	*HERC2P9*	ENSG00000184226	*PCDH9*
ENSG00000169715	*MT1E*	ENSG00000078674	*PCM1*
ENSG00000260549	*MT1L*	ENSG00000132646	*PCNA*
ENSG00000125148	*MT2A*	ENSG00000053372	*MRTO4*
ENSG00000167508	*MVD*	ENSG00000172889	*EGFL7*
ENSG00000157601	*MX1*	ENSG00000109576	*AADAT*
ENSG00000133026	*MYH10*	ENSG00000136463	*TACO1*
ENSG00000092841	*MYL6*	ENSG00000108798	*ABI3*
ENSG00000183091	*NEB*	ENSG00000099139	*PCSK5*
ENSG00000090266	*NDUFB2*	ENSG00000150048	*CLEC1A*
ENSG00000129559	*NEDD8*	ENSG00000171222	*SCAND1*

Table S4 continued

Principal Component 1		Principal Component 2	
Ensembl ID	Symbol	Ensembl ID	Symbol
ENSG00000111859	*NEDD9*	ENSG00000167775	*CD320*
ENSG00000136098	*NEK3*	ENSG00000113555	*PCDH12*
ENSG00000186575	*NF2*	ENSG00000124785	*NRN1*
ENSG00000143153	*ATP1B1*	ENSG00000115252	*PDE1A*
ENSG00000116962	*NID1*	ENSG00000154678	*PDE1C*
ENSG00000198805	*PNP*	ENSG00000186642	*PDE2A*
ENSG00000144061	*NPHP1*	ENSG00000187688	*TRPV2*
ENSG00000169418	*NPR1*	ENSG00000184588	*PDE4B*
ENSG00000185483	*ROR1*	ENSG00000075218	*GTSE1*
ENSG00000111335	*OAS2*	ENSG00000171425	*ZNF581*
ENSG00000013297	*CLDN11*	ENSG00000100311	*PDGFB*
ENSG00000135124	*P2RX4*	ENSG00000129048	*ACKR4*
ENSG00000140564	*FURIN*	ENSG00000013306	*SLC25A39*
ENSG00000117450	*PRDX1*	ENSG00000119801	*YPEL5*
ENSG00000106366	*SERPINE1*	ENSG00000131153	*GINS2*
ENSG00000197632	*SERPINB2*	ENSG00000197594	*ENPP1*
ENSG00000185630	*PBX1*	ENSG00000164035	*EMCN*
ENSG00000142546	*NOSIP*	ENSG00000161980	*POLR3K*
ENSG00000109618	*SEPSECS*	ENSG00000100625	*SIX4*
ENSG00000167772	*ANGPTL4*	ENSG00000178921	*PFAS*
ENSG00000189159	*HN1*	ENSG00000135919	*SERPINE2*
ENSG00000023902	*PLEKHO1*	ENSG00000105851	*PIK3CG*
ENSG00000137804	*NUSAP1*	ENSG00000008710	*PKD1*
ENSG00000175426	*PCSK1*	ENSG00000057294	*PKP2*
ENSG00000154781	*CCDC174*	ENSG00000117410	*ATP6V0B*
ENSG00000006327	*TNFRSF12A*	ENSG00000136404	*TM6SF1*
ENSG00000137877	*SPTBN5*	ENSG00000166851	*PLK1*
ENSG00000115252	*PDE1A*	ENSG00000071655	*MBD3*
ENSG00000182022	*CHST15*	ENSG00000165240	*ATP7A*
ENSG00000154678	*PDE1C*	ENSG00000102575	*ACP5*
ENSG00000100554	*ATP6V1D*	ENSG00000184702	*SEPT5*
ENSG00000172572	*PDE3A*	ENSG00000172965	*MIR4435-2HG*
ENSG00000187688	*TRPV2*	ENSG00000128567	*PODXL*
ENSG00000196247	*ZNF107*	ENSG00000062822	*POLD1*
ENSG00000168077	*SCARA3*	ENSG00000168002	*POLR2G*
ENSG00000143476	*DTL*	ENSG00000170891	*CYTL1*
ENSG00000100311	*PDGFB*	ENSG00000129195	*FAM64A*
ENSG00000129048	*ACKR4*	ENSG00000145390	*USP53*
ENSG00000117543	*DPH5*	ENSG00000168209	*DDIT4*
ENSG00000004799	*PDK4*	ENSG00000085224	*ATRX*
ENSG00000171314	*PGAM1*	ENSG00000099364	*FBXL19*
ENSG00000119630	*PGF*	ENSG00000196544	*BORCS6*
ENSG00000135919	*SERPINE2*	ENSG00000186871	*ERCC6L*

Table S4 continued

Principal Component 1		Principal Component 2	
Ensembl ID	Symbol	Ensembl ID	Symbol
ENSG00000133056	*PIK3C2B*	ENSG00000059769	*DNAJC25*
ENSG00000171608	*PIK3CD*	ENSG00000099260	*PALMD*
ENSG00000067225	*PKM*	ENSG00000146918	*NCAPG2*
ENSG00000104368	*PLAT*	ENSG00000166912	*MTMR10*
ENSG00000122861	*PLAU*	ENSG00000105538	*RASIP1*
ENSG00000011422	*PLAUR*	ENSG00000101695	*RNF125*
ENSG00000117410	*ATP6V0B*	ENSG00000177692	*DNAJC28*
ENSG00000136404	*TM6SF1*	ENSG00000087253	*LPCAT2*
ENSG00000083444	*PLOD1*	ENSG00000130748	*TMEM160*
ENSG00000152952	*PLOD2*	ENSG00000101220	*C20orf27*
ENSG00000114554	*PLXNA1*	ENSG00000143224	*PPOX*
ENSG00000071655	*MBD3*	ENSG00000175756	*AURKAIP1*
ENSG00000008277	*ADAM22*	ENSG00000185480	*PARPBP*
ENSG00000141682	*PMAIP1*	ENSG00000170779	*CDCA4*
ENSG00000102575	*ACP5*	ENSG00000137831	*UACA*
ENSG00000184702	*SEPT5*	ENSG00000126870	*WDR60*
ENSG00000108387	*SEPT4*	ENSG00000072041	*SLC6A15*
ENSG00000147481	*SNTG1*	ENSG00000134690	*CDCA8*
ENSG00000099817	*POLR2E*	ENSG00000074964	*ARHGEF10L*
ENSG00000170891	*CYTL1*	ENSG00000138180	*CEP55*
ENSG00000177700	*POLR2L*	ENSG00000196368	*NUDT11*
ENSG00000145990	*GFOD1*	ENSG00000090530	*P3H2*
ENSG00000052126	*PLEKHA5*	ENSG00000073711	*PPP2R3A*
ENSG00000033100	*CHPF2*	ENSG00000146859	*TMEM140*
ENSG00000189184	*PCDH18*	ENSG00000038210	*PI4K2B*
ENSG00000091127	*PUS7*	ENSG00000103381	*CPPED1*
ENSG00000154133	*ROBO4*	ENSG00000104341	*LAPTM4B*
ENSG00000168209	*DDIT4*	ENSG00000123485	*HJURP*
ENSG00000128917	*DLL4*	ENSG00000095383	*TBC1D2*
ENSG00000069812	*HES2*	ENSG00000065328	*MCM10*
ENSG00000005469	*CROT*	ENSG00000225470	*JPX*
ENSG00000164951	*PDP1*	ENSG00000162545	*CAMK2N1*
ENSG00000184840	*TMED9*	ENSG00000169826	*CSGALNACT2*
ENSG00000178075	*GRAMD1C*	ENSG00000101311	*FERMT1*
ENSG00000011258	*MBTD1*	ENSG00000024526	*DEPDC1*
ENSG00000137960	*GIPC2*	ENSG00000147642	*SYBU*
ENSG00000137501	*SYTL2*	ENSG00000022556	*NLRP2*
ENSG00000198113	*TOR4A*	ENSG00000165801	*ARHGEF40*
ENSG00000044459	*CNTLN*	ENSG00000058804	*NDC1*
ENSG00000118898	*PPL*	ENSG00000198185	*ZNF334*
ENSG00000101695	*RNF125*	ENSG00000218336	*TENM3*
ENSG00000175756	*AURKAIP1*	ENSG00000105011	*ASF1B*
ENSG00000141219	*C17orf80*	ENSG00000042088	*TDP1*

Table S4 continued

Principal Component 1		Principal Component 2	
Ensembl ID	Symbol	Ensembl ID	Symbol
ENSG00000160058	*BSDC1*	ENSG00000140563	*MCTP2*
ENSG00000072041	*SLC6A15*	ENSG00000035499	*DEPDC1B*
ENSG00000134186	*PRPF38B*	ENSG00000112304	*ACOT13*
ENSG00000090530	*P3H2*	ENSG00000168078	*PBK*
ENSG00000172731	*LRRC20*	ENSG00000197852	*FAM212B*
ENSG00000137269	*LRRC1*	ENSG00000156711	*MAPK13*
ENSG00000115107	*STEAP3*	ENSG00000145431	*PDGFC*
ENSG00000147419	*CCDC25*	ENSG00000183943	*PRKX*
ENSG00000066027	*PPP2R5A*	ENSG00000112852	*PCDHB2*
ENSG00000137522	*RNF121*	ENSG00000147697	*GSDMC*
ENSG00000133574	*GIMAP4*	ENSG00000120549	*KIAA1217*
ENSG00000149923	*PPP4C*	ENSG00000082497	*SERTAD4*
ENSG00000135002	*RFK*	ENSG00000130962	*PRRG1*
ENSG00000129534	*MIS18BP1*	ENSG00000010438	*PRSS3*
ENSG00000138587	*MNS1*	ENSG00000202515	*VTRNA1-3*
ENSG00000152953	*STK32B*	ENSG00000182916	*TCEAL7*
ENSG00000104341	*LAPTM4B*	ENSG00000176907	*C8orf4*
ENSG00000163046	*ANKRD30BL*	ENSG00000141994	*DUS3L*
ENSG00000162545	*CAMK2N1*	ENSG00000124225	*PMEPA1*
ENSG00000122862	*SRGN*	ENSG00000240065	*PSMB9*
ENSG00000110675	*ELMOD1*	ENSG00000205220	*PSMB10*
ENSG00000130827	*PLXNA3*	ENSG00000163808	*KIF15*
ENSG00000135905	*DOCK10*	ENSG00000163050	*COQ8A*
ENSG00000162409	*PRKAA2*	ENSG00000163638	*ADAMTS9*
ENSG00000118242	*MREG*	ENSG00000114698	*PLSCR4*
ENSG00000116871	*MAP7D1*	ENSG00000090971	*NAT14*
ENSG00000218336	*TENM3*	ENSG00000117643	*MAN1C1*
ENSG00000167601	*AXL*	ENSG00000134247	*PTGFRN*
ENSG00000171132	*PRKCE*	ENSG00000124212	*PTGIS*
ENSG00000042317	*SPATA7*	ENSG00000152253	*SPC25*
ENSG00000065675	*PRKCQ*	ENSG00000095303	*PTGS1*
ENSG00000176871	*WSB2*	ENSG00000073756	*PTGS2*
ENSG00000186918	*ZNF395*	ENSG00000128578	*STRIP2*
ENSG00000005483	*KMT2E*	ENSG00000186260	*MKL2*
ENSG00000128833	*MYO5C*	ENSG00000196935	*SRGAP1*
ENSG00000196562	*SULF2*	ENSG00000183775	*KCTD16*
ENSG00000145431	*PDGFC*	ENSG00000136383	*ALPK3*
ENSG00000147697	*GSDMC*	ENSG00000138650	*PCDH10*
ENSG00000171867	*PRNP*	ENSG00000138771	*SHROOM3*
ENSG00000120549	*KIAA1217*	ENSG00000013293	*SLC7A14*
ENSG00000082497	*SERTAD4*	ENSG00000105426	*PTPRS*
ENSG00000088882	*CPXM1*	ENSG00000073008	*PVR*
ENSG00000130962	*PRRG1*	ENSG00000148143	*ZNF462*

Table S4 continued

Principal Component 1		Principal Component 2	
Ensembl ID	Symbol	Ensembl ID	Symbol
ENSG00000010438	*PRSS3*	ENSG00000169213	*RAB3B*
ENSG00000189056	*RELN*	ENSG00000051180	*RAD51*
ENSG00000175352	*NRIP3*	ENSG00000166349	*RAG1*
ENSG00000111554	*MDM1*	ENSG00000114200	*BCHE*
ENSG00000176907	*C8orf4*	ENSG00000172819	*RARG*
ENSG00000125912	*NCLN*	ENSG00000113319	*RASGRF2*
ENSG00000100804	*PSMB5*	ENSG00000032219	*ARID4A*
ENSG00000116774	*OLFML3*	ENSG00000074527	*NTN4*
ENSG00000099256	*PRTFDC1*	ENSG00000126950	*TMEM35A*
ENSG00000240065	*PSMB9*	ENSG00000114115	*RBP1*
ENSG00000104047	*DTWD1*	ENSG00000171791	*BCL2*
ENSG00000163808	*KIF15*	ENSG00000049541	*RFC2*
ENSG00000144476	*ACKR3*	ENSG00000138835	*RGS3*
ENSG00000090097	*PCBP4*	ENSG00000269900	*RMRP*
ENSG00000175166	*PSMD2*	ENSG00000283029	*RN7SL1*
ENSG00000047617	*ANO2*	ENSG00000149201	*CCDC81*
ENSG00000101474	*APMAP*	ENSG00000106399	*RPA3*
ENSG00000115310	*RTN4*	ENSG00000167526	*RPL13*
ENSG00000102897	*LYRM1*	ENSG00000265681	*RPL17*
ENSG00000139946	*PELI2*	ENSG00000214026	*MRPL23*
ENSG00000128203	*ASPHD2*	ENSG00000128626	*MRPS12*
ENSG00000124212	*PTGIS*	ENSG00000164684	*ZNF704*
ENSG00000100626	*GALNT16*	ENSG00000170889	*RPS9*
ENSG00000120278	*PLEKHG1*	ENSG00000171848	*RRM2*
ENSG00000186260	*MKL2*	ENSG00000176697	*BDNF*
ENSG00000168916	*ZNF608*	ENSG00000197956	*S100A6*
ENSG00000129422	*MTUS1*	ENSG00000005187	*ACSM3*
ENSG00000138411	*HECW2*	ENSG00000137266	*SLC22A23*
ENSG00000136383	*ALPK3*	ENSG00000182492	*BGN*
ENSG00000144959	*NCEH1*	ENSG00000196876	*SCN8A*
ENSG00000092421	*SEMA6A*	ENSG00000108691	*CCL2*
ENSG00000138134	*STAMBPL1*	ENSG00000115884	*SDC1*
ENSG00000110318	*CEP126*	ENSG00000169439	*SDC2*
ENSG00000137727	*ARHGAP20*	ENSG00000154864	*PIEZO2*
ENSG00000144583	*MARCH4*	ENSG00000101194	*SLC17A9*
ENSG00000105559	*PLEKHA4*	ENSG00000127586	*CHTF18*
ENSG00000115109	*EPB41L5*	ENSG00000007908	*SELE*
ENSG00000116260	*QSOX1*	ENSG00000174175	*SELP*
ENSG00000013293	*SLC7A14*	ENSG00000001617	*SEMA3F*
ENSG00000153707	*PTPRD*	ENSG00000129595	*EPB41L4A*
ENSG00000142949	*PTPRF*	ENSG00000123219	*CENPK*
ENSG00000163661	*PTX3*	ENSG00000169718	*DUS1L*
ENSG00000117569	*PTBP2*	ENSG00000142910	*TINAGL1*

Table S4 continued

Principal Component 1		Principal Component 2	
Ensembl ID	Symbol	Ensembl ID	Symbol
ENSG00000073008	*PVR*	ENSG00000109805	*NCAPG*
ENSG00000137767	*SQRDL*	ENSG00000267313	*KC6*
ENSG00000128805	*ARHGAP22*	ENSG00000186283	*TOR3A*
ENSG00000082126	*MPP4*	ENSG00000214944	*ARHGEF28*
ENSG00000128340	*RAC2*	ENSG00000164736	*SOX17*
ENSG00000144118	*RALB*	ENSG00000250337	*LINC01021*
ENSG00000077092	*RARB*	ENSG00000164161	*HHIP*
ENSG00000113319	*RASGRF2*	ENSG00000143429	*LOC645166*
ENSG00000032219	*ARID4A*	ENSG00000206432	*TMEM200C*
ENSG00000198258	*UBL5*	ENSG00000235770	*LINC00607*
ENSG00000122257	*RBBP6*	ENSG00000176974	*SHMT1*
ENSG00000101773	*RBBP8*	ENSG00000136205	*TNS3*
ENSG00000102317	*RBM3*	ENSG00000075420	*FNDC3B*
ENSG00000114115	*RBP1*	ENSG00000110080	*ST3GAL4*
ENSG00000110092	*CCND1*	ENSG00000136830	*FAM129B*
ENSG00000171552	*BCL2L1*	ENSG00000180992	*MRPL14*
ENSG00000116741	*RGS2*	ENSG00000125901	*MRPS26*
ENSG00000117152	*RGS4*	ENSG00000136603	*SKIL*
ENSG00000129538	*RNASE1*	ENSG00000105281	*SLC1A5*
ENSG00000113916	*BCL6*	ENSG00000125351	*UPF3B*
ENSG00000149201	*CCDC81*	ENSG00000125378	*BMP4*
ENSG00000123395	*ATG101*	ENSG00000196632	*WNK3*
ENSG00000156313	*RPGR*	ENSG00000183598	*HIST2H3D*
ENSG00000164684	*ZNF704*	ENSG00000153162	*BMP6*
ENSG00000175634	*RPS6KB2*	ENSG00000189223	*PAX8-AS1*
ENSG00000176697	*BDNF*	ENSG00000234912	*SNHG20*
ENSG00000134243	*SORT1*	ENSG00000214814	*FER1L6*
ENSG00000197956	*S100A6*	ENSG00000173638	*SLC19A1*
ENSG00000182568	*SATB1*	ENSG00000103254	*FAM173A*
ENSG00000204842	*ATXN2*	ENSG00000108604	*SMARCD2*
ENSG00000182492	*BGN*	ENSG00000023608	*SNAPC1*
ENSG00000169432	*SCN9A*	ENSG00000125835	*SNRPB*
ENSG00000108691	*CCL2*	ENSG00000172331	*BPGM*
ENSG00000276409	*CCL14*	ENSG00000152377	*SPOCK1*
ENSG00000124875	*CXCL6*	ENSG00000163554	*SPTA1*
ENSG00000169439	*SDC2*	ENSG00000140319	*SRP14*
ENSG00000124145	*SDC4*	ENSG00000144681	*STAC*
ENSG00000154864	*PIEZO2*	ENSG00000115415	*STAT1*
ENSG00000132436	*FIGNL1*	ENSG00000138378	*STAT4*
ENSG00000007908	*SELE*	ENSG00000252835	*SCARNA21*
ENSG00000188404	*SELL*	ENSG00000270066	*SCARNA2*
ENSG00000112378	*PERP*	ENSG00000252481	*SCARNA13*
ENSG00000155307	*SAMSN1*	ENSG00000251791	*SCARNA6*

Table S4 continued

Principal Component 1		Principal Component 2	
Ensembl ID	Symbol	Ensembl ID	Symbol
ENSG00000135926	*TMBIM1*	ENSG00000252010	*SCARNA5*
ENSG00000142910	*TINAGL1*	ENSG00000212464	*SNORA12*
ENSG00000015532	*XYLT2*	ENSG00000206634	*SNORA22*
ENSG00000115267	*IFIH1*	ENSG00000238961	*SNORA47*
ENSG00000178980	*SELENOW*	ENSG00000200354	*SNORA71D*
ENSG00000214765	*SEPT7P2*	ENSG00000159167	*STC1*
ENSG00000154134	*ROBO3*	ENSG00000109193	*SULT1E1*
ENSG00000007384	*RHBDF1*	ENSG00000087586	*AURKA*
ENSG00000164736	*SOX17*	ENSG00000130303	*BST2*
ENSG00000167693	*NXN*	ENSG00000067715	*SYT1*
ENSG00000235505	*LOC643733*	ENSG00000149591	*TAGLN*
ENSG00000118515	*SGK1*	ENSG00000112592	*TBP*
ENSG00000166922	*SCG5*	ENSG00000239039	*SNORD13*
ENSG00000143429	*LOC645166*	ENSG00000212232	*SNORD17*
ENSG00000108854	*SMURF2*	ENSG00000196628	*TCF4*
ENSG00000136205	*TNS3*	ENSG00000137310	*TCF19*
ENSG00000127080	*IPPK*	ENSG00000185339	*TCN2*
ENSG00000075420	*FNDC3B*	ENSG00000169679	*BUB1*
ENSG00000121749	*TBC1D15*	ENSG00000156970	*BUB1B*
ENSG00000073849	*ST6GAL1*	ENSG00000270141	*TERC*
ENSG00000136830	*FAM129B*	ENSG00000090447	*TFAP4*
ENSG00000163814	*CDCP1*	ENSG00000072274	*TFRC*
ENSG00000112246	*SIM1*	ENSG00000092969	*TGFB2*
ENSG00000180992	*MRPL14*	ENSG00000120708	*TGFBI*
ENSG00000153044	*CENPH*	ENSG00000106799	*TGFBR1*
ENSG00000165271	*NOL6*	ENSG00000137801	*THBS1*
ENSG00000125351	*UPF3B*	ENSG00000100300	*TSPO*
ENSG00000164889	*SLC4A2*	ENSG00000172009	*THOP1*
ENSG00000214814	*FER1L6*	ENSG00000035862	*TIMP2*
ENSG00000090020	*SLC9A1*	ENSG00000167900	*TK1*
ENSG00000064651	*SLC12A2*	ENSG00000120802	*TMPO*
ENSG00000144136	*SLC20A1*	ENSG00000184113	*CLDN5*
ENSG00000174640	*SLCO2A1*	ENSG00000131747	*TOP2A*
ENSG00000080503	*SMARCA2*	ENSG00000146242	*TPBG*
ENSG00000102010	*BMX*	ENSG00000111669	*TPI1*
ENSG00000166311	*SMPD1*	ENSG00000140416	*TPM1*
ENSG00000117143	*UAP1*	ENSG00000067445	*TRO*
ENSG00000114850	*SSR3*	ENSG00000106804	*C5*
ENSG00000139618	*BRCA2*	ENSG00000185561	*TLCD2*
ENSG00000115415	*STAT1*	ENSG00000176890	*TYMS*
ENSG00000138378	*STAT4*	ENSG00000213967	*ZNF726*
ENSG00000126561	*STAT5A*	ENSG00000148154	*UGCG*
ENSG00000252010	*SCARNA5*	ENSG00000149823	*VPS51*

Table S4 continued

Principal Component 1		Principal Component 2	
Ensembl ID	Symbol	Ensembl ID	Symbol
ENSG00000206634	*SNORA22*	ENSG00000162692	*VCAM1*
ENSG00000201998	*SNORA23*	ENSG00000140105	*WARS*
ENSG00000212443	*SNORA53*	ENSG00000147180	*ZNF711*
ENSG00000152518	*ZFP36L2*	ENSG00000167232	*ZNF91*
ENSG00000109193	*SULT1E1*	ENSG00000159840	*ZYX*
ENSG00000109743	*BST1*	ENSG00000263934	*SNORD3A*
ENSG00000130303	*BST2*	ENSG00000144063	*MALL*
ENSG00000149591	*TAGLN*	ENSG00000214706	*IFRD2*
ENSG00000197780	*TAF13*	ENSG00000075785	*RAB7A*
ENSG00000204219	*TCEA3*	ENSG00000169282	*KCNAB1*
ENSG00000212232	*SNORD17*	ENSG00000089723	*OTUB2*
ENSG00000005436	*GCFC2*	ENSG00000173621	*LRFN4*
ENSG00000169131	*ZNF354A*	ENSG00000100162	*CENPM*
ENSG00000145022	*TCTA*	ENSG00000110104	*CCDC86*
ENSG00000003436	*TFPI*	ENSG00000116455	*WDR77*
ENSG00000072274	*TFRC*	ENSG00000111670	*GNPTAB*
ENSG00000042832	*TG*	ENSG00000142634	*EFHD2*
ENSG00000092969	*TGFB2*	ENSG00000131652	*THOC6*
ENSG00000120708	*TGFBI*	ENSG00000111058	*ACSS3*
ENSG00000069702	*TGFBR3*	ENSG00000119900	*OGFRL1*
ENSG00000100300	*TSPO*	ENSG00000196159	*FAT4*
ENSG00000104067	*TJP1*	ENSG00000129680	*MAP7D3*
ENSG00000065717	*TLE2*	ENSG00000173281	*PPP1R3B*
ENSG00000028137	*TNFRSF1B*	ENSG00000100379	*KCTD17*
ENSG00000159403	*C1R*	ENSG00000063241	*ISOC2*
ENSG00000131747	*TOP2A*	ENSG00000175471	*MCTP1*
ENSG00000146242	*TPBG*	ENSG00000091656	*ZFHX4*
ENSG00000076554	*TPD52*	ENSG00000165959	*CLMN*
ENSG00000140416	*TPM1*	ENSG00000175213	*ZNF408*
ENSG00000198467	*TPM2*	ENSG00000171241	*SHCBP1*
ENSG00000067445	*TRO*	ENSG00000116771	*AGMAT*
ENSG00000155657	*TTN*	ENSG00000150636	*CCDC102B*
ENSG00000137267	*TUBB2A*	ENSG00000136122	*BORA*
ENSG00000143367	*TUFT1*	ENSG00000187720	*THSD4*
ENSG00000117586	*TNFSF4*	ENSG00000135362	*PRR5L*
ENSG00000226053	*LOC729987*	ENSG00000133142	*TCEAL4*
ENSG00000148154	*UGCG*	ENSG00000092470	*WDR76*
ENSG00000183255	*PTTG1IP*	ENSG00000149636	*DSN1*
ENSG00000189180	*ZNF33A*	ENSG00000122786	*CALD1*
ENSG00000202048	*SNORD114-20*	ENSG00000137872	*SEMA6D*
ENSG00000063180	*CA11*	ENSG00000140451	*PIF1*
ENSG00000109906	*ZBTB16*	ENSG00000138759	*FRAS1*
ENSG00000147394	*ZNF185*	ENSG00000122490	*PQLC1*

Table S4 continued

Principal Component 1		Principal Component 2	
Ensembl ID	Symbol	Ensembl ID	Symbol
ENSG00000149050	*ZNF214*	ENSG00000278259	*MYO19*
ENSG00000163879	*DNALI1*	ENSG00000119242	*CCDC92*
ENSG00000162511	*LAPTM5*	ENSG00000156675	*RAB11FIP1*
ENSG00000263934	*SNORD3A*	ENSG00000046889	*PREX2*
ENSG00000115275	*MOGS*	ENSG00000138336	*TET1*
ENSG00000167552	*TUBA1A*	ENSG00000177192	*PUS1*
ENSG00000121966	*CXCR4*	ENSG00000111981	*ULBP1*
ENSG00000169282	*KCNAB1*	ENSG00000197646	*PDCD1LG2*
ENSG00000185803	*SLC52A2*	ENSG00000221963	*APOL6*
ENSG00000111058	*ACSS3*	ENSG00000100836	*PABPN1*
ENSG00000119900	*OGFRL1*	ENSG00000158555	*GDPD5*
ENSG00000196159	*FAT4*	ENSG00000101447	*FAM83D*
ENSG00000180801	*ARSJ*	ENSG00000167513	*CDT1*
ENSG00000187240	*DYNC2H1*	ENSG00000178605	*GTPBP6*
ENSG00000128915	*ICE2*	ENSG00000169249	*ZRSR2*
ENSG00000196449	*YRDC*	ENSG00000276180	*HIST1H4I*
ENSG00000119514	*GALNT12*	ENSG00000093009	*CDC45*
ENSG00000130309	*COLGALT1*	ENSG00000196747	*HIST1H2AI*
ENSG00000198517	*MAFK*	ENSG00000275221	*HIST1H2AK*
ENSG00000175471	*MCTP1*	ENSG00000276368	*HIST1H2AJ*
ENSG00000132321	*IQCA1*	ENSG00000276903	*HIST1H2AL*
ENSG00000175213	*ZNF408*	ENSG00000278463	*HIST1H2AB*
ENSG00000105825	*TFPI2*	ENSG00000185130	*HIST1H2BL*
ENSG00000105792	*CFAP69*	ENSG00000274290	*HIST1H2BE*
ENSG00000187720	*THSD4*	ENSG00000275713	*HIST1H2BH*
ENSG00000104723	*TUSC3*	ENSG00000278588	*HIST1H2BI*
ENSG00000133142	*TCEAL4*	ENSG00000111665	*CDCA3*
ENSG00000099219	*ERMP1*	ENSG00000213347	*MXD3*
ENSG00000121895	*TMEM156*	ENSG00000129932	*DOHH*
ENSG00000266714	*MYO15B*	ENSG00000274641	*HIST1H2BO*
ENSG00000162174	*ASRGL1*	ENSG00000275714	*HIST1H3A*
ENSG00000096872	*IFT74*	ENSG00000278272	*HIST1H3C*
ENSG00000046889	*PREX2*	ENSG00000275379	*HIST1H3I*
ENSG00000005238	*FAM214B*	ENSG00000273983	*HIST1H3G*
ENSG00000107611	*CUBN*	ENSG00000197153	*HIST1H3J*
ENSG00000165113	*GKAP1*	ENSG00000278828	*HIST1H3H*
ENSG00000114107	*CEP70*	ENSG00000274267	*HIST1H3B*
ENSG00000101152	*DNAJC5*	ENSG00000278637	*HIST1H4A*
ENSG00000196812	*ZSCAN16*	ENSG00000126453	*BCL2L12*
ENSG00000197646	*PDCD1LG2*	ENSG00000277157	*HIST1H4D*
ENSG00000128284	*APOL3*	ENSG00000273542	*HIST1H4K*
ENSG00000158270	*COLEC12*	ENSG00000197238	*HIST1H4J*
ENSG00000205683	*DPF3*	ENSG00000197061	*HIST1H4C*

Table S4 continued

Principal Component 1		Principal Component 2	
Ensembl ID	Symbol	Ensembl ID	Symbol
ENSG00000140350	*ANP32A*	ENSG00000158406	*HIST1H4H*
ENSG00000116667	*C1orf21*	ENSG00000276966	*HIST1H4E*
ENSG00000239264	*TXNDC5*	ENSG00000275126	*HIST1H4L*
ENSG00000178878	*APOLD1*	ENSG00000149781	*FERMT3*
ENSG00000124749	*COL21A1*	ENSG00000105447	*GRWD1*
ENSG00000143401	*ANP32E*	ENSG00000126391	*FRMD8*
ENSG00000140941	*MAP1LC3B*	ENSG00000160072	*ATAD3B*
ENSG00000062716	*VMP1*	ENSG00000143341	*HMCN1*
ENSG00000145349	*CAMK2D*	ENSG00000130307	*USHBP1*
ENSG00000178922	*HYI*	ENSG00000144354	*CDCA7*
ENSG00000184260	*HIST2H2AC*	ENSG00000177602	*GSG2*
ENSG00000275713	*HIST1H2BH*	ENSG00000136492	*BRIP1*
ENSG00000130300	*PLVAP*	ENSG00000124074	*ENKD1*
ENSG00000126878	*AIF1L*	ENSG00000064012	*CASP8*
ENSG00000277157	*HIST1H4D*	ENSG00000140853	*NLRC5*
ENSG00000149781	*FERMT3*	ENSG00000169604	*ANTXR1*
ENSG00000136169	*SETDB2*	ENSG00000242125	*SNHG3*
ENSG00000133687	*TMTC1*	ENSG00000118473	*SGIP1*
ENSG00000119632	*IFI27L2*	ENSG00000183011	*NAA38*
ENSG00000136492	*BRIP1*	ENSG00000256053	*APOPT1*
ENSG00000158710	*TAGLN2*	ENSG00000184384	*MAML2*
ENSG00000126653	*NSRP1*	ENSG00000145794	*MEGF10*
ENSG00000115363	*EVA1A*	ENSG00000154556	*SORBS2*
ENSG00000169604	*ANTXR1*	ENSG00000183615	*FAM167B*
ENSG00000242125	*SNHG3*	ENSG00000161551	*ZNF577*
ENSG00000121851	*POLR3GL*	ENSG00000167747	*C19orf48*
ENSG00000186812	*ZNF397*	ENSG00000163702	*IL17RC*
ENSG00000168101	*NUDT16L1*	ENSG00000176619	*LMNB2*
ENSG00000122986	*HVCN1*	ENSG00000185904	*LINC00839*
ENSG00000168497	*SDPR*	ENSG00000099910	*KLHL22*
ENSG00000198286	*CARD11*	ENSG00000135637	*CCDC142*
ENSG00000166432	*ZMAT1*	ENSG00000092208	*GEMIN2*
ENSG00000176014	*TUBB6*	ENSG00000146374	*RSPO3*
ENSG00000167553	*TUBA1C*	ENSG00000164099	*PRSS12*
ENSG00000223749	*MIR503HG*	ENSG00000102802	*MEDAG*
ENSG00000166387	*PPFIBP2*	ENSG00000233016	*SNHG7*
ENSG00000128849	*CGNL1*	ENSG00000196507	*TCEAL3*
ENSG00000129474	*AJUBA*	ENSG00000274997	*HIST1H2AH*
ENSG00000149150	*SLC43A1*	ENSG00000197903	*HIST1H2BK*
ENSG00000196507	*TCEAL3*	ENSG00000180543	*TSPYL5*
ENSG00000144283	*PKP4*	ENSG00000105499	*PLA2G4C*
ENSG00000108797	*CNTNAP1*	ENSG00000162407	*PLPP3*
ENSG00000171617	*ENC1*	ENSG00000113739	*STC2*

Table S4 continued

Principal Component 1		Principal Component 2	
Ensembl ID	Symbol	Ensembl ID	Symbol
ENSG00000143127	*ITGA10*	ENSG00000138735	*PDE5A*
ENSG00000170915	*PAQR8*	ENSG00000118640	*VAMP8*
ENSG00000143013	*LMO4*	ENSG00000068001	*HYAL2*
ENSG00000087842	*PIR*	ENSG00000159228	*CBR1*
ENSG00000130589	*HELZ2*	ENSG00000159231	*CBR3*
ENSG00000133739	*LRRCC1*	ENSG00000143537	*ADAM15*
ENSG00000150764	*DIXDC1*	ENSG00000157873	*TNFRSF14*
ENSG00000134107	*BHLHE40*	ENSG00000128918	*ALDH1A2*
ENSG00000105499	*PLA2G4C*	ENSG00000138074	*SLC5A6*
ENSG00000162407	*PLPP3*	ENSG00000106052	*TAX1BP1*
ENSG00000079102	*RUNX1T1*	ENSG00000145386	*CCNA2*
ENSG00000196139	*AKR1C3*	ENSG00000133101	*CCNA1*
ENSG00000117533	*VAMP4*	ENSG00000134057	*CCNB1*
ENSG00000162734	*PEA15*	ENSG00000118971	*CCND2*
ENSG00000068001	*HYAL2*	ENSG00000277775	*HIST1H3F*
ENSG00000121858	*TNFSF10*	ENSG00000196787	*HIST1H2AG*
ENSG00000143537	*ADAM15*	ENSG00000124635	*HIST1H2BJ*
ENSG00000168615	*ADAM9*	ENSG00000184897	*H1FX*
ENSG00000141655	*TNFRSF11A*	ENSG00000168010	*ATG16L2*
ENSG00000115604	*IL18R1*	ENSG00000119333	*WDR34*
ENSG00000196468	*FGF16*	ENSG00000162063	*CCNF*
ENSG00000137563	*GGH*	ENSG00000120337	*TNFSF18*
ENSG00000171388	*APLN*	ENSG00000186193	*SAPCD2*
ENSG00000176170	*SPHK1*	ENSG00000144824	*PHLDB2*
ENSG00000133101	*CCNA1*	ENSG00000238227	*C9orf69*
ENSG00000118971	*CCND2*	ENSG00000171004	*HS6ST2*
ENSG00000067798	*NAV3*	ENSG00000003096	*KLHL13*
ENSG00000168010	*ATG16L2*	ENSG00000110711	*AIP*
ENSG00000172578	*KLHL6*	ENSG00000141295	*SCRN2*
ENSG00000113732	*ATP6V0E1*	ENSG00000198901	*PRC1*
ENSG00000120337	*TNFSF18*	ENSG00000129691	*ASH2L*
ENSG00000127533	*F2RL3*	ENSG00000163347	*CLDN1*
ENSG00000013588	*GPRC5A*	ENSG00000137033	*IL33*
ENSG00000139597	*N4BP2L1*	ENSG00000168679	*SLC16A4*
ENSG00000129691	*ASH2L*	ENSG00000157456	*CCNB2*
ENSG00000134873	*CLDN10*	ENSG00000114767	*RRP9*
ENSG00000163347	*CLDN1*	ENSG00000174371	*EXO1*
ENSG00000162595	*DIRAS3*	ENSG00000162614	*NEXN*
ENSG00000169744	*LDB2*	ENSG00000179820	*MYADM*
ENSG00000258890	*CEP95*	ENSG00000120334	*CENPL*
ENSG00000134668	*SPOCD1*	ENSG00000073803	*MAP3K13*
ENSG00000137033	*IL33*	ENSG00000198774	*RASSF9*
ENSG00000109881	*CCDC34*	ENSG00000133083	*DCLK1*

Table S4 continued

Principal Component 1		Principal Component 2	
Ensembl ID	Symbol	Ensembl ID	Symbol
ENSG00000141526	*SLC16A3*	ENSG00000178999	*AURKB*
ENSG00000107438	*PDLIM1*	ENSG00000171451	*DSEL*
ENSG00000165915	*SLC39A13*	ENSG00000164611	*PTTG1*
ENSG00000187051	*RPS19BP1*	ENSG00000183691	*NOG*
ENSG00000154359	*LONRF1*	ENSG00000128487	*SPECC1*
ENSG00000115602	*IL1RL1*	ENSG00000017483	*SLC38A5*
ENSG00000198774	*RASSF9*	ENSG00000181218	*HIST3H2A*
ENSG00000262919	*FAM58A*	ENSG00000071539	*TRIP13*
ENSG00000167874	*TMEM88*	ENSG00000105676	*ARMC6*
ENSG00000151276	*MAGI1*	ENSG00000198542	*ITGBL1*
ENSG00000008517	*IL32*	ENSG00000145348	*TBCK*
ENSG00000183691	*NOG*	ENSG00000101670	*LIPG*
ENSG00000100784	*RPS6KA5*	ENSG00000134824	*FADS2*
ENSG00000196923	*PDLIM7*	ENSG00000200913	*SNORD46*
ENSG00000081320	*STK17B*	ENSG00000099337	*KCNK6*
ENSG00000010278	*CD9*	ENSG00000118777	*ABCG2*
ENSG00000178031	*ADAMTSL1*	ENSG00000172071	*EIF2AK3*
ENSG00000205038	*PKHD1L1*	ENSG00000129675	*ARHGEF6*
ENSG00000134986	*NREP*	ENSG00000158859	*ADAMTS4*
ENSG00000198542	*ITGBL1*	ENSG00000154734	*ADAMTS1*
ENSG00000156787	*TBC1D31*	ENSG00000112208	*BAG2*
ENSG00000138398	*PPIG*	ENSG00000130755	*GMFG*
ENSG00000101670	*LIPG*	ENSG00000138433	*CIR1*
ENSG00000152465	*NMT2*	ENSG00000146592	*CREB5*
ENSG00000110031	*LPXN*	ENSG00000131016	*AKAP12*
ENSG00000172057	*ORMDL3*	ENSG00000050344	*NFE2L3*
ENSG00000118777	*ABCG2*	ENSG00000174791	*RIN1*
ENSG00000135218	*CD36*	ENSG00000104728	*ARHGEF10*
ENSG00000179841	*AKAP5*	ENSG00000100034	*PPM1F*
ENSG00000050438	*SLC4A8*	ENSG00000110848	*CD69*
ENSG00000154734	*ADAMTS1*	ENSG00000135476	*ESPL1*
ENSG00000130513	*GDF15*	ENSG00000170160	*CCDC144A*
ENSG00000138185	*ENTPD1*	ENSG00000170381	*SEMA3E*
ENSG00000115129	*TP53I3*	ENSG00000138593	*SECISBP2L*
ENSG00000138182	*KIF20B*	ENSG00000048052	*HDAC9*
ENSG00000146592	*CREB5*	ENSG00000007312	*CD79B*
ENSG00000131016	*AKAP12*	ENSG00000166803	*KIAA0101*
ENSG00000026508	*CD44*	ENSG00000126787	*DLGAP5*
ENSG00000050344	*NFE2L3*	ENSG00000184867	*ARMCX2*
ENSG00000187608	*ISG15*	ENSG00000198826	*ARHGAP11A*
ENSG00000135968	*GCC2*	ENSG00000170312	*CDK1*
ENSG00000085063	*CD59*	ENSG00000165304	*MELK*
ENSG00000158417	*EIF5B*	ENSG00000101003	*GINS1*

Table S4 continued

Principal Component 1		Principal Component 2	
Ensembl ID	Symbol	Ensembl ID	Symbol
ENSG00000135404	*CD63*	ENSG00000094804	*CDC6*
ENSG00000106443	*PHF14*	ENSG00000159164	*SV2A*
ENSG00000110848	*CD69*	ENSG00000117399	*CDC20*
ENSG00000065308	*TRAM2*	ENSG00000164045	*CDC25A*
ENSG00000166037	*CEP57*	ENSG00000101224	*CDC25B*
ENSG00000048052	*HDAC9*	ENSG00000158402	*CDC25C*
ENSG00000110651	*CD81*	ENSG00000181634	*TNFSF15*
ENSG00000158691	*ZSCAN12*	ENSG00000100918	*REC8*
ENSG00000130052	*STARD8*	ENSG00000231711	NA
ENSG00000177697	*CD151*	ENSG00000257732	NA
ENSG00000198853	*RUSC2*	ENSG00000259001	NA
ENSG00000065609	*SNAP91*	ENSG00000266037	NA
ENSG00000159164	*SV2A*	ENSG00000233452	NA
ENSG00000162413	*KLHL21*	ENSG00000132967	NA
ENSG00000242802	*AP5Z1*	ENSG00000261269	NA
ENSG00000241399	*CD302*	ENSG00000261295	NA
ENSG00000013364	*MVP*	ENSG00000263426	NA
ENSG00000181634	*TNFSF15*	ENSG00000263740	NA
ENSG00000100918	*REC8*	ENSG00000280079	NA
ENSG00000118412	*CASP8AP2*	ENSG00000281508	NA
ENSG00000232533	NA	ENSG00000200087	NA
ENSG00000233117	NA	ENSG00000197083	NA
ENSG00000260604	NA	ENSG00000200312	NA
ENSG00000233452	NA	ENSG00000220785	NA
ENSG00000171889	NA	ENSG00000233117	NA
ENSG00000140181	NA	ENSG00000175746	NA
ENSG00000279095	NA	ENSG00000267325	NA
ENSG00000235385	NA	ENSG00000222489	NA
ENSG00000266037	NA	ENSG00000124529	NA
ENSG00000257605	NA	ENSG00000223612	NA
ENSG00000248187	NA	ENSG00000229855	NA
ENSG00000228742	NA	ENSG00000244642	NA
ENSG00000175746	NA	ENSG00000254635	NA
ENSG00000273038	NA	ENSG00000210082	NA
ENSG00000253177	NA	ENSG00000226476	NA
ENSG00000225840	NA	ENSG00000226702	NA
ENSG00000276107	NA	ENSG00000226958	NA
ENSG00000263426	NA	ENSG00000265150	NA
ENSG00000198327	NA	ENSG00000197927	NA
ENSG00000226958	NA	ENSG00000214176	NA
ENSG00000244398	NA	ENSG00000205664	NA
ENSG00000282057	NA	ENSG00000228495	NA
ENSG00000259345	NA	ENSG00000276107	NA

Table S4 continued

Principal Component 1		Principal Component 2	
Ensembl ID	Symbol	Ensembl ID	Symbol
ENSG00000257732	NA	ENSG00000198327	NA
ENSG00000228495	NA	ENSG00000276232	NA
ENSG00000230257	NA	ENSG00000140181	NA
ENSG00000215386	NA	ENSG00000237039	NA
ENSG00000231991	NA	ENSG00000230606	NA
ENSG00000207344	NA	ENSG00000197846	NA
ENSG00000168405	NA	ENSG00000237973	NA
ENSG00000226476	NA	ENSG00000260604	NA
ENSG00000269378	NA	ENSG00000239437	NA
ENSG00000165121	NA	ENSG00000235385	NA
ENSG00000231503	NA	ENSG00000248187	NA

Table S5 Genes identified in HEK293T ChIP which are differentially regulated by WT and MUT

Symbol	Ensembl ID	FPKM		
		NT	WT	MUT
HMOX1	ENSG00000100292	30.30	47.97	25.07
HIST2H2AB	ENSG00000184270	18.69	29.63	13.29
CDCA8	ENSG00000134690	7.67	12.05	6.36
HIST1H2BL	ENSG00000185130	59.24	103.33	31.13
HIST1H2BO	ENSG00000274641	82.49	137.69	72.48
HIST1H3J	ENSG00000197153	50.04	114.55	49.60
HIST1H4C	ENSG00000197061	75.85	196.47	58.17
HIST1H4H	ENSG00000158406	220.72	349.98	154.04
HIST1H2AH	ENSG00000274997	43.53	96.02	40.45
HIST1H2BJ	ENSG00000124635	137.43	346.42	127.87
WDR34	ENSG00000119333	8.97	15.29	8.18
AURKB	ENSG00000178999	9.62	17.80	9.65
GPC5	ENSG00000179399	4.20	2.08	4.70
ITGA4	ENSG00000115232	2.48	0.95	25.38
NEXN	ENSG00000162614	22.82	5.78	13.77

Dataset S1 Pairwise comparison of WT and MUT (Excel file, not included)

Dataset S2 Pairwise comparison of NT and WT (Excel file, not included)

Dataset S3 Pairwise comparison of NT and MUT (Excel file, not included)

Dataset S4 Genes located near the binding sites of ZNF408 (Excel file, not included)

All datasets are available upon request (contact: dyah.karjosukarso@radboudumc.nl).

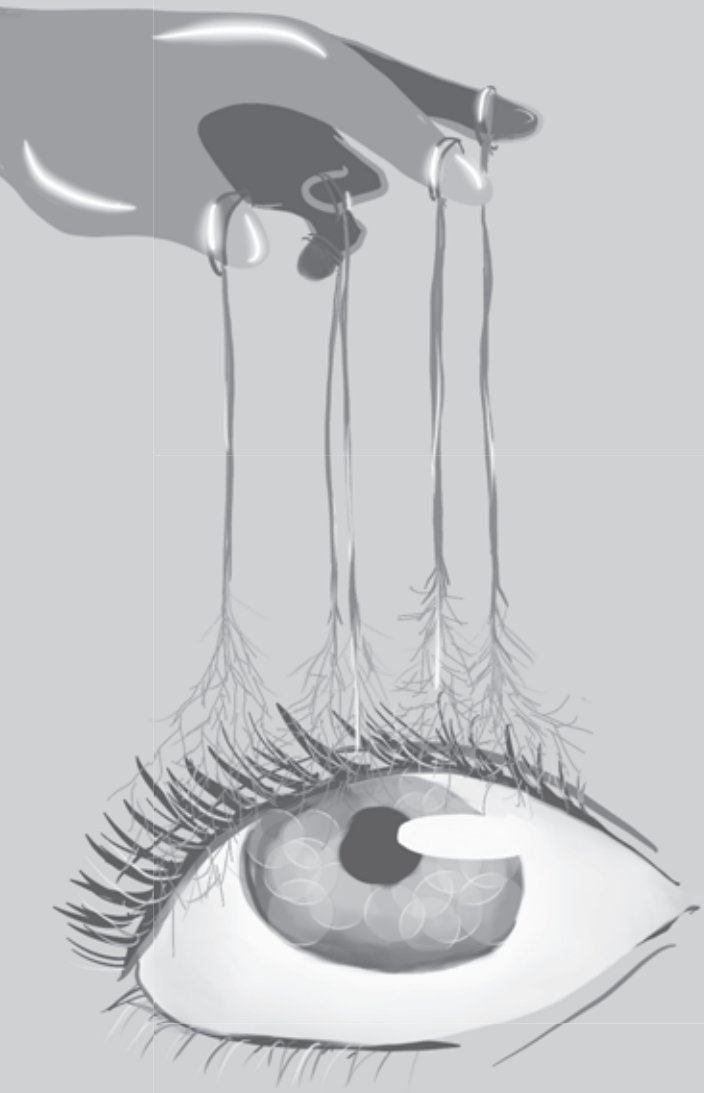

Chapter 3

Modeling *ZNF408*-associated FEVR in zebrafish results in abnormal retinal vasculature

Dyah W. Karjosukarso[1], Zaheer Ali[2], Theo A. Peters[3], Jia Qi Cheng Zhang[1], Erwin van Wijk[3], Lasse D. Jensen[2,¶], Rob W.J. Collin[1,¶]

[1]Department of Human Genetics, Donders Institute for Brain, Cognition and Behaviour, Radboud University Medical Center, Nijmegen, the Netherlands; [2]Unit of Cardiovascular Medicine, Department of Medical and Health Sciences, Linköping University, Linköping, Sweden; [3]Department of Otorhinolaryngology, Donders Institute for Brain, Cognition and Behaviour, Radboud University Medical Center, Nijmegen, the Netherlands.

¶These authors contributed equally to this work

Submitted for publication

Abstract

Familial exudative vitreoretinopathy (FEVR) is an inherited retinal disease in which the retinal vasculature is affected. Patients with FEVR typically lack or have abnormal vasculature in the peripheral retina, the outcome of which can range from mild visual impairment to complete blindness. A missense mutation (p.His455Tyr) in *ZNF408* was identified in an autosomal dominant FEVR family. Since little is known about the molecular role of ZNF408 and how its defect leads to the clinical features of FEVR, we generated two homozygous truncated *znf408* zebrafish models as well as one heterozygous and one homozygous missense *znf408* model in which the human p.His455Tyr mutation is mimicked, using CRISPR/Cas9 technology. Intriguingly, all three *znf408*-mutant zebrafish strains demonstrated progressive retinal vascular pathology, initially characterized by a deficient hyaloid vessel development at 5 dpf leading to vascular insufficiency in the retina. The generation of stable mutant lines allowed long-term follow up study which showed ectopic retinal vascular hyper-sprouting at 90 dpf and extensive vascular leakage at 180 dpf. Together, our data demonstrate an important role for znf408 in the development and maintenance of the vascular system within the retina.

3.1 Introduction

Vasculature defects in the retina are one of the leading causes of visual impairment [1]. Different developmental vision disorders resulting from retinal vasculature defects have been described, such as familial exudative vitreoretinopathy (FEVR), Norrie disease, persistent fetal vasculature, and retinopathy of prematurity (ROP), some of which have overlapping features [2]. FEVR is a rare inherited disorder which is hallmarked by an abnormal development of the vasculature in the peripheral retina. The clinical features of FEVR are heterogeneous, varying from normal vision to complete blindness [2]. Besides its diverse clinical manifestations, FEVR is also a genetically heterogeneous disorder. Defects in *FZD4*, *LRP5*, *NDP*, and *TSPAN12* are classically associated with FEVR. These genes, as well as the mutations they harbor, have been thoroughly investigated, both *in vitro* and *in vivo* (reviewed in [2, 3]). Recent genetic studies discovered more genes to be associated with FEVR, such as *ZNF408* [4], *RCBTB1* [5] and *CTNNB1* [6, 7].

A missense mutation in *ZNF408* (c.1363C>T, p.His455Tyr, NM_024741) was identified in a large autosomal dominant FEVR family [4]. We demonstrated that the encoded protein, ZNF408, is localized in the nucleus and the mutation caused mislocalization of ZNF408 to the cytoplasm [4]. Furthermore, morpholino-induced transient knockdown of *znf408* in zebrafish led to abnormal development of eye and trunk vasculature [4], suggesting it plays an important role in the development of the vasculature. However, it remains unclear what the exact role of ZNF408 is in this process, as well as how its defect results in abnormal retinal vasculature development that leads to visual impairment.

In the recent years, zebrafish has become more and more popular as a model organism to study disease mechanisms. Besides its easy maintenance and relatively low costs, 84% of known human disease-associated genes have an orthologue in this model [8]. Vision-related disorders are among the wide variety of human diseases that have been studied in zebrafish. The zebrafish retina has a layered structure which is highly similar to the human retina. Since zebrafish are diurnal organisms, their cone density is also close to that of the human retina [9]. Furthermore, the zebrafish retina is supplied by a choroidal and a retinal vasculature, the latter being derived from the hyaloid vasculature, comparable to the retinal vasculature in humans [10-12]. Finally, the availability of transgenic zebrafish lines expressing

fluorescent reporters in the cells which constitute the blood vessels, such as *Tg(fli1:GFP)* [13] and *Tg(flk1:GFP)* [14], adds an extra advantage in its application to studies of vascular-related disorders.

Although a previous morpholino-mediated knockdown study has shown that *znf408* is crucial in the development of eye and trunk vasculature in zebrafish [4], the specificity of morpholinos has been debated over the recent years [15-17]. Moreover, transient knock-down merely allows short-term investigation during early development. Finally, only the effect of an insufficient amount of a protein of interest could be observed in such knock-down studies, which is not always completely relevant for diseases inherited in an autosomal dominant manner, such as FEVR. To further study the role of ZNF408 in the vasculature development *in vivo*, we generated two homozygous zebrafish models with a frameshift mutation in *znf408* (*znf408*$^{rmc103/rmc103}$ and *znf408*$^{rmc104/rmc104}$), as well as one heterozygous and one homozygous missense *znf408* model in which the human p.His455Tyr mutation is mimicked (*znf408*$^{rmc105/+}$ and *znf408*$^{rmc105/rmc105}$), using CRISPR/Cas9 technology. This study was designed in order to determine the effect of absence (or truncation) of znf408 as well as the effect of a specific amino acid substitution such as observed in FEVR patients, which may or may not differ from the effect of *znf408* knockdown. Furthermore, the generation of stable mutant zebrafish lines would allow us to study and compare the effect of the mutations from larval stage up to adult stage, while the previous knockdown study only allowed observation at larval stage. We found that both the absence of znf408 as well as the presence of znf408 harboring the human FEVR-mutation resulted in impaired development of the hyaloid vasculature, followed by subsequent hyper-sprouting and structural destabilization of retinal vessels in the periphery of the optic disc culminating in extensive retinal vascular leakage at 180 days post fertilization (dpf). These phenotypes accurately recapitulate the disease history of FEVR in human patients, suggesting that the zebrafish mutants developed here could be exploited for developing an improved understanding of FEVR.

3.2 Materials and Methods

3.2.1 Ethics statement

Zebrafish experiments were approved by the local Animal Experimentation Committee (RU-DEC-2016-0991 and N89/15) and were performed according to the Dutch law (Wet op Dierproven 1996), the Swedish guidelines for laboratory animal research, and European regulations (Directive 86/609/EEC).

3.2.2 Zebrafish husbandry

Tupfel long fin (TLF) and *Tg(flk1:GFP)* zebrafish were maintained under standard conditions following institutional and international guidelines. Zebrafish eggs were obtained from natural spawning.

3.2.3 CRISPR/Cas9 design

The zebrafish znf408 protein sequence was aligned with the human ZNF408 protein using AlignX in VectorNTI software package, to determine the position of the fourth zinc finger domain in zebrafish znf408 (Figure S1). Subsequently, guide RNAs (gRNAs) targeting the nucleotide sequences around the fourth zinc finger domain (Figure 1a) were designed using Chopchop software (https://chopchop.rc.fas.harvard.edu/) and synthesized as previously described by Gagnon et al. [18]. A single-stranded DNA (ssDNA) donor template was used to generate the mutation that changes one of the histidine residues in the fourth zinc finger domain to a tyrosine, similar to the human p.His455Tyr mutation (Figure 1a). Next to the intended mutation, the donor template also contained silent mutations to avoid recognition by the gRNA (Figure 1a).

3.2.4 Generation of *znf408* zebrafish model

To increase the efficiency of the homology directed repair mechanism, the non-homologous end joining repair mechanism was inhibited by a splice-blocking morpholino targeting *ku70* (5'-AACTTTTTAGGCTCACCTGCATAGT-3') [19, 20]. A mix of 1 nl containing donor template (0.3 μM), gRNA (600 pg), Cas9 protein (5 ng), *ku70* morpholino (1.5 ng), phenol-red (0.01%), and KCl 0.2 M was injected using a Pneumatic Picopump pv280 (World Precision Instruments) into TLF zebrafish embryos at a one-cell stage. The injected embyros were grown into adulthood at 28°C in E3 medium (5 mM NaCl, 0.17 mM KCl, 0.33 mM $CaCl_2$, 0.33 mM $MgSO_4$, supplemented with 0.01% methylene blue). Three months post-

fertilization, adult CRISPR-injected fish were in-crossed. The offspring was raised and individually genotyped. Subsequently, the appropriate *znf408* mutants were crossed with *Tg(flk1:GFP)* fish to generate zebrafish with modified *znf408* and a GFP reporter on the blood vessels (Figure 1b). The generated fish were then in-crossed to generate homozygous models (Figure 1b).

3.2.5 Genotyping

Larvae and adult fish were genotyped by lysing the larvae or the fin of the adult fish in lysis buffer (40 mM NaOH and 0.2 mM EDTA) for 20 minutes at 95°C. For PCR amplification targeting the mutated region, 1-4 µl of the ten times diluted lysate was used. The primers fw 5'-GTGCACAGAGTGTGGCAAGT-3' and rev 5'-CACGTTGGCGAAAACACTTA-3' were used for genotyping and subsequent Sanger sequencing.

3.2.6 RNA analysis

For each RNA isolation, a pool of 25 zebrafish larvae was used. The larvae were snap frozen in liquid nitrogen at 2 days post fertilization (dpf) and either stored at -80°C or directly used for RNA isolation. The larvae were homogenized in Qiazol (Qiagen, Hilden, North Rhein Westphalia, Germany). The homogenized larvae were subjected to overnight chloroform:isopropanol precipitation using glycogen as a carrier. The precipitated RNA was subsequently purified using the Nucleospin RNA kit (Macherey Nagel, Düren, North Rhein Westphalia, Germany) following the manufacturer's instructions. cDNA was synthesized from 500-1000 ng RNA using the iScript cDNA (Bio-rad, Hercules, California, United States) synthesis kit. The obtained cDNA was used as template for *znf408* amplification using the same primers as used for genotyping. The product of this amplification was also Sanger sequenced to ensure that the mutation is transcribed into the mRNA. For normalization purposes, *actb*1 was amplified using primers fw 5'-CAACACTTCAGATCACTTCTCAGG-3' and rev 5'-CATTCTGCTCAAGGACATTGG-3'.

3.2.7 Immunohistochemistry

Zebrafish larvae at 5 dpf were incubated for 10 minutes in 10% (w/v) sucrose/PBS solution for cryo-protection, followed by embedding in Optimal Cutting Temperature (OCT) reagent and snap freezing in isopentane cooled in a liquid nitrogen bath. The cryosections (7 µm) were fixed in 4% paraformaldehyde

(PFA) for 10 minutes at room temperature followed by permeabilization in 0.01% (v/v) Tween 20/PBS for 20 minutes at room temperature. Subsequently, the cryosections were blocked in 10% normal goat serum and 2% BSA for 1 hour at room temperature. The immunostaining was performed using rabbit anti-ZNF408 antibody (1:100, Sigma). The sections were washed 3 times 5 minutes with PBS and then subjected to secondary antibody and DAPI incubation for 1 hour at room temperature. The secondary antibodies used were goat-anti-rabbit Alexa Fluor 568 (1:800, Molecular Probes, Thermo Fisher Scientific, Waltham, Massachusetts, United States). Sections were mounted using ProLong Gold (Thermo Fisher Scientific, Waltham, Massachusetts, United States). Images were taken with Zeiss Axio Imager Z2 (Zeiss, Oberkochen, Baden-Württemberg, Germany).

3.2.8 Vascular phenotyping

Vascular density, morphology and leakage was evaluated by confocal microscopy in the retina of zebrafish larvae at 5 dpf, young adults at 90 dpf or adults at 180 dpf, following intravenous or intraperitoneal injection in larvae or adults, respectively, of lysine-modified, rhodamine-conjugated dextran at 70 kDa (Thermo Scientific, Waltham, Massachusetts, United States), 30 minutes prior to euthanasia with 0.04% MS-222. Euthanized fish were then fixed overnight at 4°C in 4% PFA, enucleation was performed and in case of the adult eyes, the cornea, lens and sclera was removed as previously described [21, 22]. Tissues were mounted, vitreal side up in VectaShield (Vector, Burlingame, California, Unitesd States) and visualized using an LSM700 upright confocal microscope (Leica, Wetzlar, Hesse, Germany). Numbers of completed and anastomosed vessels or incomplete sprouts were manually counted from confocal images of hyaloid/retinal vascular areas of a specified size and density was measured as the percentage of green pixels (i.e. endothelial area) in the total area. Numbers of completed hyaloid vessels, hyaloid or retinal sprouts and the vascular densities were analyzed in a total of 6-10 individual fish per group. The plasma content in the tissue was determined as the percentage of leaded dextran (i.e. red pixels in dual-color images) in an area of interest. Leakage was determined as the plasma content in the tissue divided by the total amount of dextran-containing plasma in the area (i.e. red plus yellow pixels, the latter representing non-leaked, luminal dextran characterized by overlapping green and red signals). Plasma tissue content and leakage was analyzed in a total of 5-8 individual fish per group. Differences between the groups were evaluated using ANOVA followed by Dunnett's post-hoc test and $p<0.05$ was considered significant.

3.2.9 Visual motor response assays

Visual motor response (VMR) assays were performed on zebrafish larvae at 5 dpf using a DanioVision Observation Chamber (Noldus, Wageningen, Gelderland, the Netherlands). The larvae were individually placed in each well of a 48-well plate and subjected to 20 minutes habituation in the dark, followed by cycles of 10 minutes light OFF (dark) and 10 minutes light ON (light) for 4 hours at 28°C. For every batch of larvae, the assay was performed once in the morning and once in the afternoon using different sets of larvae. At least three independent morning and afternoon assays were performed for each genotype. Distance moved (DM, in mm) and maximum velocity (Vmax, in mm/s) were tracked per larvae per second using EthoVision software (Noldus, Wageningen, Gelderland, the Netherlands). Average DM and average Vmax of 24 wild-type larvae were compared to the average activity of 24 mutant larvae in each assay. Further, we focused our analysis on the startle response of the larvae to drastic light onset (change from light OFF to light ON). Delta DM and delta Vmax were calculated for each light onset in each assay. Delta DM or delta Vmax was defined as average DM or Vmax at light ON+1 sec and light ON+2 sec subtracted by the average DM or Vmax 30 seconds prior to light ON. Delta DM and delta Vmax of each light onset from at least three morning or afternoon assays were averaged and compared between those of wild-type larvae and mutant larvae. A two-tailed unpaired Student's t-test was employed to calculate the significant difference between wild-type and mutant larvae at each light onset. The obtained p-values were subjected to multiple testing corrections using the Benjamini-Hochberg method. All analyses were performed using R version 3.3.1.

3.3 Results

CRISPR/Cas9 technology was employed to generate mutant *znf408* zebrafish models. A guide RNA (gRNA) was designed to specifically target *znf408* around the nucleotides coding for the fourth zinc finger domain (Figure 1a). A single-stranded oligonucleotide containing the intended *znf408* c.1282C>T change was designed as donor template, flanked by 25 nucleotides long homology arms. A few silent mutations were inserted in the homology arms to avoid recognition by gRNA (Figure 1a). A mixture of gRNA, donor template and Cas9 protein was injected into one-cell staged zebrafish embryos (F0). Several genotypes were

identified in adult F1 fish, including c.1282del (*znf408*$^{rmc103/+}$), c.1282_1285del (*znf408*$^{rmc104/+}$), and c.1282C>T (*znf408*$^{rmc105/+}$) (Figure 1b). F1 fish with these genotypes were individually crossed with *Tg(flk1:GFP)* fish to generate a zebrafish line with both modified *znf408* and GFP reported on the blood vessels. The generated heterozygous fish were crossed with each other to generate homozygous fish (Figure 1c) such that both heterozygous mutant (mimicking FEVR) as well as homozygous mutant (mimicking retinitis pigmentosa) fish could be studied. RT-PCR analysis showed that in all *znf408* mutant larvae (2 dpf) the mutant mRNAs were expressed, indicating that the mutant transcripts do not fully undergo nonsense-mediated decay (Figure 2a).

The c.1282del and c.1282_1285del mutations lead to a frameshift and are predicted to generate shorter proteins that are truncated from the fourth zinc finger domain onwards, whereas c.1282C>T changes one of the core histidine residues in the fourth zinc finger domain to a tyrosine (p.His428Tyr), at the orthologous position of the p.His455Tyr mutation in human ZNF408 (Figure 1d). In each mutant generated, the predicted fourth zinc finger domain is disrupted due to the mutations introduced. We attempted to determine (mutant) znf408 protein expression, by employing one of the antibodies directed against human ZNF408. As demonstrated in Supplemental Figure S1, the region of the epitope is not well conserved between human and zebrafish proteins, nor should it recognize the truncated protein potentially present in the *znf408*$^{rmc103/rmc103}$ and *znf408*$^{rmc104/rmc104}$ mutants. Immunohistochemistry of 5 dpf larvae, however, revealed 'znf408' staining in the outer plexiform layer (OPL), both in the wild-type and in all mutant conditions (Supplemental Figure S2), suggesting the observed staining is non-specific. Znf408 was not clearly detectable in the eyes of 3 mpf fish by immunostaining (Supplemental Figure S3) nor in the eyes of 6 mpf fish (data not shown), even though *znf408* transcripts were detectable in the eyes of 90 dpf and 180 dpf fish (Figure 2b).

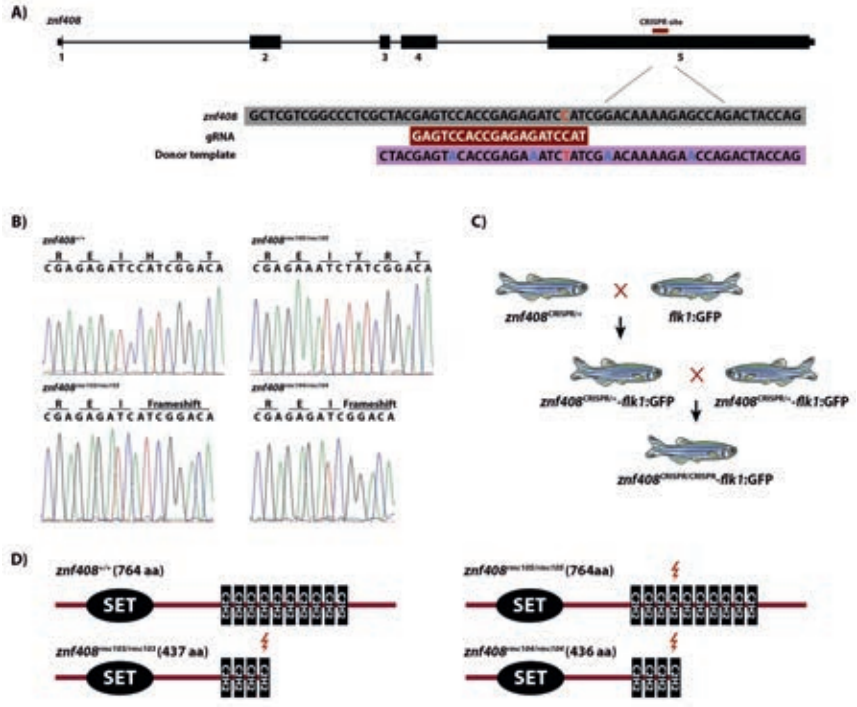

Figure 1. Generation of *znf408* zebrafish models. A) The 5 exons of zebrafish *znf408* are shown. The sequences targeted in exon 5 as well as gRNA and donor template sequences are indicated. B) Sequence analysis of wild-type, *znf408*$^{rmc105/rmc105}$, *znf408*$^{rmc103/rmc103}$, and *znf408*$^{rmc104/rmc104}$. C) The crossing of *znf408* mutants with *Tg(flk1:GFP)* line. D) Protein prediction of the znf408 mutants generated by Prosite tool (https://prosite.expasy.org/scanprosite/) based on the amino acid sequences. The length of the predicted mutant proteins is indicated.

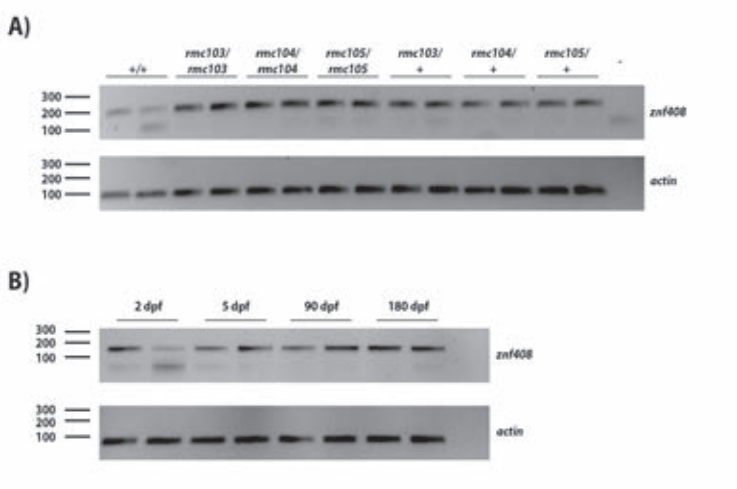

Figure 2. RT-PCR analysis of *znf408* transcripts. A) *Znf408* is expressed in wild-type and mutant larvae at 2 dpf. Two biological replicates are shown. B) *Znf408* is expressed at 2 dpf and 5 dpf larvae as well as in the eye of 3 mpf and 6 mpf wild-type fish. Two biological replicates are shown.

Next, to analyze the retinal vascular development, function and pathology in larval and adult mutant fish or controls, we injected fish at 5, 90 or 180 dpf with fluorescently-labeled 70 kDa Dextran, a method commonly used to analyze vascular perfusion, permeability and leakage, and investigated the retinal vasculature by confocal microscopy. At 5 dpf, we found a significantly reduced number of hyaloid vessels formed in all three homozygous mutant strains, as well as in heterozygous missense (*znf408*$^{rmc105/+}$) mutants (Figure 3), leading to significantly reduced hyaloid vascular density (Supplemental Figure S4). Ongoing hyaloid angiogenesis at these developmental stages was apparent by the presence of several vascular sprouts in all groups, but there were no significant differences in sprouting across the genotypes analyzed (Supplemental Figure S5). The hyaloid vessels that did develop, however, were well perfused and did not leak fluorescently-labeled dextran from the plasma into the tissue (Figure 3a and Supplemental Figure S5). In contrast to this early phenotype, homozygous mutant fish at 90 dpf developed robust retinal neovascularization as evidenced by widespread ectopic sprouting of retinal capillaries (Figures 3a and –c and Supplemental Figure S5). These new sprouts were thin and non-functional and as such did not support perfusion (Figure 3a) and did not significantly increase the density of the retinal vasculature, except for the *znf408*$^{rmc103/rmc103}$ strain (Supplemental Figure S4). Importantly, the vessels were also not leaky at this time point, as no fluorescently-labeled dextran was found outside the vascular lumen (Figure 3a and Supplemental Figure S5). Interestingly, at later stages of disease development represented by 180 dpf fish, the unstable and non-perfused sprouts seen in the 90 dpf fish had largely regressed (Figure 3a), although a smaller yet statistically significant number of ectopic sprouts still remained (Supplemental Figure S5). The retinal vascular density had, however, returned to wildtype levels in the *znf408*$^{rmc103/rmc103}$ strain (Supplemental Figure S4). Interestingly, at this stage, the retinal vasculature had become extremely leaky, as demonstrated by multiple, large edematous pools of fluorescently-labeled dextran that had accumulated under the inner limiting membrane of the retina, especially in the *znf408*$^{rmc103/rmc103}$ and *znf408*$^{rmc104/rmc104}$ strains (Figures 3a and –d and Supplemental Figure S5). Collectively, these findings demonstrate a progressive retinal vascular pathology developing in *znf408*-mutant zebrafish characterized by initially impaired hyaloid vessel development, followed by exaggerated retinal sprouting and which culminates in robust leakage and retinal edema. Importantly, this trajectory closely recapitulates the vascular changes found in patients with FEVR.

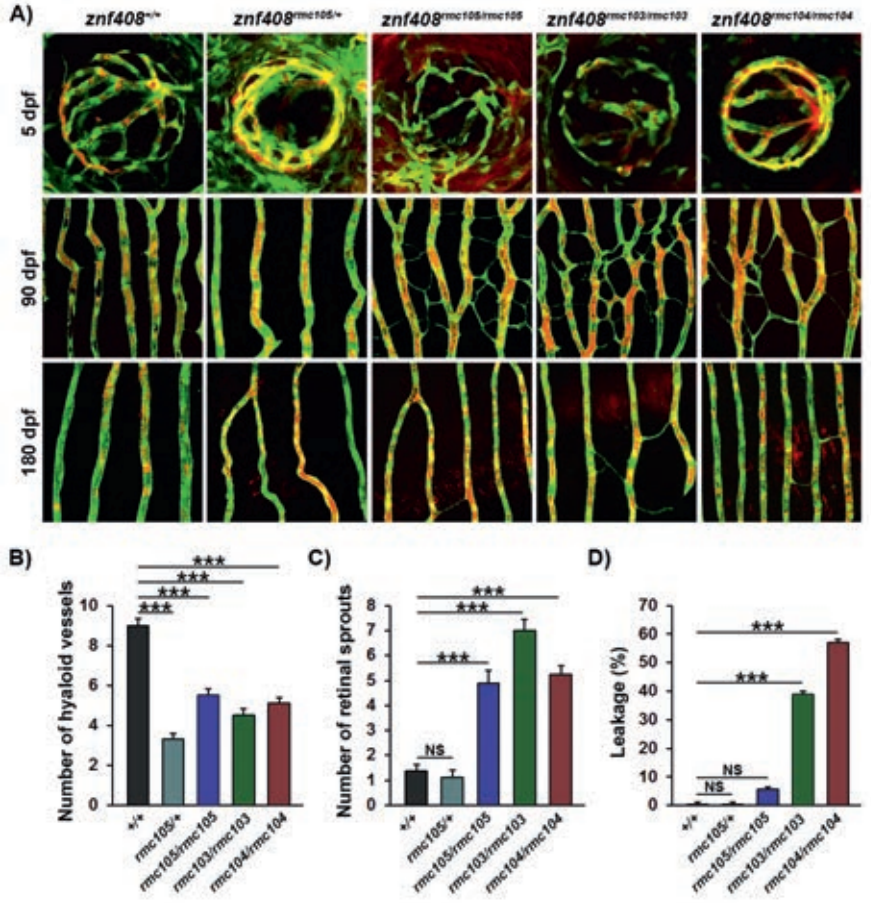

Figure 3. Progressive vascular pathology in *znf408*-mutant zebrafish larvae and adults. A) Confocal micrographs at 5, 90 or 180 dpf of the hyaloid (5 dpf, top row) or retinal vessels (90 dpf, second row and 180 dpf, third row) in *znf408*$^{+/+}$, *znf408*$^{rmc105/+}$, *znf408*$^{rmc105/rmc105}$, *znf408*$^{rmc103/rmc103}$, and *znf408*$^{rmc104/rmc104}$ zebrafish crossed onto the *Tg(flk1:GFP)* background (vessels shown in green) following injection with rhodamine-conjugated dextran (plasma shown in red). B) Quantification of the number of hyaloid vessels at 5 dpf from the groups shown in a. n=10, ANOVA: p<0.001, Dunnets post hoc: ***:p<0.001. C) Quantification of the number of sprouts in the retinal vessels at 90 dpf from the groups shown in a. n=10, ANOVA: p<0.001, Dunnets post hoc: ***:p<0.001. D) Quantification of the leaked dextran as a percentage of total dextran in the retinal vasculature at 180 dpf from the groups shown in a. n=10, ANOVA: p<0.001, Dunnets post hoc: ***:p<0.001.

To assess if there is any visual impairment in these zebrafish, 5 dpf zebrafish larvae were subjected to VMR assay. In this assay, 24 wild-type and 24 mutant larvae were placed individually in a 48-well plate and were exposed to light and dark condition every 10 minutes for 4 hours. The movements of the larvae were monitored during the assay, which is measured as distance moved (in mm) and

velocity (in mm/s). We focused our analysis on the startle response of the larvae to drastic light onset, such as the movement occurring during the switch from dark to light. Although, significant differences in startle response between wild-type and mutant larvae was not observed, there was a trend that the mutant larvae, particularly *znf408*$^{rmc103/rmc103}$ and *znf408*$^{rmc105/rmc105}$ mutants, did not respond to the light switch as much as the wild-type larvae (Figure 4).

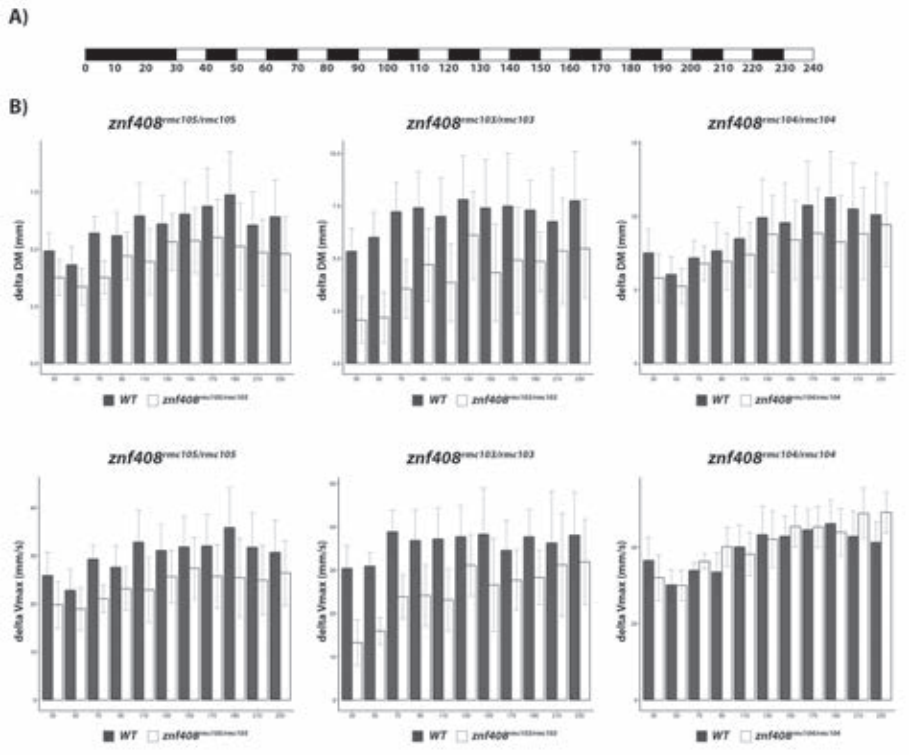

Figure 4. Mutant larvae appear to have less visuomotor response towards light. A) A schematic overview of the light treatment given to the 5 dpf larvae. Black bars denotes dark (light OFF), while white bars illustrates light (light ON) condition. Numbers underneath the bars indicate the duration of the condition in minutes. B) Bar graphs showing the startle response of wild-type vs mutant larvae. Startle response is stated as delta distance moved (DM, in mm) or delta maximum velocity (Vmax, in mm/s). Delta DM or delta Vmax was defined as average DM or Vmax at light ON+1 sec and light ON+2 sec subtracted by the average DM or Vmax 30 seconds prior to light ON.

3.4 Discussion

The identification of a mutation in *ZNF408* in an autosomal dominant FEVR family followed by further *in vitro* investigation has indicated its role in the development of vasculature [4, 23]. To further study ZNF408 *in vivo*, we generated two truncated (*znf408*$^{rmc103/rmc103}$ and *znf408*$^{rmc104/rmc104}$) and one missense (*znf408*$^{rmc105/rmc105}$) zebrafish model using CRISPR/Cas9 technology. Mutant transcripts were generated and did not seem to fully undergo nonsense-mediated decay. Immunohistochemistry analysis failed to reliably detect znf408 in zebrafish retina, possibly due to the poor conservation between the human and zebrafish amino acid sequence of ZNF408 in the region of the epitope. Nevertheless, the zebrafish models we generated clearly showed retinal vascular phenotypes at 5 dpf, 90 dpf and 180 dpf.

The presence of a zebrafish orthologue for the majority of known human disease genes and its genetic versatility render it a suitable animal model to study gene function. Moreover, the similarity of its retinal structure to that of humans, and the availability of vasculature-specific transgenic reporter lines, allowed observation of retinal vasculature development in a disease context, such as intended in this study. Although phenotypic discrepancy between morpholino and gene editing studies in zebrafish has been reported [15-17], this was not the case for *znf408*. At the larval stage, *znf408* mutant zebrafish showed delayed retinal vasculature development, similar to that observed previously in morpholino-mediated knockdown experiments [4]. This suggests the specificity of the phenotype observed upon *znf408* modification with either method. The use of gene editing to generate stable *znf408* zebrafish mutants allowed us to follow-up the phenotypic observations to adult stages.

All three mutant lines exhibited similar pathological hyaloid or retinal vascular features, strongly indicating that these phenotypes were caused by specific modification of znf408 function in these strains. In all three strains, hyaloid vessel development was stunted, suggesting that znf408 is important for angiogenesis specifically in the hyaloid vasculature. In juvenile (3 months old) mutants, however, ectopic capillary sprouting in the peripheral retina was evident, a phenotype highly reminiscent of hypoxia-induced capillary sprouting [21, 22], suggesting that the initially under-developed retinal vasculature likely led to retinal hypoxia which

in turn drove ectopic capillary sprouting. At 6 months, the immature capillary sprouts had regressed but the capillary network remained immature and highly leaky. These phenotypes closely resemble the vascular pathologies seen during progression of FEVR in humans, which also begin with a retinal vasculopathy but at more advanced stages progress to pathological retinal neovascularization and leakage [2, 24]. As such, the functions of znf408 in regulating the zebrafish retinal vasculature closely recapitulate that seen in humans.

ZNF408 encodes for a protein that belongs to the PRDM (positive regulatory domain I-binding factor 1/PRDI-BF1 and retinoblastoma-interacting zinc finger protein 1/RIZ1 homology domain containing) family. Such a protein typically contains a PRDM domain, which is often found in a subfamily of SET methyltransferases, and multiple adjacent C2H2 zinc finger domains. Members of this family have been reported to regulate gene expression either by enzymatic activity towards histone modification, or by interacting with other proteins to modify gene expression [25, 26]. The C2H2 domains of ZNF408 are conserved in several species (i.e. *Homo sapiens*, *Bos taurus*, *Canis familiaris*, *Mus musculus* and *Danio rerio*), highlighting their importance. *Znf408* mRNA was detectable in both truncated lines (*znf408*$^{rmc103/rmc103}$ and *znf408*$^{rmc104/rmc104}$), suggesting that the mutant mRNA did not undergo nonsense-mediated decay, at least not to a large extent. Therefore, a truncated znf408 may be produced in *znf408*$^{rmc103/rmc103}$ and *znf408*$^{rmc104/rmc104}$ zebrafish. However, the protein is likely not functioning properly due to the disrupted zinc finger domains, hence the retinal vasculature phenotype. We have seen in *znf408*$^{rmc105/+}$ fish, how even a single amino acid change in the fourth C2H2 domain led to the observed phenotype, comparable to that observed in all homozygous mutant lines. However, while all mutant lines exhibited similar overall phenotypes, subtle differences in severity were apparent at the 5, 90 and 180 dpf timepoints. Whereas heterozygous *znf408*$^{rmc105/+}$ mutants exhibited impaired hyaloid vessel development that was non-inferior to that seen in the homozygous mutants, the heterozygous fish at 90 and 180 dpf were not phenotypically different from wildtype controls. This suggests that while the development of hyaloid vasculature was temporarily delayed in the heterozygous *znf408*$^{rmc105/+}$ mutants, it likely recovered faster or more fully leading to retinal normoxia at 90 dpf compared to the homozygous mutants. Also at 180 dpf, the homozygous missense *znf408*$^{rmc105/rmc105}$ mutants did not exhibit the same level of vascular leakage as in the *znf408*$^{rmc103/rmc103}$ and *znf408*$^{rmc104/rmc104}$ mutants that are

predicted to produce truncated znf408 proteins. This suggests that in zebrafish znf408 additional vascular functions are associated with the region downstream of the fourth zinc finger domain.

FEVR patients carry the p.His455Tyr mutation in a heterozygous manner [4]. In zebrafish, we observed a clear phenotypic difference between *znf408*$^{rmc105/+}$ and *znf408*$^{rmc105/rmc105}$. Such a diffference was also noted in the animal models for other FEVR genes, such as *FZD4*, *LRP5*, and *TSPAN12*, in which the heterozygous knock-out mice did not show (prominent) phenotype, although both heterozygous and homozygous mutations in these genes have been reported in FEVR patients [2, 27-29]. It is still poorly understood what underlies this difference. Intriguingly, the vascular disruption observed in *znf408* mutants seemed to be specific to the hyaloid/retinal vasculature. This is in line with other studies demonstrating specific requirements for PI3K [30], VEGF-B [31], or Vitamin D [32] in the development of the hyaloid vessels in zebrafish. The specific role of these signaling pathways and whether they constitute different points in the same pathway or contribute to several independent pathways that converge on regulating retinal vascular development is an area of future investigation.

The p.His455Tyr mutation is located within one of the C2H2 domains of ZNF408 and a previous study has shown that endothelial cells overexpressing p.His455Tyr ZNF408 failed to form tube networks *in vitro*. Subsequent transcriptome analysis revealed that ZNF408 regulates the expression of genes involved in the development of vasculature, a process that appears to be disrupted by the p.His455Tyr mutation [23]. Taking into account the comparable *in vitro* versus *in vivo* phenotype, it is tempting to hypothesize that *znf408* has a similar molecular role in zebrafish and the phenotype observed is due to gene expression perturbances. Further investigation to the transcriptome of the mutant zebrafish models may shed further light on this. Analysis performed at different time points may also deepen our insight into the molecular dynamics leading to the unique phenotypes observed at the different stages.

We attempted to detect znf408 protein in the zebrafish retina by immunohistochemistry. Znf408 appeared to localize to the outer plexiform layer in the wild-type zebrafish larvae. However, a similar signal was also detected in *znf408*$^{rmc103/rmc103}$ and *znf408*$^{rmc104/rmc104}$, although the antibody epitope should not be

present in case a truncated znf408 is expressed in the mutant models. Furthermore, no reliable signal was obtained in the retina of young adult (three mpf) and adult (six mpf) zebrafish. Materials only stained with the secondary antibody did not give any fluorescent signal, indicating that there is no aspecific binding of the secondary antibody. In addition, the fluorescent signal was only obtained if the zebrafish materials were not fixed prior to cryosectioning. It is possible that there is not enough similarity between the epitope of the primary ZNF408 antibody used and the zebrafish znf408 amino acid sequence. The specificity of the antibody was previously tested by immunocytochemistry on a cellular system overexpressing HA-tagged znf408, and the fluorescent signal of the HA-tag and znf408 were overlapping, suggesting that the antibody used, in theory, could recognize zebrafish znf408, albeit overexpressed. Nevertheless, we cannot exclude whether there is any peptide in zebrafish that resembles the epitope of the primary antibody, hence the signal oberved in *znf408*$^{rmc103/rmc103}$ and *znf408*$^{rmc104/rmc104}$ mutant lines. A primary antibody directed specifically against zebrafish znf408, in combination with blocking peptides, will likely yield more reliable results.

This study corroborates the involvement of *ZNF408* in the development of retinal vasculature and also in the disease mechanism of FEVR. Intriguingly, in humans, bi-allelic loss-of-function mutations in *ZNF408* have been reported to underlie autosomal recessive retinitis pigmentosa [33, 34]. The loss of function *znf408* zebrafish models (as in *znf408*$^{rmc103/rmc103}$ and *znf408*$^{rmc104/rmc104}$) showed defective retinal vasculature development and only mild visual impairment in visuomotor assay, particularly if compared to the visual impairment observed in retinitis pigmentosa zebrafish models [35-37]. One explanation for this is that the visuomotor assay we used here is not sensitive enough, and alternatives (e.g. electroretinogram recordings, optokinetic response measurements) would be needed. Thus, it is yet to be determined how (predicted) loss of function of *znf408* (as in *znf408*$^{rmc103/rmc103}$ and *znf408*$^{rmc104/rmc104}$) showed a retinal vasculature phenotype instead of retinitis pigmentosa-like symptoms in zebrafish. If truncated znf408 is present in *znf408*$^{rmc103/rmc103}$ and *znf408*$^{rmc104/rmc104}$, it is well possible that the lost of function to the C-terminal did not disrupt photoreceptor function, albeit the apparent vasculature damage. Generation of a full *znf408* knock-out model, in which the indels are inserted as early as possible in *znf408* may provide further insight. Moreover, deeper molecular studies of our zebrafish models by using e.g. transcriptome analysis will likely increase our understanding on this apparent discrepancy.

In conclusion, we here show that disruption of *znf408*, as well as the introduction of a missense mutation mimicking *ZNF408*-associated FEVR, in zebrafish leads to abnormal development and function of the retinal vasculature system. To our knowledge, these are the first stable FEVR models in zebrafish and also the first animal models generated to study *ZNF408*, which can increase our knowledge on the development of retinal vasculature in general, and the still largely unknown mechanisms on how mutations in *ZNF408* can lead to FEVR in humans.

Acknowledgements

We would like to gratefully thank Tom Spanings, Antoon van der Horst, and Jeroen Boerrigter for technical assistance and Margo Dona for the assistance with the visuomotor assay. This work is funded by a Radboudumc PhD grant to Dyah W. Karjosukarso.

Funding

This work is funded by Radboudumc PhD grant to Dyah W. Karjosukarso.

Conflict of interest

The authors declare no conflict of interest.

References

1. Bek, T. (2013) Regional morphology and pathophysiology of retinal vascular disease. *Prog Retin Eye Res* **36**, 247-259
2. Gilmour, D. F. (2015) Familial exudative vitreoretinopathy and related retinopathies. *Eye (Lond)* **29**, 1-14
3. Nikopoulos, K., Venselaar, H., Collin, R. W., Riveiro-Alvarez, R., Boonstra, F. N., Hooymans, J. M., Mukhopadhyay, A., Shears, D., van Bers, M., de Wijs, I. J., van Essen, A. J., Sijmons, R. H., Tilanus, M. A., van Nouhuys, C. E., Ayuso, C., Hoefsloot, L. H., and Cremers, F. P. (2010) Overview of the mutation spectrum in familial exudative vitreoretinopathy and Norrie disease with identification of 21 novel variants in FZD4, LRP5, and NDP. *Hum Mutat* **31**, 656-666
4. Collin, R. W., Nikopoulos, K., Dona, M., Gilissen, C., Hoischen, A., Boonstra, F. N., Poulter, J. A., Kondo, H., Berger, W., Toomes, C., Tahira, T., Mohn, L. R., Blokland, E. A., Hetterschijt, L., Ali, M., Groothuismink, J. M., Duijkers, L., Inglehearn, C. F., Sollfrank, L., Strom, T. M., Uchio, E., van Nouhuys, C. E., Kremer, H., Veltman, J. A., van Wijk, E., and Cremers, F. P. (2013) *ZNF408* is mutated in familial exudative vitreoretinopathy and is crucial for the development of zebrafish retinal vasculature. *Proc Natl Acad Sci U S A* **110**, 9856-9861
5. Wu, J. H., Liu, J. H., Ko, Y. C., Wang, C. T., Chung, Y. C., Chu, K. C., Liu, T. T., Chao, H. M., Jiang, Y. J., Chen, S. J., and Chung, M. Y. (2016) Haploinsufficiency of RCBTB1 is associated with Coats disease and familial exudative vitreoretinopathy. *Hum Mol Genet* **25**, 1637-1647
6. Dixon, M. W., Stem, M. S., Schuette, J. L., Keegan, C. E., and Besirli, C. G. (2016) CTNNB1 mutation associated with familial exudative vitreoretinopathy (FEVR) phenotype. *Ophthalmic Genet* **37**, 468-470
7. Panagiotou, E. S., Sanjurjo Soriano, C., Poulter, J. A., Lord, E. C., Dzulova, D., Kondo, H., Hiyoshi, A., Chung, B. H., Chu, Y. W., Lai, C. H. Y., Tafoya, M. E., Karjosukarso, D., Collin, R. W. J., Topping, J., Downey, L. M., Ali, M., Inglehearn, C. F., and Toomes, C. (2017) Defects in the Cell Signaling Mediator beta-Catenin Cause the Retinal Vascular Condition FEVR. *Am J Hum Genet* **100**, 960-968
8. Richardson, R., Tracey-White, D., Webster, A., and Moosajee, M. (2017) The zebrafish eye-a paradigm for investigating human ocular genetics. *Eye (Lond)* **31**, 68-86
9. Chhetri, J., Jacobson, G., and Gueven, N. (2014) Zebrafish--on the move towards ophthalmological research. *Eye (Lond)* **28**, 367-380
10. Kaufman, R., Weiss, O., Sebbagh, M., Ravid, R., Gibbs-Bar, L., Yaniv, K., and Inbal, A. (2015) Development and origins of zebrafish ocular vasculature. *BMC Dev Biol* **15**, 18
11. Kitambi, S. S., McCulloch, K. J., Peterson, R. T., and Malicki, J. J. (2009) Small molecule screen for compounds that affect vascular development in the zebrafish retina. *Mech Dev* **126**, 464-477
12. Alvarez, Y., Cederlund, M. L., Cottell, D. C., Bill, B. R., Ekker, S. C., Torres-Vazquez, J., Weinstein, B. M., Hyde, D. R., Vihtelic, T. S., and Kennedy, B. N. (2007) Genetic determinants of hyaloid and retinal vasculature in zebrafish. *BMC Dev Biol* **7**, 114
13. Lawson, N. D., and Weinstein, B. M. (2002) In vivo imaging of embryonic vascular development using transgenic zebrafish. *Dev Biol* **248**, 307-318
14. Choi, J., Dong, L., Ahn, J., Dao, D., Hammerschmidt, M., and Chen, J. N. (2007) FoxH1 negatively modulates flk1 gene expression and vascular formation in zebrafish. *Dev Biol* **304**, 735-744
15. Eisen, J. S., and Smith, J. C. (2008) Controlling morpholino experiments: don't stop making antisense. *Development* **135**, 1735-1743
16. Schulte-Merker, S., and Stainier, D. Y. (2014) Out with the old, in with the new: reassessing morpholino knockdowns in light of genome editing technology. *Development* **141**, 3103-3104
17. Kok, F. O., Shin, M., Ni, C. W., Gupta, A., Grosse, A. S., van Impel, A., Kirchmaier, B. C., Peterson-Maduro, J., Kourkoulis, G., Male, I., DeSantis, D. F., Sheppard-Tindell, S., Ebarasi, L., Betsholtz, C., Schulte-Merker, S., Wolfe, S. A., and Lawson, N. D. (2015) Reverse genetic screening reveals poor correlation between morpholino-induced and mutant phenotypes in zebrafish. *Dev Cell* **32**, 97-108
18. Gagnon, J. A., Valen, E., Thyme, S. B., Huang, P., Akhmetova, L., Pauli, A., Montague, T. G., Zimmerman, S., Richter, C., and Schier, A. F. (2014) Efficient mutagenesis by Cas9 protein-mediated oligonucleotide insertion and large-scale assessment of single-guide RNAs. *PLoS One* **9**, e98186

19. Bladen, C. L., Navarre, S., Dynan, W. S., and Kozlowski, D. J. (2007) Expression of the Ku70 subunit (XRCC6) and protection from low dose ionizing radiation during zebrafish embryogenesis. *Neurosci Lett* **422**, 97-102

20. Slijkerman, R., Goloborodko, A., Broekman, S., de Vrieze, E., Hetterschijt, L., Peters, T., Gerits, M., Kremer, H., and van Wijk, E. (2018) Poor Splice-Site Recognition in a Humanized Zebrafish Knockin Model for the Recurrent Deep-Intronic c.7595-2144A>G Mutation in USH2A. *Zebrafish* **15**, 597-609

21. Cao, R., Jensen, L. D., Soll, I., Hauptmann, G., and Cao, Y. (2008) Hypoxia-induced retinal angiogenesis in zebrafish as a model to study retinopathy. *PLoS One* **3**, e2748

22. Rouhi, P., Jensen, L. D., Cao, Z., Hosaka, K., Lanne, T., Wahlberg, E., Steffensen, J. F., and Cao, Y. (2010) Hypoxia-induced metastasis model in embryonic zebrafish. *Nat Protoc* **5**, 1911-1918

23. Karjosukarso, D. W., van Gestel, S. H. C., Qu, J., Kouwenhoven, E. N., Duijkers, L., Garanto, A., Zhou, H., and Collin, R. W. J. (2018) An FEVR-associated mutation in *ZNF408* alters the expression of genes involved in the development of vasculature. *Hum Mol Genet* **27**, 3519-3527

24. Kashani, A. H., Brown, K. T., Chang, E., Drenser, K. A., Capone, A., and Trese, M. T. (2014) Diversity of retinal vascular anomalies in patients with familial exudative vitreoretinopathy. *Ophthalmology* **121**, 2220-2227

25. Fog, C. K., Galli, G. G., and Lund, A. H. (2012) PRDM proteins: important players in differentiation and disease. *Bioessays* **34**, 50-60

26. Hohenauer, T., and Moore, A. W. (2012) The Prdm family: expanding roles in stem cells and development. *Development* **139**, 2267-2282

27. Xu, Q., Wang, Y., Dabdoub, A., Smallwood, P. M., Williams, J., Woods, C., Kelley, M. W., Jiang, L., Tasman, W., Zhang, K., and Nathans, J. (2004) Vascular development in the retina and inner ear: control by Norrin and Frizzled-4, a high-affinity ligand-receptor pair. *Cell* **116**, 883-895

28. Kato, M., Patel, M. S., Levasseur, R., Lobov, I., Chang, B. H., Glass, D. A., 2nd, Hartmann, C., Li, L., Hwang, T. H., Brayton, C. F., Lang, R. A., Karsenty, G., and Chan, L. (2002) Cbfa1-independent decrease in osteoblast proliferation, osteopenia, and persistent embryonic eye vascularization in mice deficient in Lrp5, a Wnt coreceptor. *J Cell Biol* **157**, 303-314

29. Junge, H. J., Yang, S., Burton, J. B., Paes, K., Shu, X., French, D. M., Costa, M., Rice, D. S., and Ye, W. (2009) TSPAN12 regulates retinal vascular development by promoting Norrin- but not Wnt-induced FZD4/beta-catenin signaling. *Cell* **139**, 299-311

30. Alvarez, Y., Astudillo, O., Jensen, L., Reynolds, A. L., Waghorne, N., Brazil, D. P., Cao, Y., O'Connor, J. J., and Kennedy, B. N. (2009) Selective inhibition of retinal angiogenesis by targeting PI3 kinase. *PLoS One* **4**, e7867

31. Jensen, L. D., Nakamura, M., Brautigam, L., Li, X., Liu, Y., Samani, N. J., and Cao, Y. (2015) VEGF-B-Neuropilin-1 signaling is spatiotemporally indispensable for vascular and neuronal development in zebrafish. *Proc Natl Acad Sci U S A* **112**, E5944-5953

32. Merrigan, S. L., and Kennedy, B. N. (2017) Vitamin D receptor agonists regulate ocular developmental angiogenesis and modulate expression of dre-miR-21 and VEGF. *Br J Pharmacol* **174**, 2636-2651

33. Habibi, I., Chebil, A., Kort, F., Schorderet, D. F., and El Matri, L. (2017) Exome sequencing confirms *ZNF408* mutations as a cause of familial retinitis pigmentosa. *Ophthalmic Genet* **38**, 494-497

34. Avila-Fernandez, A., Perez-Carro, R., Corton, M., Lopez-Molina, M. I., Campello, L., Garanto, A., Fernandez-Sanchez, L., Duijkers, L., Lopez-Martinez, M. A., Riveiro-Alvarez, R., Da Silva, L. R., Sanchez-Alcudia, R., Martin-Garrido, E., Reyes, N., Garcia-Garcia, F., Dopazo, J., Garcia-Sandoval, B., Collin, R. W., Cuenca, N., and Ayuso, C. (2015) Whole-exome sequencing reveals *ZNF408* as a new gene associated with autosomal recessive retinitis pigmentosa with vitreal alterations. *Hum Mol Genet* **24**, 4037-4048

35. Corral-Serrano, J. C., Messchaert, M., Dona, M., Peters, T. A., Kamminga, L. M., van Wijk, E., and Collin, R. W. J. (2018) C2orf71a/pcare1 is important for photoreceptor outer segment morphogenesis and visual function in zebrafish. *Sci Rep* **8**, 9675

36. Dona, M., Slijkerman, R., Lerner, K., Broekman, S., Wegner, J., Howat, T., Peters, T., Hetterschijt, L., Boon, N., de Vrieze, E., Sorusch, N., Wolfrum, U., Kremer, H., Neuhauss, S., Zang, J., Kamermans, M., Westerfield, M., Phillips, J., and van Wijk, E. (2018) Usherin defects lead to early-onset retinal dysfunction in zebrafish. *Exp Eye Res* **173**, 148-159

37. Messchaert, M., Dona, M., Broekman, S., Peters, T. A., Corral-Serrano, J. C., Slijkerman, R. W. N., van Wijk, E., and Collin, R. W. J. (2018) Eyes shut homolog is important for the maintenance of photoreceptor morphology and visual function in zebrafish. *PLoS One* **13**, e0200789

Supplementary materials

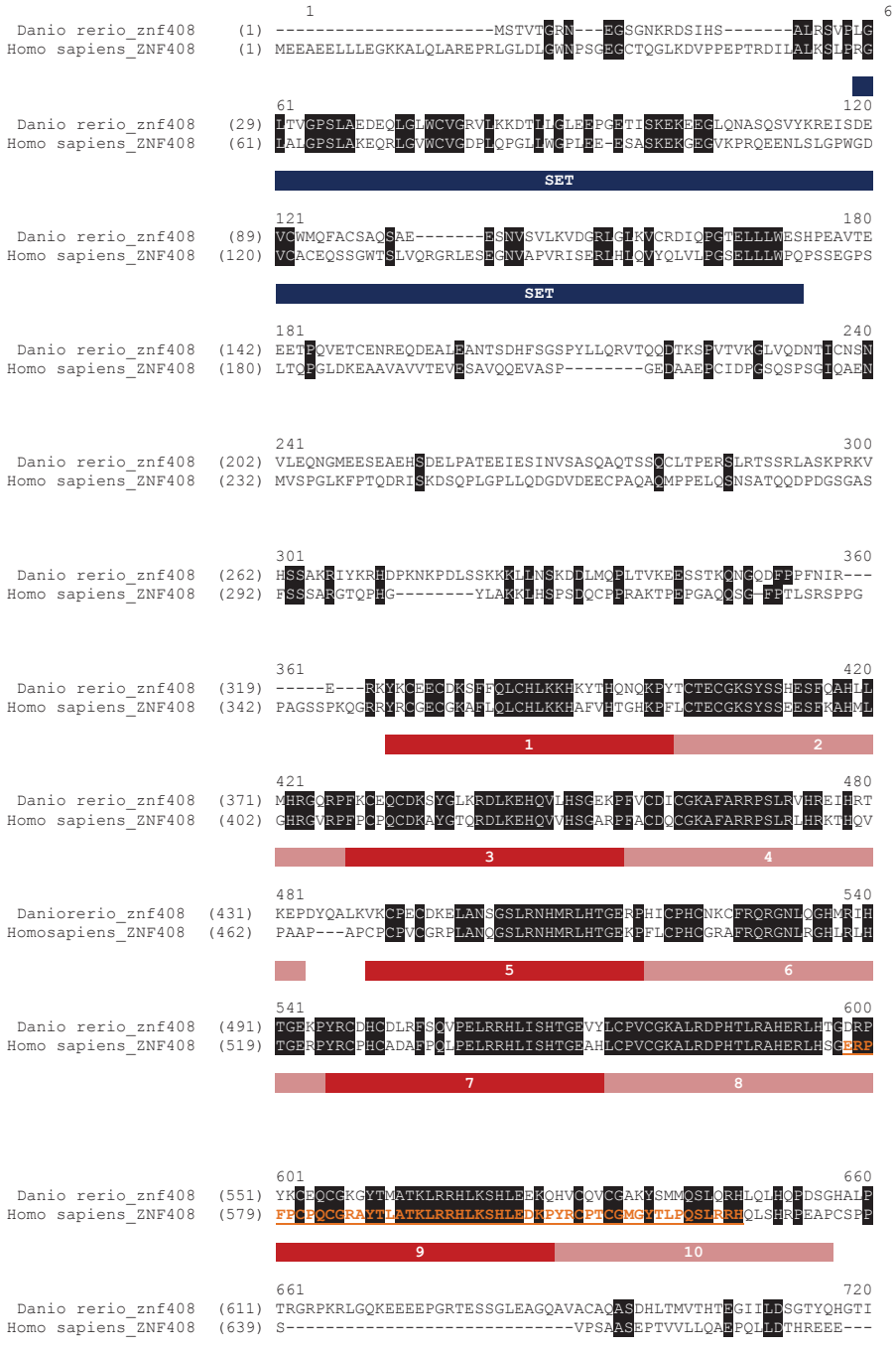

```
                          721                                                 780
 Danio rerio_znf408  (671) VLGKGAEKELDRIELSEDIIEIPISDENTNIVVQEQTSKGLSLQEQEVNAECTVEASSDC
Homo sapiens_ZNF408  (667) ------------VSPARDVVEVTISES----------------QEK-------------C

                          781                                 815
 Danio rerio_znf408  (731) IVLP-EQDANSCLVIIQGQDGLSSVAETVEIETVV
Homo sapiens_ZNF408  (686) FVVPEEPDAAPSLVLIHKDMGLGAWAEVVEVEMGT
```

Figure S1. Sequence alignment of human ZNF408 protein with zebrafish znf408 protein. Identical residues in all sequences are white on a black background. The predicted domains of ZNF408 protein are indicated. The epitope of the ZNF408 antibody used in this manuscript is indicated by orange color and underline.

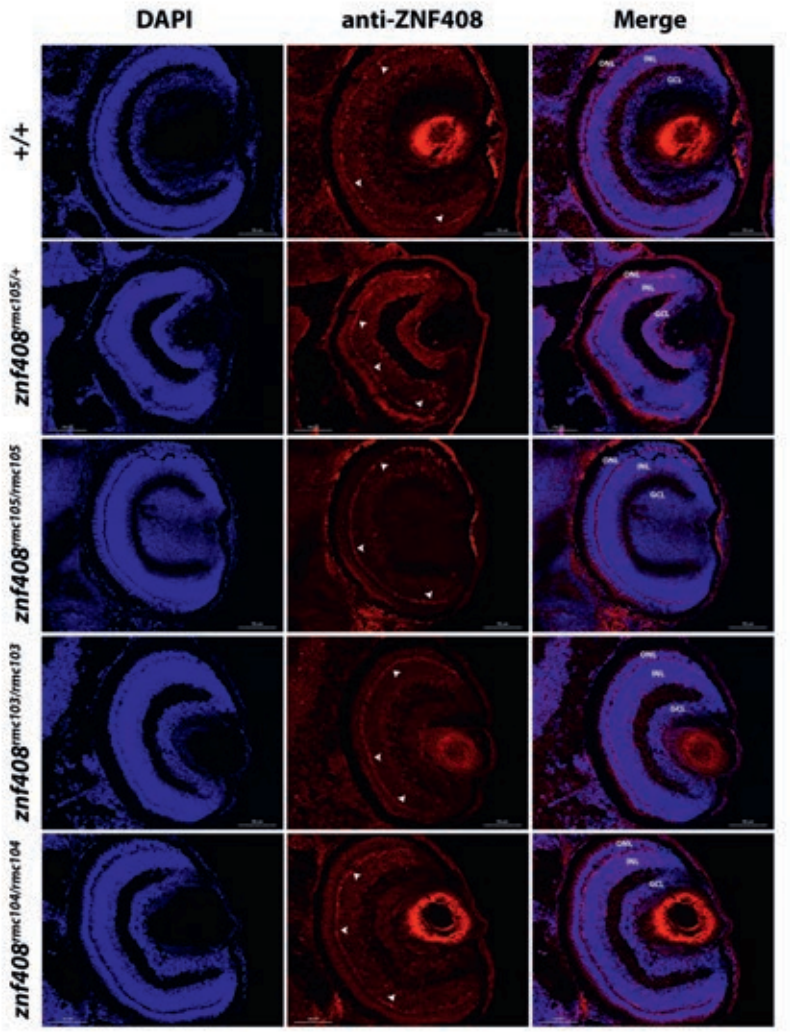

Figure S2. Znf408 is localized in the outer plexiform layer and can be detected in wild-type and mutant larvae at 5 dpf. The signal for znf408 is indicated with white arrowheads and the three nuclear layers of the retina are denoted. The detection of the signal in the truncated mutant larvae renders the results as doubtful. Scale bar is 50 μm.

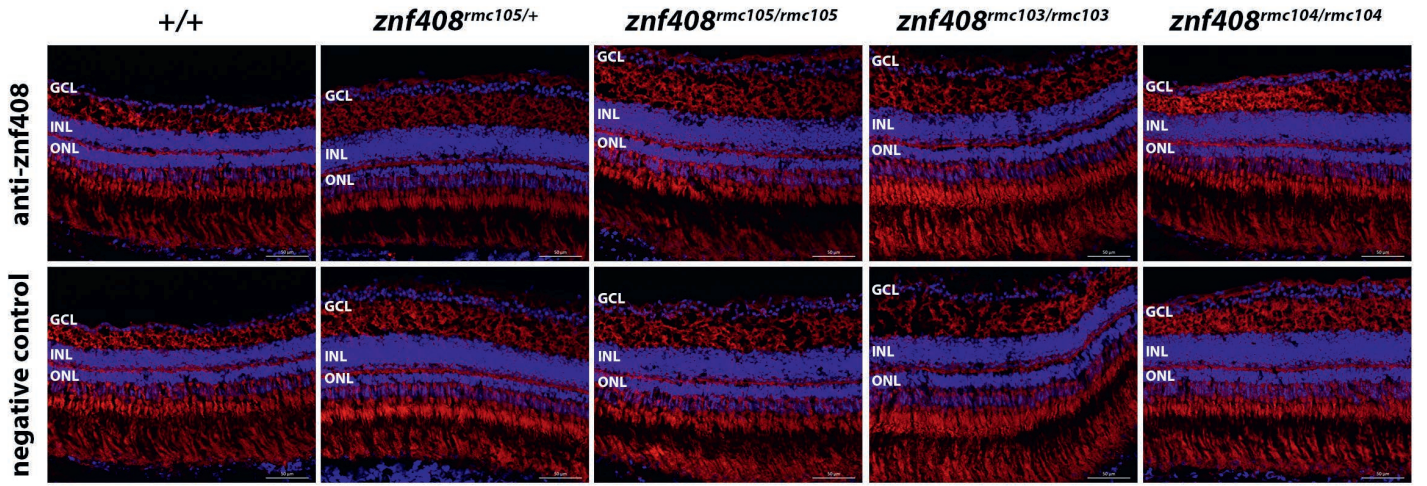

Figure S3. Znf408 was not detectable in the eyes of 90 dpf fish by immunostaining. A representative image per condition is shown and compared to the negative controls, i.e. sections that are only treated with secondary antibody. Scale bar is 50 µm.

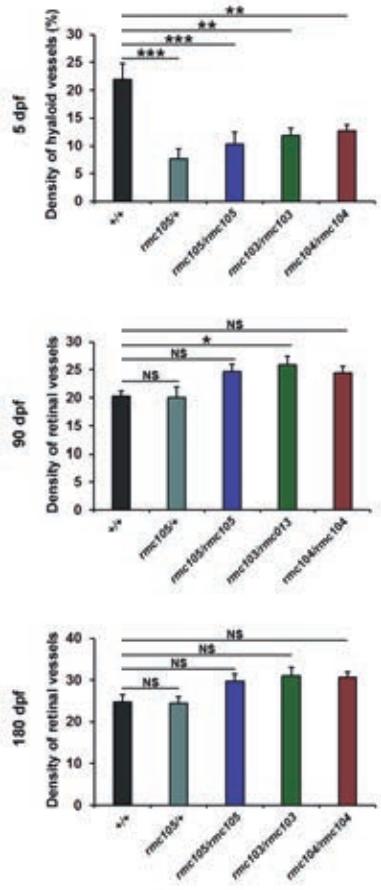

Figure S4. ***Znf408*-mutant zebrafish larvae have lower density of hyaloid vasculature, compared to the wild-type.** Quantification of hyaloid and retinal vasculature at 5, 90, and 180 dpf. n=10, ANOVA: p<0.001, Dunnets post hoc: ***:p<0.001

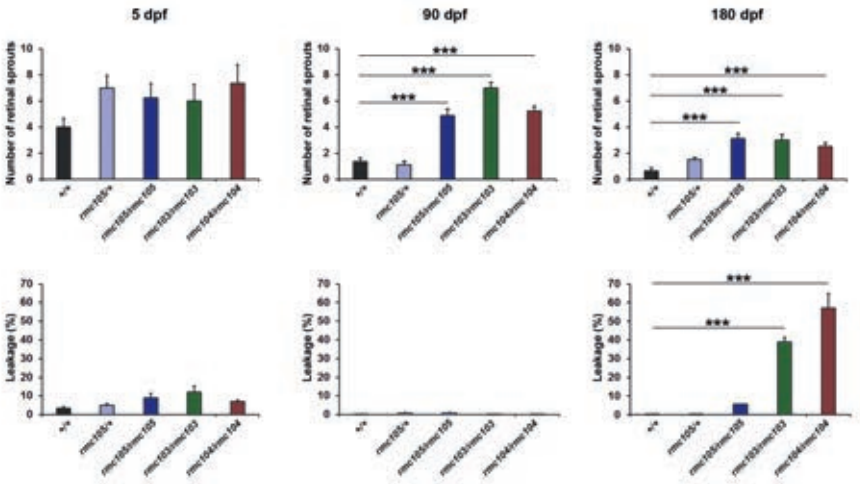

Figure S5. Quantification of sprouting and leakage in the retinal vessels at 5 dpf, 90 dpf, and 180 dpf. Each group has n=5-8, ANOVA: p<0.001, Dunnets post hoc: ***:p<0.001.

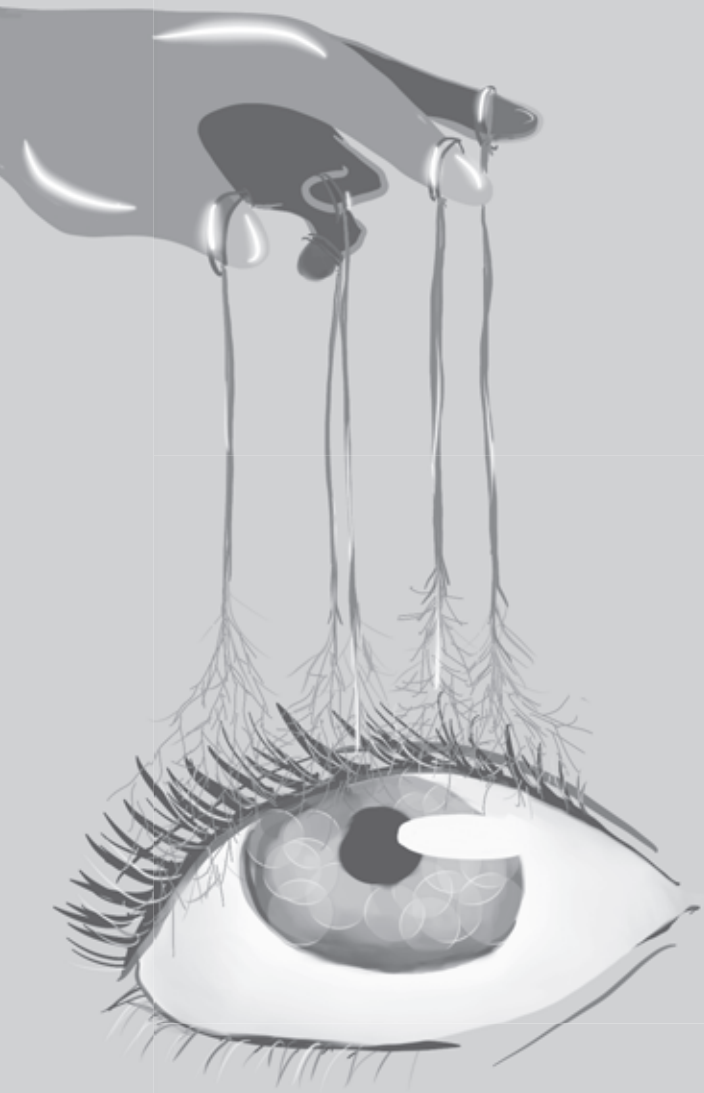

Chapter 4

Application of patient-specific iPSC-derived endothelial cells to study non-penetrance in *ZNF408*-associated familial exudative vitreoretinopathy

Dyah W. Karjosukarso[1], Lonneke Duijkers[2], Anita Hoogendoorn[2], Jia Qi Cheng Zhang[2], Katrin Linda[1], Frans P.M. Cremers[1], Huiqing Zhou[3,4], Rob W.J. Collin[1]

[1]Department of Human Genetics, Donders Institute for Brain, Cognition and Behaviour, Radboud University Medical Center, Nijmegen, the Netherlands;
[2]Department of Human Genetics, Radboud University Medical Center, Nijmegen, the Netherlands;
[3]Department of Molecular Developmental Biology, Faculty of Science, Radboud Institute for Molecular Life Sciences, Radboud University, Nijmegen, the Netherlands;
[4]Department of Human Genetics, Radboud Institute for Molecular Life Sciences, Radboud University Medical Center, Nijmegen, the Netherlands;

Abstract

Familial exudative vitreoretinopathy (FEVR) is an inherited retinal disorder that is primarily characterized by absence or abnormal development of vasculature in the peripheral retina. Heterogeneous clinical features and genetic causes have been observed in FEVR. Moreover, reduced penetrance has also been reported in up to 25% of mutation carriers. Nevertheless, it still largely unknown what causes reduced penetrance in FEVR. A mutation in *ZNF408* (c.1363C>T, p.His455Tyr) was identified in an autosomal dominant FEVR family and non-penetrance of this mutation was observed in two unaffected individuals. In this study, we performed a pilot investigation whether it is possible to generate patient-specific endothelial cells from induced pluripotent stem cells (iPSCs) and used the obtained cells as *in vitro* model of FEVR in order to study *ZNF408*-associated reduced penetrance. Primary fibroblasts cultures were generated from skin biopsies and then reprogrammed into iPSCs. Subsequently, the iPSCs were differentiated to endothelial lineage and then characterized by immunostaining, gene expression analysis, and *in vitro* tube formation assay. The obtained endothelial cells from controls, patient, and unaffected mutant carrier were comparable with respect to morphology, expression of endothelial cells markers, as well as their angiogenic ability. A trend of lower differentiation efficiency towards endothelial cells was observed in both the patient and the unaffected mutant carrier, when compared to controls. Furthermore, the expression of *ZNF408* in the unaffected mutant carrier was approximately 2-fold lower than in patient and controls. Altogether, this pilot study showed that it is possible to generate patient-specific endothelial cells and characterize them to study reduced penetrance in FEVR. To this end, the experiments performed in this study, however, did not explain the underlying cause of reduced penetrance in FEVR.

4.1 Introduction

Familial exudative vitreoretinopathy (FEVR) was first described by Criswick and Schepens [1]. It is an inherited retinal disorder, which is hallmarked by the absence or abnormal development of vasculature in the peripheral retina [2-4]. Various clinical features are observed in FEVR patients, whose manifestations can range from no visual symptom to complete blindness [5]. Furthermore, it is a genetically heterogeneous disorder. Mutations in multiple genes have so far been found to be associated with FEVR [6-14].

Collin *et al.* reported a mutation in *ZNF408* (c.1363C>T, p.His455Tyr) in a large autosomal dominant FEVR family [7]. Besides its presence in FEVR patients, this mutation was also detected in two unaffected family members, suggesting reduced penetrance. Both unaffected family members inherited the mutation from one affected parent and possessed a different wild-type allele compared to their affected sibling (Figure 1).

Non-penetrance is defined as a state in which the presence of a genotype trait does not manifest in the expected phenotype. In FEVR, non-penetrance has been observed in up to 25% of mutation carriers [15]. The penetrance of a genetic variant can be influenced by multiple factors, for instance, gene expression levels, epigenetic modifications, environment, gender, age, allele dosage or modifier genes [16]. The underlying cause(s) of reduced penetrance in FEVR are still hardly understood.

To investigate the cause of non-penetrance, one would need patient material, which has the appropriate genetic background, derived from a relevant tissue. Since retinal vasculature is affected in FEVR, we considered endothelial cells as a relevant *in vitro* model. Although it is not possible to directly access retinal endothelial cells from FEVR patients, recent advances in cellular technology have shown the feasibility of generating patient-specific endothelial cells (ECs) from induced pluripotent stem cells (iPSCs), and subsequently employ the generated iPSC-derived ECs (iPSC-ECs) to study vascular diseases (reviewed in [17, 18]). Moreover, Gu *et al.* recently showed the application of iPSC-ECs to study reduced penetrance observed in familial pulmonary arterial hypertension [19].

In this study, we employed iPSC-ECs to study a non-penetrance case observed in *ZNF408*-associated FEVR. Skin biopsy-derived primary fibroblast cultures were obtained from one of the unaffected mutation carriers (UMC) and her affected sibling (Figure 1). The generated fibroblasts were reprogrammed to a pluripotent state and subsequently, differentiated into the endothelial lineage. Flow cytometry was employed to sort the cells into a homogeneous endothelial cell population and also to assess the differentiation efficiency. Furthermore, the characteristics of the obtained endothelial cells were examined by immunostaining, gene expression analysis, as well as *in vitro* tube formation assay. The properties of endothelial cells derived from the patient and the UMC were compared to each other and also to controls.

4.2 Materials and Methods

4.2.1 Ethical statement

Written informed consent was obtained from all participants. This study was approved by the Local Ethics Committee and conducted in adherence to the tenets of Declaration of Helsinki.

4.2.2 Fibroblast culture

Skin biopsies were obtained from two healthy individuals (male and female), one FEVR patient (female), and one unaffected mutation carrier (female). Primary fibroblast cultures were derived from the obtained skin biopsy. The fibroblasts were cultured in DMEM supplemented with 20% FCS, 1% sodium pyruvate, and 1% Pen/Strep.

4.2.3 Fibroblast reprogramming to iPSCs

Primary fibroblast lines were reprogrammed into iPSCs by lentiviral transduction of pluripotency genes *OCT3/4*, *NANOG*, *KLF4*, and *c-MYC*, following the standard procedures of the Stem Cell Technology Center of the Radboud University Medical Center, as previously described [20]. The pluripotency of the obtained cells was examined by immunocytochemistry of pluripotency markers (Figure S1 and S2).

4.2.4 iPSC and hESC culture

Human embryonic stem cells (hESCs, WA09(H9)) were obtained from WiCell. iPSCs and hESCs were cultured in Essential 8 flex medium (Thermo Fisher Scientific) on Matrigel coated culture dishes (1:15 dilution, BD Biosciences). The colonies were split every 4-7 days.

4.2.5 iPSC and hESC differentiation to endothelial cells

The differentiation of hESCs and iPSCs to endothelial cells was performed following the protocol described earlier by Patsch *et al.* [21]. Briefly, iPSCs were seeded as single cells with the density of 300,000 cells per well of a 12-well plate coated with Matrigel (1:15 dilution, BD Biosciences). The cells were seeded in Essential 8 Flex medium (Thermo Fisher Scientific) supplemented with 10 μM Rock inhibitor Y-27632 (Sigma Aldrich). The following day the medium was changed into mesoderm induction medium, which consisted of DMEM/F12 (Sigma Aldrich) and Neurobasal (Thermo Fisher Scientific) medium in 1:1 ratio, supplemented with 1% N2 (Thermo Fisher Scientific), 2% B27 (Thermo Fisher Scientific), 25 ng/μl BMP4 (Sigma Aldrich), and 6 μM CHIR-99021 (Bio-Techne). Three days later, the cells were further specified to an endothelial lineage for two days. The endothelial induction medium contained StemPro-34 SFM medium (Thermo Fisher Scientific) supplemented with 1% L-alanyl-L-glutamine (Sigma Aldrich), 2 μM forskolin (Sigma Aldrich) and 200 ng/μl VEGF (Peprotech). The endothelial induction medium was renewed daily until day 6. On the sixth day, the cells were sorted for CD31+ cells by flow cytometry (see below) and were re-plated on 12-well plate coated with 0.01 mg/ml bovine fibronectin (Promocell). The endothelial cells were expanded to confluency in Endothelial Growth Medium 2 (Promocell) supplemented with 50 ng/μl VEGF (Peprotech). The medium was refreshed every 48 hours until the cells reached confluency and were harvested.

4.2.6 Fluorescent activated cell sorting (FACS)

At day 6 of differentiation, the cells were dissociated as single cells. Three million cells were resuspended in 200 μl FACS buffer (1 mM EDTA, 25 mM HEPES pH 7, and 1% FCS in PBS), and stained with CD31-FITC antibody (Beckman Coulter) for 45 min on ice. The stained cells were washed once with PBS and filtered through 70 μm filter to remove cell clumps. Subsequently, the cells were sorted through 85 μm nozzle of Aria cell sorter (Becton Dickinson). The percentage of CD31+ cells was analyzed using Kaluza Analysis 2.1 software (Beckman Coulter) based

on 10,000 events. One-way ANOVA followed by Tukey's multiple comparison test was employed in the statistical analysis of three independent experiments.

4.2.7 DNA analysis

Genomic DNA was isolated from fibroblasts, hESC-derived endothelial cells instead of hESC- derived endothelial cells (hESC-ECs), and iPSC-ECs using QIAamp DNA mini kit (Qiagen) following the manufacturer's instructions. The region containing *ZNF408* c.1363C>T mutation was amplified from 25 ng DNA using fw 5'-CCTGGCCAAGAAGTTACACAG-3' and rev 5'-TTTCTCCTGTATGGAGCCTCA-3' primers. The amplified products were subsequently subjected to Sanger sequencing.

4.2.8 *In vitro* tube formation assay

The hESC-ECs and iPSC-ECs were seeded on 96-well plate coated with Matrigel (BD Biosciences) at a density of 1.5 x 10^4 cells per well. Twenty hours later, the cells were stained with 6 μM Calcein Red (Thermo Fisher Scientific). Cells were imaged on an EVOS cell imaging station. The tube networks were quantified using the online Wimtube tool from Wimasis (https://www.wimasis.com/en/products/13/WimTube). Two images were quantified per condition in three independent experiments. The data obtained were subjected to one-way ANOVA with Tukey's multiple comparison post-hoc analysis.

4.2.9 Immunocytochemistry

Fibroblasts were cultured on a 12-well plate with coverslips, whereas hESC-ECs and iPSC-ECs were grown on a 12-well plate with coverslips coated with 0.01 mg/ml bovine fibronectin (Promocell). Upon confluency, the cells were fixed with 2% PFA for 20 min at room temperature. The cells were then permeabilized using 1% Triton X-100 in PBS (v/v) for 5 min, followed by 2 x 5 min washes in PBS and blocking with 2% BSA in PBS (w/v) for 20 min. The fibroblasts were stained with rabbit anti ZNF408 (1:100, Biorbyt) for 2h at room temperature. Alternatively, the iPSC-ECs were stained with the following primary antibodies, sheep anti CD31 (1:100, R&D Systems), goat anti VE-cadherin (1:100, R&D Systems), and rabbit anti ZNF408 (1:100, Biorbyt) for 2 h at room temperature. After 3 x 5 min washes in PBS, secondary antibodies were introduced. The secondary antibody used in fibroblast staining was goat anti rabbit Alexa Fluor 488, while the secondary antibodies used in iPSC-EC staining were donkey anti sheep Alexa Fluor 488,

donkey anti goat Alexa Fluor 647, and donkey anti rabbit Alexa Fluor 568. Secondary antibodies were used in a dilution of 1:500 (Thermo Fisher Scientific). Following 3 x 5 min washes in PBS and rinsing in Milli-Q, the cells were mounted using Vectashield with DAPI (Vector Laboratories). The slides were imaged on Zeiss Axio Imager.

4.2.10 Gene expression analysis by qPCR

Total RNA was isolated from fibroblasts, hESC, and iPSC-derived endothelial cells using the Macherey Nagel RNA extraction kit, following the manufacturer's instructions. The obtained RNA (1000 ng) was used to synthesize cDNA using the iScript cDNA synthesis kit (Bio-Rad) according to the instruction manual. Quantitative real-time PCR (qPCR) was performed using GoTaq qPCR master mix (Promega). The primers used are listed in Supplementary Table 1. Three technical replicates of each condition were measured in three independent experiments. One-way ANOVA with Dunnet's post-hoc analysis was utilized in the statistical analysis of fibroblasts qPCR and Kruskal-Wallis test followed by Dunns post-hoc analysis was used in the analysis of hESC-ECs and iPSC-ECs qPCR.

4.2.11 Statistical analysis

Statistical tests used in the data analysis of the different experiments are described in detail in the sections that belong to the corresponding experiments.

4.3 Results

Skin biopsies were obtained from an FEVR patient and her unaffected sibling who also carries the p.His455Tyr mutation (Figure 1). Haplotype analysis showed that both individuals inherited the mutant allele from the father, but inherited a different wild-type allele from the mother (Figure 1) [7].

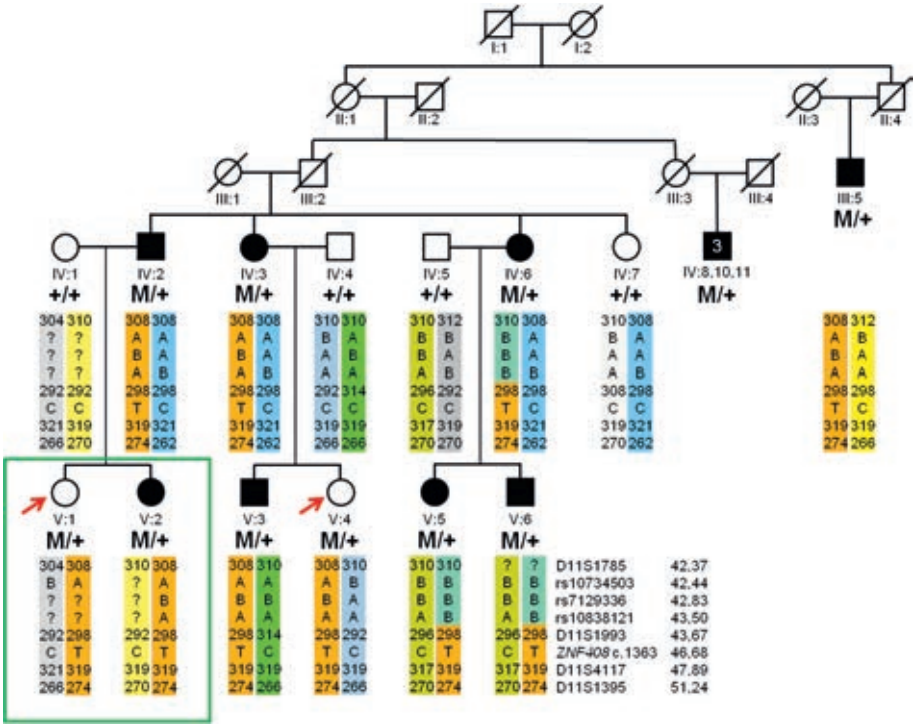

Figure 1. Pedigree of the autosomal dominant FEVR family. Square denotes male and circle represents female. Filled squares or circles indicate affected individuals. Haplotype analysis of chromosome 11p11.2 is shown below each individual. Unaffected *ZNF408* c.1363C>T mutation carriers (V:1 and V:4) are indicated with red arrows. The individuals participating in this study (V:1 and V:2) are marked with a green rectangle. Modified from Collin *et al.* [7].

Primary fibroblast cultures were derived from these skin biopsies. Subsequently, the obtained cells were characterized at DNA, RNA, and protein level. Sanger sequencing showed that fibroblasts derived from both individuals have the heterozygous *ZNF408* c.1363C>T mutation (Figure 2a), that was absent in a fibroblast culture derived from a healthy control. Gene expression analysis showed no significant difference in *ZNF408* expression between the three conditions (Figure 2b). Immunocytochemistry showed that ZNF408 is expressed at the protein level and localized in the nuclei of the fibroblasts (Figure 2c).

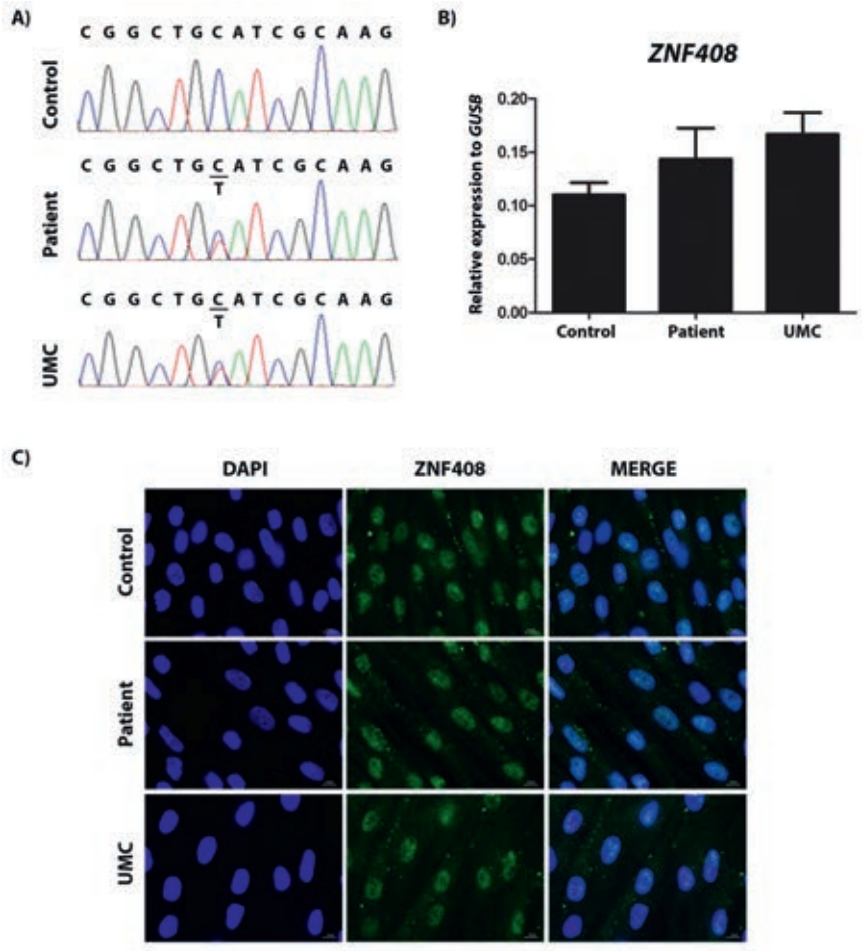

Figure 2. Preliminary study in skin biopsy-derived fibroblasts. A) Sanger sequencing to confirm the presence of *ZNF408* c.1363C>T variant at genomic DNA level in fibroblasts. B) Gene expression analysis of *ZNF408* in control individual, FEVR patient and UMC. Gene expression is plotted as fold-change relative to housekeeping gene, *GUSB*. No significant difference was observed. C) Immunostaining of ZNF408 in control individual, FEVR patient and UMC fibroblasts. Scale bar is 10 μm.

Since primary fibroblasts are not a completely relevant *in vitro* model to study vasculature-related diseases such as FEVR, we opted to use these cells to generate patient-specific endothelial cells in this study. To generate such an *in vitro* model, the obtained fibroblasts were reprogrammed into iPSCs and subsequently, differentiated into endothelial cells. The reprogramming into iPSCs was performed by lentiviral transduction of pluripotency genes *OCT3/4*, *NANOG*, *KLF4*, and *c-MYC*. The pluripotency of the obtained iPSCs was verified by immunostaining of pluripotency markers (Figure S1). We used two control iPSC lines in this study,

which were also reprogrammed by lentiviral transduction. The pluripotency tests of these lines are presented in Figure S2. Additionally, the iPSC lines and hESC line used in this study were subjected to Sanger sequencing to confirm that both patient and UMC line carry the *ZNF408* c.1363C>T mutation and that it is absent in the control iPSC lines as well as in the hESC line (Figure S3).

The iPSC and hESC were differentiated into the endothelial lineage following a protocol previously described by Patsch *et al.* [21]. Briefly, the pluripotent cells were directed to the mesodermal lineage for 4 days and subsequently, specified to the endothelial lineage for 2 days. The obtained endothelial cells were sorted for cells expressing CD31, an endothelial cell marker, at day 6 to obtain a homogeneous cell population. The CD31+ cells were then grown to confluency and harvested 4-5 days after sorting (Figure 3). All the obtained endothelial cells showed a similar morphology (Figure 3). Nevertheless, different survival rate upon post-sorting seeding and growth rate between the different iPSC-EC lines were observed. These were based on daily observations and were not quantified in this study, therefore, no data could be shown.

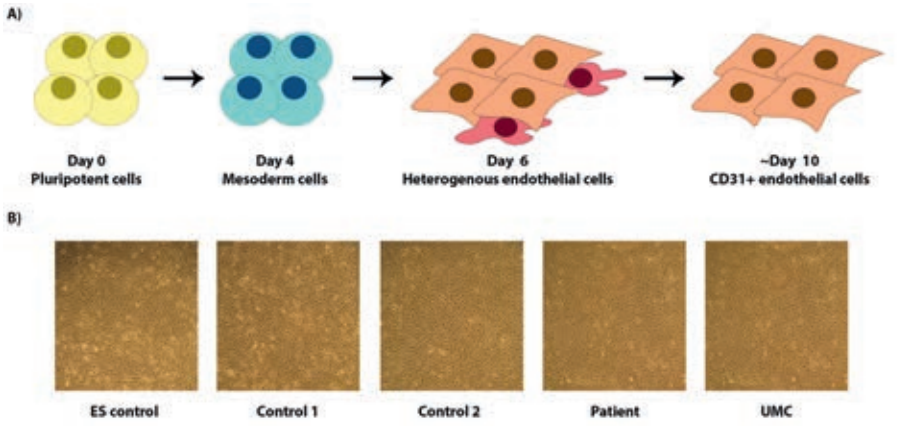

Figure 3. Differentiatiation of pluripotent cells into endothelial cells. A) Schematic illustration of differentiation procedure. B) Phase contrast images of the obtained CD31+ endothelial cells. The images were taken at 10x objective magnification using a Canon IXU 95 IS camera attached to the microscope. Therefore, no scalebar could be drawn.

As indicated above, the hESC and control iPSC lines seem to differentiate slightly more efficient into the endothelial lineage, compared to the patient iPSC and UMC iPSC lines. In three independent differentiation experiments performed in

this study, there were less CD31+ cells obtained from patient iPSC and UMC iPSC lines, compared to the control lines. Although this difference was not statistically significant, there seems to be a trend which is consistent in three independent experiments. Figure 4 shows representative flow cytometry results of one of the differentiation experiments as well as the average of CD31+ cells obtained from each line in the three experiments.

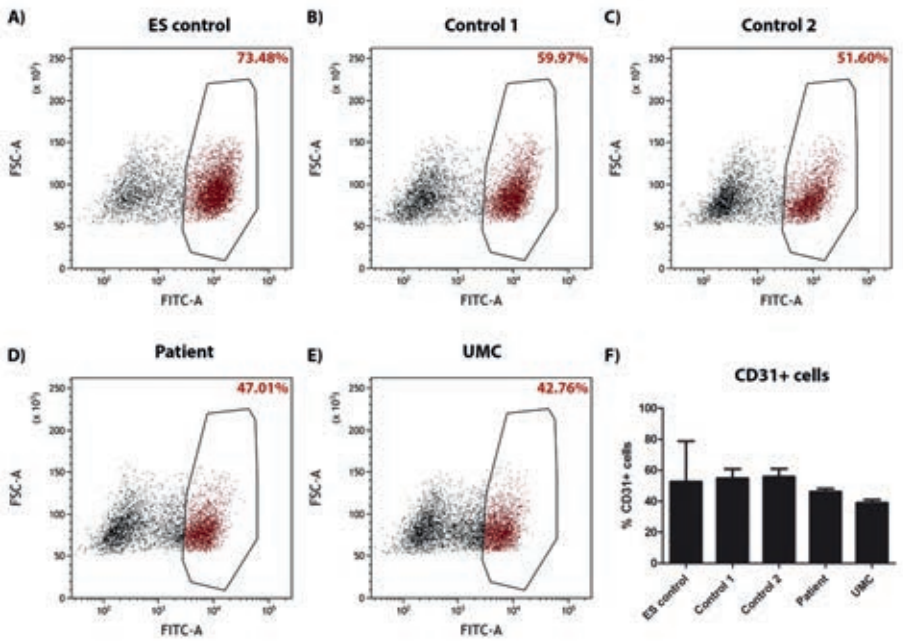

Figure 4. A trend of lower differentiation efficiency of patient iPSC and UMC iPSC. A) - E) Dot plots of the flow cytometry for cells positively labeled with CD31-FITC (red dots). Black dots represent CD31-negative cells. The percentage of CD31+ cells is indicated in each plot. F) Bar graph depicting the average of CD31+ cells (in percentage) in three independent experiments. Error bars indicate standard deviation. Statistical analysis was performed using one-way Anova followed by Tukey's multiple comparison test. No statistical significance difference was observed.

Immunocytochemistry was employed to further determine whether the obtained cells contained endothelial characteristics. Besides CD31, another endothelial cell marker, VE-cadherin (also known as CD144), was studied. Based on the results obtained in the immunostaining, the cell populations obtained were purely endothelial cells, expressing both CD31 and VE-cadherin (Figure 5). Additionally, we also stained for ZNF408 to determine whether there is any difference in ZNF408 localization in control, patient and UMC-derived endothelial cells. In all lines, ZNF408 is localized in the nucleus of the cell (Figure 5). We also observed

some signal in the cytoplasm in some cells. However, this signal was occasionally present in endothelial cells derived from different sources without an apparent pattern in three independent experiments. Therefore, it is tempting to suggest that these are aspecific signals.

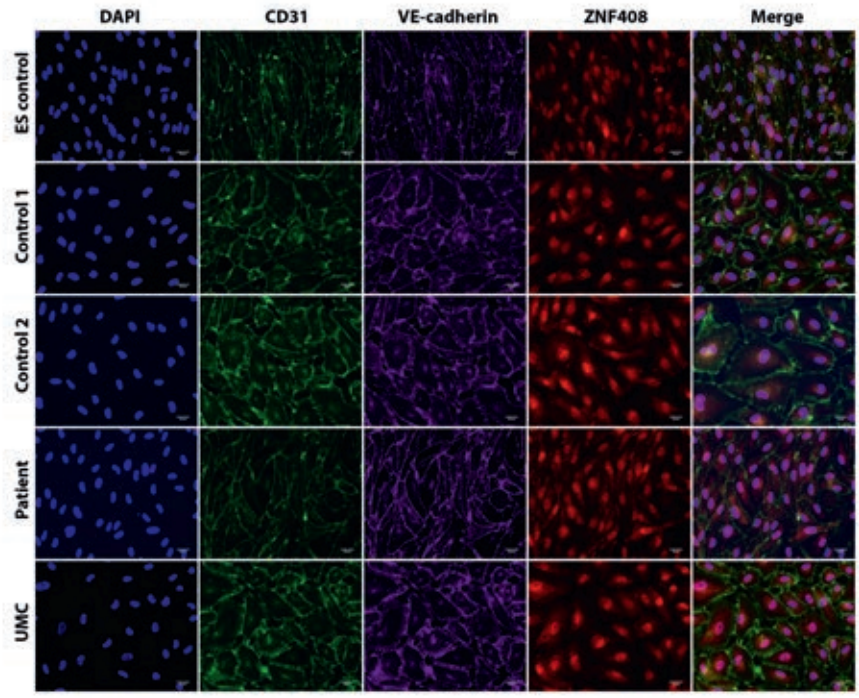

Figure 5. The obtained endothelial cells expressed endothelial cell markers, CD31 and VE-cadherin, and ZNF408 is localized in the nuclei of these cells. Immunostaining images were taken with similar exposure time for all the cell lines. Scale bar is 50 μm.

Gene expression analysis showed that the expression of *OCT4*, a pluripotency marker, was highest at day 0 and decreased throughout the differentiation (Figure S4). This indicates that the cells used to start the differentiation were pluripotent and subsequently, underwent differentiation. Two mesoderm lineage markers tested, *T* and *MIXL1*, were upregulated at day 4, suggesting that the cells were specified to a mesoderm lineage at that point.

Gene expression analysis of endothelial cell markers, *CDH5* and *PECAM1* (coding for VE-cadherin and CD31, respectively), confirmed the immunostaining results. Both genes were upregulated when differentiated, compared to day 0 and day 4.

Harvest day is defined as the day the endothelial cells were confluent and therefore, harvested for immunostaining, RNA isolation, and *in vitro* tube formation assay. Day 0 and day 4 refers to pluripotent and mesodermal state, respectively. Another endothelial cell marker, von-Willebrand factor (*VWF*) was also upregulated, further confirming the endothelial specification of the cells. The expression level of *ZNF408* was also measured and interestingly, it seems to be quite variable between individuals and also between the three independent experiments performed. It is also intriguing that the expression level of *ZNF408* in UMC is approximately half of the one observed in the patient. This was also observed previously in another independent experiment (Figure S5).

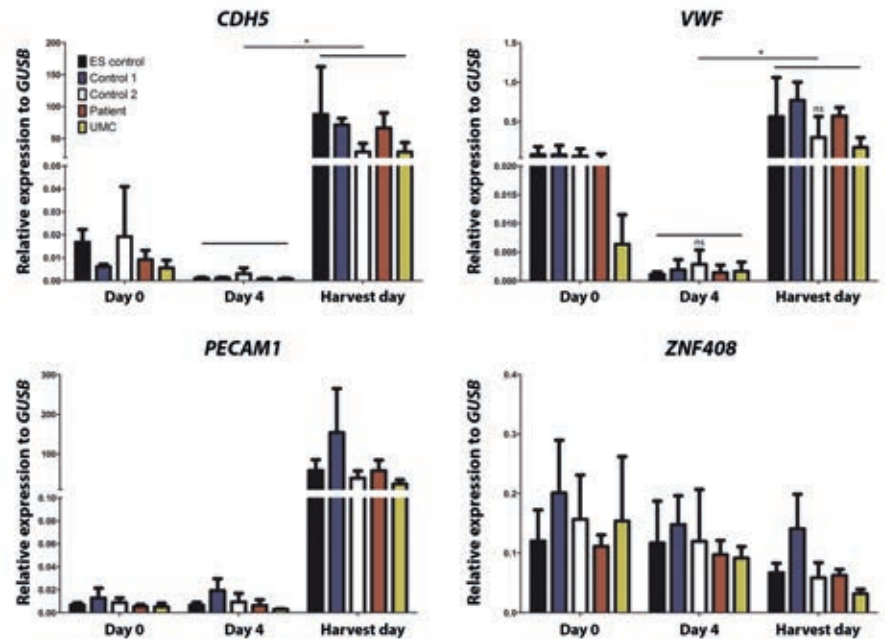

Figure 6. The obtained endothelial cells expressed endothelial cell markers and variable *ZNF408* expression. Gene expression is plotted as fold-change relative to housekeeping gene, *GUSB*. Error bars represent standard deviation of three independent experiments. Statistical analysis was performed using Kruskal-Wallis test, followed by Dunns post-hoc analysis. Statistical significance (p-value <0.05) is denoted with *. Ns in *VWF* graph indicates that among the 5 conditions compared between the Day 4 and Harvest day, no statistical significance was observed for control 2.

Finally, the obtained endothelial cells were subjected to an *in vitro* tube formation assay to study their endothelial behavior. In this assay, the endothelial cells were seeded at low density on extracellular matrix (Matrigel) and incubated for 16-20

hours to allow them to form capillary networks *in vitro*. However, no apparent difference in their ability to form capillary networks was observed between the different cell lines (Figure 7). The images obtained were quantified for branching points, number of tubes, as well as tube length. No significant difference was observed between the conditions, suggesting that the obtained endothelial cells have comparable angiogenic ability.

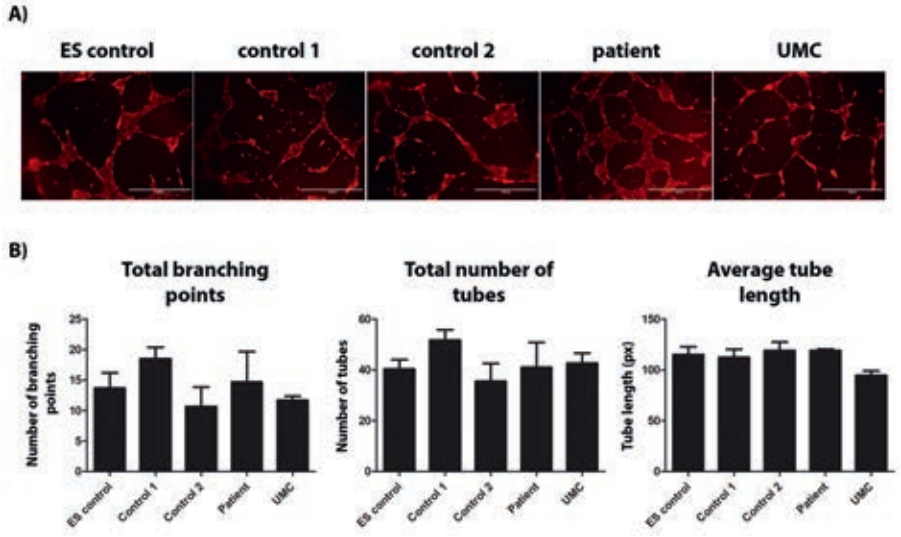

Figure 7. No apparent difference was observed in *in vitro* tube formation assay. A) Representative images of tube networks formed by the obtained endothelial cells. Scale bar is 1000 µm. B) Quantification of the tube networks from three independent experiments, each of which consists of two technical replicates. Error bars depict standard error of the mean. No significance difference was observed between the conditions.

4.4 Discussion

In this study, we aimed to use iPSC-ECs as *in vitro* model to study reduced penetrance in FEVR. Skin biopsy-derived fibroblasts from an FEVR patient with the *ZNF408* c.1363C>T mutation and her sister who is unaffected despite carrying this mutation were reprogrammed into iPSCs. Subsequently, the obtained iPSC lines were differentiated into endothelial cells. The differentiation protocol used proved to be robust and yielded consistent results in three independent experiments. No remarkable difference in morphology and endothelial cell characteristics was observed between endothelial cells derived from control, patient and UMC iPSC

lines. Patient and UMC iPSC lines showed a slightly lower differentiation efficiency towards endothelial cell lineage. Lastly, endothelial cells derived from UMC iPSC showed lower *ZNF408* expression in comparison to those derived from patient and controls.

Although the iPSC-ECs derived from controls, patient, and UMC did not show any remarkable difference in the aforementioned endothelial characteristics, different survival and growth rate post-sorting was observed (data not shown). Gu *et al.* showed in a reduced penetrance study using iPSC-EC that despite similar behavior in the *in vitro* tube formation assay, cells may have different survival and adhesion ability [19]. Besides, cell migration is also one of the functional assays often used to characterize endothelial cells. It would be valuable to characterize the obtained iPSC-ECs in more detail with cell survival, cell adhesion, and cell migration assays, to further learn about the potential similarities and differences of the iPSC-ECs lines. Additionally, the iPSC-ECs used in the experiments in this study were passage 1, obtained directly after the sorting procedure, which was due to time constraints. Other studies using endothelial cells derived from pluripotent cells often used later passages, such as passage 3-8 in Gu *et al.* and passage 4 in Patsch *et al.* [19, 21]. The experiments performed in this study would need to be repeated at other passages, to ensure reproducibility of the results and thereby, a just conclusion can be drawn about the *in vitro* behavior of the cells.

A trend of lower differentiation efficiency towards the endothelial lineage was observed in patient and UMC iPSC lines. This was seen consistently in three independent experiments conducted. Although it is tempting to assume that this showed that patient and UMC iPSC lines are not able to optimally generate endothelial cells, it may also be influenced by the unique characteristics of each iPSC line. Patsch *et al.*, the authors of the differentiation protocol, mentioned that the optimal seeding density and CHIR 99021 concentration (*i.e.* GSK3β inhibitor used to direct differentiation towards mesoderm lineage) may differ for each pluripotent cell line [21]. In this study, similar seeding density and CHIR concentration were utilized for all the lines to enable a fair comparison. Therefore, the possibility that the conditions applied are not always optimal for patient and UMC iPSC lines cannot be excluded.

An intriguing difference between iPSC-ECs is the lower expression of *ZNF408* in UMC-derived endothelial cells, compared to patient and controls. Although the difference is not statistically significant, such difference was observed consistently in several experiments and only observed at the endothelial state. It is tempting to hypothesize that this difference in *ZNF408* expression may be the underlying cause in the observed non-penetrance. However, it is unclear how lower *ZNF408* expression in UMC would protect against FEVR, while controls have comparable or higher *ZNF408* expression than patient-derived cells. Cooper *et al.* summarized some examples of non-penetrance cases with differential allelic expression, none of which is similar to this [16]. Furthermore, in our previous study, we showed that *ZNF408* is involved in the development of vasculature [22]. Such hypothesis is only logical if the mutant p.His455Tyr allele is inactive in UMC, leading to the approximately 2-fold lower expression compared to patient-derived cells. As such, the inactivity of the mutant allele may protect the UMC against FEVR and that 50% expression of the wild-type *ZNF408* is likely to be sufficient for proper retinal vasculature development. An allele-specific expression experiment on the iPSC-ECs is required to prove this hypothesis. If confirmed, the investigation should be continued to discover what causes this allele-specific expression and what the molecular consequences of it are. Regardless whether this hypothesis is proven or not, a transcriptome profiling of iPSC-ECs obtained may shed further light into the molecular mechanisms underlying *ZNF408*-associated non-penetrance observed in this family.

Considering the images obtained from immunostaining experiments, there seems to be background staining of ZNF408 in the cytoplasm of iPSC-ECs generated in this study. It may be improved by optimizing the staining protocol or choosing an alternative antibody. Nonetheless, it is interesting how immunostaining of endogenous ZNF408 in fibroblasts and iPSC-ECs showed nuclear staining in individuals with and without the p.His455Tyr mutation, despite the previous finding in which overexpression of p.His455Tyr mutant in COS1 cells showed cytoplasmic localization [7]. Such discrepancy has been observed previously, when comparing endogenous and artificial overexpression systems [23]. Furthermore, the difference in cellular system used and *ZNF408* expression in each system may also influence the localization.

As interesting as these findings are, one must realize that this preliminary study is only based on experiments performed on one clone of each iPSC line. It has been demonstrated that such iPSC-based modelling studies require more controls and patients to attain reliable data [24]. It may be advantageous to repeat the experiments on other clones of these iPSC lines in order to exclude any findings influenced by interclonal variability. Furthermore, the generation of isogenic control iPSC lines by CRISPR/Cas9 technology may exclude the variability of different genetic backgrounds of the donor. Additionally, this study only consists of one example of non-penetrance of *ZNF408* c.1363C>T in FEVR. Expanding the study to the other *ZNF408* c.1363C>T non-penetrance branch of the family as well as other cases of non-penetrance in (*ZNF408*-associated) FEVR, would allow a better investigation and a deeper understanding of the underlying mechanism, provided that the individuals are willing to participate.

Since only the patient was subjected to whole exome sequencing in the previous study by Collin *et al.* [7], we cannot exclude the possibility that there are other genetic variants that differ between patient and UMC that may contribute to the non-penetrance observed. Haplotype analysis showed that patient and UMC inherited a different wild-type allele from their mother [7]. Comprehensive sequence analysis, such as whole exome sequencing or whole genome sequencing, may aid in identifying any other genetic variant(s) that may influence the difference in phenotype between these individuals.

Altogether, this study showed that it is possible to robustly generate patient-specific endothelial cells to model FEVR *in vitro*, which open the avenues to study reduced penetrance in FEVR. Further investigations are required to validate the findings observed in this study. It has yet to be determined whether reduced penetrance in FEVR has a universal cause, regardless of the genetic cause. Lastly, although as a developmental disease the window of opportunity is rather small, the identification of the factor(s) that protect the UMCs from FEVR may lead the path to the development of a potential treatment for FEVR patients.

Acknowledgements

We gratefully acknowledge the subjects that participated in this study. We would like to thank Prof. Ronald Roepman for providing the gender-matched iPSC control line; Anke van Dijk, Tessa van der Heijden, and Louet Koolen from the Stem Cell Technology Center of the Radboudumc; Saskia van der Velde-Visser and Marlie Jacobs-Camps for cell culture assistance; Prof. Camiel Boon and Nathalie Bax for skin biopsy taking; Rob Woestenenk for assistance with FACS, and Thea van der Velden for providing CD31-FITC antibody.

Funding

This work is funded by Radboudumc PhD grant to Dyah W. Karjosukarso.

Conflict of interest

The authors declare no conflict of interest.

References

1. Criswick, V.G. and C.L. Schepens, *Familial exudative vitreoretinopathy.* Am J Ophthalmol, 1969. **68**(4): p. 578-94.
2. Canny, C.L. and G.L. Oliver, *Fluorescein angiographic findings in familial exudative vitreoretinopathy.* Arch Ophthalmol, 1976. **94**(7): p. 1114-20.
3. Miyakubo, H., K. Hashimoto, and S. Miyakubo, *Retinal vascular pattern in familial exudative vitreoretinopathy.* Ophthalmology, 1984. **91**(12): p. 1524-30.
4. Miyakubo, H., N. Inohara, and K. Hashimoto, *Retinal involvement in familial exudative vitreoretinopathy.* Ophthalmologica, 1982. **185**(3): p. 125-35.
5. Boonstra, F.N., et al., *Clinical and molecular evaluation of probands and family members with familial exudative vitreoretinopathy.* Invest Ophthalmol Vis Sci, 2009. **50**(9): p. 4379-85.
6. Chen, Z.Y., et al., *A mutation in the Norrie disease gene (NDP) associated with X-linked familial exudative vitreoretinopathy.* Nat Genet, 1993. **5**(2): p. 180-3.
7. Collin, R.W., et al., *ZNF408 is mutated in familial exudative vitreoretinopathy and is crucial for the development of zebrafish retinal vasculature.* Proc Natl Acad Sci U S A, 2013. **110**(24): p. 9856-61.
8. Nikopoulos, K., et al., *Next-generation sequencing of a 40 Mb linkage interval reveals TSPAN12 mutations in patients with familial exudative vitreoretinopathy.* Am J Hum Genet, 2010. **86**(2): p. 240-7.
9. Wu, J.H., et al., *Haploinsufficiency of RCBTB1 is associated with Coats disease and familial exudative vitreoretinopathy.* Hum Mol Genet, 2016. **25**(8): p. 1637-47.
10. Panagiotou, E.S., et al., *Defects in the Cell Signaling Mediator beta-Catenin Cause the Retinal Vascular Condition FEVR.* Am J Hum Genet, 2017. **100**(6): p. 960-968.
11. Poulter, J.A., et al., *Mutations in TSPAN12 cause autosomal-dominant familial exudative vitreoretinopathy.* Am J Hum Genet, 2010. **86**(2): p. 248-53.
12. Toomes, C., et al., *Mutations in LRP5 or FZD4 underlie the common familial exudative vitreoretinopathy locus on chromosome 11q.* Am J Hum Genet, 2004. **74**(4): p. 721-30.
13. Robitaille, J., et al., *Mutant frizzled-4 disrupts retinal angiogenesis in familial exudative vitreoretinopathy.* Nat Genet, 2002. **32**(2): p. 326-30.
14. Jiao, X., et al., *Autosomal recessive familial exudative vitreoretinopathy is associated with mutations in LRP5.* Am J Hum Genet, 2004. **75**(5): p. 878-84.
15. Nikopoulos, K., et al., *Overview of the mutation spectrum in familial exudative vitreoretinopathy and Norrie disease with identification of 21 novel variants in FZD4, LRP5, and NDP.* Hum Mutat, 2010. **31**(6): p. 656-66.
16. Cooper, D.N., et al., *Where genotype is not predictive of phenotype: towards an understanding of the molecular basis of reduced penetrance in human inherited disease.* Hum Genet, 2013. **132**(10): p. 1077-130.
17. Cochrane, A., et al., *Advanced in vitro models of vascular biology: Human induced pluripotent stem cells and organ-on-chip technology.* Adv Drug Deliv Rev, 2018.
18. Klein, D., *iPSCs-based generation of vascular cells: reprogramming approaches and applications.* Cell Mol Life Sci, 2018. **75**(8): p. 1411-1433.
19. Gu, M., et al., *Patient-Specific iPSC-Derived Endothelial Cells Uncover Pathways that Protect against Pulmonary Hypertension in BMPR2 Mutation Carriers.* Cell Stem Cell, 2017. **20**(4): p. 490-504 e5.
20. Sangermano, R., et al., *Photoreceptor Progenitor mRNA Analysis Reveals Exon Skipping Resulting from the ABCA4 c.5461-10T-->C Mutation in Stargardt Disease.* Ophthalmology, 2016. **123**(6): p. 1375-85.
21. Patsch, C., et al., *Generation of vascular endothelial and smooth muscle cells from human pluripotent stem cells.* Nat Cell Biol, 2015. **17**(8): p. 994-1003.
22. Karjosukarso, D.W., et al., *An FEVR-associated mutation in ZNF408 alters the expression of genes involved in the development of vasculature.* Hum Mol Genet, 2018. **27**(20): p. 3519-3527.
23. Stadler, C., et al., *Immunofluorescence and fluorescent-protein tagging show high correlation for protein localization in mammalian cells.* Nat Methods, 2013. **10**(4): p. 315-23.
24. Germain, P.L. and G. Testa, *Taming Human Genetic Variability: Transcriptomic Meta-Analysis Guides the Experimental Design and Interpretation of iPSC-Based Disease Modeling.* Stem Cell Reports, 2017. **8**(6): p. 1784-1796.

Supplementary Materials

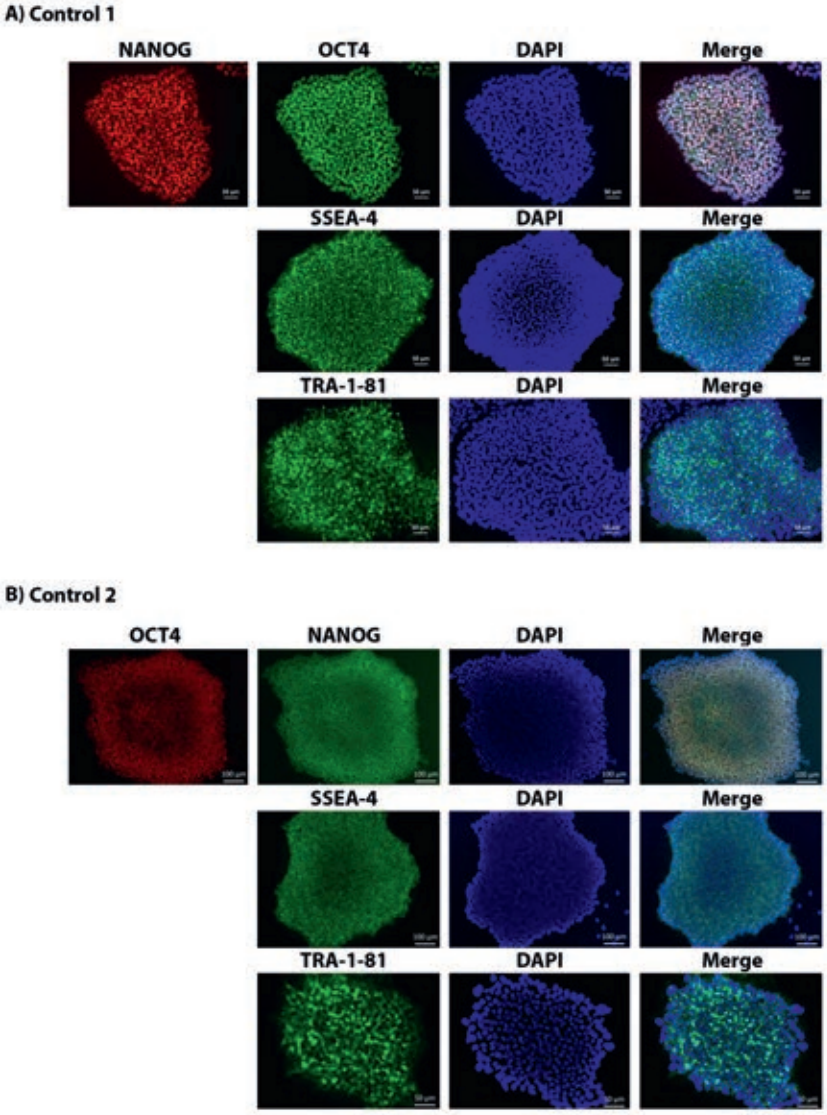

Figure S1. Immunocytochemistry of pluripotency markers of one clone of A) control 1 and B) control 2. Scale bars of all images of control 1 is 50 µm. Scale bars of the images in the top and middle row of control 2 are 100 µm, whereas those of the images in the last row are 50 µm. Images courtesy of Stem Cell Technology Center, Radboudumc.

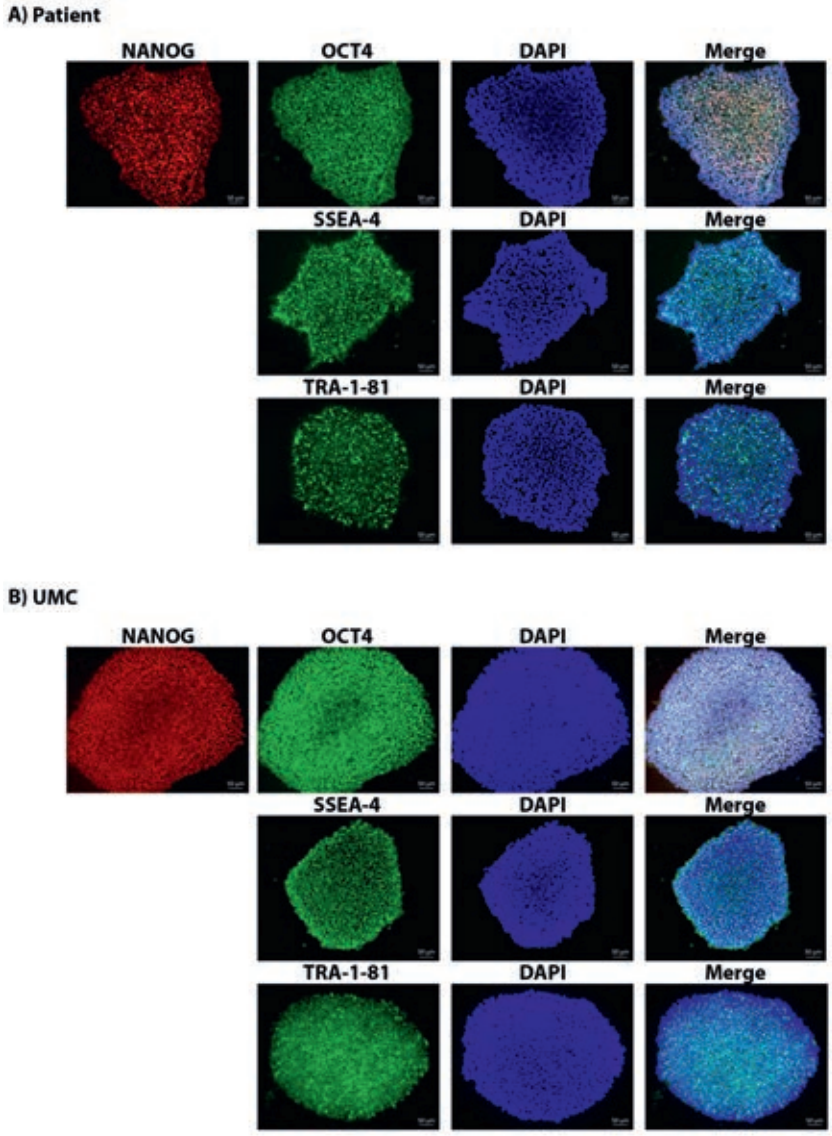

Figure S2. Immunocytochemistry of pluripotency markers of one clone of A) patient and B) UMC. Scale bars of all images are 50 μm. Images courtesy of Stem Cell Technology Center, Radboudumc.

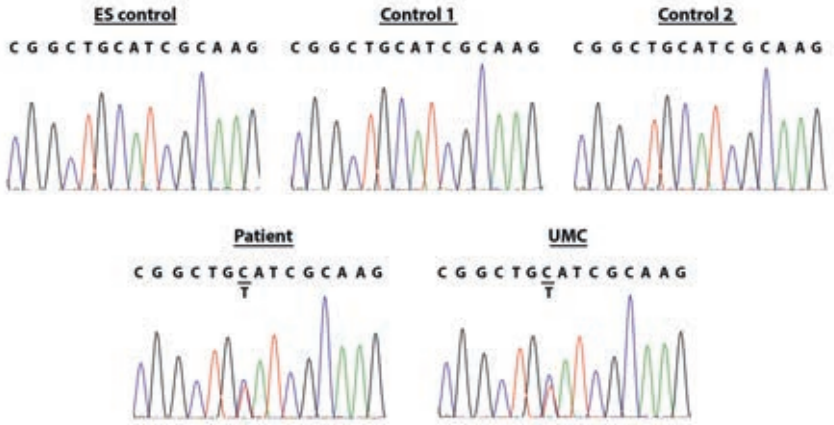

Figure S3. iPSCs derived from the patient and UMC carried the heterozygous *ZNF408* c.1363C>T mutation, which is absent in the controls. Sanger sequencing of the obtained pluripotent stem cells used in this study. The mutation is indicated.

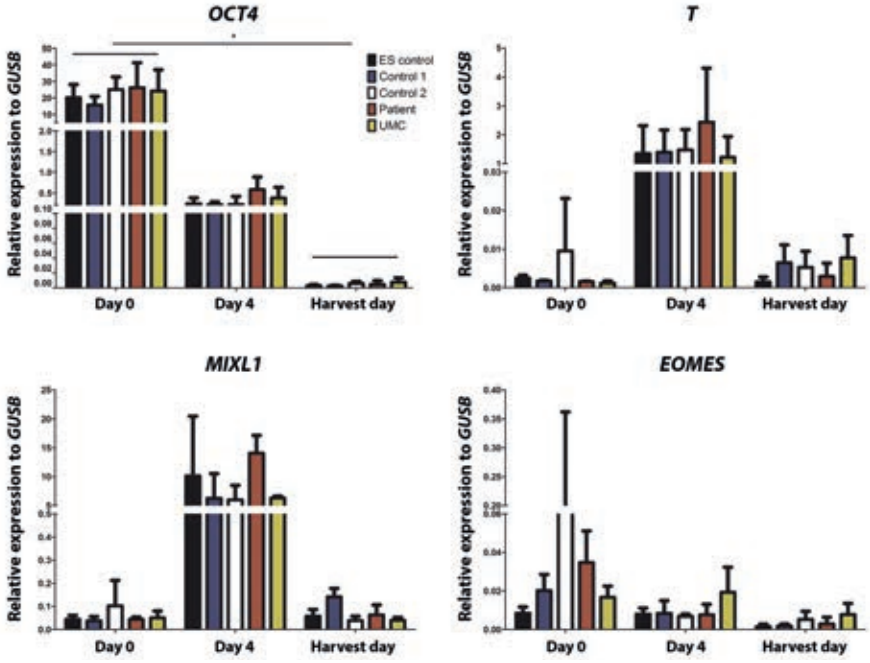

Figure S4. Gene expression analysis of pluripotency and mesoderm markers. Gene expression is plotted as fold-change relative to housekeeping gene, *GUSB*. Error bars represent standard deviation of three independent experiments. Statistical analysis were performed using Kruskal-Wallis test, followed by Dunns post-hoc analysis. Statistical significance (p-value <0.05) is denoted with *.

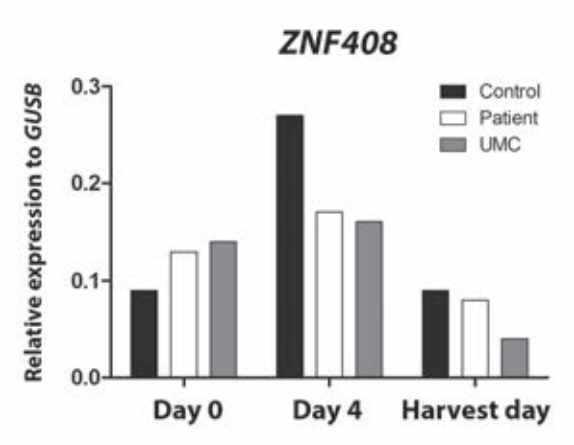

Figure S5. Gene expression analysis in an independent differentiation experiment showing lower *ZNF408* expression in UMC. Gene expression is plotted as fold-change relative to housekeeping gene, *GUSB*. Control iPSC line used in this experiment is similar to control 1 used in the other experiments described in this chapter.

Table S1 qPCR primer sequences

Gene	Forward Primer (5'-3')	Reverse Primer (5'-3')
GUSB	AGAGTGGTGCTGAGGATTGG	CCCTCATGCTCTAGCGTGTC
OCT4	GTTCTTCATTCACTAAGGAAGG	CAAGAGCATCATTGAACTTCAC
CDH5	AGGACGCTTTCACCATTGAG	TCATGTATCGGAGGTCGATG
VWF	GACTGTCCAGTGTGTGAGGTG	AGGCTTCACAGGTGAGGTTG
PECAM1	TCGGACAGTGGGACGTATATC	ATGACCTCAAACTGGGCATC
ZNF408	GAGGAGTCTGCCTCCAAGG	CCAGCCAGAACTCTGCTCAC
T	TGCTTCCCTGAGACCCAGTT	GATCACTTCTTTCCTTTGCATCAAG
EOMES	CGCCACCAAACTGAGATGAT	CACATTGTAGTGGGCAGTGG
MIXL1	GTATGGTTCCAGAACAGGCG	GTTCCAGGAGCACAGTGGTT

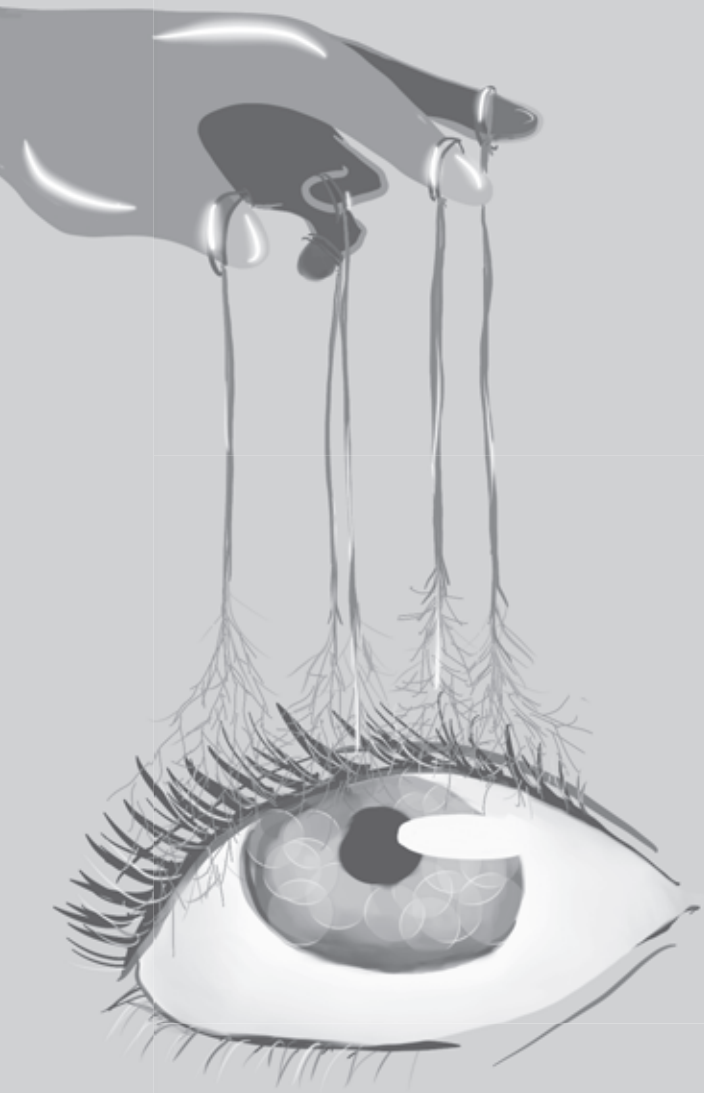

Chapter 5

Detection and quantification of a *KIF11* mosaicism in a subject presenting familial exudative vitreoretinopathy with microcephaly

Dyah W. Karjosukarso[1,2], Frans P.M. Cremers[1,2], C. Erik van Nouhuys[3], Rob W.J. Collin[1,2]

[1]Department of Human Genetics and
[2]Donders Institute for Brain, Cognition and Behaviour, Radboud University Medical Center, Nijmegen, the Netherlands;
[3]Royal Dutch Visio, Centre of Expertise for Blind and Partially Sighted People, Nijmegen, The Netherlands.

European Journal of Human Genetics (2018) **26:** 1819-1823

Abstract

Familial exudative vitreoretinopathy (FEVR) is an inherited retinal disorder which is primarily characterized by abnormal development of retinal vasculature. In this study, we reported a subject presenting the clinical features of FEVR as well as microcephaly. Screening of the *KIF11* gene in this patient revealed a novel heterozygous protein-truncating variant (c.2717del, p.(Leu906*), NM_004523.3). Segregation analysis in the unaffected parents using Sanger sequencing suggested the variant to be present in a mosaic state in the unaffected mother. *KIF11* exon 19 which harbors the variant was amplified from the proband and her father as well as three different tissues of the mother, followed by amplicon-based deep sequencing. This analysis revealed that the variant is present in different tissues of the mother at various rates, i.e. in blood (16.9%), saliva (20.7%), or skin biopsy-derived fibroblast cells (6.6%). These data demonstrate the importance of deep sequencing in unaffected parents upon detection of a genetic defect in isolated cases to detect possible mosaicism, enabling more reliable recurrence risk assessment and thereby improve genetic counseling.

5.1 Introduction

Familial exudative vitreoretinopathy (FEVR) is a clinically and genetically heterogeneous disorder, primarily characterized by abnormal development of the retinal vasculature [1, 2]. A serious manifestation of FEVR is a falciform retinal fold, a condition leading to visual impairment at young age [3].

Variants in *KIF11* have been reported in individuals with FEVR plus microcephaly, as well as in progressive retinal dystrophy and syndromic patients exhibiting microcephaly, lymphedema, chorioretinal dysplasia and/or intellectual disability [4-8]. *KIF11* variants can occur *de novo*, or be inherited from one of the parents [4-6]. Although missense variants have been reported, the majority of *KIF11* variants that lead to FEVR are protein-truncating variants [4-6, 9]. *KIF11* encodes the protein Eg5, which is involved in mitosis [10]. *In vitro* inhibition of Eg5 resulted in impaired endothelial cell proliferation and migration [11]. Furthermore, *kif11* zebrafish mutants showed defects in glial development [12]. These data underscore the importance of Eg5 in angiogenesis and central nervous system development, which may explain the abnormal retinal vasculature development and microcephaly observed in patients carrying variants in *KIF11*.

In this study, a novel heterozygous protein-truncating variant in *KIF11* was identified in a subject presenting FEVR and microcephaly. The variant was detected in mosaic state in the mother. The level of mosaicism in different tissues of the mother was accurately determined by deep sequencing.

5.2 Materials and Methods

5.2.1 Subjects and clinical evaluation

A subject with FEVR and microcephaly as well as both her unaffected parents participated in this study. The proband underwent ophthalmological and neurological examination. Clinical examinations were followed-up for 17 years. Following the identification of a genetic mosaicism, the mother was also extensively examined with different ophthalmological tests as well as a measure of head circumference. Written informed consent was obtained from all participants. This study was approved by the local Ethics Committee and conducted according to the tenets of the Declaration of Helsinki.

5.2.2 Genetic analysis

All exons and intron-exon boundaries of the *KIF11* gene were screened for potentially causative DNA variants in the proband by Sanger sequencing and a causative variant was identified. Subsequently, exon 19 of *KIF11* was amplified from the proband, her father, and three different tissues of her mother. The amplicons were subjected to Sanger sequencing as well as Ion semiconductor sequencing (Ion Personal Genome Machine, Thermo Fisher Scientific, Waltham, Massachussetts, USA) as described previously [13]. The genetic analysis are explained in detail in the Supplementary Information. The variant that was detected has been submitted to the LOVD database (https://databases.lovd.nl/shared/genes/KIF11, individual IDs: 00154935 and 00154936).

5.3 Results

The proband is a female patient who was born after a normal gestation and delivery. She was found to have nystagmus, convergent strabismus and mild microcephaly at an early age. At 3 years of age, low visual acuity and strabismus of the right eye was noted. Occlusion of the left eye was tried for a short period without success and strabismus was corrected by surgery. At the age of 7, best corrected visual acuity (BCVA) of the right eye was *finger counting* and of the left eye 20/50. Neurological examination at the same age disclosed slight psychomotor retardation. A computer tomography (CT) scan showed no structural abnormalities of the brain and ventricles, nor any cerebral calcifications; the skull circumference was 48 cm (<p2; second percentile). Laboratory tests for metabolic disorders and toxoplasmosis

were negative. Fundus examination at the age of 9 showed a prominent falciform retinal fold running from the optic disk to the inferior-temporal periphery in the right eye (Figure 1a). Some retinal vessels were observed outside the fold and no abnormalities were noted in the peripheral retina. Besides those shown in the fundus picture, some white tissue attached to the pars plana was also observed. In the left eye, areas of retinal pigmented epithelium atrophy (Figure 1b) and an abrupt termination of the temporal retinal vessels was observed in the equatorial area: the more peripheral part of the retina is avascular and shows some local areas of RPE atrophy. During 17 years of follow-up, no significant changes in the anterior segments and fundi of both eyes were noted, nor did visual acuity decline. The patient died at 28 years of age by a cause that is unrelated to the phenotype described here.

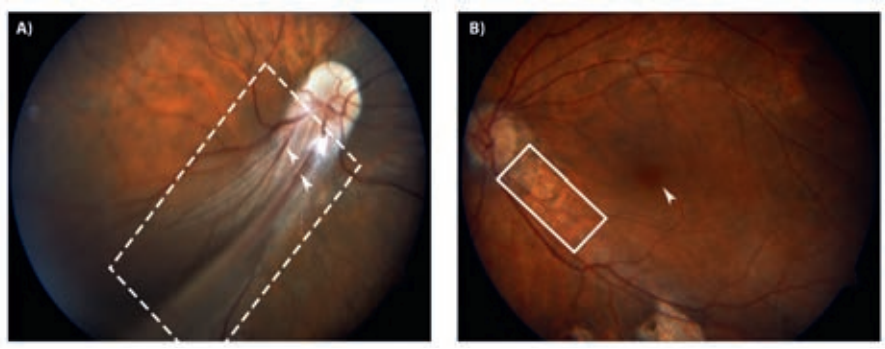

Figure 1. Fundus photographs of the posterior retina of the proband demonstrating FEVR. A) Fundus picture of the right eye, showing a prominent falciform retinal fold (indicated with a dashed box) with several retinal vessels (indicated with white arrowheads) extending from the optic disk in inferior-temporal direction to the fundus periphery. The posterior retina is included in the fold and no macula could be detected. The retina outside the fold is attached and shows some retinal vessels. B) Fundus picture of the left eye reveals areas of retinal pigmented epithelium (RPE) atrophy (indicated with a solid box) around the optic disk and along the inferior-temporal vessels. The macula (indicated with a white arrowhead) is slightly ectopic.

Since the clinical features present in the proband resemble those of FEVR and microcephaly, *KIF11* was Sanger sequenced from blood DNA to detect potentially causative DNA variants. A novel heterozygous one base-pair deletion that immediately results in premature termination of the protein (c.2717del; p.(Leu906*), hg19, NM_004523.3) was detected (Figure 2a-c). While the variant was not present in the father (Figure 2c), small peaks of the mutant allele were detected in the mother's blood DNA, suggesting a mosaicism.

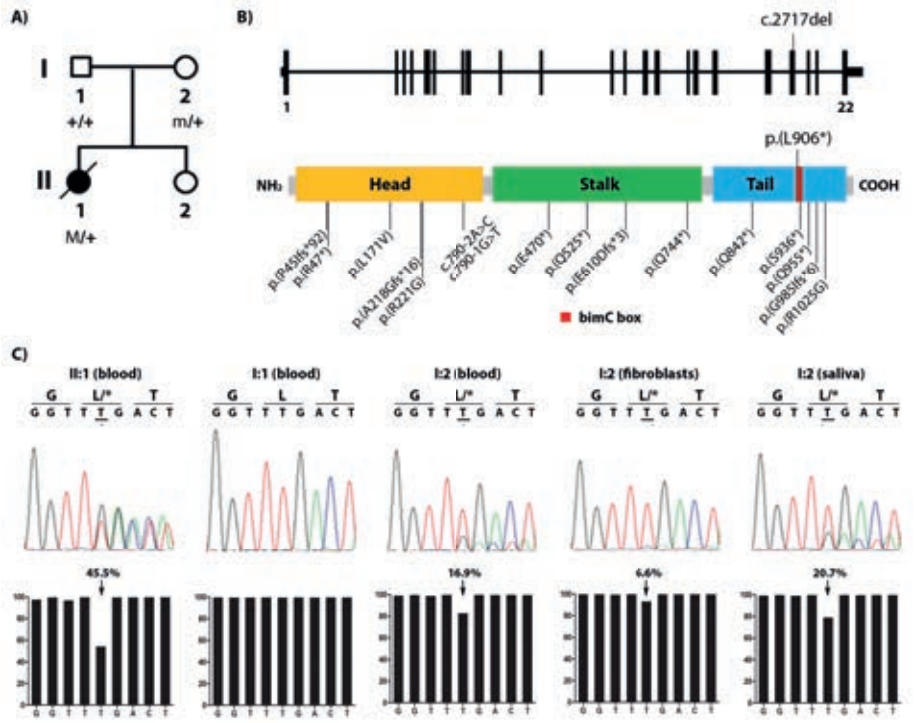

Figure 2. Genetic analysis of *KIF11* in a patient with FEVR and microcephaly. A) Pedigree of the family described in this study. The affected proband is depicted with a filled symbol. Slash indicates deceased person. M denotes germ line variant, m denotes mosaic variant; B) Schematic representation of the *KIF11* gene and the encoded Eg5 protein (adapted from Ostergaard *et al.* [7]). The variant identified in this study is depicted above the scheme. Other *KIF11* variants reported in subjects with FEVR and microcephaly cases are indicated below the protein [4-6, 9]. cDNA positions corresponding to the indicated protein variants are listed in Table 1; C) Sequencing results of the *KIF11* variant. Sanger sequencing electropherograms are shown in the upper panel, whereas the relative amount of reads obtained from Ion semiconductor sequencing are depicted below in bar graphs. The percentage of reads per given nucleotide is defined as the amount of reads called for a base among the total reads that cover that specific nucleotide. The percentage of reads having the c.2717del variant are indicated above the graph.

To further investigate this finding, *KIF11* exon 19 which harbors the variant was amplified from blood-derived DNA from the proband and her father as well as DNA of three different tissues from the mother (peripheral blood lymphocytes, skin biopsy-derived fibroblasts, and saliva), followed by amplicon-based deep sequencing using the Ion Personal Genome Machine. For each sample, more than 200,000 reads were obtained. This analysis confirmed that the variant was present heterozygously (45.5% of the reads) in the proband (Figure 2c) and absent in the father. It also revealed that the variant was present in the mother's blood, saliva, and fibroblasts at a frequency of 16.9%, 20.7%, and 6.6%, respectively. This not only confirms that the mother is mosaic for this variant, but also demonstrates that the degree of mosaicism can differ between tissues (Figure 2c).

Table 1 ***KIF11*** **variants associated with FEVR**

Variant (cDNA)	Variant (protein)	Reference
c.131_132dup	p.(Pro45Ilefs*92)	Hu *et al.* [5]
c.139C>T	p.(Arg47*)	Robitaille *et al.* [4]
c.511C>G	p.(Leu171Val)	Li *et al.* [6]
c.652dup	p.(Ala218Glyfs*16)	Robitaille *et al.* [4]
c.661A>G	p.(Arg221Gly)	Robitaille *et al.* [4]
c.790-2A>C	p.(?)	Li *et al.* [6]
c.790-1G>T	p.(?)	Robitaille *et al.* [4]
c.1408G>T	p.(Glu470*)	Robitaille *et al.* [4]
c.1573C>T	p.(Gln525*)	Li *et al.* [6]
c.1830_1833del	p.(Glu610Aspfs*3)	Rao *et al.* [9]
c.2230C>T	p.(Gln744*)	Hu *et al.* [5]
c.2524C>T	p.(Gln842*)	Li *et al.* [6]
c.2717del	p.(Leu906*)	This manuscript
c.2807C>G	p.(Ser936*)	Li *et al.* [6]
c.2863C>T	p.(Gln955*)	Hu *et al.* [5]
c.2952_2955del	p.(Gln985Ilefs*6)	Hu *et al.* [5]
c.3073A>G	p.(Arg1025Gly)	Li *et al.* [6]

Following the identification of the mosaicism in the mother, a detailed clinical re-examination was performed, at an age of 57. At a young age, no visual or ocular problems had been reported. When she was 18 years old, she started wearing contact lenses to correct a light myopia of both eyes. Operations for cataract with lens implantation were done in both eyes at age 53. Ophthalmological examination showed normal best corrected visual acuity (right eye: 20/30 and left eye: 20/25). Her head circumference was 55 cm and thereby falls within the normal range. The eye position was straight and good binocular functions were present. Both anterior segments showed a well-positioned artificial lens with minimal opacification of the posterior lens capsule. Slitlamp-biomicroscopy showed posterior poles with a normal configuration of the macula and the vascular arcades of the retina. The peripheral retina was completely vascularized and did not show any dystrophic signs. In conclusion, no signs of FEVR or microcephaly were present in the mother of the proband.

5.4 Discussion

A heterozygous variant in *KIF11* (c.2717del, p.(Leu906*)) was detected in a patient presenting FEVR and microcephaly. It was inherited from the mother, who carries the variant in mosaic state at various rates in different tissues (blood, fibroblasts, and saliva). Besides the identification of the genetic defect in this patient, this

study also demonstrates the importance of genetic testing in parents and provides insight in the required amount of Eg5, the protein encoded by *KIF11*, for normal development.

To date, two suspected *KIF11* mosaic cases have been reported in literature [4, 5]. Robitaille *et al.* reported two siblings carrying identical *KIF11* variants that were not detected in the healthy parents by Sanger sequencing [4], whereas Hu *et al.* reported a case in which a mosaicism was suspected via subcloning experiments [5]. To our knowledge, this is the first report in which a *KIF11* mosaicism is accurately detected in different tissues of an individual using amplicon-based deep sequencing. This technique may allow the detection of mosaicism that occurs at a low rate which may be undetectable by Sanger sequencing. The presence of the variant in germ cells and somatic cells of the mother indicates that the variant has arisen early in embryonic development, prior to primordial germ cell differentiation (before ~15 mitotic divisions) [14]. Although it cannot be assessed experimentally, we can assume a similar degree of mosiacism present in the germline compared to those detected in saliva and blood, which contain cells originating from ectoderm and mesoderm, respectively. Thereby, we can also hypothesize on the chance of offspring being affected. Thus, the robust detection of mosaicism in unaffected parents can allow more accurate recurrence risks assessments and thereby facilitate better genetic counseling.

In this study, the mosaicism was quantified in three different tissues populated by cells originating from mesoderm (blood and fibroblasts) and ectoderm (saliva). Leukocytes (mesoderm) contamination in the saliva sample may occur [15]. The presence of the variant in these tissues corresponds with the abnormal development of retinal vasculature and microcephaly observed in the patient, which are defects in the development of organs predominantly populated by cells originating from mesoderm and ectoderm, respectively.

A difference in the mosaicism rate was detected in blood *vs.* fibroblasts, despite both originating from mesoderm. Although this may indicate that the variant occurred after further mesoderm specification, its presence in the germ cells of the mother suggests that the difference is more likely due to an artifact of the *in vitro* culturing of fibroblasts, which has been shown previously in lymphoblastoid cell lines [15]. Therefore, fresh materials which have not undergone any *in vitro* culturing should be used to detect mosaicisms.

KIF11 variants reported in subjects with FEVR and microcephaly are equally distributed throughout the Eg5 protein (Figure 2b) [4-6, 9], further highlighting the importance of both the N- and C- terminal part of Eg5 for proper functioning in spindle localization, as shown previously [10]. The variant that is identified in this study lies in the bimC box, a sequence motif surrounding a potential phosphorylation site at the C-terminus of the protein. It is known that Eg5 phosphorylation at this site (specifically at threonine residue 927) is required for its mitotic spindle association during mitosis [10, 16]. The data obtained in this study also allow the speculation of the amount of Eg5 required for a cell to function normally. Assuming a full loss-of-function of the mutated allele and considering the average mosaicism rate detected in the mother (20%), it is tempting to assume that a similar degree of mosaicism is present in other tissues, and thus that ~80% of normal Eg5 protein is sufficient for normal development. Given that a heterozygous variant results in developmental defects, the minimum required amount of Eg5 likely lies between 50 and 80%.

In summary, the findings in this study demonstrates the importance of deep sequencing of parental DNA following the identification of genetic defects in isolated cases to detect possible mosaicism. It will allow a reliable recurrence risk assessment and thereby improve genetic counseling. It is not only relevant for subjects with FEVR and microcephaly, but also for other genetic disorders with a similar mode of inheritance.

Acknowledgments

We gratefully acknowledge the subjects that participated in this study. We would like to thank Dr. Kornelia Neveling and Ronny Derks from the Genomics Technology Center of Radboudumc for assistance with Ion semiconductor sequencing, Michael Kwint for assistance with analysis of the Ion semiconductor sequencing data, Dr. Alexander Hoischen for helpful discussions on mosaicisms, Dr. Wendy van Zelst-Stams for skin biopsy taking, and Saskia van der Velde-Visser for cell culture assistance.

Funding

This work is funded by Radboudumc PhD grant to Dyah W. Karjosukarso.

Conflict of interest

All authors declare no conflict of interest.

References

1. Criswick VG, Schepens CL (1969) Familial exudative vitreoretinopathy. *Am J Ophthalmol* **68:** 578-594
2. Gilmour DF (2015) Familial exudative vitreoretinopathy and related retinopathies. *Eye (Lond)* **29:** 1-14
3. van Nouhuys CE (1981) Congenital retinal fold as a sign of dominant exudative vitreoretinopathy. *Albrecht Von Graefes Arch Klin Exp Ophthalmol* **217:** 55-67
4. Robitaille JM, Gillett RM, LeBlanc MA, Gaston D, Nightingale M, Mackley MP, Parkash S, Hathaway J, Thomas A, Ells A, *et al.* (2014) Phenotypic overlap between familial exudative vitreoretinopathy and microcephaly, lymphedema, and chorioretinal dysplasia caused by KIF11 mutations. *JAMA Ophthalmol* **132:** 1393-1399
5. Hu H, Xiao X, Li S, Jia X, Guo X, Zhang Q (2016) KIF11 mutations are a common cause of autosomal dominant familial exudative vitreoretinopathy. *Br J Ophthalmol* **100:** 278-283
6. Li JK, Fei P, Li Y, Huang QJ, Zhang Q, Zhang X, Rao YQ, Li J, Zhao P (2016) Identification of novel KIF11 mutations in patients with familial exudative vitreoretinopathy and a phenotypic analysis. *Sci Rep* **6:** 26564
7. Ostergaard P, Simpson MA, Mendola A, Vasudevan P, Connell FC, van Impel A, Moore AT, Loeys BL, Ghalamkarpour A, Onoufriadis A, *et al.* (2012) Mutations in KIF11 cause autosomal-dominant microcephaly variably associated with congenital lymphedema and chorioretinopathy. *Am J Hum Genet* **90:** 356-362
8. Birtel J, Gliem M, Mangold E, Tebbe L, Spier I, Muller PL, Holz FG, Neuhaus C, Wolfrum U, Bolz HJ, *et al.* (2017) Novel Insights Into the Phenotypical Spectrum of KIF11-Associated Retinopathy, Including a New Form of Retinal Ciliopathy. *Invest Ophthalmol Vis Sci* **58:** 3950-3959
9. Rao FQ, Cai XB, Cheng FF, Cheng W, Fang XL, Li N, Huang XF, Li LH, Jin ZB (2017) Mutations in LRP5,FZD4, TSPAN12, NDP, *ZNF408*, or KIF11 Genes Account for 38.7% of Chinese Patients With Familial Exudative Vitreoretinopathy. *Invest Ophthalmol Vis Sci* **58:** 2623-2629
10. Sawin KE, Mitchison TJ (1995) Mutations in the kinesin-like protein Eg5 disrupting localization to the mitotic spindle. *Proc Natl Acad Sci U S A* **92:** 4289-4293
11. Exertier P, Javerzat S, Wang B, Franco M, Herbert J, Platonova N, Winandy M, Pujol N, Nivelles O, Ormenese S, *et al.* (2013) Impaired angiogenesis and tumor development by inhibition of the mitotic kinesin Eg5. *Oncotarget* **4:** 2302-2316
12. Barresi MJ, Burton S, Dipietrantonio K, Amsterdam A, Hopkins N, Karlstrom RO (2010) Essential genes for astroglial development and axon pathfinding during zebrafish embryogenesis. *Dev Dyn* **239:** 2603-2618
13. Diekstra A, Bosgoed E, Rikken A, van Lier B, Kamsteeg EJ, Tychon M, Derks RC, van Soest RA, Mensenkamp AR, Scheffer H, *et al.* (2015) Translating sanger-based routine DNA diagnostics into generic massive parallel ion semiconductor sequencing. *Clin Chem* **61:** 154-162
14. Campbell IM, Shaw CA, Stankiewicz P, Lupski JR (2015) Somatic mosaicism: implications for disease and transmission genetics. *Trends Genet* **31:** 382-392
15. Gajecka M (2016) Unrevealed mosaicism in the next-generation sequencing era. *Mol Genet Genomics* **291:** 513-530
16. Blangy A, Lane HA, d'Herin P, Harper M, Kress M, Nigg EA (1995) Phosphorylation by p34cdc2 regulates spindle association of human Eg5, a kinesin-related motor essential for bipolar spindle formation in vivo. *Cell* **83:** 1159-1169

Supplementary materials

Genetic analysis

DNA was isolated from peripheral blood lymphocytes of proband and her parents using a standard salting-out procedure. In addition, DNA was isolated from saliva and skin biopsy-derived fibroblasts cell line of the unaffected mother using Chemagic STAR DNA Saliva4k (Perkin Elmer Chemagen, Baesweiler, Germany), kit and QIAamp DNA mini kit (Qiagen, Hilden, Germany), according to manufacturer's instructions, respectively.

All exons and intron-exon boundaries of the *KIF11* gene were screened for potentially causative DNA variants in the proband by Sanger sequencing. The primers used for this screening are listed in Supplementary Table 1. Exon 19 of *KIF11* that harbors the causative mutation was amplified from the proband, her father, and three different tissues of her mother (peripheral blood lymphocytes, saliva, and fibroblasts). The amplicons were subjected to Sanger sequencing as well as Ion semiconductor sequencing (Ion Personal Genome Machine, Thermo Fisher Scientific). The resulting fastq files were analyzed and converted into BAM files in SeqNext software (JSI), and visualized in Integrated Genomics Viewer (IGV, Broad Institute).

Table S1 ***KIF11*** **primers**

Fragment Name	Sequence (5'- to 3'-)	Fragment size (bp)
*KIF11*_ex1_F	AGTACCGGGTAGAGAGCGGG	315
*KIF11*_ex1_R	CTGGACCGCGCAGTAGG	
*KIF11*_ex2_3_F	TAGTTAGTGAAAATGTCATTGATAACC	627
*KIF11*_ex2_3_R	GCAACAAGAGTGAAACTCCG	
*KIF11*_ex4_F	CCACTGTGCCTGGCTTG	259
*KIF11*_ex4_R	CAAGACAGAGGCCCTCAAAC	
*KIF11*_ex5_6_F	GGCCCATGTATTTTAACTGCC	639
*KIF11*_ex5_6_R	CACCCCAATTTGACTTTCTCC	
*KIF11*_ex7_F	TCCTGTTTTCAGTATTTCAGAAGC	236
*KIF11*_ex7_R	GGACAAAATTTCAAGCTGCTC	
*KIF11*_ex8_F	TTATTTTGCTGGCGATTTAATAC	489
*KIF11*_ex8_R	ATCCGCCCACCTTGGAC	
*KIF11*_ex9_F	AAAGGTTGGGCATAGTGGTC	360
*KIF11*_ex9_R	CCTTCCATGGGCAATTTAAC	
*KIF11*_ex10_F	ATTTGTTGCATGTCCTTCCC	234
*KIF11*_ex10_R	AAGTTTTACTTCAAATAGCCTGTTATC	
*KIF11*_ex11_F	CACTTGGGTATCAAGTGATGG	404
*KIF11*_ex11_R	GACCCTGGGAGGCAGAG	
*KIF11*_ex12_F	CCGGGTAACTTCTTACAACTTTTG	417
*KIF11*_ex12_R	GGACAGAAATACCATTTGGGG	
*KIF11*_ex13_F	TATGTACCACCACACCCAGC	475
*KIF11*_ex13_R	TGACACCGTCATCTATGTTTCAC	
*KIF11*_ex14_F	TCTTTGAAATGGTTTGAACGG	367
*KIF11*_ex14_R	GGAAGAAAGAATAGCAGTTAACATTG	
*KIF11*_ex15_16_F	TTTAATGTGAATGTTTAGCTACCAAAG	576
*KIF11*_ex15_16_R	TCAGCTTTTACAGTATTCAGATTGTG	
*KIF11*_ex17_F	TCACTTCCACTGCTTTCCTC	564
*KIF11*_ex17_R	GCACAAATACGCAATGAAAAG	
*KIF11*_ex18_F	GAGCCAGACTGTCCACGTTC	557
*KIF11*_ex18_R	CACAAAACGAGATCATCTGTAAGC	
*KIF11*_ex19_F	GGAAAAGGTAAGGGAAAATATGATG	417
*KIF11*_ex19_R	AAATTTCTGTCAGGCAATGG	
*KIF11*_ex20_F	TGACAGGTAGCAAGACTGATCC	368
*KIF11*_ex20_R	TCACATGAAGTCAGCCACATC	
*KIF11*_ex21_F	TCAAAGCTGCTGTTACTCTTGTG	277
*KIF11*_ex21_R	TTCTGCTCACCACGAACAATAC	
*KIF11*_ex22_F	TTTTGCCTATAACCCAGAGAAC	578
*KIF11*_ex22_R	GGAGTGTAGTGGTGTACCTTTGG	

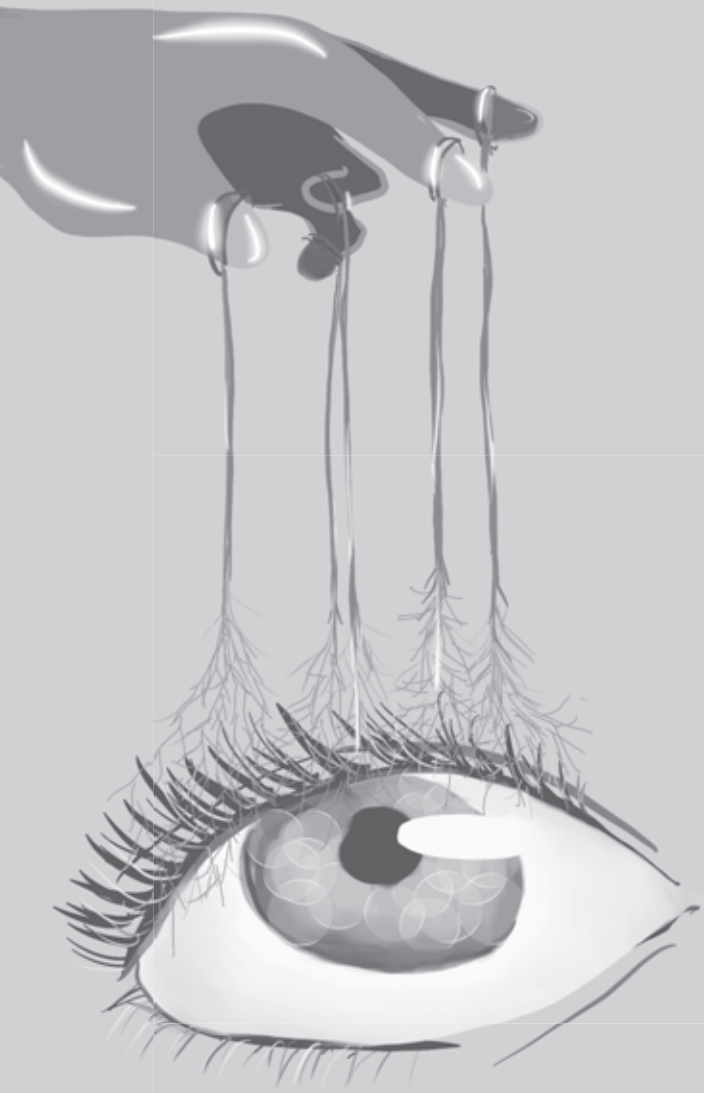

Chapter 6

General discussion

Familial exudative vitreoretinopathy (FEVR) was first described by Criswick and Schepens in 1969 [1]. Since then, efforts have been made to elucidate the genetic cause of this inherited retinal defect. A few years ago, a missense mutation (p.His455Tyr) in *ZNF408* was identified as the underlying genetic cause in an autosomal dominant FEVR family [2]. Afterwards, more genetic variants in *ZNF408* were found to be associated with FEVR in other studies [3-6], as well as in another inherited eye disease, retinitis pigmentosa [7, 8]. Nevertheless, how defects in *ZNF408* result in these diseases is poorly understood. In this study, we focused on deciphering the molecular role of ZNF408, particularly in the development of (retinal) vasculature, and how defect(s) in *ZNF408* can give rise to the clinical features observed in FEVR. We also aimed to identify other genetic cause(s) of FEVR and related diseases.

6.1 ZNF408 in the development of (retinal) vasculature

The identification of a genetic variant in *ZNF408* that causes FEVR suggested its involvement in the development of the (retinal) vasculature. Since this first finding, more genetic studies have reported other *ZNF408* variants in a handful of FEVR cases [3-6], emphasizing the role of ZNF408 in vasculature development. Abnormal eye and trunk vasculature development observed upon morpholino-induced knockdown of *znf408* in zebrafish further strengthened this hypothesis [2]. We continued modeling of *znf408* in zebrafish and showed abnormal retinal vasculature development in *znf408* mutant zebrafish (Chapter 3)

FEVR is hallmarked by the absence of or abnormal vasculature in the peripheral retina, while the primary vascular layer can be either normal or abnormal, depending on the severity of the disease. This suggests that FEVR is likely a disorder of angiogenesis instead of vasculogenesis. This was supported by the observation in murine models of FEVR in which the deeper retinal plexuses are absent, whereas the primary retinal plexus is still present [9]. The *znf408* zebrafish models described in this thesis also showed presence of retinal vasculature, albeit delayed and abnormally developed (Chapter 3). Altogether, these indicate that ZNF408 plays a role in retinal angiogenesis.

To better understand the molecular role of ZNF408, particularly in (retinal) angiogenesis, we opted to use endothelial cells as an *in vitro* model. In Chapter 2, we overexpressed wild-type and p.His455Tyr mutant ZNF408 in human umbilical

vein endothelial cells (HUVEC) and observed that the overexpression of mutant ZNF408 disrupts the ability of HUVEC to form a capillary-like network in an *in vitro* tube formation assay, thus mimicking the abnormal retinal vasculature observed in FEVR patients. Transcriptomics analysis was performed on these cellular models whose results suggested a role for ZNF408 in various biological processes. Importantly, this analysis showed that the p.His455Tyr mutation alters the normal gene expression regulated by ZNF408, which may underlie the observed cellular phenotype. Gene ontology analysis of the differentially regulated genes showed that wild-type ZNF408 upregulates genes that are associated with nucleosome assembly and protein heterotetramerization, whereas its downregulated genes are associated with biological processes relevant to the vasculature development (e.g. response to hypoxia, cell adhesion, and angiogenesis). The latter led us to the hypothesis that wild-type ZNF408 supports the development of vasculature by downregulating the expression of genes that inhibit this process.

We further looked for the mechanism by which ZNF408 regulates gene expression. Since it has ten zinc finger domains, we assumed that it functions by binding to DNA and acting as a transcription factor. Chromatin immunoprecipitation followed by next generation sequencing (ChIP-Seq) performed in HEK293T cells showed that the p.His455Tyr mutation reduced the DNA binding ability of ZNF408 (Chapter 2). Nonetheless, little overlap was observed between the genes identified in the transcriptomics analysis and the ChIP-Seq experiment. The difference in cellular systems used in both experiments as well as the relatively low number of binding sites detected may contribute to this. The latter also implies that ZNF408 does not bind directly to DNA to regulate gene expression and suggests that its effect on gene expression is likely to be an indirect effect. Although DNA binding is the most commonly described activity of zinc finger domains, RNA binding and protein binding have also been described [10, 11]. Besides zinc finger domains, ZNF408 is also predicted to have a PRDM (positive regulatory domain I-binding factor 1/PRD1-BF1 and retinoblastoma-interacting zinc finger protein 1/RIZ1 homology domain containing) domain, near its N-terminus. The PRDM domain is a subfamily of SET methyltransferase. Such PRDM proteins typically have multiple adjacent zinc finger domains, as predicted in ZNF408. Members of this family are usually involved in the regulation of gene expression by acting as histone methyltransferase or as co-factor by binding to other proteins [12, 13]. Further investigation on ZNF408 interacting partners may shed more light into its mechanism of action in regulating gene expression.

To further study the role of ZNF408 *in vivo*, we generated two truncated and one missense *znf408* zebrafish model using CRISPR/Cas9 technology (Chapter 3). In both truncated *znf408* models, a frameshift was created that is predicted to result in a truncated protein. Alternatively, in the missense model, one of the core histidines of the fourth zinc finger domain was substituted with a tyrosine residue, mimicking the p.His455Tyr mutation identified in FEVR patients. The *znf408* zebrafish models showed a delay in retinal vasculature development at 5 days post-fertilization, abnormal sprouting at 3 months post-fertilization, as well as vascular leakage at 6 months post-fertilization (Chapter 3). In Chapter 2, we observed altered gene expression by the p.His455Tyr mutation, which may underlie the cellular phenotype observed. It is tempting to hypothesize that the phenotypes observed in the zebrafish models are also due to altered gene expression caused by modified *znf408*. Seventy percent of human genes have an orthologue in the zebrafish genome [14]. Indeed, 188 out of 227 genes that are differentially regulated by wild-type and p.His455Tyr ZNF408, as described in Chapter 2, have a zebrafish orthologue based on the Biomart database. It would be interesting to do transcriptomics analysis in the *znf408* zebrafish models to determine whether similar sets of genes are affected by the genetic modification of *znf408* in these models. A time-course transcriptomics analysis would be very informative, since the gene expression may change over time, which may underlie the different phenotypes that were observed at different time points.

FZD4, *LRP5*, *TSPAN12*, and *NDP* are the genes that are most frequently mutated in FEVR and thus are also the most studied [9]. The proteins encoded by these genes are involved in the Norrin/β-catenin signaling pathway [15]. In this pathway, TSPAN12 aids the formation of the FZD4-LRP5 receptor complex for Norrin (the protein encoded by NDP). Binding of Norrin to its receptor complex activates the pathway, which leads to the translocation of β-catenin to the nucleus where it regulates the expression of its downstream target genes [15]. Recently, mutations in *CTNNB1*, the gene encoding for β-catenin, were identified in FEVR patients, further corroborating the association of the Norrin signaling pathway to FEVR [16]. Additionally, a recently identified causative gene for FEVR, *RCBTB1*, was also suggested to be involved in the nuclear localization of β-catenin [17]. Based on these findings, it is tempting to hypothesize that *ZNF408* is also involved in this pathway. None of the FEVR genes, however, were found to be regulated by ZNF408 (Chapter 2). Thus, it is unlikely that ZNF408 is located upstream of the

pathway, regulating its activity. *ZNF408* is neither included in the list of β-catenin target genes in Wnt homepage maintained by the Nusse lab (https://web.stanford.edu/group/nusselab/cgi-bin/wnt/target_genes) nor in a comprehensive study of β-catenin target genes by Herbst *et al.* [18]. Furthermore, ZNF408 is also not included in the knowledge map of β-catenin molecular function developed by Celen *et al.*, which comprises its post-translational modifications, protein-protein interactions, disease-associated mutations, transcription factors co-activated by β-catenin and their targets, as well as the major processes in which β-catenin is known to participate [19]. Therefore, it is unlikely that it is involved in that pathway neither as an interaction partner of β-catenin nor as one of the target genes of β-catenin. Additionally, almost none of ZNF408-regulated genes were found in this knowledge map, suggesting different roles of ZNF408 and β-catenin in the regulation of gene expression. Involvement in the Norrin/β-catenin pathway has also not been observed for *ATOH7*, another FEVR gene [20]. *ATOH7* encodes a bHLH transcription factor which is crucial for retinal ganglion formation [21]. This indicates that, although the majority of FEVR genes are involved in the Norrin/β-catenin pathway, it is well possible that *ZNF408*, similar to *ATOH7*, is involved in another pathway, defects in which eventually can lead to FEVR features.

6.2 A surprise from ZNF408

In Chapter 2, we described how the p.His455Tyr mutation alters the normal gene expression regulated by wild-type ZNF408. Besides downregulating genes that are involved in the development of vasculature, wild-type ZNF408 upregulates the expression of genes associated with nucleosome assembly and protein heterotetramerization. The majority of these genes encode for histone proteins. These suggest the involvement of ZNF408 in chromatin remodeling. It is known that the expression of histone genes are cell-cycle regulated and controlled, both at the transcriptional and post-transcriptional level [22]. Furthermore, 8 out of 15 genes within the minute overlap between the transcriptome data and the ChIP-Seq results, encode histone proteins. As mentioned previously, ZNF408 belongs to the family of PRDM proteins and members of this family have been described to play a role in histone modifications, either directly or indirectly [12]. Taking this into account, it is very well possible that ZNF408 is also involved in chromatin remodeling. In addition, the enrichment of these gene ontology terms were found in the transcriptome analysis as well as the ChIP-Seq data, experiments which were performed on two different cell systems. This tempted us to hypothesize that it is the major role of ZNF408 in different cellular systems, although the genes

regulated may differ per system. In this light, the differential expression of the histone genes we observed could well be the driving force of the other differential expression observed in this analysis. Further investigation of interaction partners of ZNF408, such as by proteomics profiling and RNA pull-down assays, as well as other epigenetic profiling experiments may shed more light on this.

6.3 Defects in *ZNF408* lead to different phenotypes

Mutations in *ZNF408* have also been reported in autosomal recessive retinitis pigmentosa (RP) cases [7, 8], which is characterized by a rod-cone photoreceptor degeneration. Although it is not uncommon that different mutations in one gene manifest different clinical features, the clinical features of RP and FEVR are quite distinct and the genotype-phenotype correlations still need to be established. Mutations causing FEVR and RP are either missense or stop mutations that are spread throughout the gene (Figure 1, Table 1), implying that there is no clear correlation between the type and position of the mutation and the resulting clinical features. Immunohistochemistry in human and mouse retina showed that ZNF408 is expressed in the vasculature as well as the photoreceptor cells. We were not able to reliably detect znf408 in zebrafish retina (Chapter 3). The truncated *znf408* zebrafish models we generated are supposedly a good model for *ZNF408*-associated RP which is inherited in autosomal recessive manner. Despite the mild visual impairment observed at 5 dpf, no apparent neuronal degeneration was observed at different stages of these models. Instead, we observed abnormal vasculature development similar to the missense zebrafish model.

Mutations in *ZNF408* that are detected in FEVR are inherited in an autosomal dominant manner, whereas those found in RP cases have an autosomal recessive inheritance pattern [2-8]. Such an inheritance pattern was also observed in *RCBTB1*, in which mutations were detected in (autosomal dominant) FEVR or (autosomal recessive) retinal degeneration with RP as one of the ocular features [17, 23]. Such a correlation has not been observed for other FEVR genes. Although this suggests a correlation between the inheritance pattern and the phenotypic outcome, it is still unclear which mutations cause which phenotype and how. Further studies on the genotype-phenotype correlation of *ZNF408* and the resulting clinical features will be required to understand this. The studies described in this thesis may have paved a way towards elucidating the role of ZNF408, particularly in the pathogenesis of FEVR, but similar studies in the context of RP would shed further light on this and thereby, assist in disease management.

Table 1 Variants reported in *ZNF408*

cDNA Variant NM_024741	Protein Variant NM_024741	cDNA Variant NM_001184751	Protein Variant NM_001184751	Exac Allele Frequency	PhyloP*	SIFT	PolyPhen-2	Grantham	Ref
FEVR									
c.130C>T	p.(Pro44Ser)	c.106C>T	p.(Pro36Ser)	0	-0.6219	Tolerated	Benign	74	[5]
c.377G>A	p.(Ser126Asn)	c.353G>A	p.(Ser118Asn)	0.00004942	2.022	Deleterious	Possibly Damaging	46	[2, 3]
c.443G>A	p.(Arg148Gln)	c.419G>A	p.(Arg140Gln)	0.00001667	1.042	Tolerated	Benign	43	[6]
c.694A>G	p.(Met232Val)	c.670A>G	p.(Met224Val)	0	-0.896	Tolerated	Benign	21	[5]
c.758G>A	p.(Gly253Asp)	c.734G>A	p.(Gly245Asp)	0	0.028	Tolerated	Benign	94	[3]
c.1107del	p.(Lys370Serfs*118)	c.1083delG	p.(Lys362Serfs*118)						[3]
c.1285G>A	p.(Val429Met)	c.1261G>A	p.(Val421Met)	0.00006669	2.266	Deleterious	Probably Damaging	21	[3]
c.1363C>T	p.(His455Tyr)	c.1339C>T	p.(His447Tyr)	0.00001689	6.0599	Deleterious	Probably Damaging	83	[2]
c.1496C>T	p.(Pro499Leu)	c.1472C>T	p.(Pro491Leu)	0.000008537	1.299	Deleterious	Probably Damaging	98	[3]
c.1517G>A	p.(Arg506His)	c.1493G>A	p.(Arg498His)	0	3.8359	Deleterious	Probably Damaging	29	[3]
c.1757G>A	p.(Arg586His)	c.1733G>A	p.(Arg578His)	0.00003448	2.0759	Deleterious	Possibly Damaging	29	[3]
c.1987_1990del	p.(Glu663Argfs*36)	c.1963_1966del	p.(Glu655Hisfs*36)						[3]
c.2145G>T	p.(Glu715Asp)	c.2121G>T	p.(Glu707Asp)	0	1.4329	Deleterious	Probably Damaging	58	[5]
c.2149G>A	p.(Glu717Lys)	c.2125G>A	p.(Glu709Lys)	0.000009935	0.646	Deleterious	Possibly Damaging	56	[3]
FEVR-digenic**									
c.892G>A	p.(Gly298Ser)	c.868G>A	p.(Gly290Ser)	0.0002401	0.4199	Tolerated	Benign	56	[4]
c.1987_1990del	p.(Glu663Argfs*36)	c.1963_1966del	p.(Glu655Hisfs*36)						[4]
c.1988G>C	p.(Arg663Thr)	c.1964G>C	p.(Arg655Thr)	0.00002629	0.966	Tolerated	Benign	71	[4]
arRP***									

cDNA Variant NM_024741	Protein Variant NM_024741	cDNA Variant NM_001184751	Protein Variant NM_001184751	Exac Allele Frequency	PhyloP*	SIFT	PolyPhen-2	Grantham	Ref
c.358_359del	p.(Ala122Leufs*2)	c.334_335del	p.(Ala114Leufs*2)						[7]
c.653-1G>T	p.(?)	c.629-1G>T	p.(?)						[8]
c.1621C>T	p.(Arg541Cys)	c.1597C>T	p.(Arg533Cys)	0.00001723	0.337	Deleterious	Possibly Damaging	180	[7]
c.1304G>A****	p.(Arg435Gln)	c.1280G>A	p.(Arg427Gln)	0.0001336	2.1349	Deleterious	Probably Damaging	43	[24]

*PhyloP100way score from www.varsome.com

** These variants were reported to be present together with another variant in other FEVR genes in one individual.

*** These variants are homozygous variants.

****This variant was reported in a case of autosomal recessive retinal degeneration, which subtype was not specified by the authors.

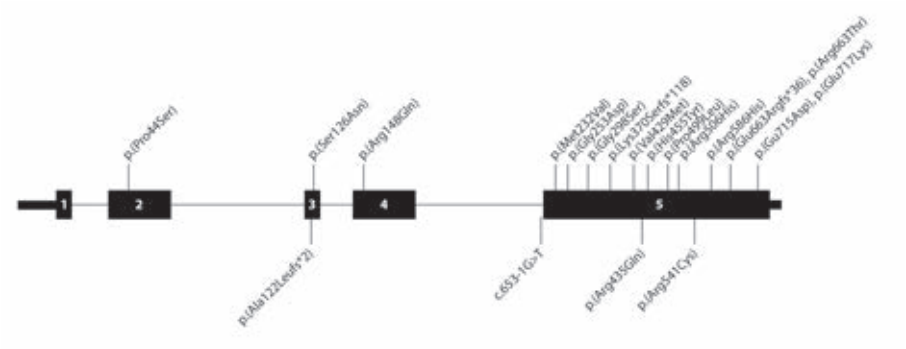

Figure 1. Schematic representation of variants reported in *ZNF408*. Variants reported in FEVR cases are depicted on the top, whereas those reported in RP and other cases are illustrated on the bottom. The protein variant nomenclature is based on transcript NM_024741.

6.4 Complexity of FEVR genetics

The advancement of molecular technologies has allowed researchers to identify the genetic causes in a large number of FEVR cases. As mentioned previously, *FZD4*, *LRP5*, *TSPAN12*, and *NDP*, are the genes most frequently mutated in FEVR. Recent gene hunting efforts have added *ZNF408*, *RCBTB1*, *ATOH7*, and *CTNNB1* to the list of causative genes for FEVR [2, 16, 17, 20]. However, there are still a number of unsolved FEVR cases [9]. The remaining genetic causes of the unsolved cases can be either defect(s) in a novel gene or variant(s) located outside the coding region of known genes. A series of digenic cases of FEVR has also been recently reported [4]. Most of the FEVR genes were identified either by targeted Sanger sequencing or whole-exome sequencing, which does not allow the investigator to identify genetic defects outside the coding region or structural variants. The ever-decreasing cost of sequencing, together with the improvement in data analysis, will soon allow whole-genome sequencing (WGS) to be broadly available for the identification of the genetic cause of any inherited disease, thereby, providing means to identify underlying causes in the unsolved FEVR cases.

The clinical features of FEVR have also been found to be accompanied by other symptoms. For example, a syndrome called osteoporosis pseudoglioma, in which patients present bone abnormalities and FEVR characteristics, is caused by mutations in *LRP5* [25]. Another example is Norrie disease, an X-linked disease caused by *NDP* mutations, in which hearing impairment and sometimes intellectual impairment are detected next to FEVR-like ocular features [26]. FEVR symptoms have also been observed accompanied by microcephaly, a

clinical presentation associated with mutations in *KIF11* [27]. In Chapter 5, we demonstrated that a *KIF11* variant can be present in a mosaic manner in a healthy individual. If the variant is present in the germ cells, the variant can be transmitted to the offspring causing unexpected manifestation of the disease. Although we were the first to quantify the mosaicism of *KIF11* associated with FEVR and microcephaly in different tissues, it has been previously suspected in other *KIF11* cases [27, 28]. This finding raises the question whether mosaicisms can also be present in other cases of FEVR. Low grade mosaicisms can be difficult to detect using Sanger sequencing, and therefore may be missed. Based on our findings, it is important to screen both parents of FEVR patient with deep sequencing to detect potential mosaicisms in isolated FEVR cases, in which the genetic variant in the patient would commonly be considered as *de novo*, to improve genetic counseling.

Phenotypic variability, even within a family, is often observed in FEVR. In addition, reduced penetrance has been observed in approximately 25% of FEVR mutation carriers [29]. The penetrance of a genetic variant can be influenced by many factors, *e.g.*, epigenetic modification, allele dosage, modifier gene(s), copy number variants, gene expression level, environmental factors [30]. In Chapter 4, we present a preliminary study of *in vitro* investigation of reduced penetrance in *ZNF408*-associated FEVR. There are two unaffected individuals who carry the *ZNF408* p.His455Tyr mutation in the large autosomal dominant FEVR family described by Collin *et al.* [2]. One of these unaffected mutation carriers (UMC) is included in this preliminary study, together with her affected sister (Chapter 4). Due to the requirement of relevant patient material, an *in vitro* study of the underlying cause of non-penetrance can be challenging. For instance, in case of a disease such as FEVR, patient material from retinal vasculature would be required, which is both practically and ethically challenging. Fortunately, advances in the application of induced pluripotent stem cell (iPSC) technology have allowed the generation of theoretically any relevant material from patient-derived iPSCs. In the study described in Chapter 4, we used iPSCs obtained from the UMC and her sister to generate patient-specific endothelial cells, a relevant cell type for vasculature-related disorders. This pilot study showed us how iPSC-derived endothelial cells can be used as an *in vitro* model to study reduced penetrance in FEVR. Further molecular and cellular characterization of the generated endothelial cells may reveal the underlying cause of reduced penetrance of *ZNF408*-associated FEVR. The cause of reduced penetrance in *ZNF408* associated-FEVR may or may

not be similar to the cause of reduced penetrance observed in FEVR cases with mutations in other genes. Nevertheless, the method presented can be applied to any FEVR case to have better insight on the reduced penetrance often observed in this disease.

6.5 Implications of this study to diagnostics

The clinical diagnosis of FEVR is usually performed by ocular examination accompanied by fluorescein angiography. The diagnosis may be facilitated by screening of asymptomatic family members. Furthermore, genetic analysis is recommended for proper counseling, taking into account that FEVR is a lifelong disease, whose unpredictable progression requires regular follow-up [31].

So far, the majority of molecular diagnosis of FEVR is performed either by Sanger sequencing or targeted next-generation sequencing of known genes. Whole exome sequencing was employed in the genetic analysis of FEVR cases in which no defect was found in the known genes, which led to the identification of several novel genes in recent years [2, 16, 17]. As mentioned previously, whole exome sequencing analysis only allowed the detection of variants within the coding regions of the genome. With the decreasing sequencing costs and development of analysis tools, whole genome sequencing is likely to be more powerful in the identification of novel genetic defects in FEVR, within as well as outside the coding regions. The identification of genetic defects in the unsolved FEVR cases not only provides more insight into the molecular basis of the disease, but also is essential for diagnostics and thereby, disease management and counseling. Additionally, deep sequencing may be required to identify mosaicisms in isolated cases of FEVR, such as the case presented in Chapter 5 of this thesis.

Detection of known variants in known genes can easily facilitate diagnosis and future counseling. There are plenty of *in silico* programs, databases, and guidelines that can aid in the classification of a new variant in a known gene. However, if the candidate pathogenic variant is a new variant in a novel gene, it can be quite challenging to determine whether it is the causative variant. Functional characterization of such variants is required, next to the *in silico* predictions. In this thesis, we subjected two *in vitro* models of *ZNF408*-associated FEVR to *in vitro* tube formation assay (Chapter 2 and 4). One of the *in vitro* models is HUVEC overexpressing wild-type and mutant ZNF408 via lentiviral transduction, in

which there was a striking difference between wild-type and mutant ZNF408. We also performed a pilot study in which we differentiated patient-derived iPSCs into endothelial cells, for which no striking difference was observed between cells obtained from healthy individual *vs* a patient. As this is a pilot study, there are plenty of technical improvements which may influence the results of the *in vitro* tube formation assay. Nonetheless, such *in vitro* models and assay can be employed to assess the effect of the candidate variant in relevant models and assays, thereby facilitating the molecular diagnosis and disease management.

6.6 Towards treatment or prevention of FEVR

Laser photocoagulation is one of the common treatments for the vascular leakage and exudates observed in FEVR patients. Surgical intervention is often recommended in cases with retinal detachment [31]. Several different groups have tried to employ intravitreal injection of anti-VEGF therapy, such as those used in treating wet age-related macular degeneration, as additional treatment of the neovascularization in FEVR [32-34]. Despite the promising results, these studies were conducted on a small scale and for relatively short period of time. Therefore, further research into the efficacy and safety is required.

Gene therapy has been successfully applied in the treatment of some inherited retinal disorders and is under development for some other retinal diseases. A hallmark example is the delivery of *RPE65* for the treatment of Leber congenital amaurosis [35]. However, FEVR is a developmental disease, which means there is a small window of opportunity to correct the developmental defect. In the era of iPSC differentiation technologies, cell replacement therapy may have more potential in restoring the absent or abnormal retinal vasculature in FEVR. Nevertheless, such a therapy is commonly patient-specific, i.e. iPSCs need to be obtained from the specific patient, the genetic defect needs to be be corrected, and patient-specific cells must be generated. As such, it requires a lot of time, money, and facilities to treat a patient with FEVR. Considering these, together with the heterogeneity of FEVR, a more universal treatment is required.

Since the Norrin/β-catenin signaling is deficient in FEVR (and alike diseases), targeting this pathway is a potential therapeutic approach. Treatment with Norrin has been shown to restore the vascular defects in the retinas of mice with Norrie disease as well as in oxygen-induced retinopathy mice [36-40]. However, other

components of the Norrin/β-catenin signaling pathway may also be defective in FEVR, for instance, loss of function of FZD4 and LRP5, the receptor and co-receptor of Norrin. As a more general therapeutic approach, Wang *et al.* targeted GSK3β, a component of Norrin/β-catenin signaling that phosphorylates β-catenin which results in the degradation of β-catenin [41]. Intraperitoneal injection of lithium to *Lrp5*$^{-/-}$ mice reversed the vascular phenotype and partially restored visual function [41]. Although this effect should still be tested on other FEVR animal models, this finding opens a new avenue for a universal treatment of FEVR and other Norrin/Wnt-related vascular eye diseases. In addition, lithium is an FDA-approved treatment that has been used to treat mental disorders, even during pregnancy, rendering its safety. However, considering that human retinal vasculature develops *in utero* instead of postnatally as in mice, the safety to treat fetuses and infants with lithium should still be determined.

FEVR can also be caused by mutations in *ZNF408* and *ATOH7*, both of which have not been shown to be related to the Norrin/β-catenin signaling. Lithium treatment may or may not be advantageous for FEVR caused by mutations in these genes. Other molecules may also have potential in the treatment of FEVR, for which the screening can be done *in vitro* and *in vivo*. *In vitro* tube formation assays can be applied in studies determining angiogenesis-modulating activity of drugs in a high-throughput manner [42]. Furthermore, Kitambi *et al.* performed a screening of small molecules to study their influence on retinal vasculature development in zebrafish [43]. Taking such possibilities into account, the *in vitro* and *in vivo* models of FEVR, such as some that are described in this thesis (Chapter 2, Chapter 3, and Chapter 4), can thus be used in identifying potential drugs for the treatment of FEVR.

Given its heterogenous nature, it is likely that combination of treatments will be required to halt the disease progression of FEVR. The deeper insight into the molecular mechanisms underlying this disease not only facilitates diagnosis and disease management, but also paves the way to design and recommend better treatments for FEVR.

6.7 Concluding remarks

Advancement of technologies in the field of ophthalmology, genetics, and molecular biology has advanced the knowledge into FEVR and its cause significantly, since

its first description in 1969. Diagnosis methods and classification of disease stages are established. The genetic cause of a large number of FEVR cases also can be explained, thanks to the persistent genetic studies in the last decades. *In vitro* and *in vivo* studies of FEVR-associated genes have shed light into the molecular aetiology of the disease. Nevertheless, there are many more aspects to investigate, such as identifying the genetic causes of the remaining FEVR cases, mechanisms that lead to FEVR, as well as development of potential treatments. The studies presented in this thesis were aimed to touch upon these issues and have deepened the understanding of the molecular basis of FEVR, particularly *ZNF408*-associated FEVR, as well as providing new tools for the investigation of disease mechanisms and potential treatments.

REFERENCES

1. Criswick VG, Schepens CL (1969) Familial exudative vitreoretinopathy. *Am J Ophthalmol* **68:** 578-594
2. Collin RW, Nikopoulos K, Dona M, Gilissen C, Hoischen A, Boonstra FN, Poulter JA, Kondo H, Berger W, Toomes C*, et al.* (2013) *ZNF408* is mutated in familial exudative vitreoretinopathy and is crucial for the development of zebrafish retinal vasculature. *Proc Natl Acad Sci U S A* **110:** 9856-9861
3. Li JK, Li Y, Zhang X, Chen CL, Rao YQ, Fei P, Zhang Q, Zhao P, Li J (2018) Spectrum of Variants in 389 Chinese Probands With Familial Exudative Vitreoretinopathy. *Invest Ophthalmol Vis Sci* **59:** 5368-5381
4. Li Y, Peng J, Li J, Zhang Q, Li J, Zhang X, Fei P, She K, Zhao P (2018) The characteristics of digenic familial exudative vitreoretinopathy. *Graefes Arch Clin Exp Ophthalmol* **256:** 2149-2156
5. Musada GR, Syed H, Jalali S, Chakrabarti S, Kaur I (2016) Mutation spectrum of the FZD-4, TSPAN12 AND *ZNF408* genes in Indian FEVR patients. *BMC Ophthalmol* **16:** 90
6. Salvo J, Lyubasyuk V, Xu M, Wang H, Wang F, Nguyen D, Wang K, Luo H, Wen C, Shi C*, et al.* (2015) Next-generation sequencing and novel variant determination in a cohort of 92 familial exudative vitreoretinopathy patients. *Invest Ophthalmol Vis Sci* **56:** 1937-1946
7. Avila-Fernandez A, Perez-Carro R, Corton M, Lopez-Molina MI, Campello L, Garanto A, Fernandez-Sanchez L, Duijkers L, Lopez-Martinez MA, Riveiro-Alvarez R*, et al.* (2015) Whole-exome sequencing reveals *ZNF408* as a new gene associated with autosomal recessive retinitis pigmentosa with vitreal alterations. *Hum Mol Genet* **24:** 4037-4048
8. Habibi I, Chebil A, Kort F, Schorderet DF, El Matri L (2017) Exome sequencing confirms *ZNF408* mutations as a cause of familial retinitis pigmentosa. *Ophthalmic Genet* **38:** 494-497
9. Gilmour DF (2015) Familial exudative vitreoretinopathy and related retinopathies. *Eye (Lond)* **29:** 1-14
10. Brayer KJ, Segal DJ (2008) Keep your fingers off my DNA: protein-protein interactions mediated by C2H2 zinc finger domains. *Cell Biochem Biophys* **50:** 111-131
11. Iuchi S (2001) Three classes of C2H2 zinc finger proteins. *Cell Mol Life Sci* **58:** 625-635
12. Fog CK, Galli GG, Lund AH (2012) PRDM proteins: important players in differentiation and disease. *Bioessays* **34:** 50-60
13. Hohenauer T, Moore AW (2012) The Prdm family: expanding roles in stem cells and development. *Development* **139:** 2267-2282
14. Richardson R, Tracey-White D, Webster A, Moosajee M (2017) The zebrafish eye-a paradigm for investigating human ocular genetics. *Eye (Lond)* **31:** 68-86
15. Nikopoulos K, Venselaar H, Collin RW, Riveiro-Alvarez R, Boonstra FN, Hooymans JM, Mukhopadhyay A, Shears D, van Bers M, de Wijs IJ*, et al.* (2010) Overview of the mutation spectrum in familial exudative vitreoretinopathy and Norrie disease with identification of 21 novel variants in FZD4, LRP5, and NDP. *Hum Mutat* **31:** 656-666
16. Panagiotou ES, Sanjurjo Soriano C, Poulter JA, Lord EC, Dzulova D, Kondo H, Hiyoshi A, Chung BH, Chu YW, Lai CHY*, et al.* (2017) Defects in the Cell Signaling Mediator beta-Catenin Cause the Retinal Vascular Condition FEVR. *Am J Hum Genet* **100:** 960-968
17. Wu JH, Liu JH, Ko YC, Wang CT, Chung YC, Chu KC, Liu TT, Chao HM, Jiang YJ, Chen SJ*, et al.* (2016) Haploinsufficiency of RCBTB1 is associated with Coats disease and familial exudative vitreoretinopathy. *Hum Mol Genet* **25:** 1637-1647
18. Herbst A, Jurinovic V, Krebs S, Thieme SE, Blum H, Goke B, Kolligs FT (2014) Comprehensive analysis of beta-catenin target genes in colorectal carcinoma cell lines with deregulated Wnt/beta-catenin signaling. *BMC Genomics* **15:** 74
19. Celen I, Ross KE, Arighi CN, Wu CH (2015) Bioinformatics Knowledge Map for Analysis of Beta-Catenin Function in Cancer. *PLoS One* **10:** e0141773
20. Kondo H, Matsushita I, Tahira T, Uchio E, Kusaka S (2016) Mutations in ATOH7 gene in patients with nonsyndromic congenital retinal nonattachment and familial exudative vitreoretinopathy. *Ophthalmic Genet* **37:** 462-464
21. Gao Z, Mao CA, Pan P, Mu X, Klein WH (2014) Transcriptome of Atoh7 retinal progenitor cells identifies new Atoh7-dependent regulatory genes for retinal ganglion cell formation. *Dev Neurobiol* **74:** 1123-1140
22. Rattray AM, Muller B (2012) The control of histone gene expression. *Biochem Soc Trans* **40:** 880-885

23. Coppieters F, Ascari G, Dannhausen K, Nikopoulos K, Peelman F, Karlstetter M, Xu M, Brachet C, Meunier I, Tsilimbaris MK, *et al.* (2016) Isolated and Syndromic Retinal Dystrophy Caused by Biallelic Mutations in RCBTB1, a Gene Implicated in Ubiquitination. *Am J Hum Genet* **99:** 470-480
24. Biswas P, Naeem MA, Ali MH, Assir MZ, Khan SN, Riazuddin S, Hejtmancik JF, Riazuddin SA, Ayyagari R (2018) Whole-Exome Sequencing Identifies Novel Variants that Co-segregates with Autosomal Recessive Retinal Degeneration in a Pakistani Pedigree. *Adv Exp Med Biol* **1074:** 219-228
25. Gong Y, Slee RB, Fukai N, Rawadi G, Roman-Roman S, Reginato AM, Wang H, Cundy T, Glorieux FH, Lev D, *et al.* (2001) LDL receptor-related protein 5 (LRP5) affects bone accrual and eye development. *Cell* **107:** 513-523
26. Meindl A, Berger W, Meitinger T, van de Pol D, Achatz H, Dorner C, Haasemann M, Hellebrand H, Gal A, Cremers F, *et al.* (1992) Norrie disease is caused by mutations in an extracellular protein resembling C-terminal globular domain of mucins. *Nat Genet* **2:** 139-143
27. Robitaille JM, Gillett RM, LeBlanc MA, Gaston D, Nightingale M, Mackley MP, Parkash S, Hathaway J, Thomas A, Ells A, *et al.* (2014) Phenotypic overlap between familial exudative vitreoretinopathy and microcephaly, lymphedema, and chorioretinal dysplasia caused by KIF11 mutations. *JAMA Ophthalmol* **132:** 1393-1399
28. Hu H, Xiao X, Li S, Jia X, Guo X, Zhang Q (2016) KIF11 mutations are a common cause of autosomal dominant familial exudative vitreoretinopathy. *Br J Ophthalmol* **100:** 278-283
29. Boonstra FN, van Nouhuys CE, Schuil J, de Wijs IJ, van der Donk KP, Nikopoulos K, Mukhopadhyay A, Scheffer H, Tilanus MA, Cremers FP, *et al.* (2009) Clinical and molecular evaluation of probands and family members with familial exudative vitreoretinopathy. *Invest Ophthalmol Vis Sci* **50:** 4379-4385
30. Cooper DN, Krawczak M, Polychronakos C, Tyler-Smith C, Kehrer-Sawatzki H (2013) Where genotype is not predictive of phenotype: towards an understanding of the molecular basis of reduced penetrance in human inherited disease. *Hum Genet* **132:** 1077-1130
31. Tauqeer Z, Yonekawa Y (2018) Familial Exudative Vitreoretinopathy: Pathophysiology, Diagnosis, and Management. *Asia Pac J Ophthalmol (Phila)* **7:** 176-182
32. Lu YZ, Deng GD, Liu JH, Yan H (2018) The role of intravitreal ranubizumab in the treatment of familial exudative vitreoretinopathy of stage 2 or greater. *Int J Ophthalmol* **11:** 976-980
33. Quiram PA, Drenser KA, Lai MM, Capone A, Jr., Trese MT (2008) Treatment of vascularly active familial exudative vitreoretinopathy with pegaptanib sodium (Macugen). *Retina* **28:** S8-12
34. Tagami M, Kusuhara S, Honda S, Tsukahara Y, Negi A (2008) Rapid regression of retinal hemorrhage and neovascularization in a case of familial exudative vitreoretinopathy treated with intravitreal bevacizumab. *Graefes Arch Clin Exp Ophthalmol* **246:** 1787-1789
35. Bennett J, Ashtari M, Wellman J, Marshall KA, Cyckowski LL, Chung DC, McCague S, Pierce EA, Chen Y, Bennicelli JL, *et al.* (2012) AAV2 gene therapy readministration in three adults with congenital blindness. *Sci Transl Med* **4:** 120ra115
36. Ohlmann A, Scholz M, Goldwich A, Chauhan BK, Hudl K, Ohlmann AV, Zrenner E, Berger W, Cvekl A, Seeliger MW, *et al.* (2005) Ectopic norrin induces growth of ocular capillaries and restores normal retinal angiogenesis in Norrie disease mutant mice. *J Neurosci* **25:** 1701-1710
37. Ohlmann A, Seitz R, Braunger B, Seitz D, Bosl MR, Tamm ER (2010) Norrin promotes vascular regrowth after oxygen-induced retinal vessel loss and suppresses retinopathy in mice. *J Neurosci* **30:** 183-193
38. Dailey WA, Drenser KA, Wong SC, Cheng M, Vercellone J, Roumayah KK, Feeney EV, Deshpande M, Guzman AE, Trese M, *et al.* (2017) Norrin treatment improves ganglion cell survival in an oxygen-induced retinopathy model of retinal ischemia. *Exp Eye Res* **164:** 129-138
39. Tokunaga CC, Chen YH, Dailey W, Cheng M, Drenser KA (2013) Retinal vascular rescue of oxygen-induced retinopathy in mice by norrin. *Invest Ophthalmol Vis Sci* **54:** 222-229
40. Zeilbeck LF, Muller BB, Leopold SA, Senturk B, Langmann T, Tamm ER, Ohlmann A (2016) Norrin mediates angiogenic properties via the induction of insulin-like growth factor-1. *Exp Eye Res* **145:** 317-326
41. Wang Z, Liu CH, Sun Y, Gong Y, Favazza TL, Morss PC, Saba NJ, Fredrick TW, He X, Akula JD, *et al.* (2016) Pharmacologic Activation of Wnt Signaling by Lithium Normalizes Retinal Vasculature in a Murine Model of Familial Exudative Vitreoretinopathy. *Am J Pathol* **186:** 2588-2600
42. Arnaoutova I, Kleinman HK (2010) In vitro angiogenesis: endothelial cell tube formation on gelled basement membrane extract. *Nat Protoc* **5:** 628-635
43. Kitambi SS, McCulloch KJ, Peterson RT, Malicki JJ (2009) Small molecule screen for compounds that affect vascular development in the zebrafish retina. *Mech Dev* **126:** 464-477

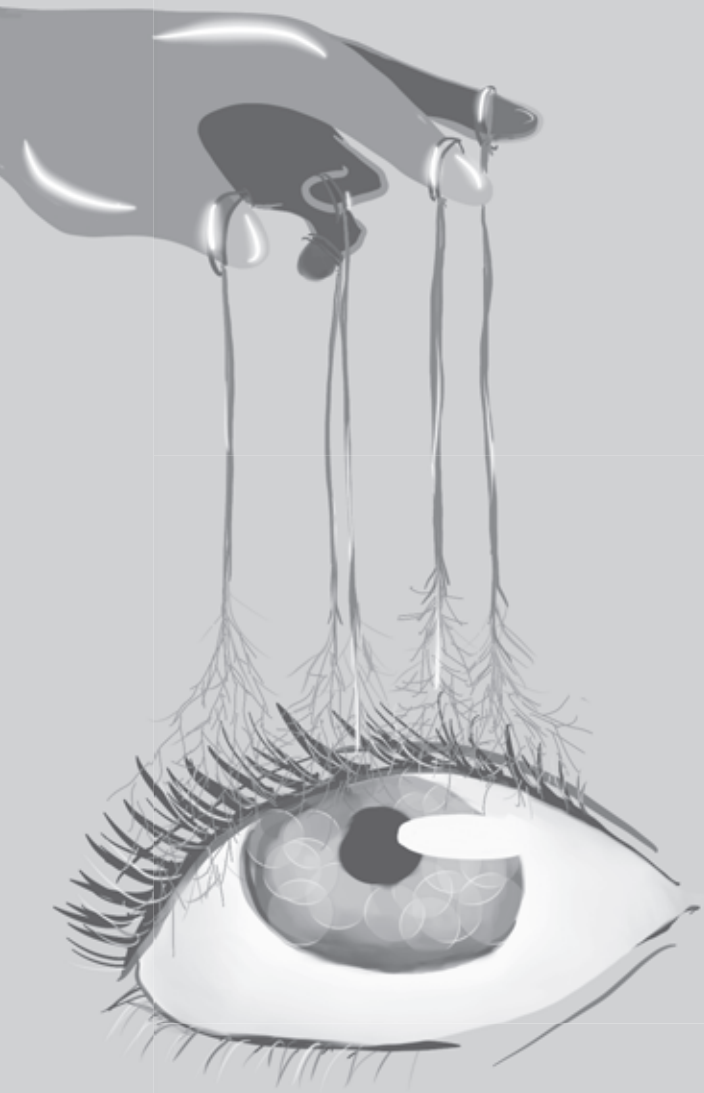

Chapter 7

Summary/Samenvatting/Intisari

Summary

Vision plays a crucial role in one's life. The human eye consists of numerous delicate parts which have different functions. The retina is the part of the eye that is responsible to catch the light signal from the environment and convert it into neural impulses for the brain to perceive. The retina has a high metabolic activity, which is supported by nutrients supplied through blood vessels. Vasculature defects in the retina represent one of the major causes of visual impairment. Background information on the structure of the retina and the development of retinal vasculature are provided in **Chapter 1**. This thesis focuses on a subtype of visual impairment termed familial exudative vitreoretinopathy (FEVR). It is an inherited retinal disorder hallmarked by abnormal or absence of vasculature in the peripheral retina. This disease is also explained extensively in **Chapter 1**. Finally, relevant *in vivo* and *in vitro* models to study retinal vasculature as well as molecular and cellular technologies used in this thesis are described in **Chapter 1**.

A few years ago, a mutation in *ZNF408* (c.1363C>T, p.His455Tyr) was identified in an autosomal dominant FEVR family. Despite subsequent experiments in cells and zebrafish which suggest the involvement of ZNF408 in the development of retinal vasculature, little is known about its molecular function. In **Chapter 2**, an *in vitro* study on the role of ZNF408 in regulating gene expression and how the p.His455Tyr mutation affects its function is presented. Transcriptome profiling showed that ZNF408 regulates the expression of genes relevant to the development of vasculature, which is altered by the p.His455Tyr mutation. Further molecular experiments suggest that ZNF408 regulates gene expression in an indirect manner.

To further study the function of *znf408 in vivo*, *znf408* zebrafish models were generated (**Chapter 3**). Deletions that are predicted to lead to a truncated protein were introduced in two zebrafish models, one with a 1 bp deletion and the other with a 4 bp deletion. A missense model was also generated, in which a 1 bp substitution was applied to mimic the human p.His455Tyr mutation. Characterization of the mutant models showed delayed retinal vasculature development at larval stage, abnormal sprouting in young adults, and vascular leakage in adults. These indicate the suitability of these models as animal model of FEVR and also to further study *znf408* in retinal vasculature development *in vivo*.

FEVR is a clinically and genetically heterogeneous disease. Furthermore, reduced penetrance has been observed in approximately 25% of mutation carriers in FEVR. It is still unclear what is the underlying cause of the observed reduced penetrance. In **Chapter 4**, a pilot study of reduced penetrance in *ZNF408*-associated FEVR is presented. Induced pluripotent stem cells of an FEVR patient with the *ZNF408* c.1363C>T mutation and her sister who is unaffected despite carrying the same mutation, as well as those from control individuals were differentiated into endothelial cells. The obtained endothelial cells showed comparable morphology, expression of endothelial cell markers, and angiogenic behavior. A trend of lower differentiation efficiency towards endothelial lineage was observed in the induced pluripotent stem cell lines derived from the patient and the unaffected mutant carrier. Furthermore, endothelial cells derived from the unaffected mutant carrier had an approximately 2-fold lower *ZNF408* expression compared to patient and controls. Further research is required to determine whether these results are reproducible in other circumstances and also to gain deeper insight into the molecular mechanisms of reduced penetrance in FEVR. Nonetheless, this pilot study showed how patient-specific endothelial cells can be generated from induced pluripotent stem cells and that the obtained endothelial cells can be employed in studying reduced penetrance in FEVR.

As a genetically heterogeneous disease, mutations in other genes have been reported in FEVR patients. In **Chapter 5**, the identification of a mutation in *KIF11* in a patient presenting FEVR and microcephaly is described. Further genetic study revealed that the mutation was inherited from the unaffected mother who is mosaic for the mutation. This study showed the importance of thorough genetic assessment of unaffected parents, particularly in an isolated cases, to enable more reliable recurrence risk assessment and hence, better genetic counseling.

Finally, in **Chapter 6,** the role of ZNF408 in the development of (retinal) vasculature based on *in vitro* and *in vivo* findings is discussed. Transcriptome profiling suggested a possible role of ZNF408 in chromatin remodeling. This unexpected finding is also discussed in **Chapter 6**. Besides monogenic FEVR, variants in *ZNF408* have also been reported in retinitis pigmentosa and digenic FEVR. All variants that have been reported in *ZNF408* and how different variants lead to different phenotypes are summarized and discussed in **Chapter 6**, followed by a discussion on the complexity of FEVR genetics. Finally, the impact of the studies presented in this thesis to diagnostics, disease management, and potential therapeutics for FEVR are discussed.

Samenvatting

Het vermogen om te kunnen zien speelt een cruciale rol in iemands leven. Het menselijk oog bestaat uit talloze gevoelige delen met verschillende functies. Het netvlies is het deel van het oog dat verantwoordelijk is voor het opvangen van lichtsignalen uit de omgeving, en deze om te zetten in neurale impulsen voor de hersenen om waar te nemen. Het netvlies heeft een hoge metabole activiteit, die wordt ondersteund door voedingsstoffen die via bloedvaten worden aangevoerd. Een defect vaatstelsel in het netvlies is dan ook een belangrijke oorzaak van visuele stoornissen. Achtergrondinformatie over de structuur van het netvlies en de ontwikkeling van het vaatstelsel van het netvlies wordt gegeven in **Hoofdstuk 1**. Dit proefschrift richt zich op een subtype van visuele beperking genaamd 'familial exudative vitreoretinopathy' (FEVR). Dit is een erfelijke netvliesaandoening gekenmerkt door abnormale of afwezigheid van vaatstelsels in het randgebied van het netvlies. Deze ziekte wordt ook uitgebreid toegelicht in **Hoofdstuk 1**. Tot slot worden relevante *in vivo* en *in vitro* modellen voor het bestuderen van vaatstelsels van het netvlies, alsook de moleculaire en cellulaire technologieën die in dit proefschrift worden gebruikt beschreven in **Hoofdstuk 1**.

Enkele jaren geleden werd een mutatie in *ZNF408* (c.1363C>T, p.His455Tyr) geïdentificeerd in een autosomaal dominante FEVR-familie. Ondanks latere experimenten in cellen en zebravissen, die wijzen op de betrokkenheid van *ZNF408* bij de ontwikkeling van het vaatstelsel in het netvlies, is er weinig bekend over de moleculaire functie ervan. In **Hoofdstuk 2** wordt een *in vitro* studie gepresenteerd over de rol van ZNF408 bij het reguleren van gen expressie en hoe de p.His455Tyr-mutatie dit proces beïnvloedt. Transcriptoom analyse toonde aan dat *ZNF408* de expressie reguleert van genen die relevant zijn voor de ontwikkeling van het vaatstelsel, en hoe deze werden veranderd door de mutatie p.His455Tyr. Verdere moleculaire experimenten wijzen erop dat ZNF408 genexpressie op een indirecte manier reguleert.

Om de functie van *znf408 in vivo* verder te bestuderen, werden *znf408* zebravismodellen gegenereerd (**Hoofdstuk 3**). Deleties waarvan werd voorspeld dat ze tot een frameshift mutatie zouden leiden, werden geïntroduceerd in twee zebravismodellen, één met een deletie van 1 bp en de andere met een deletie van 4 bp. Een *missense*-model werd ook gegenereerd, waarbij een 1 bp substitutie werd

toegepast om de menselijke p.His455Tyr-mutatie na te bootsen. Karakterisering van de mutante modellen toonde vertraagde ontwikkeling van het vaatstelsel van het netvlies in het larvale stadium, abnormale vertakkingen bij jongvolwassen vissen, en vasculaire lekkage bij volwassen vissen. Deze resultaten geven de geschiktheid van deze modellen aan als diermodel voor FEVR en ook voor verdere studies van *znf408* in de ontwikkeling van *in vivo* vaatstelsels van het netvlies.

FEVR is een klinisch en genetisch heterogene ziekte. Verder wordt een verminderde penetrantie waargenomen bij ongeveer 25% van mutatiedragers bij FEVR. Het is nog steeds onduidelijk wat de onderliggende oorzaak is van deze verminderde penetrantie. In **Hoofdstuk 4** wordt een pilotstudie van verminderde penetrantie in *ZNF408*-geassocieerde FEVR gepresenteerd. Geïnduceerde pluripotente stamcellen van een FEVR-patiënt met de *ZNF408* c.1363C>T-mutatie en haar zuster, die niet is aangedaan ondanks het dragen van dezelfde mutatie, alsook die van controle-individuen, werden gedifferentieerd in endotheelcellen. De verkregen endotheelcellen vertoonden vergelijkbare morfologie, expressie van endotheliale celmarkers en angiogeen gedrag. Een trend van lagere differentiatie-efficiëntie naar endotheliale origine werd waargenomen in de geïnduceerde pluripotente stamcellijnen afgeleid van de patiënt en de gezonde mutatie drager. Bovendien hadden endotheelcellen afgeleid van de gezonde mutatie drager een ongeveer 2-voudig lagere *ZNF408*-expressie in vergelijking met de patiënt en controles. Verder onderzoek is nodig om te bepalen of deze resultaten reproduceerbaar zijn in andere omstandigheden en ook om een dieper inzicht te krijgen in de moleculaire mechanismen van verminderde penetrantie in FEVR. Niettemin toonde deze pilotstudie aan hoe patiënt-specifieke endotheelcellen kunnen worden gegenereerd uit geïnduceerde pluripotente stamcellen en dat de verkregen endotheelcellen kunnen worden gebruikt voor het bestuderen van verminderde penetrantie in FEVR.

Zijnde een genetisch heterogene ziekte, zijn er ook mutaties in andere genen gerapporteerd bij FEVR patiënten. **Hoofdstuk 5** beschrijft de identificatie van een mutatie in *KIF11* bij een patiënt met FEVR en microcefalie. Verdere genetische studies onthulden dat de mutatie werd geërfd van de niet-aangedane moeder die drager en mozaïek is voor de mutatie. Deze studie toonde het belang aan van een grondige genetische beoordeling van niet-getroffen ouders, met name in geïsoleerde gevallen, om betrouwbaardere risicobeoordelingen mogelijk te maken en dus betere

genetische counseling.

In **Hoofdstuk 6** wordt de rol van ZNF408 in de ontwikkeling van het vaatstelsel (netvlies) op basis van onze *in vitro* en *in vivo* bevindingen besproken. Transcriptoomprofilering stelde een mogelijke rol van ZNF408 in chromatine-hermodellering voor. Deze onverwachte bevinding wordt ook besproken in **Hoofdstuk 6**. Naast monogene FEVR zijn ook varianten in *ZNF408* gerapporteerd bij retinitis pigmentosa en digene FEVR. Alle varianten die zijn gerapporteerd in *ZNF408* en hoe verschillende varianten leiden tot verschillende fenotypen worden samengevat en besproken in **Hoofdstuk 6**, gevolgd door een discussie over de complexiteit van FEVR-genetica. Ten slotte worden de bevindingen van de onderzoeken uit dit proefschrift gekoppeld aan de diagnostiek, het omgaan met de ziekte, en potentiële nieuwe behandelingen voor FEVR.

Intisari

Penglihatan memiliki peranan penting dalam kehidupan seseorang. Mata manusia terdiri dari berbagai bagian yang fungsinya beragam. Retina adalah bagian dari mata yang berfungsi untuk menerima rangsangan cahaya dari lingkungan dan mengubahnya menjadi impuls saraf untuk kemudian diproses oleh otak. Retina memiliki aktivitas metabolisme yang tinggi. Aktivitas ini didukung oleh nutrisi yang disalurkan melalui pembuluh darah. Kerusakan pembuluh darah di retina merupakan salah satu penyebab utama gangguan penglihatan. Struktur retina dan perkembangan pembuluh darah di retina dijelaskan di **Bab 1**. Salah satu subtipe gangguan penglihatan yang disebut familial exudative vitreoretinopathy (FEVR) adalah fokus dari tesis ini. FEVR adalah kelainan retina turunan yang ditandai oleh tidak adanya atau abnormalitas pada pembuluh darah di retina perifer. Penyakit ini juga dijelaskan secara mendalam pada **Bab 1**. Model *in vivo* dan *in vitro* yang relevan untuk mempelajari pembuluh darah di retina serta teknologi molekuler dan seluler yang digunakan dalam tesis ini diuraikan pada **Bab 1**.

Beberapa tahun yang lalu, mutasi pada *ZNF408* (c.1363C>T, p.His455Tyr) diidentifikasi dalam keluarga dengan FEVR yang diturunkan secara dominan autosom. Meskipun percobaan selanjutnya dalam sel dan ikan zebra menunjukkan keterlibatan *ZNF408* dalam perkembangan pembuluh darah di retina, belum banyak yang diketahui tentang fungsi molekulernya. **Bab 2** berisi penjelasan mengenai studi *in vitro* tentang peranan ZNF408 dalam mengatur ekspresi gen dan bagaimana mutasi p.His455Tyr dapat mempengaruhi fungsinya. Analisa transkriptomik menunjukkan bahwa ZNF408 mengatur ekspresi gen yang relevan untuk perkembangan pembuluh darah, yang diubah oleh mutasi p.His455Tyr. Hasil eksperimen molekuler lebih lanjut mengindikasikan bahwa ZNF408 mengatur ekspresi gen secara tidak langsung..

Untuk mempelajari lebih lanjut fungsi *znf408 in vivo*, rekayasa gen *znf408* dilakukan pada ikan zebra (**Bab 3**). Dua delesi yang diperkirakan untuk menimbulkan protein yang lebih pendel diaplikasikan pada gen *znf408* di ikan zebra, yang pertama delesi 1 bp dan yang kedua delesi 4 bp. Satu model *missense* juga dihasilkan, yang mana substitusi 1 bp diaplikasikan untuk menyerupai mutasi p.His455Tyr pada manusia. Karakterisasi model-model mutan ini menunjukkan terhambatnya perkembangan pembuluh darah retina pada tahap larva, kelainan

pertumbuhan cabang pada tahap ikan muda, dan kebocoran pembuluh darah pada tahap ikan dewasa. Hasil karakterisasi ini menunjukkan bahwa model-model ini sesuai untuk meneliti peranan *znf408* lebih lanjut dalam perkembangan pembuluh darah retina secara *in vivo*.

FEVR adalah penyakit yang heterogen, baik secara klinis maupun genetik. *Reduced penetrance* telah diamati pada sekitar 25% mutasi *carrier* dalam FEVR. Namun, penyebabnya belum diketahui secara jelas. Studi awal mengenai *reduced penetrance* dalam FEVR yang disebabkan oleh *ZNF408* diuraikan di dalam **Bab 4**. Sel punca ber-pluripotensi dari seorang pasien FEVR dan saudara perempuannya yang tidak menunjukkan gejala FEVR walaupun juga mempunyai mutasi di gen *ZNF408*, dan juga sel punca ber-pluripotensi dari individu sehat (kontrol), didiferensiasikan menjadi sel endotel. Sel-sel endotel yang dihasilkan dari beberapa individual ini menunjukkan morfologi, ekspresi marker-marker sel endotel, dan karakteristik angiogenik yang sebanding satu sama lain. Efisiensi diferensiasi sel-sel punca dari pasien FEVR dan saudarinya untuk menjadi sel endotel cenderung lebih rendah dibandingkan dengan sel-sel punca dari kontrol. Lebih lanjut, sel endotel yang dihasilkan dari individu sehat yang mempunyai mutasi pada gen *ZNF408* memiliki ekspresi gen *ZNF408* sekitar 2 kali lebih rendah dibandingkan dengan pasien FEVR dan kontrol. Penelitian lebih lanjut diperlukan untuk menentukan apakah hasil ini dapat direproduksi dan juga untuk mendapatkan wawasan yang lebih dalam tentang mekanisme molekuler dari *reduced penetrance* dalam FEVR. Meskipun demikian, penelitian awal ini menunjukkan bagaimana sel endotel dapat didiferensiasikan dari sel punca pasien dan sel endotel yang dihasilkan dapat digunakan untuk mempelajari *reduced penetrance* dalam FEVR.

Sebagai penyakit yang heterogen secara genetik, mutasi pada gen selain *ZNF408* telah dilaporkan pada pasien FEVR. **Bab 5** mendeskripsikan identifikasi mutasi pada gen *KIF11* pada pasien dengan FEVR dan mikrosefali. Studi genetik lebih lanjut menunjukkan bahwa mutasi ini diwarisi dari ibu yang tidak memiliki FEVR yang mosaik untuk mutasi ini. Studi ini menunjukkan pentingnya evaluasi genetik menyeluruh dari orang tua meskipun tidak memiliki FEVR, terutama dalam kasus yang sporadik, sehingga penilaian risiko turunan dapat lebih akurat dan pada akhirnya konseling genetik yang lebih baik dapat diberikan.

Peran ZNF408 dalam perkembangan pembuluh darah (di retina) berdasarkan temuan *in vitro* dan *in vivo* dibahas di dalam **Bab 6**. Hasil analisa transkriptomik mengacu pada kemungkinan peran ZNF408 dalam modifikasi kromatin. Temuan tak terduga ini juga dibahas di dalam **Bab 6**. Semua varian yang telah dilaporkan dalam *ZNF408* dan bagaimana varian yang berbeda menimbulkan fenotip yang berbeda dirangkum dan dibahas di dalam **Bab 6**, diikuti dengan diskusi tentang kompleksitas genetika FEVR. Selanjutnya, dampak dari studi yang disajikan dalam tesis ini untuk diagnostik, manajemen penyakit, dan kemungkinan terapi untuk FEVR juga dibahas di **Bab 6**.

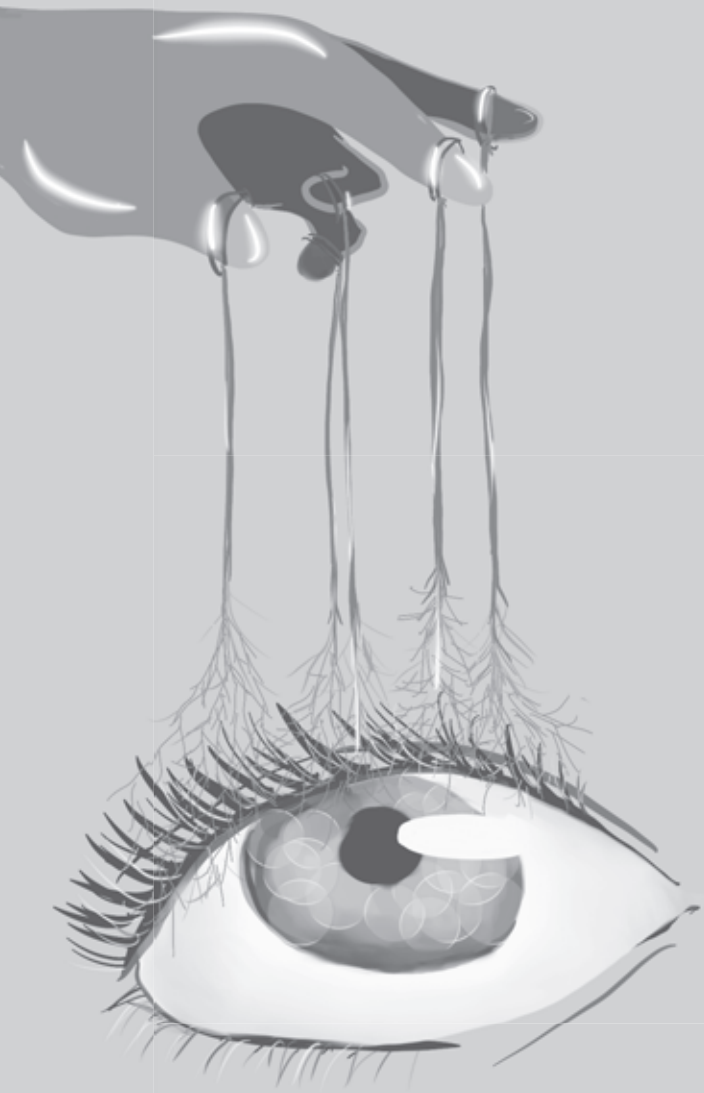

About the author

Dyah Winiarty Karjosukarso was born on March 1, 1992 in Ujung Pandang, Indonesia. She moved to the Netherlands in 2008 to follow the Life Sciences program at the Hogeschool van Arnhem en Nijmegen. After obtaining her Bachelor of Applied Sciences degree in 2012, she received a scholarship to join the research master Molecular Mechanisms of Disease at the Radboud University, the Netherlands. During her master study, she performed two internships. The first one was related to the topic presented in this thesis, at the Department of Human Genetics at the Radboudumc, under supervision of Dr. Rob Collin and Dr. Huiqing Zhou. She chose stem cell research for her second internship, which was performed at the lab of Prof. Roger Pedersen at the Anne McLaren Laboratory of Regenerative Medicine, University of Cambridge, under supervision of Dr. Sasha Mendjan. She obtained the internal Radboudumc PhD grant to continue the project she worked on during her first master internship and started in October 2014 as a PhD student in the Blindness Genetic Therapy group of Dr. Rob Collin at the Department of Human Genetics at the Radboudumc in Nijmegen, the Netherlands. In March 2019, she joined the lab of Dr. Klaas Mulder at the Department of Molecular Developmental Biology, Radboud Institute of Molecular Life Sciences, as a postdoctoral fellow, to study head and neck cancer using single cell technologies.

List of publications

Detection and quantification of a KIF11 mosaicism in a subject presenting familial exudative vitreoretinopathy with microcephaly
Karjosukarso DW, Cremers FPM, van Nouhuys CE, Collin RWJ.
European Journal of Human Genetics (2018) **26:** 1819-1823

Hypermorphic and hypomorphic AARS alleles in patients with CMT2N expand clinical and molecular heterogeneities
Weterman MAJ, Kuo M, Kenter SB, Gordillo S, **Karjosukarso DW**, Takase R, Bronk M, Oprescu S, Ruissen F, Witteveen RJW, Bienfait HME, Breuning M, Verhamme C, Hou YM, Visser M, Antonellis A, Baas F.
Human Molecular Genetics (2018) **27:** 4036-4050

An FEVR-associated mutation in ZNF408 alters the expression of genes involved in the development of vasculature
Karjosukarso DW, van Gestel SHC, Qu J, Kouwenhoven EN, Duijkers L, Garanto A, Zhou H, Collin RWJ
Human Molecular Genetics (2018) **27:** 3519-3527

Defects in the Cell Signaling Mediator β-Catenin Cause the Retinal Vascular Condition FEVR
Panagiotou ES, Sanjurjo Soriano C, Poulter JA, Lord EC, Dzulova D, Kondo H, Hiyoshi A, Chung BH, Chu YW, Lai CHY, Tafoya ME, **Karjosukarso D**, Collin RWJ, Topping J, Downey LM, Ali M, Inglehearn CF, Toomes C.
American Journal of Human Genetics (2017) **100:** 960-968

NANOG and CDX2 pattern distinct subtypes of human mesoderm during exit from pluripotency.
Mendjan S, Mascetti VL, Ortmann D, Ortiz M, **Karjosukarso DW**, Ng Y, Moreau T, Pedersen RA
Cell Stem Cells (2014) **15:** 310-325

Acknowledgements

This PhD adventure is finally coming to an end. The completion of thesis would not be possible without the help and support of many people, some of which I would like to specially thank.

First of all, **Rob**, a heartfelt thanks for your supervision all these years. From my master internship, writing the PhD proposal, and the PhD journey itself. I am happy that you gave me the chance to try different techniques during my PhD and to work on my project the way I want. I have learnt a lot from you and your optimism helped me through the difficult phases. Thank you for always believing in me!

Jo, I am grateful that I can always come to you with questions. Thank you for helping me find my way with ChIP-Seq and RNA-Seq experiments. I appreciate a lot our conversation when I was in doubt about the next step in my career, which resulted in my current position. Thank you!

Frans, thank you for your interest and input for my project. You got more involved towards the end of my PhD and thanks to your structured working style, it is possible to finish it on time. Thank you for all your input during the thesis meetings as well as your detailed corrections for this thesis.

The **BGT group**: **Alex**, **Lonneke**, **Anita**, **Julio**, **Muriël**, **Matthijs**, and **Tess**. Thank you for your input during group meetings and the great atmosphere in the group. **Alex**, I cannot say this enough, thank you for all the ask-Alex questions. I would still be figuring out how to do my experiments without your help. **Julio**, the imaging guru and tortilla chef, it was great to spend the PhD with you. **Muriël**, we spent a lot of time together, at the fish and also outside work. It was great working with you and thanks for the nice time as well as for the great trip to ARVO Baltimore, Washington, and New York. **Lonneke**, you were always there, during my internship and when I came back for my PhD. Thank you for all your help and the nice time. I am happy that you are willing to be my paranymph during my thesis defense. **Anita**, thank you for your help at the end of my project and also the nice time, both in the lab and at the fish.

The other **ZAT-lab members**: **Erwin**, **Erik**, **Margo**, **Ralph**, **Theo**, **Lisette**, and **Sanne**. Thank you all for all the input on zebrafish work and the nice time in the lab. **Margo**, I learned a lot about the fish from you and also had many gezellig moments. Thanks! **Theo**, you made a lot of blocks and sections for me. Thank you for all your help.

The co-authors of my chapters, without whom this thesis will not be finished. **Bas**, thank you for all your help with data analysis and statistics. It was awesome that I could just turn my chair and asked as many questions as I wanted. **Jieqiong**, thank you for your help with the ChIP-Seq and RNA-Seq experiments. **Evelyn**, thanks for introducing me to the ChIP-Seq world. **Lasse and Zaheer**, it was great working with you. I am happy that we found your poster in ARVO and collaborate since then. Fingers crossed for the zebrafish manuscript. **Katrin**, our story goes a long way, but in this instance, thanks for your magic with my iPSC lines. I would not have Chapter 4 of this thesis without your help. **Erik van Nouhuys**, thank you for all your help with the clinical side of the project.

My students: **Mariya** and **Jia Qi**, thank you for your enthusiasm and contribution to my project. I hope you learn from it as much as I have learnt from you. Best wishes for your future career.

The **Q4 PhD room**: **Anouk**, **Zeinab**, **Elly**, **Katrin**, **Joanna**, **Ting**, **Suzanne**, **Teun**, **Manon**, **Britt**, **Jason**, **Eline**, **Janine**, **Francesca**, **Renske**, and **Sarita**. Thank you for the great time in the office and the nice bowling night. Good luck to you all!

The **fish facility team**: **Tom**, **Antoon**, and **Jeroen**. Thank you for all your help and advice. Also, for taking such a great care of the zebrafish.

Other colleagues in Human Genetics, who has helped me, with experiments, finding things, and/or the nice chitchats. **Riccardo**, **Galuh**, **Bjorn**, **Michael**, **Simon**, **Anke**, **Louet**, **Tessa**, **Silvia**, **Lilian**, **Ideke**, **Minh**, **Brooke**, **Maryam**, **Sylvia**, **Kaman**, **Saskia**, and **Marlie**, thank you all!

Friendship is one of the greatest gift of life and I am blessed with a lot of great friends who stayed with me through good and bad times. The **Nijmegen gang**, **Andhyk**, **Okta**, **Sam**, **Tammy**, **Rebecca**, **Richard**, **Eko**, **Alin**, **Bella**, **Eugin**, and **Meily**, from

the HAN till now that most of you are not living in Nijmegen anymore, it is never a dull moment with you all :) I am happy that we still meet each other and have fun together. **Eugin**, you rock! Good luck finishing your PhD :) **Mirna**, thank you for all the good times, hunting for good food, and going to the movies. **Tammy**, I am happy that I can always count on you, mbar! **Bella**, you were there since my very first day in the Netherlands. It is not only my journey, but also yours. Thank you for the awesome cover and being my paranymph. Basically, thank you for always being there for me. **Kris**, it was full of trials and tribulations, but also good times. Thank you for your listening ears, help, and company.

Mbak Mira dan **Mas Tyas**, makasih untuk semuanya. **Papa** dan **Mama**, terima kasih sudah mengizinkan dede ke Belanda. Terima kasih untuk support dan doa Mama Papa, sampai semua ini bisa selesai dengan baik.

Donders Graduate School for Cognitive Neuroscience

For a successful research Institute, it is vital to train the next generation of young scientists. To achieve this goal, the Donders Institute for Brain, Cognition and Behaviour established the Donders Graduate School for Cognitive Neuroscience (DGCN), which was officially recognized as a national graduate school in 2009. The Graduate School covers training at both Master and PhD level and provides an excellent educational context fully aligned with the research programme of the Donders Institute.

The school successfully attracts highly talented national and international students in biology, physics, psycholinguistics, psychology, behavioral science, medicine and related disciplines. Selective admission and assessment centers guarantee the enrolment of the best and most motivated students.

The DGCN tracks the career of PhD graduates carefully. More than 50% of PhD alumni show a continuation in academia with postdoc positions at top institutes worldwide, e.g. Stanford University, University of Oxford, University of Cambridge, UCL London, MPI Leipzig, Hanyang University in South Korea, NTNU Norway, University of Illinois, North Western University, Northeastern University in Boston, ETH Zürich, University of Vienna etc.. Positions outside academia spread among the following sectors: specialists in a medical environment, mainly in genetics, geriatrics, psychiatry and neurology. Specialists in a psychological environment, e.g. as specialist in neuropsychology, psychological diagnostics or therapy. Positions in higher education as coordinators or lecturers. A smaller percentage enters business as research consultants, analysts or head of research and development. Fewer graduates stay in a research environment as lab coordinators, technical support or policy advisors. Upcoming possibilities are positions in the IT sector and management position in pharmaceutical industry. In general, the PhDs graduates almost invariably continue with high-quality positions that play an important role in our knowledge economy.

For more information on the DGCN as well as past and upcoming defenses please visit:
http://www.ru.nl/donders/graduate-school/phd/

Data management

Type of data	Subject to privacy (yes/no)	Way of anonymization	Storage
Research data	Yes	All patients received an untraceable number, the identity of the patient is only known by the research PI and treating physician.	Research data were stored in numbered lab journals from October 2014 – November 2016. From then onwards, research data were documented in Labguru in the Vitreoretinopathies project: https://radboudumc.labguru.com/knowledge/projects/711. Access to the data are restricted to PI and direct users.
Antibodies	No	Not applicable	Antibodies were registered in the antibody database from the Department of Human Genetics in Labguru: https://radboudumc.labguru.com/biocollections/antibodies. Antibodies were stored with a traceable number in the assigned freezer/fridge at the Department of Human Genetics, according to the manufacturer's instructions.
Fluorescence images	No	Not applicable	Fluorescence imaging data were stored on the private network of the Blindness Genetics Therapy group at the Department of Human Genetics: T:\PIgroup-Rob-Collin\02 Microscopy images\06 Dyah Karjosukarso.
Plasmids and viruses	No	Not applicable	Plasmids were registered in the Blindness Genetics Therapy database and assigned to a pGT-number. H:\GR Theme groups\10 PI Group Rob Collin\05 Vector_AAV_AON Database. Plasmids were stored in the assigned freezer at -80°C at the Department of Human Genetics.
Patient-derived cell lines	Yes	All patients received an untraceable number, the identity of the patient is only known by the research PI and treating physician.	Cell lines received a traceable number and were registered at the cell culture facility of the Department of Human Genetics. Cell lines were frozen in liquid nitrogen and stored in the assigned freezer at -80°C at the Department of Human Genetics. The number of the cell lines used can be found in the labjournal of Dyah Karjosukarso, stored at the Department of Human Genetics or in Labguru in the Vitreoretinopathies project: https://radboudumc.labguru.com/knowledge/projects/711. Contact person to find the cell lines in the assigned freezer: Saskia van der Velde-Visser.
Other cell lines	No	Not applicable	Cell lines were stored with a traceable number at the cell culture facility at the Department of Human Genetics, according to the manufacturer's instructions. The number of the cell lines used can be found in the labjournal of Dyah Karjosukarso, stored at the Department of Human Genetics or in Labguru in the Vitreoretinopathies project: https://radboudumc.labguru.com/knowledge/projects/711. Contact person to find the cell lines in the assigned freezer: Saskia van der Velde-Visser.
Next generation sequencing data	Yes	All patients received an untraceable number, the identity of the patient is only known by the research PI and treating physician.	Raw data of next generation sequencing experiments were stored on the private network of the Blindness Genetics Therapy group at the Department of Human Genetics: T:\PIgroup-Rob-Collin\12 NGS_data_DK.

n.a.: not applicable.

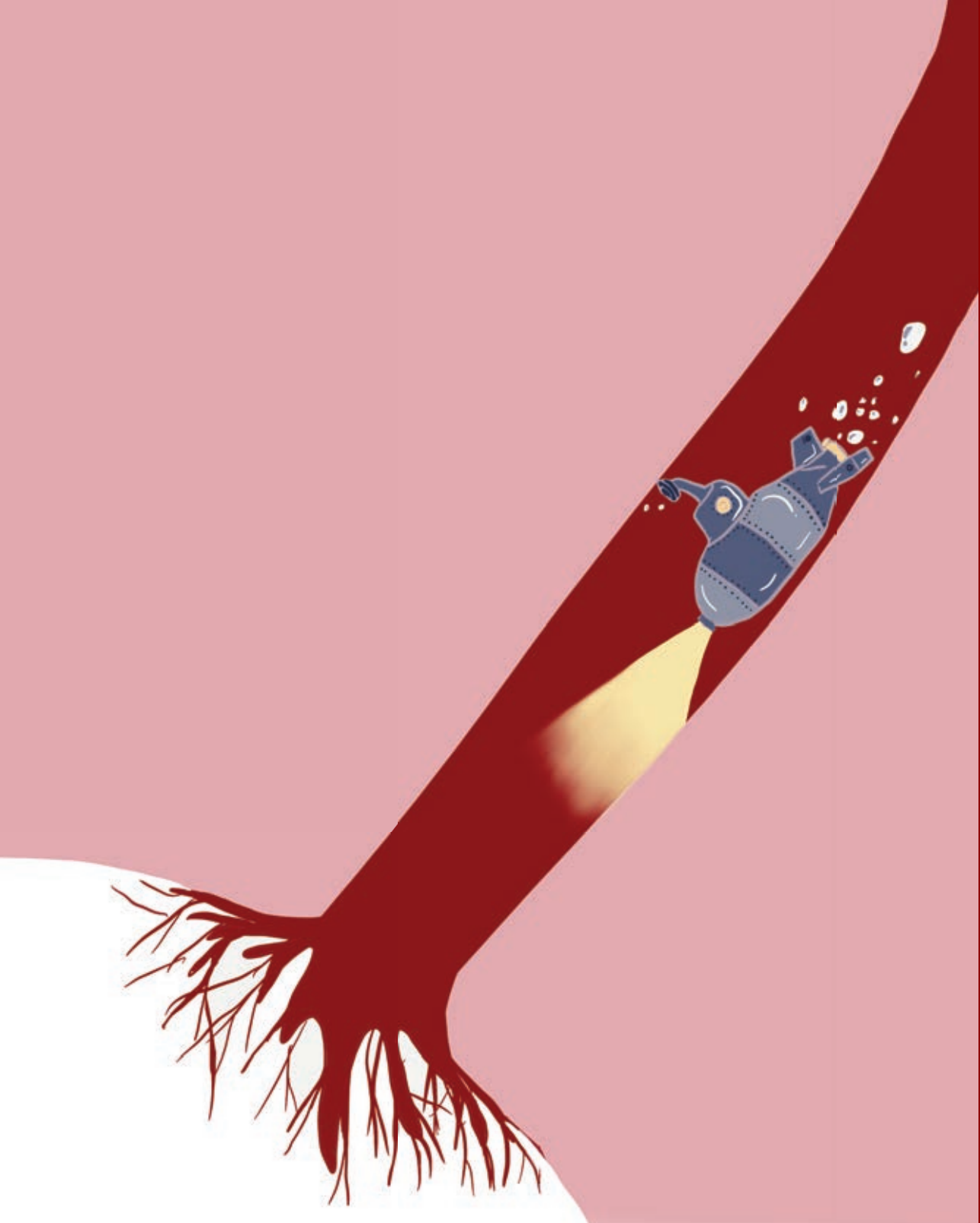

DONDERS INSTITUTE

Max Planck Institute for Psycholinguistics

Radboud University

Radboudumc